Princetonlaan 6
3584 CB Utrecht
P.O. Box 80015
3508 TA Utrecht
The Netherlands

www.tno.nl

T +31 88 866 42 56
F +31 88 866 44 75

TNO report

TNO 2015 R10740 | Final Report

Improved sweet spot identification and smart development using integrated reservoir characterization (Phase 2)

Date	01 June 2015
Author(s)	Susanne Nelskamp Tanya Goldberg Sander Houben Kees Geel Laura Wasch Roel Verreussel Thijs Boxem

Number of pages	133
Number of appendices	8
Customer	EBN B.V., Windershall Noordzee B.V.
Project name	Sweet Spot Identification PHASE 2
Project number	060.05919

Summary

In contrast to mature shale gas plays, for which extensive exploration drilling is and was possible, exploration in the Netherlands is very challenging in the absence of dedicated exploration wells. This project therefore aimed at developing and applying a methodology for shale gas exploration that builds on the synthesis of existing information and data from vintage wells in addition to analyses of outcrop analogues and core material in order to identify the most promising targets for shale gas presence and production. Ultimately, this will reduce the need to drill hundreds of wells and to rely on production data for the same purpose.

The study focuses on the main geological parameters controlling the in-situ shale gas presence: e.g., the thickness and lateral distribution, quality and quantity of organic matter, mineral composition and maturation history. For this purpose the Posidonia Shale Formation in four wells from the Dutch subsurface, as well as an outcrop analogue (Jet Rock Formation of the Cleveland Basin), were analytically studied in detail by generating mineralogical, palynological, inorganic and organic geochemical data. Well-logs from Dutch on- and offshore wells were used for detailed well correlation and property mapping. When combined with the detailed outcrop and core-analyses, these correlations and compilations are pivotal for underpinning the processes that control the deposition, distribution and quality of the shale gas / source rock in a regional, paleogeographic context.

According to the well-log patterns, the Posidonia Shale Formation can be easily traced in high detail throughout the Netherlands, largely because of its strong cyclic signal and little lateral heterogeneity with respect to thickness. Correlation across basins was achieved using stable carbon isotope measurements on the organic material. Total organic carbon (TOC) content is generally high in the lower half of the formation, as seen from measurements and calculated TOC logs.Geochemical proxies, biomarker and palynological facies all point towards the installation of a sharp chemocline and anoxic to euxinic water column conditions as the main driving factor for TOC enrichment. It seems that localised areas with increased subsidence in salt rim synclines are characterized by maximum TOC contents. This may suggest that there is a relation to water depth and/or created accommodation space when it comes to pinpointing TOC-sweet spots. Next to that, the overall temporally homogeneously distributed TOC-trends suggest that the entire basin was susceptible to stratification and enhanced preservation of organic matter. Indications for a strong control of coastal and/or fluvial proximity was not found.

The overall mineralogical composition of the Posidonia Shale Formation consists of clay, clay to silt sized quartz and primary (biogenic) and early diagenetic carbonates. The calculated brittleness of the formation is mainly related to the carbonate content. Conspicuous carbonate concretions are recorded in several discrete strata, occurring in conjunction with high TOC-content. They are a product of microbial anoxygenic oxidation of organic-matter and methane occurring below a stratified water column.

In order to assess the quality of the Posidonia Shale Formation as a shale gas target, several parameters were compared to those of the main shale gas plays in the US. With respect to organic matter content and quality, the Posidonia Shale

Formation strongly resembles the US shales. The environmental processes that determine the deposition of organic matter rich shales in comparable depositional environments appear to be quite similar as well, since the same cyclicity that was observed in the Posidonia Shale Formation could also be observed in several US shales. However the overall thickness and maturity of the Posidonia Shale Formation is lower and brittleness is enhanced by carbonate rocks.

This project therefore shows that it is possible to identify promising shale gas targets or areas of superior source-rock quality from available exploration data. A better understanding of processes that lead to the deposition of organic-rich shales helps in understanding and predicting the distribution and quality of these areas and thus reducing the need for extensive exploration drilling in order to identify shale gas targets.

This report compiles the results of the second phase of the project entitled “Improved Sweet Spot Identification and Smart Development Using Integrated Reservoir Characterization”, carried out within the Innovation Program Upstream Gas as part of the Dutch Top Sector Policy “Energy”. Data and results from the first phase were incorporated and extended in this study.

Contents

1 Section 1 – Background

1.1 Introduction

This project is carried out in the context of the Innovation Program Upstream Gas and is part of the Dutch Top Sector policy 'Energy'. The project is titled 'Improved sweet spot identification and smart development using integrated reservoir characterization (Phase 2)'. The total budget of the project is 200,000.- €, half of the budget is accounted for by the Dutch government. The other half is funded by the two industrial partners Energie Beheer Nederland (EBN) and Wintershall Noordzee B.V..

1.1.1 Background of study – project plan

Since well data from shale gas and coalbed methane (CBM) plays is limited and poorly understood, it is crucial to develop non-conventional methods to optimize gas recovery and mitigate production risks, thereby enabling economic development of these plays. Therefore, the full suite of available subsurface and field data and -methods needs to be integrated to successfully use well log responses for 1) identification, 2) characterization of sweet spots and 3) reservoir behaviour predictions. The first phase of the project (Phase 1: 2012-2013) focused on the integrated sedimentological and petrophysical reservoir characterization, leading to a better understanding of shale plays and insight into the ideal paleoenvironments that offer most favourable shale gas conditions. All data and interpretations were translated and upscaled to log scale to suit the tools of the operator. The second phase will build on the results so far to validate hypothesis, calibrate geochemical data and to investigate which concepts can be assumed to be generally favourable for shale gas plays.

The first stage Sweet Spot project Phase 2 is focussed on the calibration and further interpretation of geochemical data. For the calibration of the present geochemical composition the collected samples will be analysed for clay-fraction XRD. The mineral composition, especially the clay fraction and the clay composition, will give an indication of the hydraulic fracturing potential of the identified zones, especially when the results of this study are linked to the results of the hydraulic fracturing and well placement study of TNO and the fracture network study of Utrecht University According to Gasparik et al. (2012) the clay composition is furthermore the main factor influencing the amount of adsorbed gas in the Posidonia Shale Formation. Extending upon the XRD results, Rock-Eval analysis will be performed to gain insight into the differences in the type of the organic fraction of the samples will be assessed for the different zones and linked to the identified biofacies. The organic material gives an indication of the total hydrocarbon generation potential of the individual zones. According to current knowledge (e.g. Passey et al., 2010) overmature oilprone type II source rocks appear to have the most potential. Most Posidonia shale data indicate Kerogen Type 2 or 3 but more detailed knowledge on the vertical and lateral variability in potential kerogen type will serves economic purposes. Based on the results of the palynological biofacies study from the first phase of the project (Phase1) the organic matter type can be linked to specific depositional environments, helping the conditions and high-potential zones to be better identified (e.g. for biosteering).

The second stage of the Sweet Spot project Phase 2 is based on the hypothesis formulated in the project's Phase 1. It is designed to both test the hypothesis and gain insight into sweet spots in the Dutch on- and offshore. Comparison of the geochemical data from the Whitby Shale (UK) to the Posidonia shale in the Netherlands will give insights into the correlation and extrapolation potential of sweetspots basin-wide. In this respect it is important to understand the regional versus basin-wide paleoenvironmental setting. Extending the dataset towards the deeper zones of the NWGB using offshore wells from the Netherlands, gives us more control in the lateral extent of the prolific shales and also further increases our understanding on the play. This project integrates and discusses large scale controlling parameters such as the influence of the Boreal Realm, the change to multi-basinal patterns and terrestrial inputs from structural highs.

Using all data, interpretations, correlations and hypotheses from both the first and second phase of the Sweet Spot project, we aim to translate the Posidonia Shale Formation's specific characteristics and properties to more generalized concepts concerning shale plays. For this analogy, several proven shale gas plays are cross referenced based on published data and data provided by the Sweet Spot's project industrial partners. Not only is this translation of concepts of importance for shale occurrences from different geographical locations, but ii can also act as an introduction for future research on under explored shale play intervals in the Dutch subsurface.

1.1.2 Geological description (modified from the SSI1 report)

The Toarcian Posidonia Shale Formation is part of a very distinctive global stratigraphic interval with a present-day distribution from central to northwestern Europe, comprising the surface and subsurface of the U.K. (Mulgrave Shale Member), Germany (Posidonienschiefer, or Ölschiefer, Figure 3) and France (Schistes Carton). Given the relatively uniform lithological characters (dark-grey to brownish-black, bituminous, fissile claystones and siltstones) and thickness (mostly around 30-60 m) across these basins, it is commonly suggested that the deposition of the Posidonia Shale took place over a large oceanic domain during a period of high eustatic level, restricted circulation in the water column and relative tectonic quiescence. The present-day distribution of these stratigraphic units was probably controlled by erosion at basin margins and non-deposition over bounding paleotopographic highs (Pletsch et al., 2010). The official Dutch nomenclature (Van Adrichem Boogaert and Kouwe, 1993-1997) describes the Posidonia Shale Formation as deposited in a low-energy pelagic environment under oxygen-deficient conditions, partly controlled by a eustatic phase of high sea level; however, recent research suggests that this simplistic process and environmental framework should be reconsidered (e.g. Ghadeer and Macquaker, 2011; Trabucho-Alexandre et al., 2012).

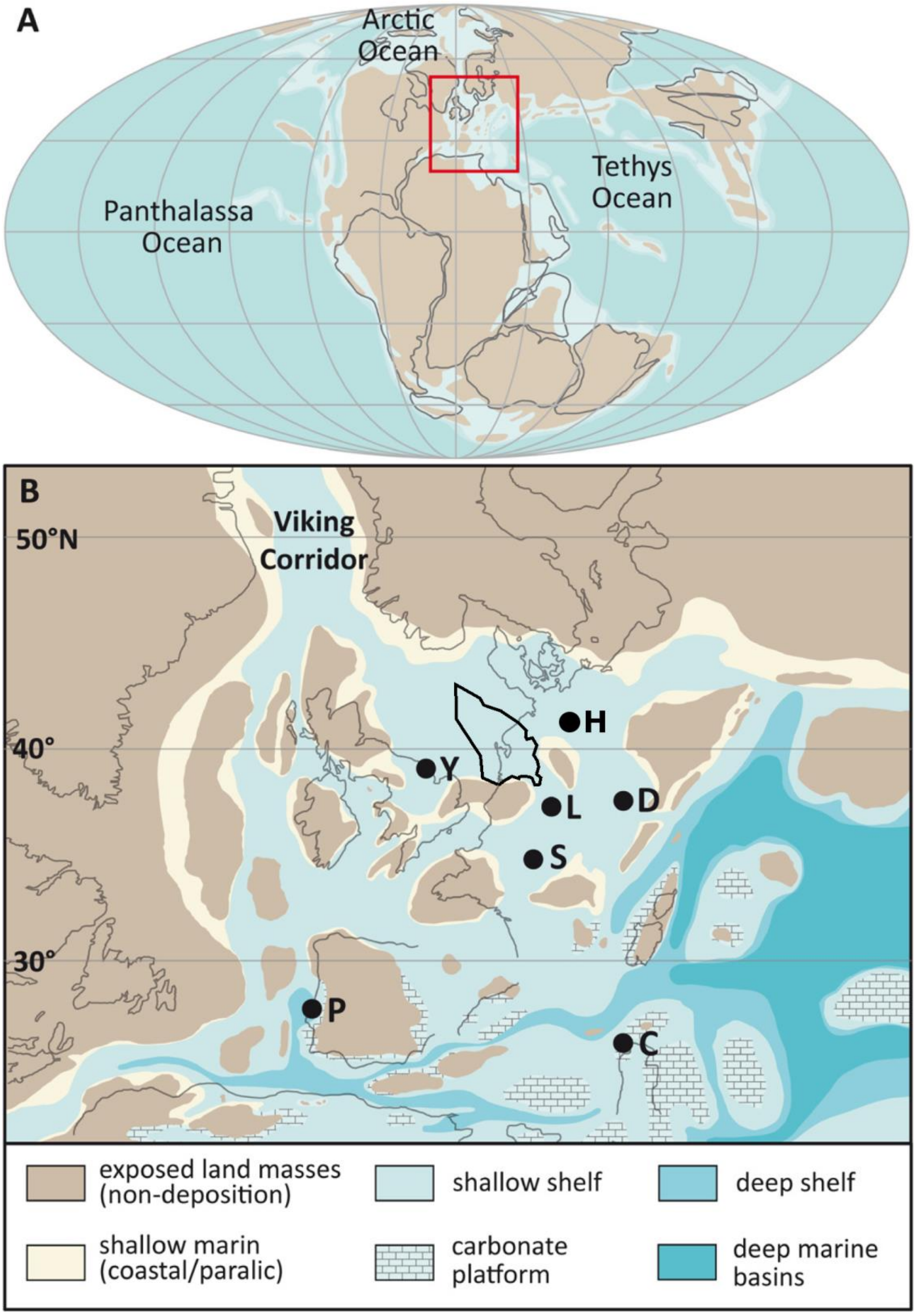

Figure 1-1 Paleogeographic setting during the Toarcian with location of the study areas (modified after Ruebsam et al., 2014). Y: Yorkshire/Whitby, UK, H: Hils syncline, Germany, L: Lorraine Sub-Basin, Luxembourg, D: Dotternhausen, Germany, S: Sancerre, France, P: Peniche, Portugal, C: Colle di Sogno, Italy

In the Netherlands, the formation is restricted to the axes of Late Jurassic rift basins (West Netherlands Basin and its extension into the Roer Valley Graben, the Central Netherlands Basin, and isolated locations in the Lower Saxony Basin in the onshore and Broad Fourteens Basin and Dutch Central Graben in the offshore, Figure 1-2). The common view is that the sediments deposited outside the basin centres were locally eroded in parts of the Netherlands due to inversion events (Wong et al., 2007), although this hypothesis is debated following observations of syn-sedimentary tectonics in the Early Jurassic. The Posidonia Shale Formation conformably overlies the non-bituminous claystones of the Lower Jurassic Aalburg Formation, although bituminous intervals have been identified also in the Aalburg Formation (De Jager et al., 1996), and it is conformably overlain by non-bituminous clay- and siltstones of the Middle Jurassic Werkendam Formation (Van Adrichem Boogaert and Kouwe 1993-1997; TNO-NITG, 2004), although hiatuses and unconfomities were identified at several locations.

The Posidonia Shale Formation consists of dark-grey to brownish-black bituminous fissile claystones and forms a very distinctive interval throughout the subsurface of the Netherlands. It isrecognizable by its high gamma ray and resistivity readings on wire-line logs (Van Adrichem Boogaert and Kouwe, 1993-1997). Evaluation of wireline log responses showed that subdivisions can be made into distinct zones within the Posidonia Shale Formation, which are correlatable between wells throughout the basin (see chapter 2.6). A similar vertical zonation of the Posidonia Shale Formation is observed also in Germany (locally referred as the Posidonienschiefer Formation) on the basis of both geochemical and sedimentological parameters (e.g. Röhl et al., 2001; Frimmel et al., 2004; Schwark and Frimmel, 2004).

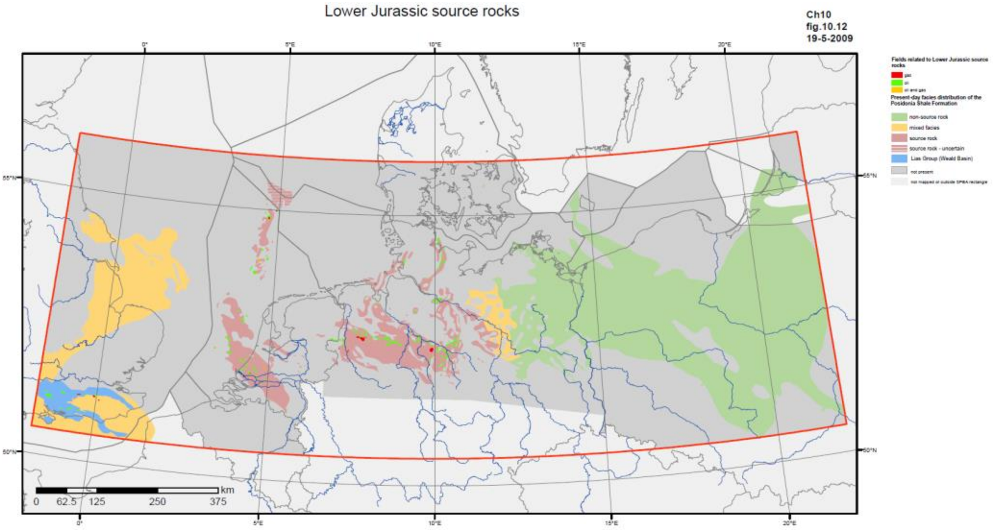

Figure 1-2 Source rock facies map of the Posidonia Shale Formation and its equivalents (Doornenbal and Stevenson, 2010)

1.2 Localities

1.2.1 *Runswick Bay – Cleveland Basin*

For Phase 2 of the Sweet Spot project, the samples collected in Runswick Bay in the Whitby Mudstone Formation (UK) were revisited. The results from Phase 1 this project were used for integration and interpretation together with the new samples analysed from the Netherlands. Furthermore XRD measurements were made on a number of samples and used to calibrate the XRF and ICP-MS analyses from Phase 1. A detailed description of the geology and sedimentary evolution of the area is given in the report of phase 1.

Figure 1-3 Locality of the sampling location in Runswick Bay in the Cleveland Basin (north is down)

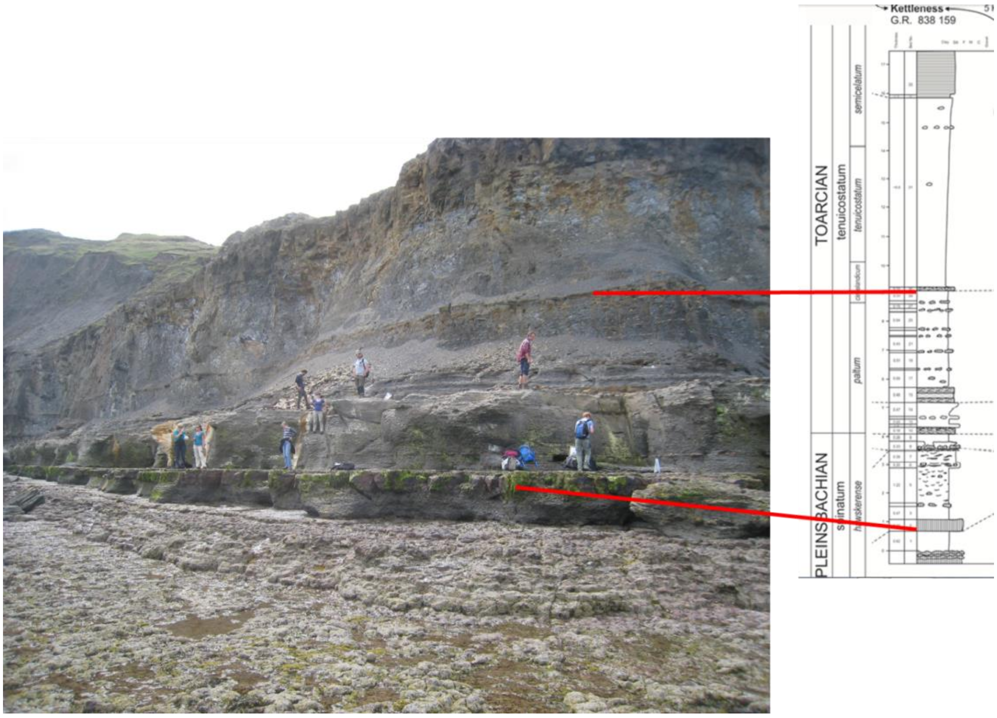

Figure 1-4 Outcrop photo of the studied section at the locality of Kettleness, East of Runswick Bay. Stratigraphic column shown to the right (Field notes handout).

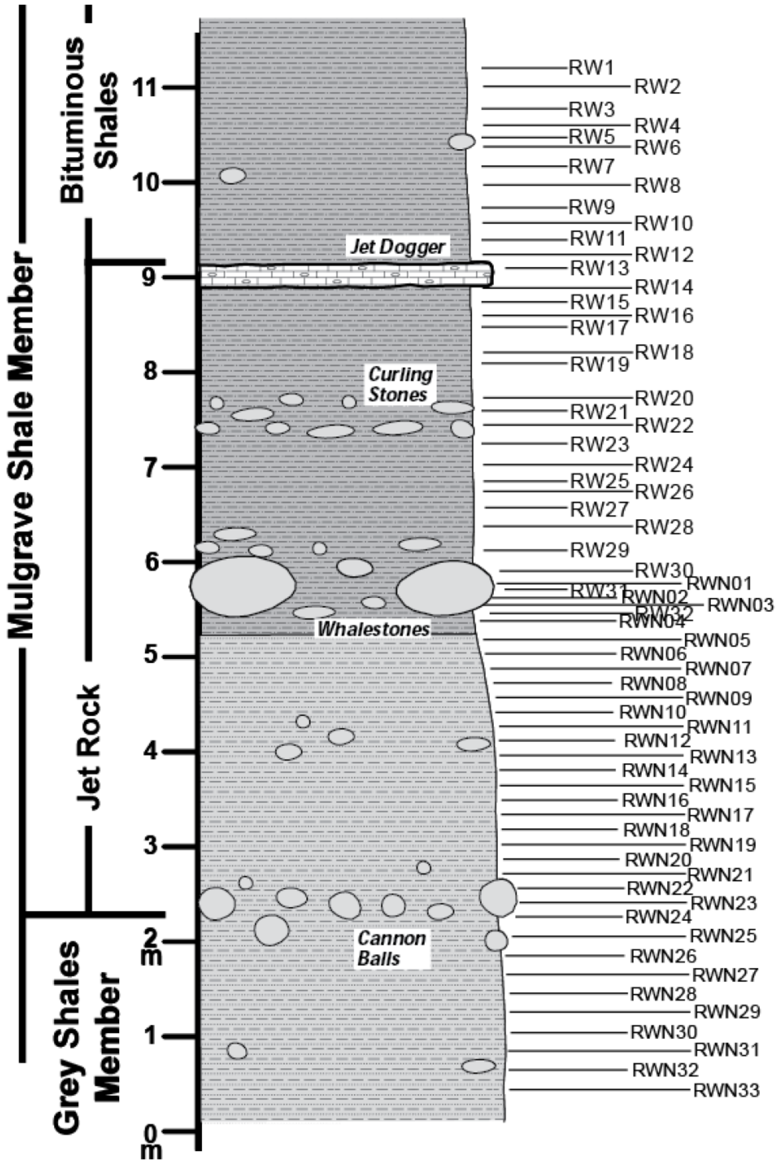

Figure 1-5 Stratigraphic section showing the vertical position of the samples taken for Phase 1 of the project along the Whitby outcrop.

1.2.2 *The Netherlands*

In order to achieve a wider spread of information, two wells in the Dutch onshore and offshore (F11-01 and RWK-01) were selected in addition to the already studied well LOZ-01. These wells were chosen for the availability of sample material in the Posidonia Shale Formation as well as for their location. Additional analyses were available for well L05-04.

For the log correlation and mapping exercise all wells in the Dutch offshore that penetrated the Posidonia Shale Formation and had good quality digital logs available were selected. For a complete list of wells see Appendix A.

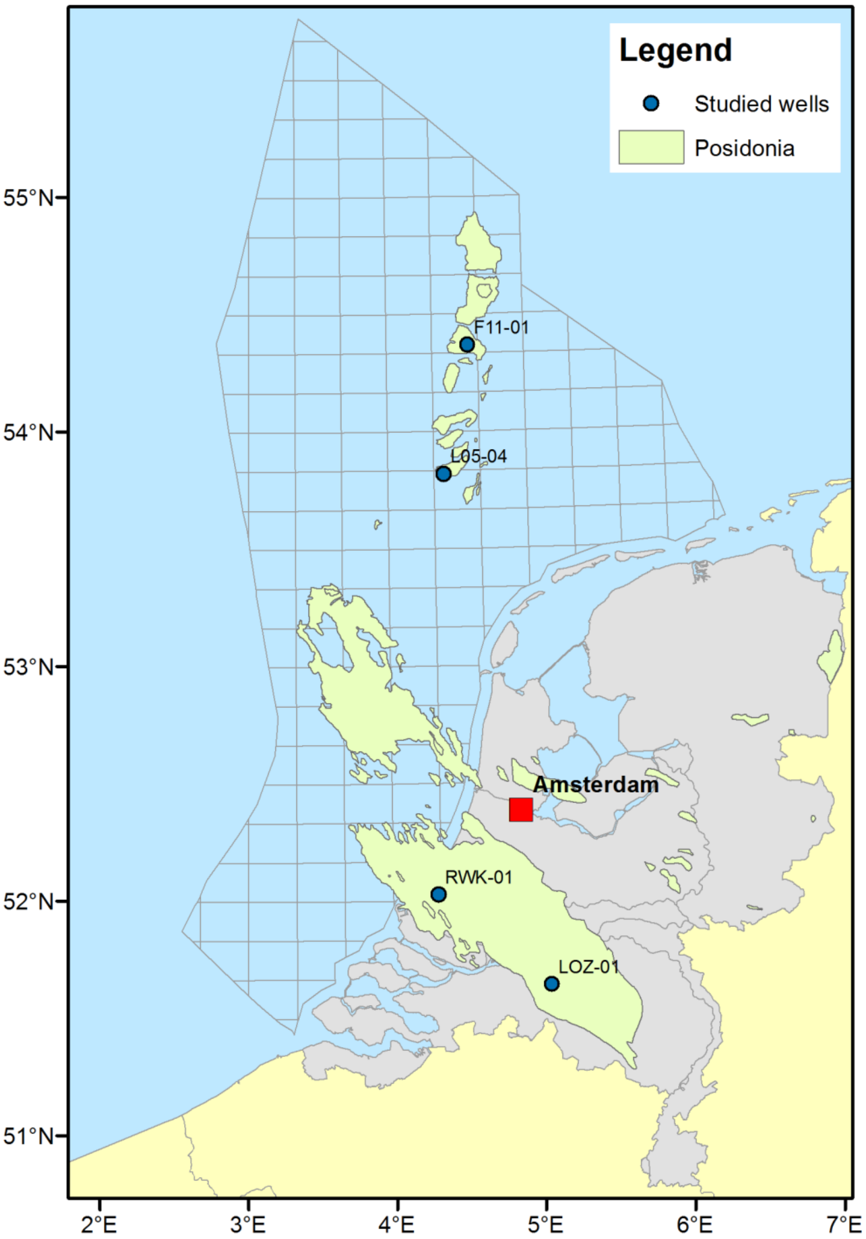

Figure 1-6 Distribution of the Posidonia Shale Formation in the Netherlands and location of the studied wells

1.2.3 *Germany*

The Posidonia Shale Formation equivalent in Germany is referred as the Posidonien Schiefer or Lias ε, and is present in the North German Lower Saxony Basin, the Rhine Graben and the Molasse Basin in the south (Figure 1-7). In several locations the formation is cropping out or is very close to the surface, such as in the area of the Hils Syncline in the Lower Saxony Basin (including in the study). Six shallow research wells were drilled in the Hils Syncline, that cover a maturity sequence from very immature in well Wenzen (0.48 %Ro) to overmature in well Haddensen (1.45 %Ro, Mann and Müller, 1987).

Figure 1-7 Distribution map of the Posidonienschiefer in Germany (from Andruleit et al., 2012), the striped areas are regions that were deemed interesting for shale gas exploration

The wells of the Hils Syncline have been intensely studied in the past (e.g., Mann et al., 1985; Mann and Müller, 1987; Littke et al., 1988, 1991; Rullkötter et al., 1988; Leythaeuser et al., 1988). Published and unpublished well logs were used to extend the log correlation used in this study into Germany (Mann and Müller (1987) and internal confidential report of the FZ Jülich).

1.2.4 *Luxemburg*

The Posidonia Shale equivalent in Luxembourg are the Schistes Bitumineux. They are found on the eastern margin of the Paris Basin. Samples from a shallow well (FR-210-006) in Esch-Alzette in Luxembourg were analysed for organofacies and elemental composition in the context of the PhD thesis of Jinli Song and the results are published as Song et al. (2014). In the context of this study the samples were analysed for $\delta^{13}C$ to be able to include the results into the same stratigraphic framework.

2 Section 2 – Data

During the course of this project, samples from several different locations were analysed using different methods. In this section the methods and results of these analyses are described.

Table 2-1 Number of samples of each location analysed in the context of this study

	Total no. samples	Major and trace elements	Paly-nology	Fe-Speci-ation	TOC	$\delta^{13}C$	XRD	SEM	TS
Rijswijk	64	50	50	30	30	30	5	10	10
F11-1	30	30	30	28	30	30	4	n/a	n/a
Whitby	SSI1	SSI1	SSI1	30	done	avail.	10	n/a	n/a
Total	**94**	**80**	**80**	**88**	**60**	**60**	**19**	**10**	**10**

2.1 Stable carbon isotopes

In the context of the Sweet Spot Identification projects 1 and 2 several stable carbon isotope analyses of organic matter were measured on several different locations (LOZ-01, F11-01, L05-04, RWK-01, Luxembourg) and were correlated to previously measured or published results (AND-06, WED-01, Whitby (Hesselbo et al., 2000; Kemp et al., 2005), Dotternhausen (Röhl et al., 2001)

2.1.1 Methods

The technique used for isotope analysis was the Elemental Analyser - Isotope Ratio Mass Spectrometry (EA-IRMS). For this technique, samples and reference materials are weighed into tin capsules, sealed and then loaded into an automatic sampler on a Europa Scientific Roboprep-CN sample preparation module. From there, they were dropped into a furnace held at 1000 °C and combusted in the presence of oxygen. The tin capsules flash combust, raising their temperature in the region of the sample to ~1700 °C. The combusted gases are swept in a helium stream over a combustion catalyst (Cr_2O_3), copper oxide wires (to oxidize hydrocarbons) and silver wool to remove sulphur and halides. The resultant gases (N_2, NOx, H_2O, O_2, and CO_2) are swept through a reduction stage of pure copper wires held at 600 °C. This removes any oxygen and converts NOx species to N_2. A magnesium perchlorate chemical trap removes water. Carbon dioxide is separated from nitrogen by a packed column gas chromatograph held at an isothermal temperature of 100 °C. The resultant CO_2 chromatographic peak enters the ion source of the Europa Scientific 20-20 IRMS where it is ionised and accelerated. Gas species of different mass are separated in a magnetic field then simultaneously measured using a Faraday cup collector array to measure the isotopomers of CO_2 at m/z 44, 45, and 46. Both references and samples are converted and analysed in this manner. The analysis proceeds in a batch process, whereby a reference is analysed followed by a number of samples and then another reference.

2.1.2 *Results*

All measured stable carbon isotope curves show the same typical negative isotope excursion for the lower Toarcian. These curves were correlated by calculating a relative depth, The relative depth was calculated by the following formula:

$$\text{Relative depth (RD)} = (MD\_S_x - MD\_S_{x-1}) * F + RD\_S_{x-1}$$

Equation 2-1 Equation used to calculate the relative depth for the isotope correlation. MD_S_x: measured depth of the sample for which the relative depth is calculated, MD_S_{x-1}: measured depth of the sample stratigraphically below S_x, F: factor applied to the thickness (see Table 2-2), RD_S_{x-1}: relative depth of the sample stratigraphically below S_x

In this study depth was calculated relative to well F11-01, which served as a reference point. For all other locations the thickness of the intervals was adjusted until the curves were correlated. The relative adjustments to the thickness of the intervals is shown in Table 2-2. The resulting correlation can be seen in Appendix H.

Table 2-2 Factor F applied to the thickness of the different intervals to calculate the relative depth of the different correlated locations based on the fitting of the stable isotope curve

	F11-01	L05-04	Rijswijk	LOZ-01	Whitby	Dottern-hausen	Luxem-bourg
T1	1	1		1	1	2 - 8	
T2	1	1	1	1	1.2 - 1.9	3.5	1.3
T3	1	1	0.8	0.65	1.8	3.5	2
T4			0.8	0.65	1.8	3 - 4	0.6
T5			0.8	0.65	1.2 - 0.55	2	0.5
T6				0.65	0.55		

2.2 Fe-speciation, XRF and ICP-MS

2.2.1 Methodology

The Fe-speciation analyses were performed at TNO. Four Fe fractions were determined using a sequential extraction scheme described by Poulton & Canfield (2005).

1) Fe-carbonate: mainly ankerite and siderite
2) Fe-oxides and hydroxides: mainly hematite, goethite and ferrihydrite
3) Fe-magnetite
4) Fe-pyrite

For the extraction 0.1 g of sample powder was used in 10 ml of extraction fluid. First, the Fe-carbonates were extracted using a 1 M solution of sodium acetate, adjusted to a pH of 4.5. The samples were placed in a heated shaker at 50 °C during a 48 hour extraction. Iron oxides were extracted in a 2 hour extraction at room temperature using a solution of 50 g/L sodium dithionite and buffered to a pH of 4.8 with 0.35 M acetic acid and 0.2 M sodium citrate. The third step Fe-magnetite fraction was extracted with 0.2 M ammonium oxalate and 0.17 M oxalic acid solution for 6 hour at room temperature. The final step consisted of extracting the Fe-pyrite using concentrated nitric acid in a 2 hour extraction at room temperature. The iron concentrations in the extraction fluids were determined using photo spectroscopy. A 2:1 solution of 4 M NH4-acetate/14.4 M acetic acid and 1 g/L phenanthroline/2% (v/v) concentrated HCl was used. Hydroxyl-ammonium-chloride in 2% concentrated HCl was used as reducing agent. Absorbance was measured at a wavelength of 510 nm.

For samples from F11-01 and RWK-01 total organic carbon and element compositions were measured at Chemostrat, UK. Major element compositions were measured using XRF and trace element compositions were measured on the ICP-MS. For Runswick Bay element data is taken from the Sweetspot Phase 1 study.

2.2.1.1 REDOX ENVIRONMENT

Organic material is preferentially preserved in anoxic conditions. The development of anoxic conditions in the Tethyan epicontinental sea in the Toarcian is thought to be related with intense freshwater runoff during the early Toarcian warm climatic conditions that led to the development of a pycnocline (e.g. Bailey, 2003). A pycnocline (= chemocline) is a salinity stratification of the water column with less saline water at the top and more saline water at the bottom. The pycnocline restricts mixing between the top and bottom water layers and leads to oxygen depletion in the bottom water layer. One main factor driving oxygen depletion is the decay of ascending organic matter. Organic matter becomes oxidised under oxic conditions and thus consumes oxygen. High primary productivity can enhance or even be the sole cause for anoxic conditions.

Fe-speciation

The behaviour of reactive iron minerals during transport, deposition and diagenesis in marine sediments is well constrained (Canfield, 1989; Canfield et al., 1992; Poulton et al., 2004; Raiswell and Canfield, 1998; Poulton and Raiswell, 2002; Poulton and Canfield, 2011), and the careful application of improved techniques (Poulton and Canfield, 2005) can provide detailed insights into local palaeoredox conditions. The proxy is based on the presence or absence of enrichments in (bio)geochemically available Fe minerals (termed highly reactive Fe; FeHR) in marine sediments, including ferric oxides, Fe carbonates, magnetite and pyrite. Ratios of highly reactive Fe to total Fe (FeHR/FeT) that exceed 0.38, provide strong evidence for anoxic depositional conditions (Figure 2-1). Providing FeHR/FeT is > 0.38, the extent of pyritisation of the highly reactive Fe pool (FeP/FeHR) defines whether the bottom water was anoxic and ferruginous (Fe-rich) or euxinic (containing H_2S). Although a threshold of 0.8 was originally set as the upper limit for ferruginous conditions (Anderson and Raiswell, 2004), this was based on an older extraction scheme for evaluating FeHR, and values of about 0.7 and above are now considered likely to indicate bottom water euxinia, while lower values reflect ferruginous water column conditions (März et al., 2008; Poulton and Canfield, 2011). It is possible for FeP/FeHR to indicate sulfidic conditions but FeHR/FeT to indicate oxic to dysoxic consitions. In this case the sulfate reduction, that produces H_2S, is occurring close to but below the sediment/water interface.

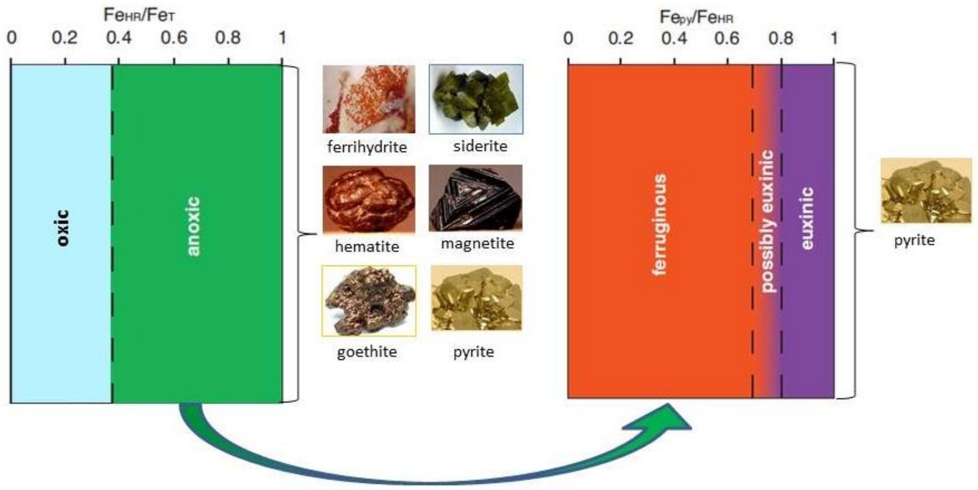

Figure 2-1 Fe-speciation relationship to bottom water redox conditions (modified after Poulton and Canfield, 2011).

Redox sensitive elements

Under oxic water column conditions redox sensitive elements such as Mo, U, V, and Cr are not extensively enriched in deposited sediments, with the result that concentrations are generally close to the terrestrial input values (Brumsack and Gieskers, 1983; Algeo, 2004; Tribovillard et al., 2006). Under anoxic to sulfidic conditions, a change in the charge and/or speciation of the redox sensitive elements promotes a decrease in their solubility, allowing authigenic enrichment to varying degrees (dependent on the particular element and the availability of sulphide). Uranium is sequestered into organic rich sediments under suboxic to anoxic conditions due to reduction of soluble U_6^+ to more immobile U_4^+ (Klinkhammer & Palmer, 1991; Dunk et al., 2002; Tribovillard et al., 2006; Partin et al., 2013), a process that does not require the presence of dissolved sulfide (Anderson et al., 1989; Barnes and Cochran, 1993). Vanadium is similarly enriched in anoxic sediments due to formation of vanadyl ions (VO_2^-), which are readily adsorbed to the substrate or form organometallic ligands (Emerson and Huestead, 1991; Morford and Emmerson, 1999). However, further sedimentary enrichment may occur in the presence of H_2S as V_4^+ is reduced to V_3^+ and precipitated as a (hydr)oxide or taken up by geoporphyrins (Breit and Wanty, 1991; Wanty and

Goldhaber, 1992; März et al., 2008). Molybdenum is the most sensitive of these elements to dissolved sulfide availability, and shows enhanced to near-quantitative removal from solution under highly euxinic conditions (Zheng et al., 2000, Helz et al., 2004, Algeo and Lyons, 2006, Algeo and Tribovillard, 2009).

TOC/P

A further redox indicator is the total organic carbon over phosphorous ratio. Phosphorous is delivered to the ocean via riverine input. It is the main nutrient for marine organisms and is therefore largely present in biomass. When organic biomass passes an oxic water column it is mostly oxidised thus releasing organic carbon (as CO_2) and P. While carbon dioxide escapes, the greater portion of P is trapped as fourapatite or sorbed and fixed to Fe-(oxyhydr)oxides. Under anoxic conditions the majority of organic matter is not remineralised and both TOC and P remain in the sediment. In conclusion, TOC/P ratios are higher in anoxic conditions and lower in oxic conditions (Figure 2-2). This relationship is however not straight forwards, as the carbon/phosphorous ratio is also governed by the type of organism. Lipid poor phytoplankton (e.g. coccolithophorids and cyanobacteria) have a lower C/P ratios than lipid-rich organisms (e.g. diatoms). Furthermore, burial diagenesis results in a differential loss of C to P. TOC/P ≥ 50, expressed in molar concentration (mol organic carbon/mol P) is thought to reflect anoxic conditions (Algeo & Ignall, 2007).

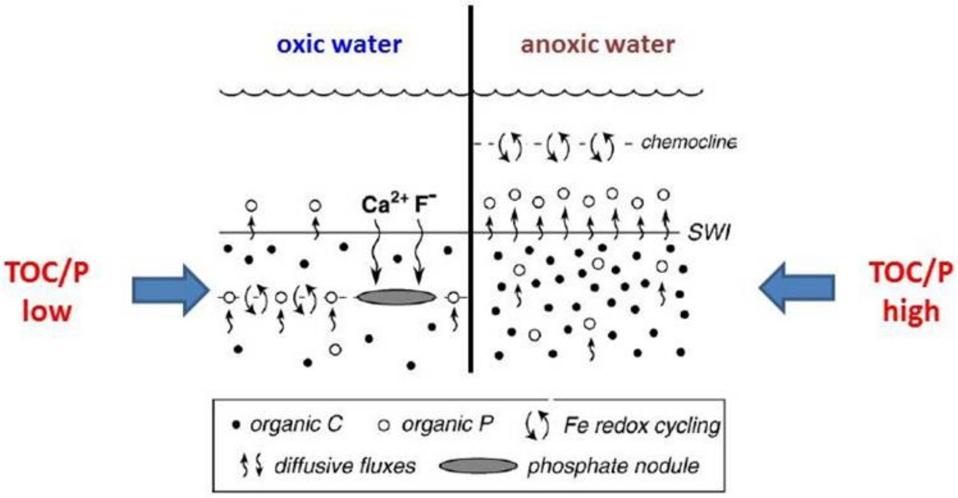

Figure 2-2 Behaviour of organic matter and phorphorous in oxic and anoxic water. SWI = sediment-water interface (modified after Algeo and Ingall, 2007).

2.2.2 Results

2.2.2.1 Runswick Bay

Throughout the analysed section at Runswick Bay, Fe-speciation points to persistent anoxic bottom water conditions, with FeHR/FeT > 0.38 (Figure 2-3). Short-lived oxic intervals at seasonal or yearly cannot be resolved as our analyses of Fe-speciation covers ca. 1 to 2 cm intervals of sediment, with a resolution of roughly 2 cm per ky. Interestingly the indicator for sulphidic conditions (FeP/FeHR) is mostly at or above the threshold to euxinic conditions, indicating that hydrogen sulphide was present in bottom waters, albeit not permanently.

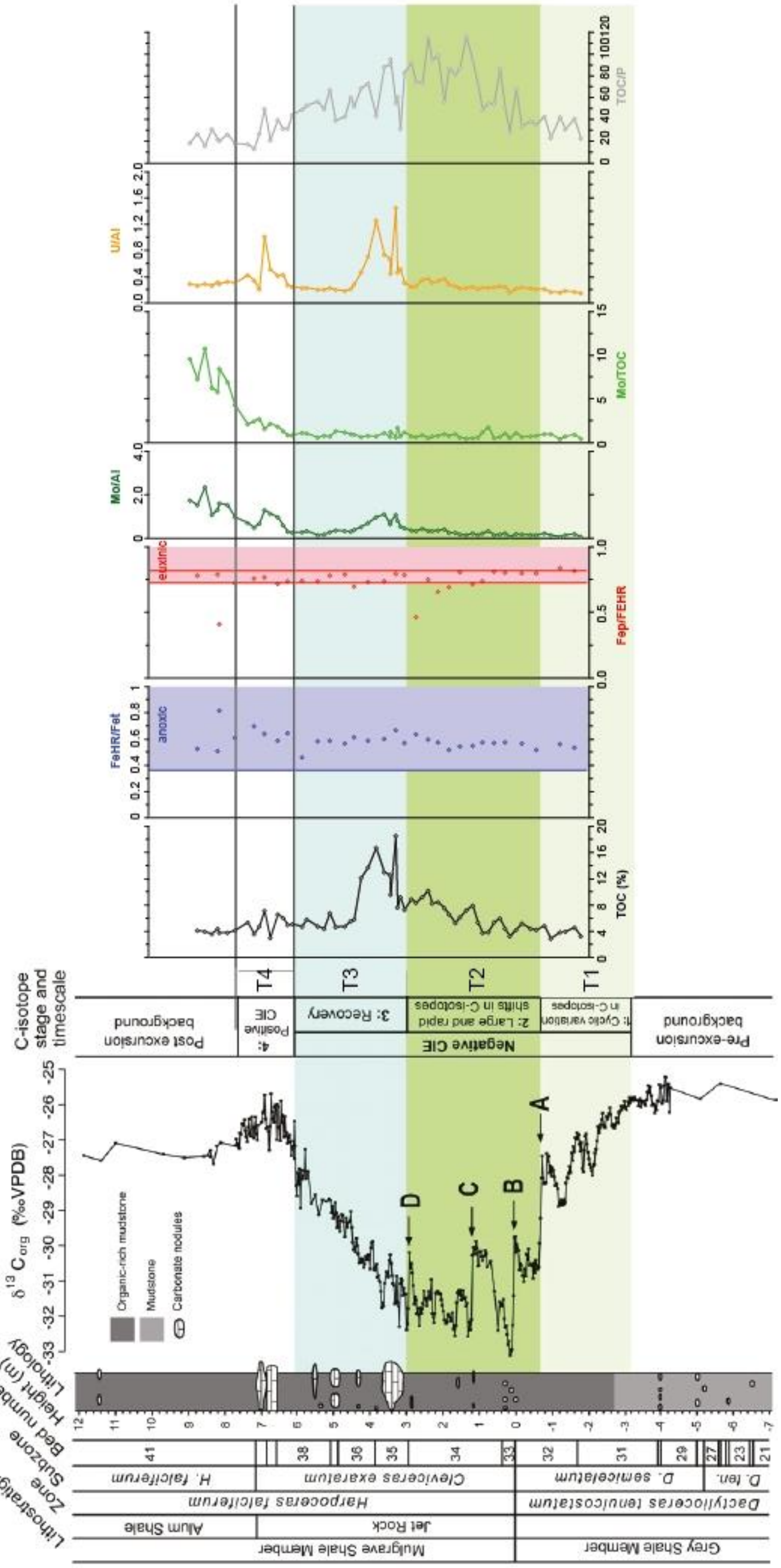

Figure 2-3 Redox proxies Runswick.

TOC/P increases significantly from the Grey Shales towards the Jet Rock and decreases again towards the Bituminous Shales. TOC/P is ≥ 50, except in the Bituminous Shale unit, where TOC/P falls partially below 50. The anoxic conditions are consistent with the Fe-speciation results. TOC/P indicates a temporal trend in the degree of anoxia, with a peak between ca. 0 and 3 m (T2). The post decrease in TOC/P is most likely related to a change in phytoplankton type (possible increase in lipid poor species).

The redox sensitive trace elements were normalised to Al in order to remove influence of differential sedimentation. The high TOC peak (around 4m above Jet Rock) corresponds with U/Al, V/Al and Mo/Al peaks, referring either to the affinity of these elements towards organic matter and/or to enhanced anoxic conditions. Mo/Al shows less enrichment than U and V and generally increases towards the top of the section. Considering that Mo is a stronger redox indicator and the fact that Fe-speciation indicates continuously anoxic and possibly euxinic conditions, we conclude that the peaks are driven by organic matter affinity.

In summary, the bottom water redox conditions do not change throughout the studied period and there is also no relation to TOC. On the contrary, the palynology shows quite a variation in the fauna, which is related to changes in the upper part of the water column. The conclusion for Runswick Bay is that within the studied interval the amount of TOC is entirely related to surface productivity.

2.2.2.2 F11-01

Similar to the Runswisk Bay setting, Fe-speciation at the F11-01 site indicates anoxic bottom water conditions throughout the studies section. Below ~2664m (T1) FeP/FeHR is below 0.7, indicating non-sulfidic conditions (Figure 2-4). With some fluctuation FeP/FeHR increases and indicates sulfidic bottom water conditions at the top of the section (T2 and T3). TOC/P increases from below 50 to above 200 in T1 and remains high. The trend towards higher concentrations can also be seen in the redox sensitive elements (Mo, U and V). This corresponds with a contemporaneous increase in TOC. Although the redox sensitive trace elements are strongly connected to organic matter content, the sum of the geochemical parameters points to an increase in the water column anoxia and euxinia within the Posidonia Shale Formation. In a recent publication by Trabucho-Alexandre et al. (2012) pyrite framboid sizes were analysed. An average framboid size below 6 nm and a narrow size distribution indicates sulfidic conditions above the sediment water column (Wignal & Newton, 1998). Pyrite framboid size decrease from 6 nm to ~4nm within the Posidonia formation. The pyrite size distribution also narrows during T2 indicating sulfidic water column conditions. This is consistent with the other redox indicators.

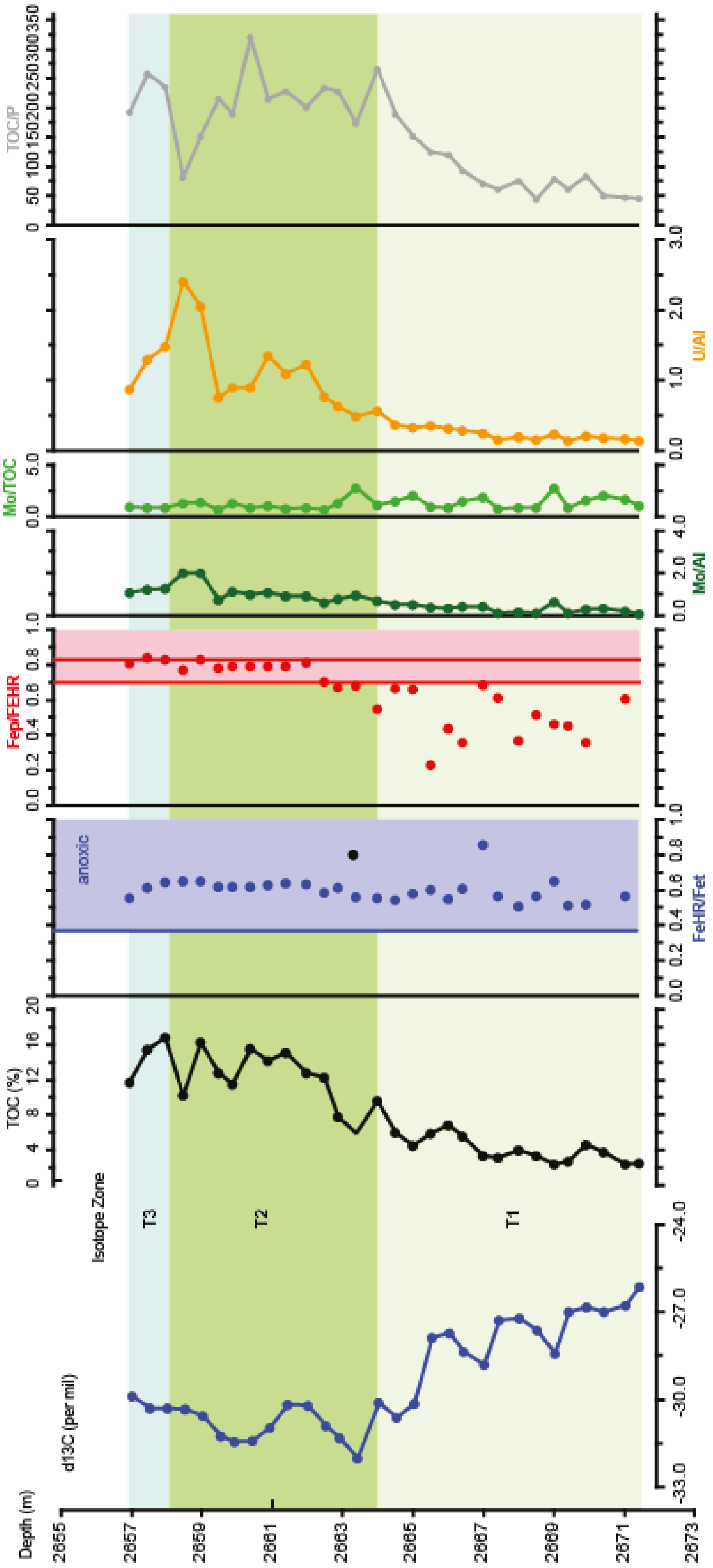

Figure 2-4 Redox proxies F11-1

Although we have not generated any data for L05-04, Trabucho-Alexandre et al. (2012) record a clear decrease in pyrite framboid size (from 10nm to 4nm) and in size distribution from the Aalburg and into the Posidonia formation. This points to similar redox conditions for L05-04 as in F11-01.

2.2.2.3 *RWK-01*

Fe-speciation and TOC/P in the Aalburg Formation samples shows dyoxic to fully oxic bottom water conditions. Redox sensitive trace elements remain low.

During deposition of the Posidonia Formation FeHR/FeT indicates anoxic bottom water (similar to F11-01). During T2 and lower T3 FeP/FeHR is variable but indicates a change from ferruginous to sulfidic bottom water. TOC/P increases through T2 and remains well above the anoxic threshold up until T5. The top part of the Posidinia formation sulfidic conditions prevail mostly. As in previous sections U/Al and V/Al follow the TOC trend. Mo/Al has some relation to TOC but shows a strong increase during T4 and T5. A decline in TOC/P as well as Mo/Al occurs during T6. TOC/P may also be influenced by the type of organic matter, however a deepening of the chemocline towards the sediment water interface is more likely.

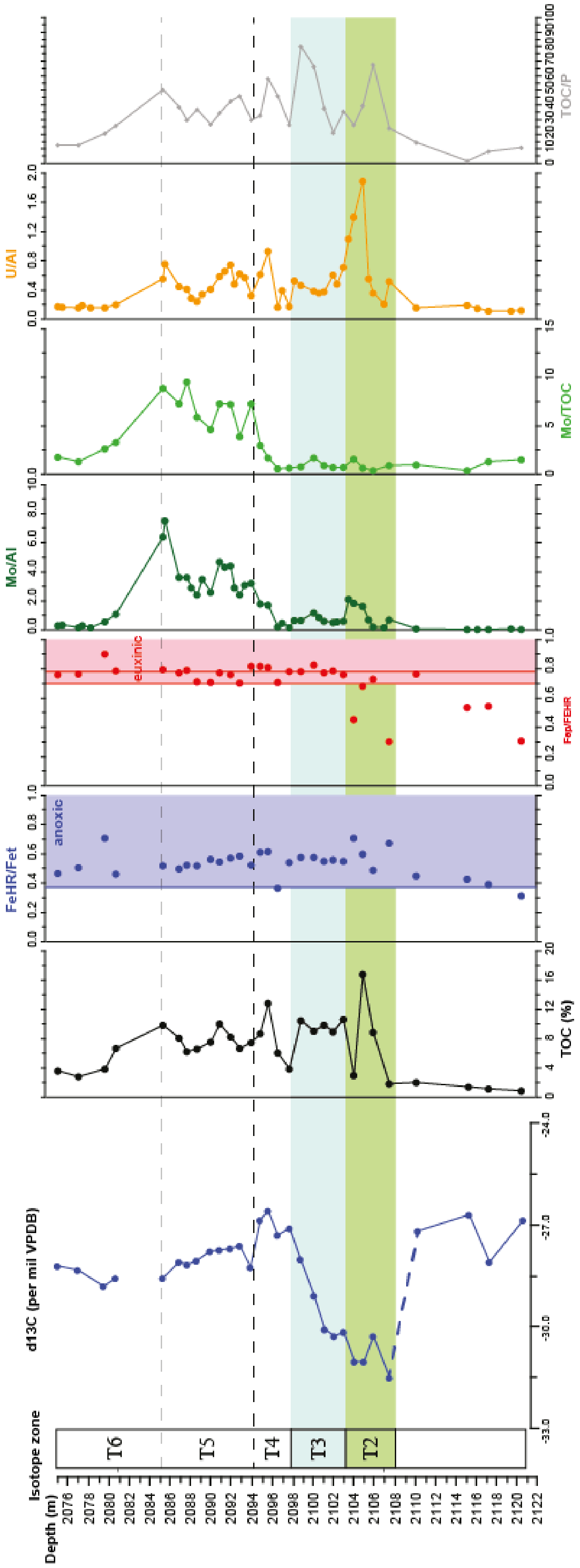

Figure 2-5 Redox proxies RWK-1

2.2.3 Synthesis

2.2.3.1 Redox variation across the basin

The bottom water redox conditions are relatively similar in all studied sections (predominantly anoxic). Sulfidic water conditions mostly fluctuate from below to above the sediment-water interface in Runswick. RWK-01, F11-1 and probably L05-04 have a very similar redox environment, with a change from non-sulfidic in T1 to sulphidic conditions around T2. This is connected to an upward movement of the chemocline, which at times reached the photic zone. Although conditions were similar across the basin, the F11-01 section shows a stronger sulfidic signal in the top part of the section (up to bottom of T3). The sections was not cored above T3, which makes interpretation above this level difficult.

2.2.3.2 Water mass restriction

From T1 to T3 Mo and U concentrations are relatively low despite favourable conditions for redox-sensitive trace element deposition. This is commonly explained by strong element drawdown under prolonged anoxic conditions without replenishment. These element depletion have been postulated to be worldwide, due to widespread anoxia (e.g. Pearce et al., 2008). An alternative theory postulates that the element depletion and anoxia was local due to basinal water mass restriction and poor exchange with the global ocean (McArthur et al., 2008).

In zones T4 and T5 anoxic conditions still prevail and Mo increases in both Runswick and RWK-01 sections. Similar relations are seen in literature and are explained by stronger water mass mixing and less basinal restriction (Pearce et al., 2008; McArthur et al., 2008). U and V do not follow this increase. This may be related to the strong affiliation of the elements to organic matter, which is generally low in the upper zones.

The relationship between TOC and Mo (in anoxic settings) is thought to reflect the state of water mass restriction (Algeo et al., 2007). Mo is used because it is readily drawn down in anoxic conditions and becomes depleted in the water column in restricted basins such as the Black Sea today. Mo is normalised to TOC because TOC is also enriched in anoxic conditions but is not dependant on water mass restriction. Low Mo/TOC values are apparent in zones 1 to 3 in the three studied sections. This changes to higher values in zones 4 to 6 reflected by a steeper slope between the two parameters (Figure 2-6). A further observation is that in the F11-1 and RWK-01 sections Mo/TOC values are higher in zones 4 to 6 than in the Runswick section. This may be due to a stronger water mass exchange with the open ocean. Another possibility may be stronger Mo influx from the continent.

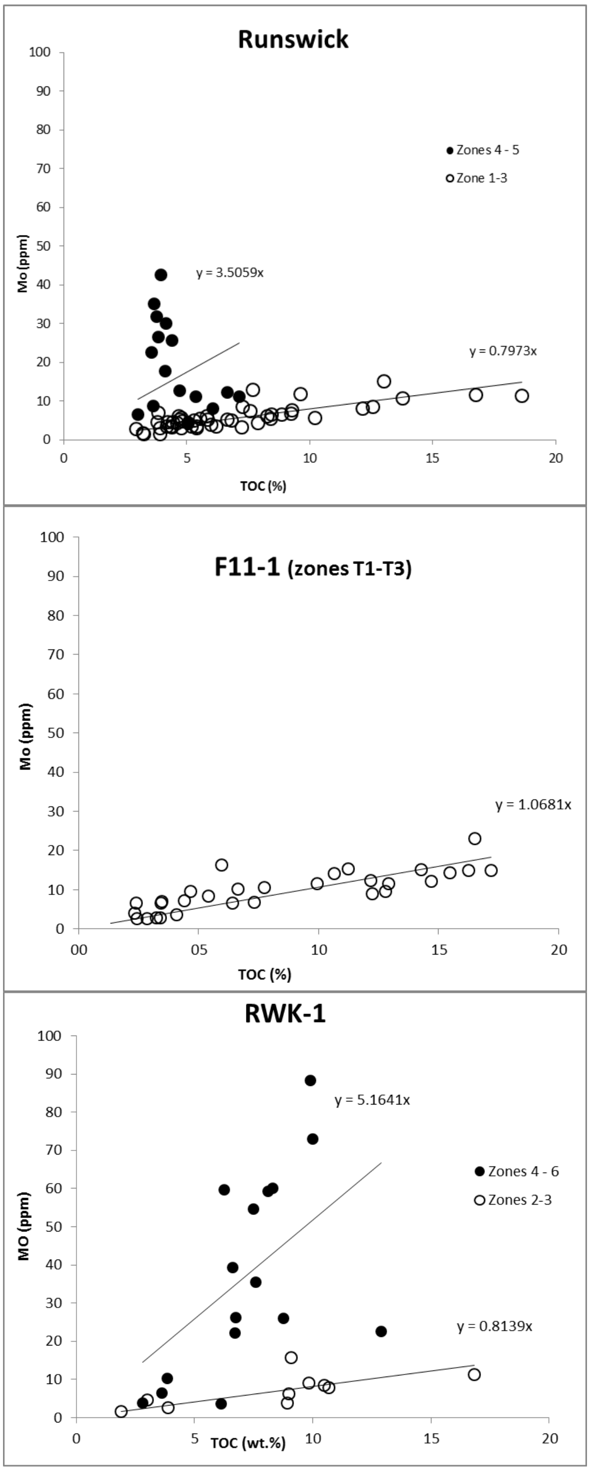

Figure 2-6 Mo (ppm) vs total organic carbon.

2.2.3.3 *Terrestrial influx*

Terrestial influx can be seen in the amount of detrital material, such as detrital clay, quartz and heavy minerals. Authigenic input is mostly reflected by TOC and carbonate content. Influence of terrestrial influx is also evident by the percentage of wood and sporomorphs (see chapter 2.4). Zr can be taken as a proxy for zircon mineral content, as zircon is solely derived from detrital input and not formed in the ocean. The assumption is that there is no change in provenance. In F11-01 (T1 to bottom T3) terrestrial influx does not seem to change much according to Zr. In Runswick Zr also decreases during T1 and T2, remains stable during T3/T4 and shows a slight increase in T5. A higher influence of terrestrial material in the grey shales has been previously reported by French et al. (2014) from biomarker evidence. In RWK-01 Zr increases in the Aalburg Formation, stays relatively stable from T2 to T5 and increases again during T6. Comparing Zr content across sections shows a pretty similar pattern in all (time-equivalent) levels.

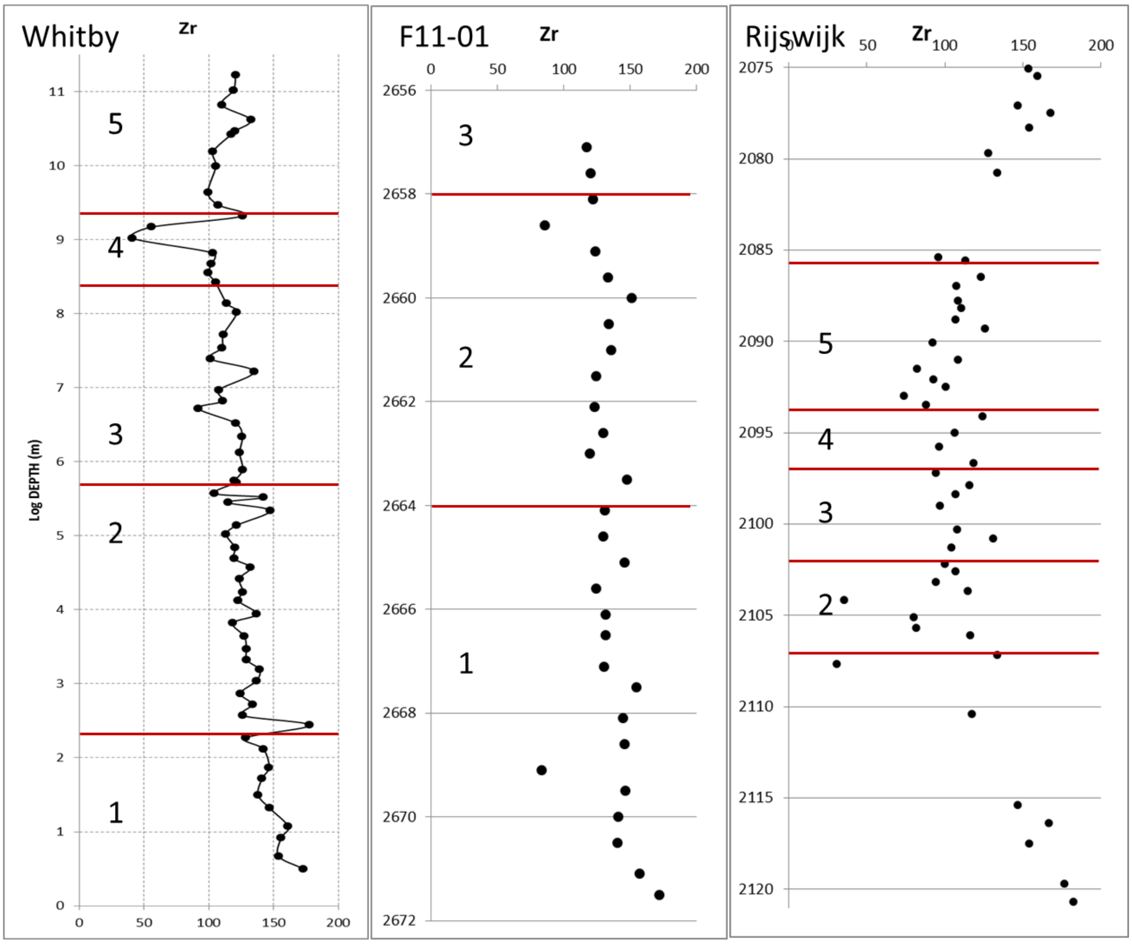

Figure 2-7 Zr mineral content for the locations of Whitby, F11-01 and Rijswijs as derived from ICP-MS

2.3 SEM and EDX chemical mapping

The main research question addressed here is “Can regional trends be identified in primary and secondary carbonate occurrence and in the related porosity and fraccability?”. To understand the carbonate occurrence in the Posidonia Shale data of different sources is integrated. Chemistry (ICP) and mineralogy (XRD) is used to study the total carbonate content of the samples. Microscopy (SEM) is performed on thin-sections to determine the relative timing of carbonate formation and to assess a primary versus secondary nature. Interpretations of primary biogenic carbonate are compared with data from the biostratigraphy. Finally the data will be integrated with correlated log zones to see which regional trends can be identified.

Samples were selected from Rijswijk-01 (RWK) for which suitable core samples were available. This set was complemented with samples from LOZ-01 (LOZ) that were available from previous projects.

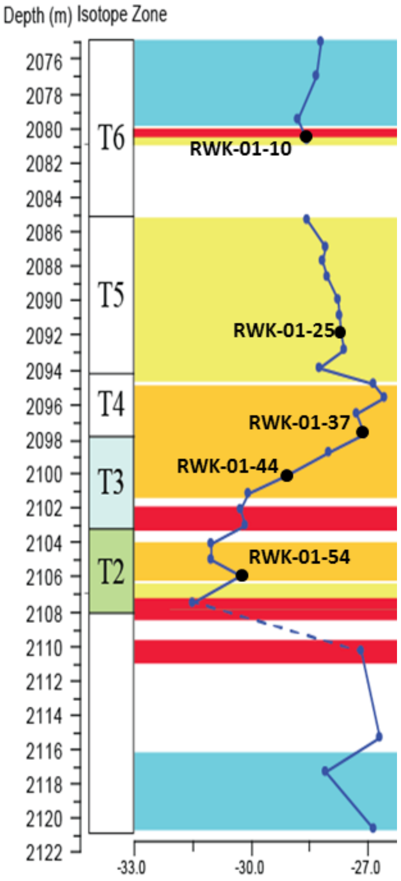

Figure 2-8 Location of the selected samples for well Rijswijk-01

2.3.1 *Methodology*

The mineral content and occurrences are studied with SEM and EDX chemical mapping. An example is given below in Figure 2-9. The SEM image shows the different grey scales of the minerals with pyrite and rutile in white and fossils in light grey (Figure 2-9a). For other minerals the grey tone is more similar and chemical mapping helps distinguishing minerals over an area of the thin section, providing an overview of their distribution in 2D. A 100 times magnification is used for each mapping to aid comparison of different samples. Note that all pictures are taken with the bedding direction vertically. The colours attributed to the chemical maps is also the same for each mapping. Figure 2-9 shows examples of the selected combinations of chemical elements to best distinguish different minerals. Calcium is shown in yellow and magnesium in red resulting in yellow for calcite and orange for dolomite (Figure 2-9b). Aluminium is coloured pink and silica blue giving clay in purple and quartz in blue (Figure 2-9b). Figure 2-9c shows albite in blue green by combining sodium and green and silica in blue. Iron (yellow) and sulphur (red) are also shown in this figure indicating pyrite in orange. Titanium is can be shown to distinguish rutile from pyrite as they are both show white on the BSE image (Figure 2-9d). The fossils also contain phosphor (Figure 2-9e). A higher aluminium intensity in the chemical map in indicates the presence of kaolinite in the illite/smectite clay matrix (Figure 2-9f). Chemical maps are made for different locations in the thin sections to investigate the petrography and the carbonate occurrence in particular.

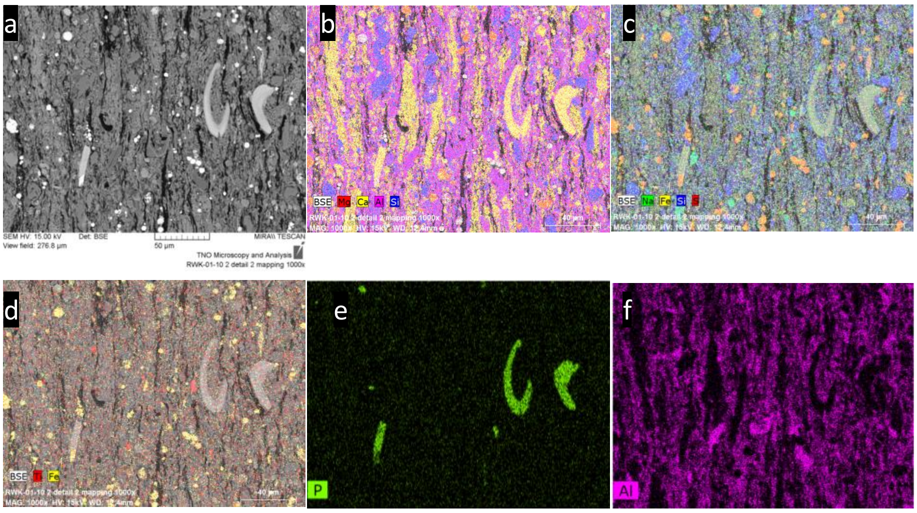

Figure 2-9 BSE view combined with chemical intensity maps indicating the mineral distribution at 1000x magnification (~250 x 200 µm view).

2.3.2 *Results*

2.3.2.1 *General characteristics Posidonia Shale Formation in RWK-01*

The largest particles in the RWK samples are fossil shell fragments which can be up to 1 mm in size and occur in distinct laminations. Dolomite is the second largest component in the RWK shales and can be up to 60 µm large. Note that we always refer to dolomite even through all rims and some cores contain iron and are therefore actually ankerite. Dolomite is generally equally distributed throughout a sample but the total amount varies for the different samples. The grains are subhedral to euhedral and straight crystal faces and rhombohedral shapes are generally observed. Dolomites have a darker magnesium rich core and an iron richer rim. Although some crystals grew adjacent to each other no clear indication of overgrowth was found. Dolomite does occur in a range of sizes but no evidence of multiple phases of dolomite growth was found. Pyrite crystallizes within the shale as generally less than 10 µm sized framboids but some larger single crystals were observed. Pyrite can occur as inclusion in dolomite indicating early diagenetic growth. The detrital grains are dominantly quartz with minor albite and mica. Quartz is well rounded and can be up to 20 µm in size, however a major part of the quartz occurs as much smaller clay sized grains associated with clay. Clay and quartz forms the matrix of the shale samples and makes up more than 50% of the sample. Elongated lumps of organic matter can be identified but are difficult to distinguish from cracks due to their black colour. Both clay and organic matter are orientated parallel to bedding but is often distorted and draped around dolomite crystals. This suggest that dolomite formed early before major compaction. The matrix also contains elongated bedding-parallel patches of calcite or smaller patches of calcite dispersed throughout the sample. The calcite patches contain small less than 2 µm fragments of fossil calcite or larger parts of structured fossil calcite. No clear in-situ growth calcite crystals are observed indicating that calcite is of primary detrital origin. The petrography of the samples indicates a detrital clay, quartz and (calcite) fossil deposition with early diagenetic pyrite and subsequent dolomite crystallization.

2.3.2.2 RWK-01-10 (2080.5 m)

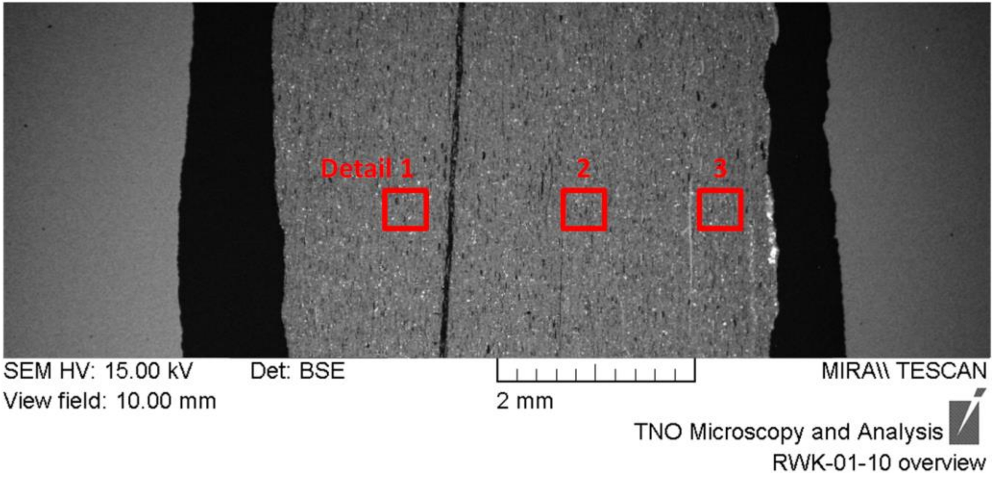

Figure 2-10 Overview of RWK-01-10 indicating the location but not the size of detail pictures and chemical maps 1-3. The bedding direction is vertical.

The overview picture of RWK-01-10 does not show clear laminations. The lighter ‘stripes’ visible represent higher concentrations of fossils or pyrite framboids. In three locations chemical maps are made to assess if there are differences in mineral content (Figure 2-10, Figure 2-11). The mineral content is quite similar, characterised by a high fossil content and low dolomite content in a clay matrix with bedding-parallel patches of calcite and quartz. Dolomite is quite small (up to 20 µm), near-euhedral in shape and exhibits clear dark cores and light iron rich rims. The black parts are both cracks and organic matter, difficult to distinguish with the SEM. Map 3 shows larger black particles that were identified as organic matter by the higher sulphur content compared to the resin in the cracks.

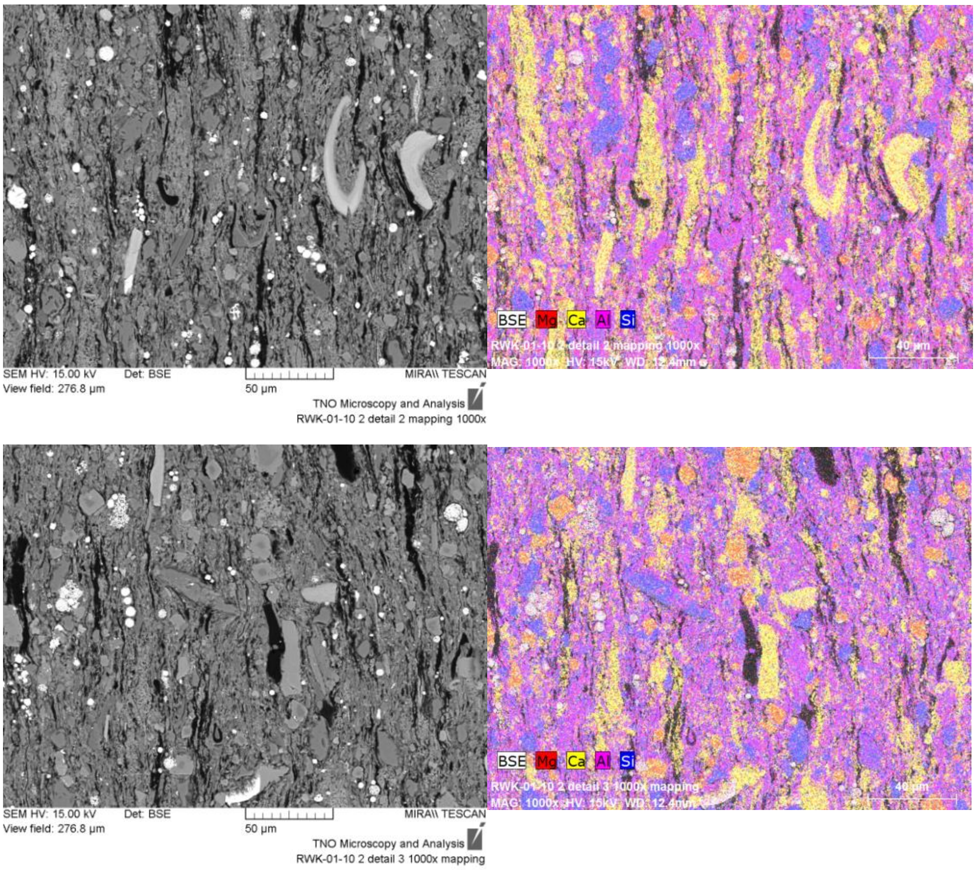

Figure 2-11 BSE views of detail 2 and 3 combined with their Mg-Ca-Al-Si chemical intensity maps indicating the carbonate-silicate mineral distribution at 1000x magnification (~250 x 200 µm view).

2.3.2.3 *RWK-01-25 (2091.5 m)*

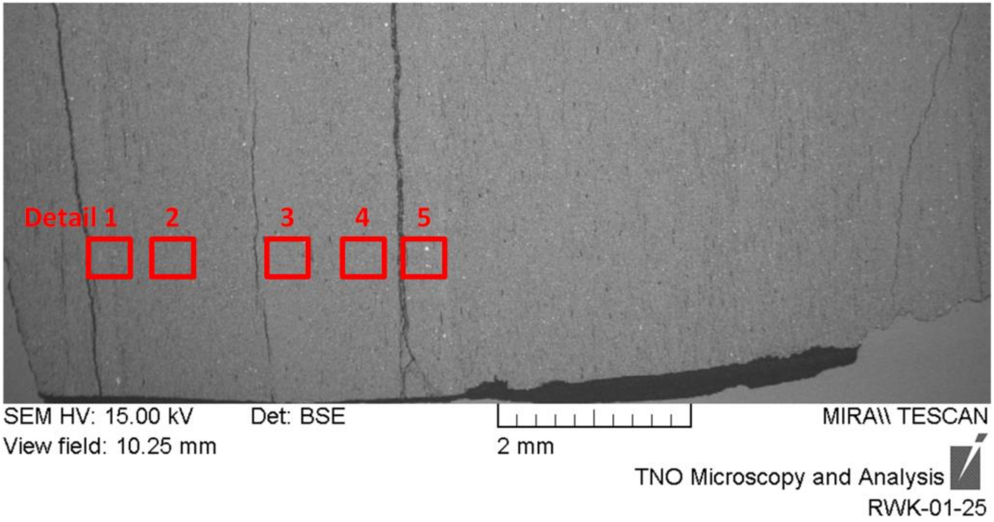

Figure 2-12 Overview of RWK-01-25 indicating the location but not the size of detail pictures and chemical maps 1-5. The bedding direction is vertical.

The overview picture of RWK-01-25 shows laminations by differences in grey tone (Figure 2-12). In five visually different laminations chemical maps are made to assess the difference in mineral content (Figure 2-13). Compared to RWK-01-10 the dolomite content is higher and the crystals larger (up to 40 µm). Especially the larger dolomite crystals are anhedral and do not always show the clear core and rim as observed for RWK-01-10. The higher dolomite content results in a lower clay and quartz matrix content. Larger (up to 10 µm) quartz grains occur scattered throughout the sample and do not form clear patches. The calcite content is variable on a 1000x magnification scale as mappings 1 to 5 show different amounts and sizes of calcite patches. Roughly spherical calcite structures can be filled with kaolinite, indicated by a higher pink intensity (compared to the matrix) surrounded by a yellow calcite.

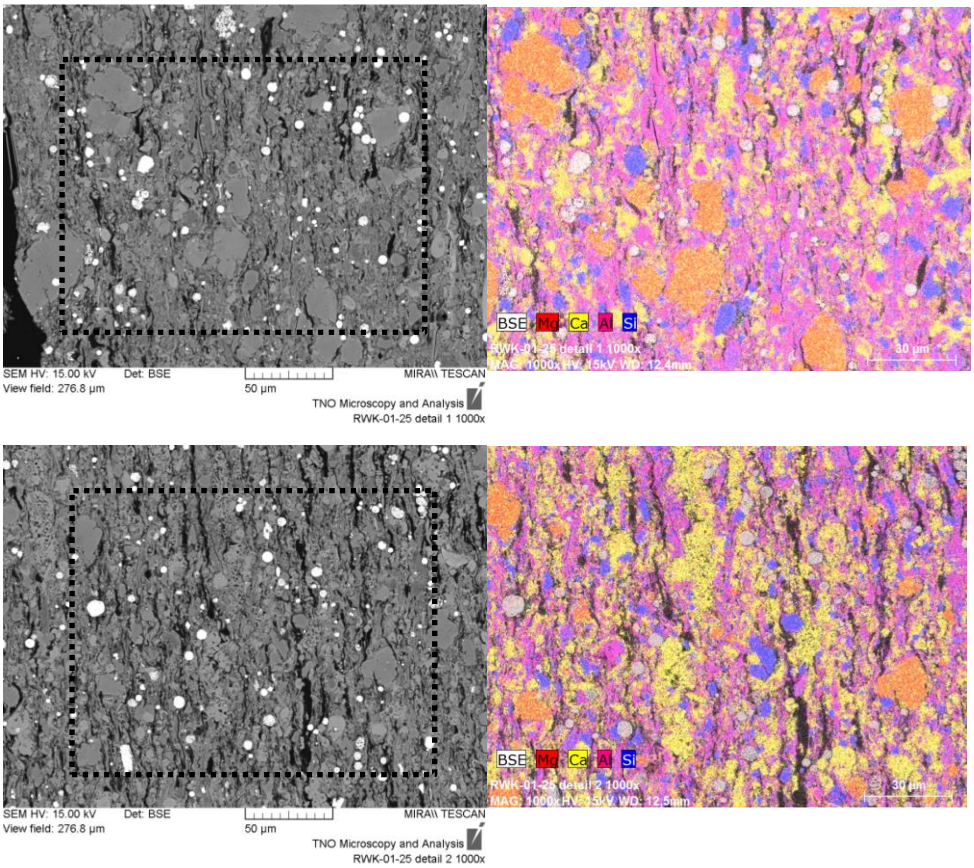

Figure 2-13 BSE views of detail 1 and 2 combined with their Mg-Ca-Al-Si chemical intensity maps indicating the carbonate-silicate mineral distribution at 1000x magnification (~250 x 200 µm view). The chemical maps may deviate slightly in size, shown by a dotted rectangle in the SEM image.

2.3.2.4 RWK-01-37 (Depth?)

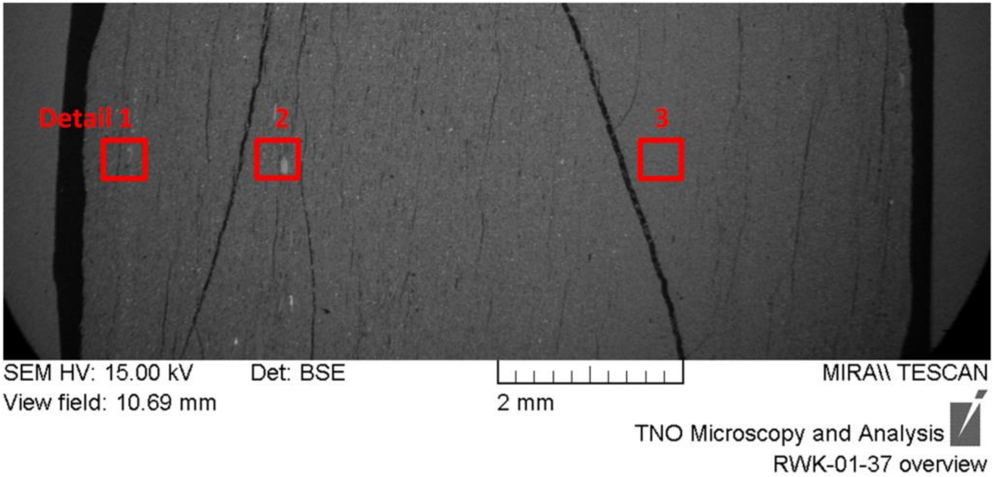

Figure 2-14 Overview of RWK-01-37 indicating the location but not the size of detail pictures and chemical maps 1-3. The bedding direction is vertical.

RWK-01-37 has a dolomite content higher than RWK-01-10 and lower than RWK-01-25 (Figure 2-15). The crystals are generally up to 20 µm in size and an- to euhedral. Map 1 shows a band of large dolomite crystals associated with larger quartz grains as well. Calcite can be quite dispersed in the matrix (Map 3) or occur in large patches (Map 2). Map 2 was made in an fossil rich lamination (see overview) which matches with the higher calcite content. This map also contains an elongated high sulphur feature which is high in calcium as well.

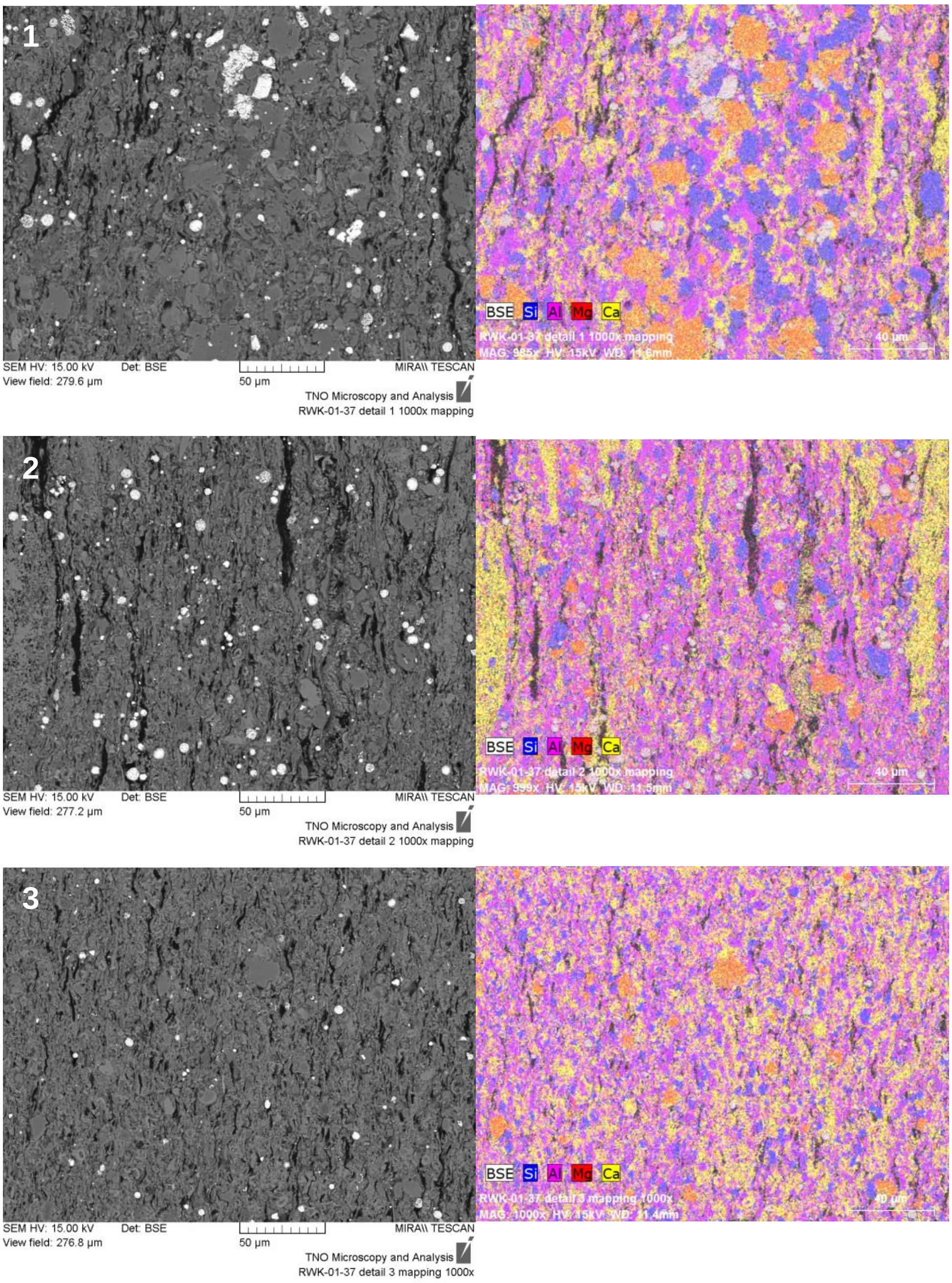

Figure 2-15 BSE views of detail 1, 2 and 3 combined with their Mg-Ca-Al-Si chemical intensity maps indicating the carbonate-silicate mineral distribution at 1000x magnification (~250 x 200 µm view).

2.3.2.5 RWK-01-44 (2100.8 m)

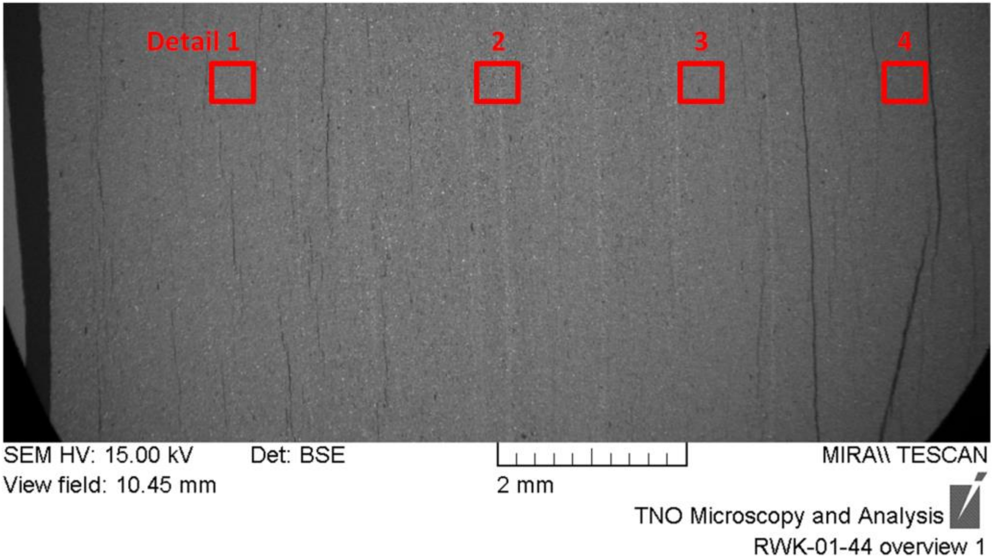

Figure 2-16 Overview of RWK-01-44 indicating the location but not the size of detail pictures and chemical maps 1-4. The bedding direction is vertical.

RWK-01-44 has a low dolomite as well as calcite content (Figure 2-17). The maps all indicate that the sample is matrix dominated containing mainly clay and quartz with some dispersed calcite, dolomite and pyrite. Even though the overview image shows some laminations the mineral content is quite similar; the laminated appearance only caused by a higher pyrite content.

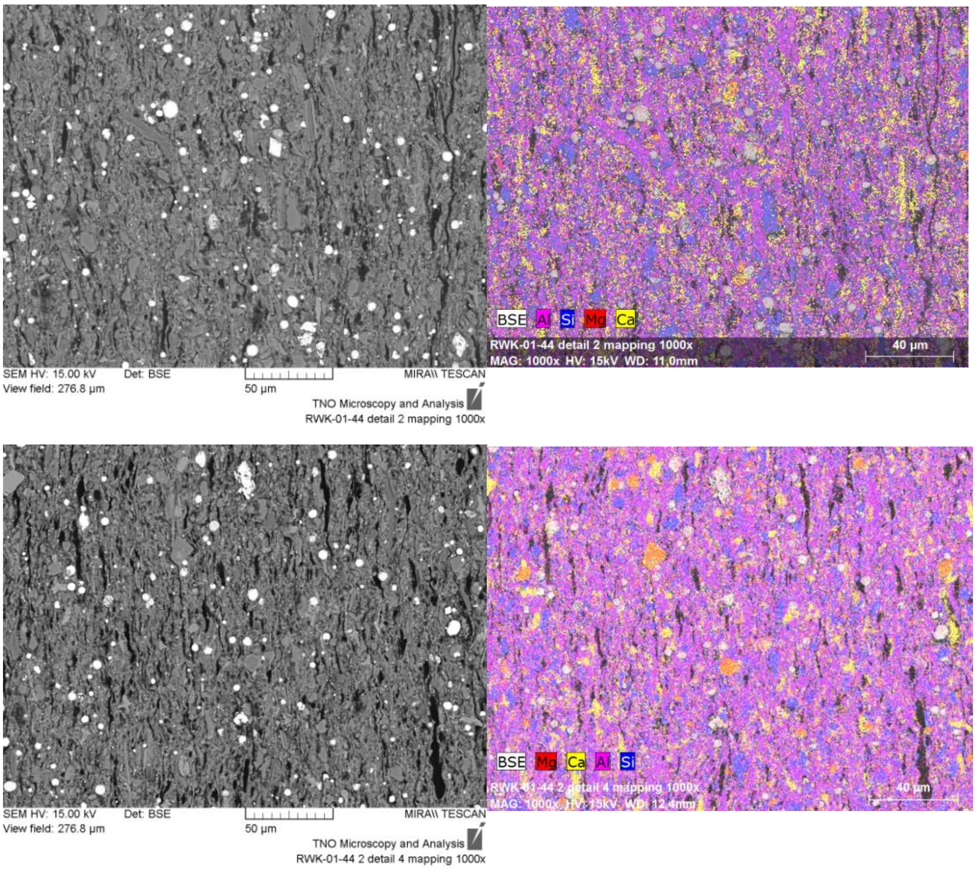

Figure 2-17 BSE views of detail 2 and 4 combined with their Mg-Ca-Al-Si chemical intensity maps indicating the carbonate-silicate mineral distribution at 1000x magnification (~250 x 200 µm view). One SEM image deviates in size, the chemical map location shown by a dotted rectangle in the SEM image.

2.3.2.6 *RWK-01-54 (2105.7 m)*

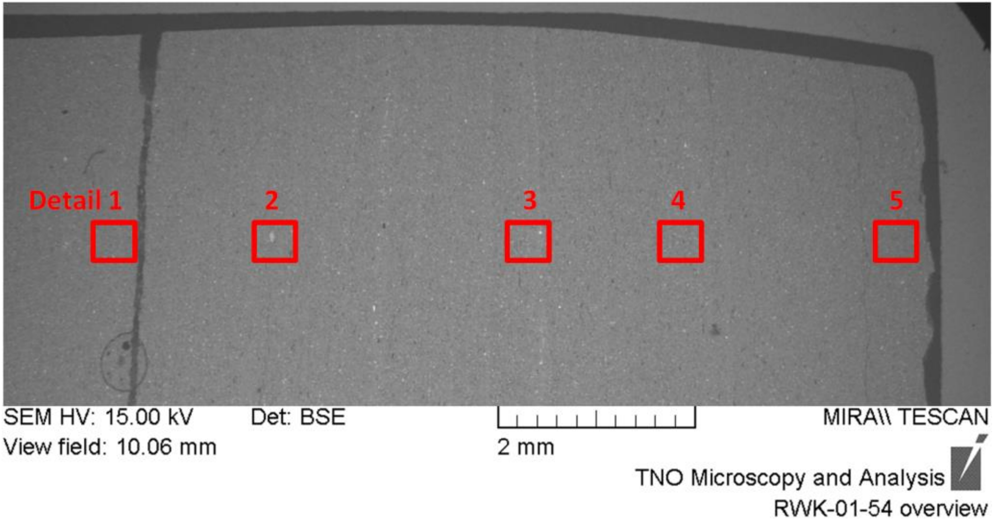

Figure 2-18 Overview of RWK-01-54 indicating the location but not the size of detail pictures and chemical maps 1-5. The bedding direction is vertical.

RWK-01-54 clearly has the highest dolomite content of all studied samples (Figure 2-19). Dolomite crystals occur in a range of sizes from <5 to 60 µm. The differences between the dolomite core and rim is clearly visible, with the width of the rim being comparable for the different sized crystals. Because of the high grain content the organic matter and clay is not directed bedding-parallel but often draped around or distorted by dolomite crystals.

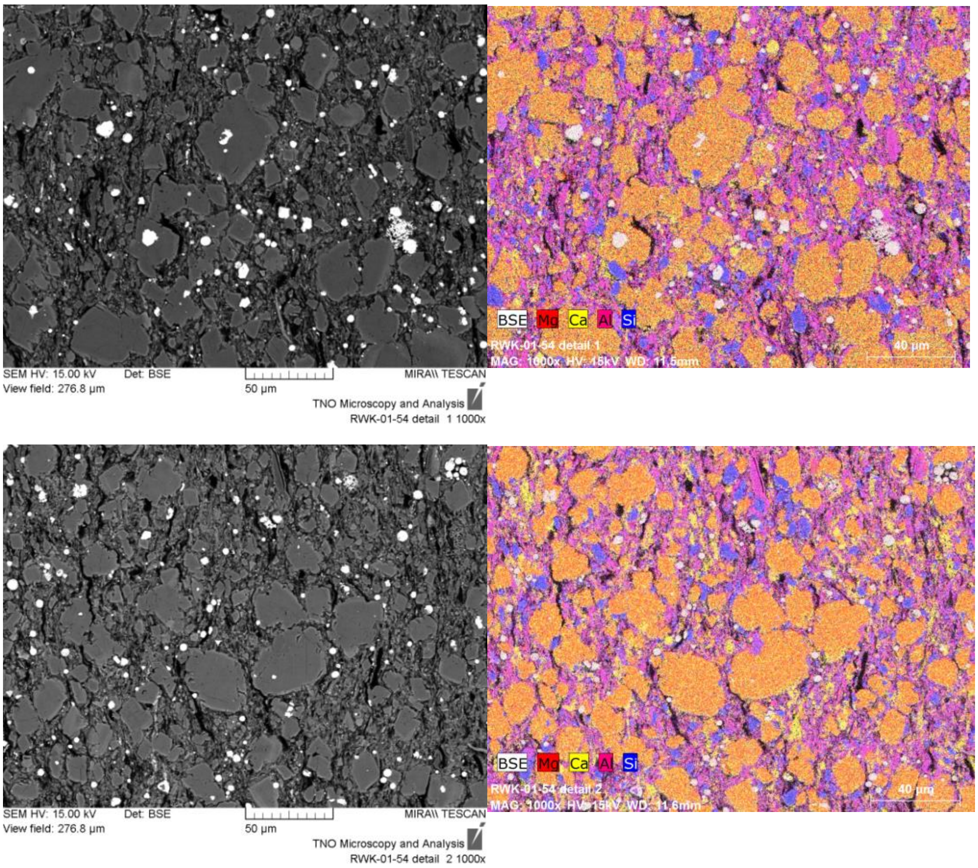

Figure 2-19 BSE views of detail 1 and 2 combined with their Mg-Ca-Al-Si chemical intensity maps indicating the carbonate-silicate mineral distribution at 1000x magnification (~250 x 200 µm view).

2.3.2.7 LOZ-01-36 (2489 m)

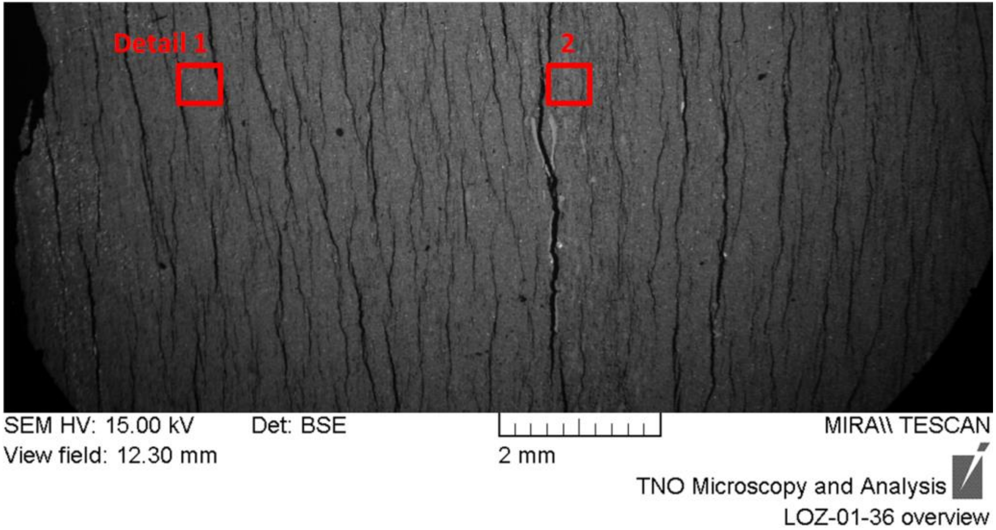

Figure 2-20 Overview of LOZ-01-36 indicating the location but not the size of detail pictures and chemical maps 1-2. The bedding direction is vertical.

The LOZ samples are more fractured than the RWK samples which could be an original feature are could be attributed to differences in drying or sample preparation(Figure 2-20). The LOZ thin sections were made for a different project by a different manufacturer and the quality is far less (surface more uneven and higher tendency for charging). The general characteristics for the two wells are similar with LOZ samples also showing large dolomite crystals within a clay-quartz matrix containing bedding-parallel fine grained calcite patches and pyrite framboids (Figure 2-21). The main difference is the appearance of the dolomite which is severely fractured. This could be due to a higher degree of compaction although the loosely packed calcite patches do not support this.

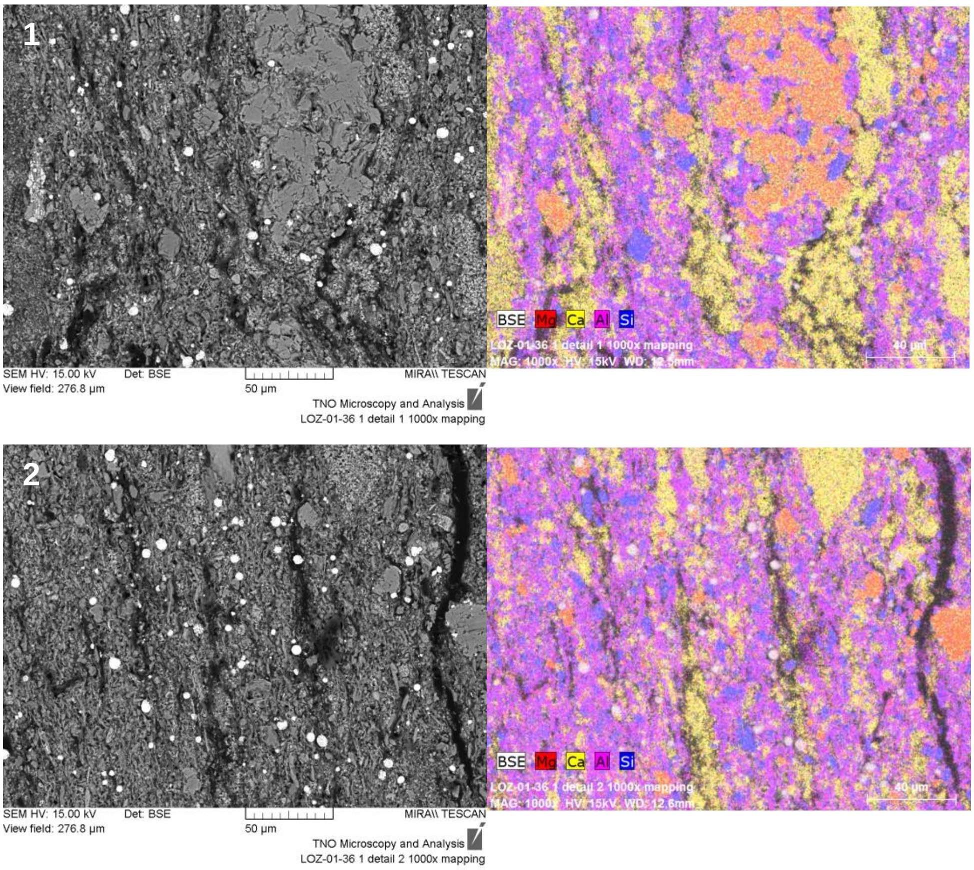

Figure 2-21 BSE views of detail 1 and 2 combined with their Mg-Ca-Al-Si chemical intensity maps indicating the carbonate-silicate mineral distribution at 1000x magnification (~250 x 200 µm view).

2.3.2.8 *LOZ-01-40 (2503 m)*

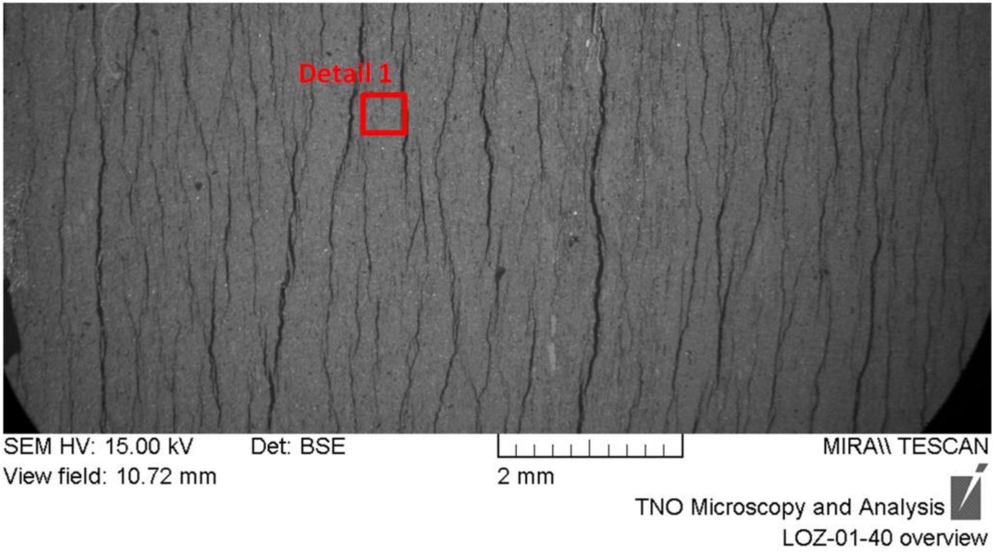

Figure 2-22 Overview of LOZ-01-40 indicating the location but not the size of detail pictures and chemical map 1. The bedding direction is vertical.

LOZ-01-40 appears very similar to LOZ-01-36, showing abundant fractures and a homogeneous grey tone apart from the bedding-parallel fossil rich bands (Figure 2-22, Figure 2-23).

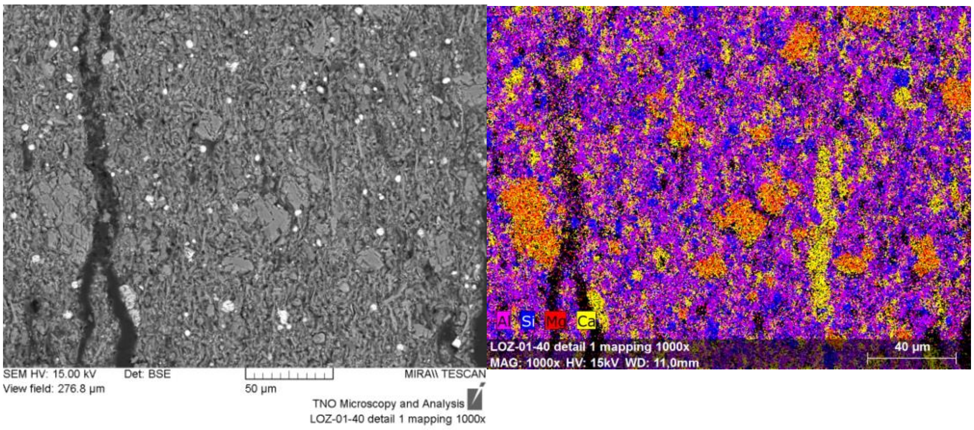

Figure 2-23 BSE views of detail 1 combined with the Mg-Ca-Al-Si chemical intensity maps indicating the carbonate-silicate mineral distribution at 1000x magnification (~250 x 200 µm view).

2.3.2.9 *Dolomite: SEM imaging and EDX analyses*

Pictures of dolomite crystals were collected for all samples to assess the nature of dolomite occurrence (Figure 2-24). RWK-01-10 dolomites have multiple growth zones with a dark grey core that is not visible in RWK-01-25 and RWK-01-37 and RWK-01-54. RWK-01-44 also contains dolomite crystals with more growth zones but only in isolated cases. The different zones within a dolomite crystal indicate change in the chemistry of the pore fluid they crystallised from but not necessarily different stages of dolomite growth. This could be observed by clear overgrowth (possibly with a different crystal orientation), however such evidence was not found.

In all samples dolomite occurs as euhedral rhombs but can exhibit anhedral sides where growth occurs against pyrite or quartz grains (see for example RWK-01-25). Partial dissolution could have occurred causing irregularities at certain crystal faces. Pyrite inclusions are often observed. Together with the observation of dolomite growth interrupted by pyrite framboids, this indicates dolomite precipitation after pyrite. This agrees with the general concept of early diagenetic pyrite growth followed by dolomite when sulphur is depleted and the pH rises. The early precipitation of dolomite is further supported by clay draping around the dolomite grains indicating that dolomite was present before major compaction. Growth of dolomite within the clay matrix could be an explanation for the silica and aluminium content of the dolomite as measured by SEM EDX.

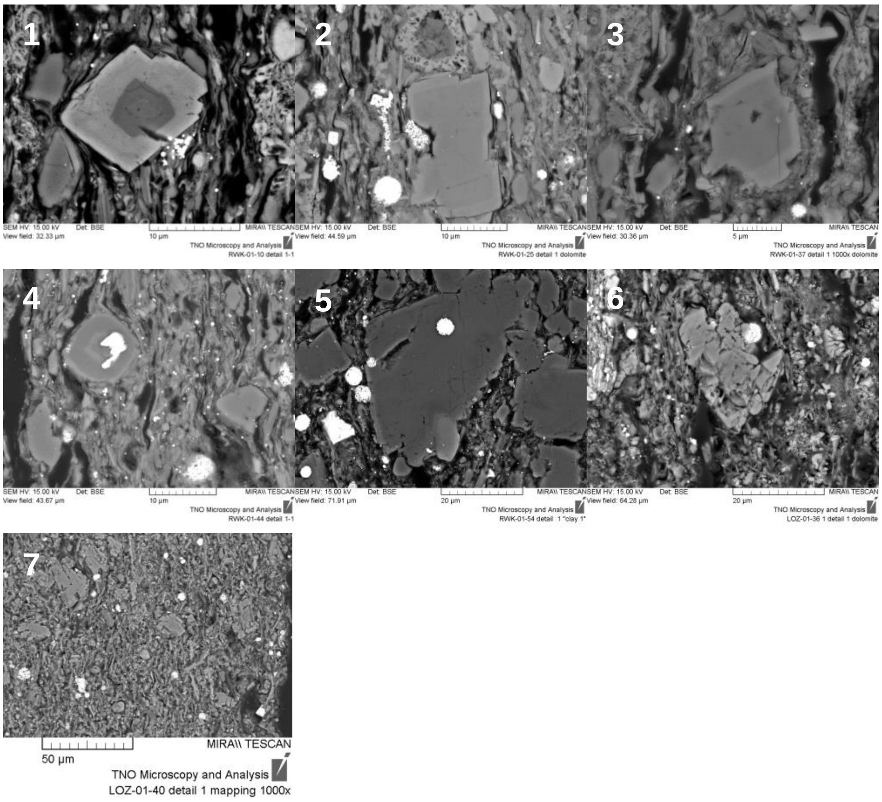

Figure 2-24 BSE images (note the different scales) of dolomite occurrence in the different samples

2.3.2.10 Calcite fossil content: SEM imaging

Pictures of calcite patches were collected for all samples to assess the nature of calcite occurrence. The calcite occurrence is quite similar for the different samples as the same type of fossils are observed. The calcite patches contain fine grained µm sized fractions of fossils with larger 2-5 µm sized elliptical coccolith fossils (for example RWK-01-37 detail 3 calcite 2, Figure 2-25). Structured calcite is also found, often still intact with a round shape containing kaolinite (for example RWK-01-44 detail 3). Some larger calcite grains occur (for example RWK-01-10 detail 2 calcite). Since almost all calcite can be attributed to fossil content, no evidence was found for secondary calcite formation. Hence the calcite content is related to initial in-situ sedimentation and no late digenetic enrichment occurred.

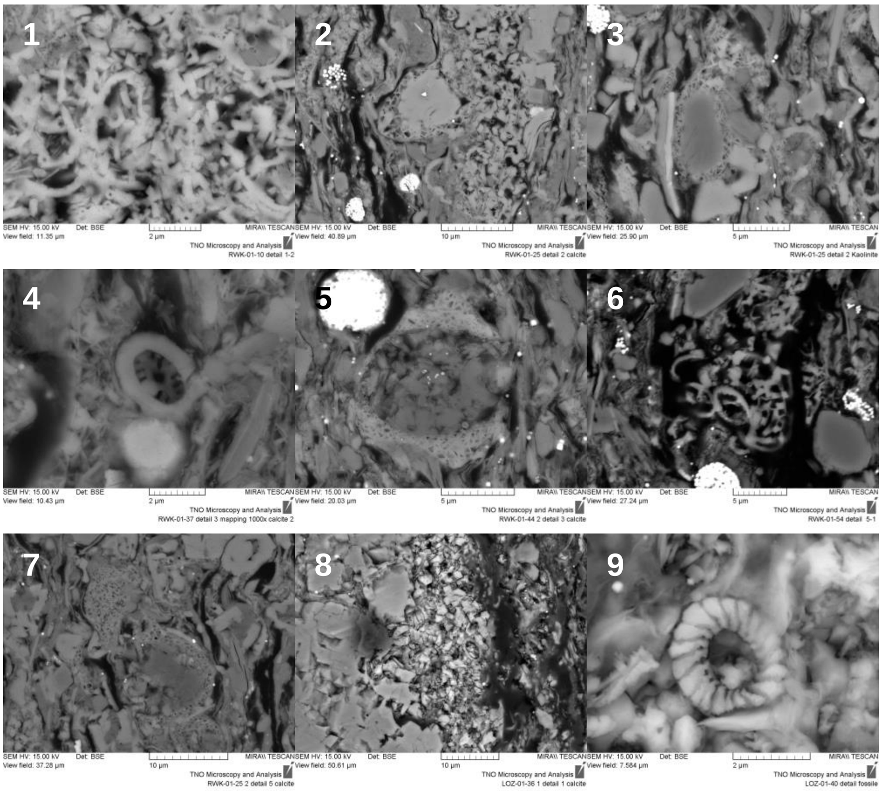

Figure 2-25 BSE images (note the different scales) of calcite fossil occurrence in the different samples.

2.3.2.11 *Chemical composition ICP*

ICP chemical measurements were performed on RWK-01 samples but are not available for the LOZ-01 samples. For both wells chemical measurements were taken by SEM EDX. Here we compare the chemical signature on the samples selected for thin sections.

Chemical characteristics samples and mapped areas
The relative ICP abundances (Figure 2-26) yield the following sample comparison:

- RWK-01-10 (2080.5): Low Mg, Medium Ca, Medium Al & Si
- RWK-01-25 (2091.5): Medium Mg, High Ca, Low Al & Si
- RWK-01-37 (2097.2): Low Mg, High Ca, Low Al & Si
- RWK-01-44 (2100.8): Low Mg, Low Ca, High Al & Si
- RWK-01-54 (2105.7): High Mg, High Ca, Low Al & Si

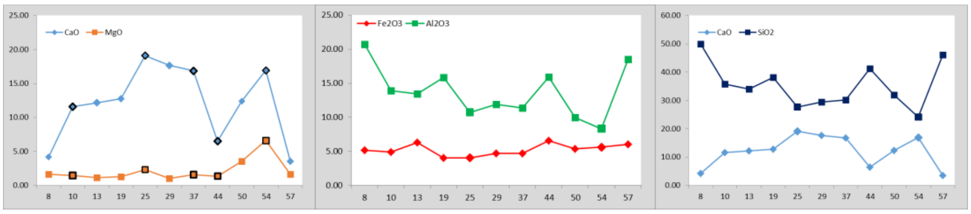

Figure 2-26 Plots of the chemical composition of the selected samples (ICP, wt%)

The relative abundances (Figure 2-26) agree with the SEM mineral observations. The high magnesium samples have a high dolomite content, the high calcium samples a high calcite content and the high aluminium-silica sample a high amount of quartz-clay matrix. When plotted the ICP shows clear correlation between elements which is also shown by the total EDX measurements of the mapped areas (all measured at 275x magnification). Silica and calcium content are negatively correlated indicating a higher silica (clay and quartz) content with lower carbonate content (Figure 2-27a). Sample RWK-01-54 has a lower calcium content for the amount of silica, since this sample contains an exceptionally high amount of dolomite (and hence magnesium). When adding calcium and magnesium – giving total carbonate content – the correlation is very good (Figure 2-27b). Aluminium and silica are positively correlated (Figure 2-27c, d) since clay and quartz occur in the matrix. In general the correlations show that the Posidonia shale mineralogy is characterised by a varying amount of carbonate content versus matrix content; with a high carbonate giving a relatively low amount of matrix and vice versa.

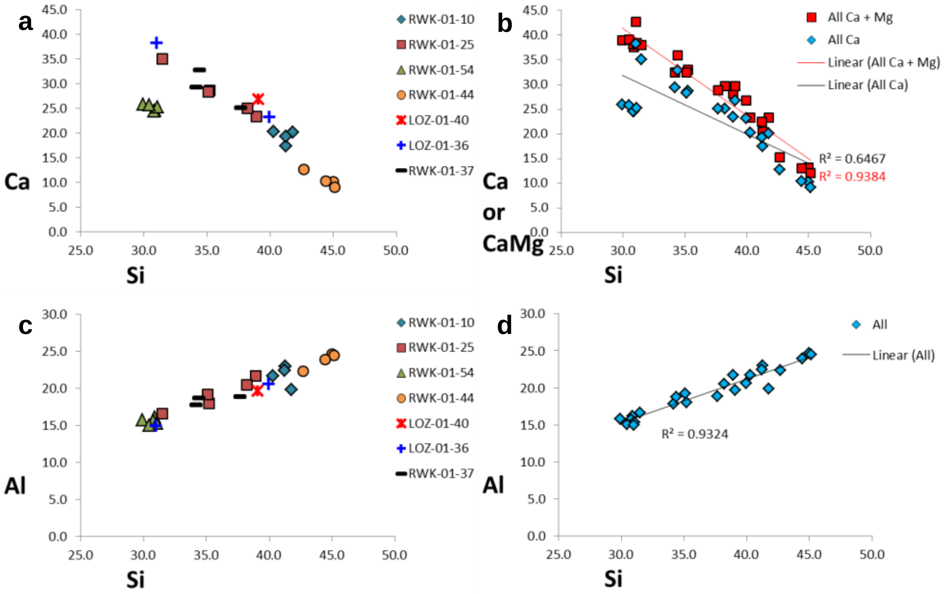

Figure 2-27 Plots of total EDX measurements of the mapped areas for different samples.

Chemical characteristics dolomite

Measurements of dolomite cores and rims were taken to investigate possible different phases of dolomite precipitation. The chemical composition was normalised to only Ca, Mg and Fe to avoid effects of Si and Al impurities and uncertainties in C and O due to measuring limitation and carbon coating. The SEM images did not provide evidence for secondary dolomite growth as no overgrowths were observed. However there were differences in zoning that are also captured by the chemical analyses. Iron substitutes for magnesium in dolomite and variations in iron content do occur (Figure 2-28a). These are internal variations while most samples overlap in iron content. RWK-0-44 shows different types that could be related to different stages of dolomite growth, however, these differences could also be attributed to changes in the local chemical environment. Unfortunately only one measurement was taken from RWK-01-54 which might show additional dolomite growth just by the high amount of dolomite present in the sample. When magnesium and iron are taken together and plotted against Ca the spread in dolomite chemistry is visualized (Figure 2-28b). The different measurements in the samples show some spread, with no clear clustering. This indicates that either different dolomite growth phases occurred similar for all samples or that all dolomite grew in one phase affected by the differences in local (lamination scale) chemistry.

The clustering of different samples for the dolomite rim measurements probably indicates different local iron supply for the different samples (Figure 2-29).

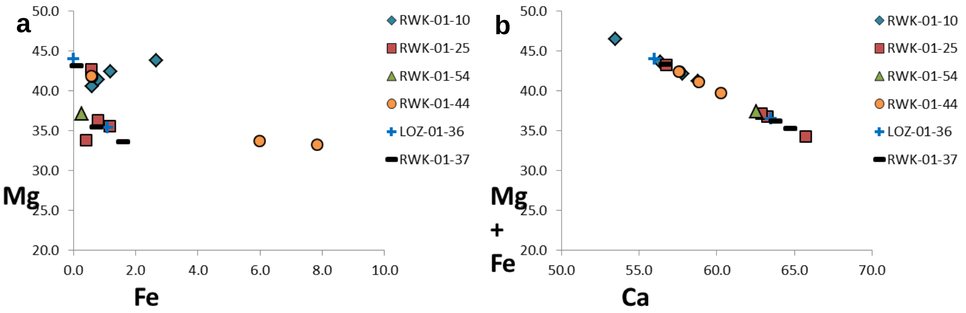

Figure 2-28 Chemical composition of dolomite cores.

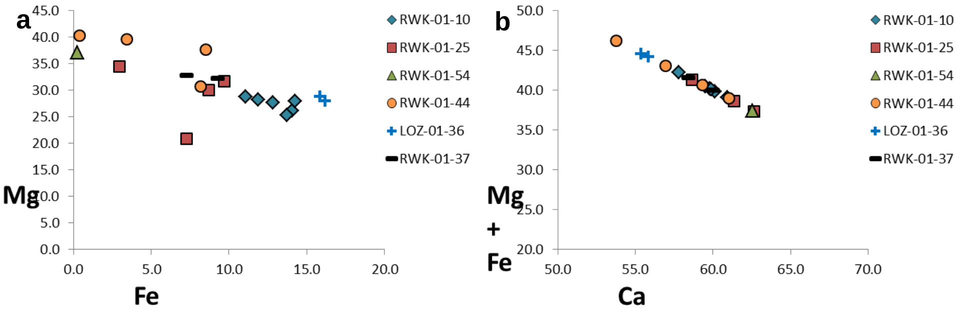

Figure 2-29 Chemical composition of dolomite rims.

2.3.3 *Synthesis*

- The RWK-01 characterisation is summarised in Figure 2-30.
- The petrography of the samples indicates detrital clay, quartz and (calcite) fossil deposition with early diagenetic pyrite and subsequent early dolomite crystallization.
- The Posidonia shale chemistry is basically characterised by a range in carbonate versus silicate matrix content. Due to the association of quartz and clay in the matrix, they correlate positively (in contrast to sandstones for example).
- The carbonate content is mainly determined by the calcite content except for some dolomite rich layers.
- The calcite content reflects the initial in-situ sedimentation of fossil fragments. The calcite fossil (remnant) occurrence is the same for all samples although the content varies.
- The dolomite content is related to early pre-compaction diagenetic processes. All dolomite shows an iron rich rim indicating depletion of magnesium towards the end of dolomization.
- No later phases of carbonate enrichment/precipitation were identified.

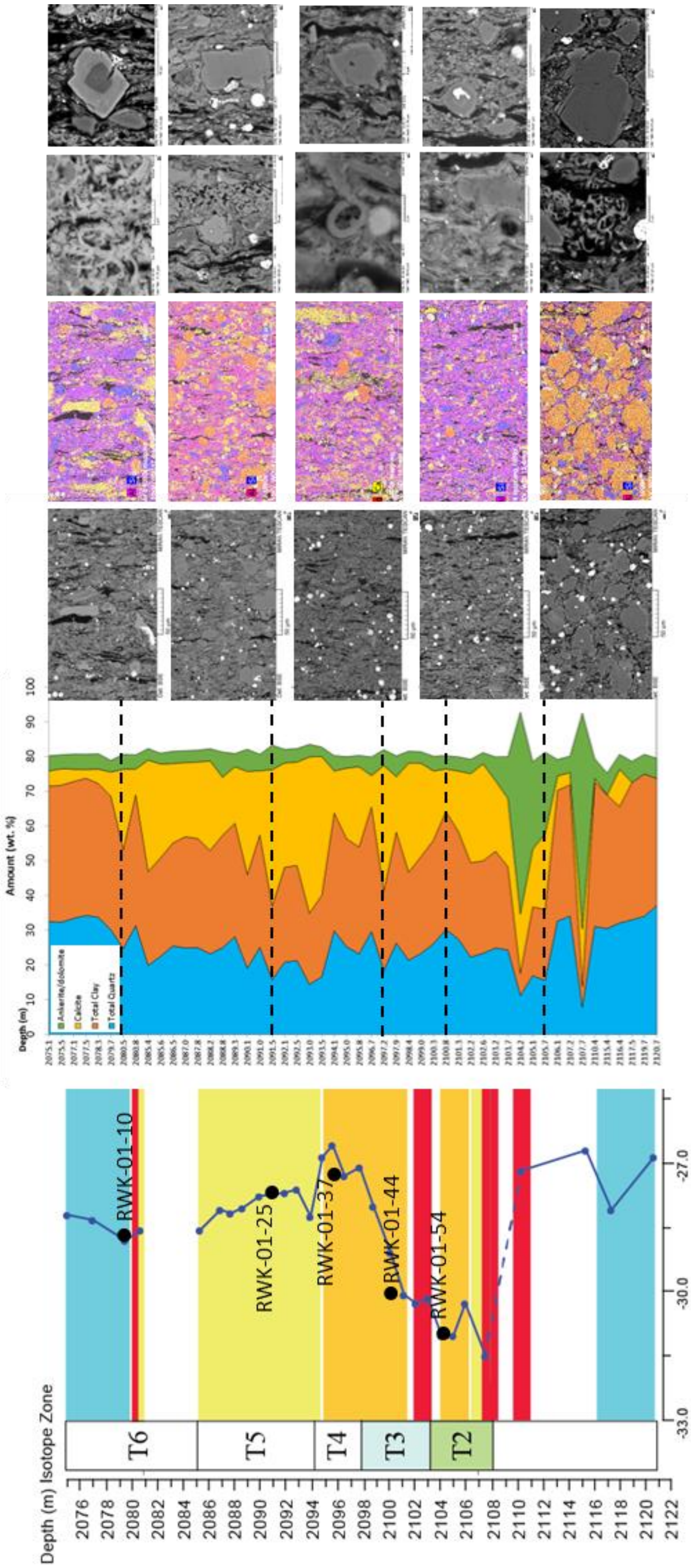

Figure 2-30 Summary of the results of the RWK-01 mineralogical characterisation. All the samples show the same mineralogical components in varying amounts: depositional calcite (fossils) and early diagenetic dolomite in a clay-quartz-pyrite matrix.

2.4 Palynology

2.4.1 Methodology

By studying the composition of organic-matter assemblages, information on the biological and environmental development of the surface-water environment can be obtained. This particularly regards primary productivity, the degree of stratification and the related chemocline migration. Patterns in terrestrial influx and climate can also be deduced since marine assemblages typically also contain fractions of terrestrial derived material.

2.4.1.1 Processing

Standard palynological processing was applied for all samples, including HCl for decalcification, destruction of mineral matrix with HF and subsequent sieving over a 15 µm mesh sieve. The organic residues were mounted on glass slides using glycerin jelly. Although the samples were extremely rich in organic matter, no oxidation step was applied in order to keep the structureless organic matter preserved. For Rijswijk and Well F11-01 we have experimented with the addition of exote Lycopodium to a known sample weight, allowing for assessment of the absolute abundance of palynomorphs per gram. This is sometimes extremely difficult due to the high density of organic-matter and palynomorphs.

2.4.1.2 Quantification

In principal, three rows were counted using the 40x objective. Illumination with ultra violet light was applied for the identification of small acritarchs and other palynomorphs. Because acritarchs and other small palynomorphs are often concealed within so-called faecal pellets, the bright fluorescence of these cells under ultraviolet light facilitates identification. The counts of the organic matter assemblages and of the palynomorph assemblages are displayed in “closed SUM” diagrams. The counts of the dinoflagellate cysts and of the pollen and spores are displayed in saw-blade distributional panels. A short description of the various groups identified is provided in the following section.

2.4.2 Palynogical groups

The organic matter or palynofacies assemblages consist of 4 groups:

1. Structureless Organic Matter (SOM): This type of organic matter consists of a mid-size to large (50 to 300µ) particles with no obvious structure, i.e. no cell walls, vessels etc. Two types are distinguished:

   Type 1 is more or less translucent and is in general less massive than Type 2.

   Type 2 is not translucent, darker and more massive than Type 1. Type 2 may reach 300µ, which is in the same range size as medium sand.

In most cases, Type 2 particles reveal small “hidden” palynomorphs when studied under ultra-violet light (instead of “normal” transmitted light). Apparently, this type represents aggregates of organic-matter, likely related to faecal pellets, resulting from extremely high biological productivity and subsequent consumption.

2. Wood: These are organic matter particles that can be attributed to wood remains. Three types are distinguished.

3. Palynomorphs These are (mostly unicellular) organic matter particles that constitute individual biological entities. This group is further subdivided and is displayed in “closed SUM” diagrams.

The palynomorph assemblages are subdivided in the following sub-categories.

1. Sphaericals: These are relatively small spherical particles with no obvious ultra-structure such as spines, granules or openings. Their biological origin is not fully clear, but it is generally thought that they are attributed to the cysts (or phycomae), representing part of the life-cycle of photosynthetic prasinophyte algae (like *Tasmanites*, see below).
2. Acritarchs: These are small algal cysts that cannot be attributed to either dinoflagellate cysts or resting cysts of known algae. In marine palynological assemblages, acritarchs are always present but usually quite rare. They are restricted to marine environments.
3. *Tasmanites*: They are Prasinophyte algae, a class of unicellular green algae in the Division of Chlorophyta. High abundance of *Tasmanites* occurs when reactive nitrogen and phosphorous become freely available in the photic zone (Prauss, 2007; Van de Schootbrugge et al., 2013). This typically happens when surface-water stratification intensifies or destabilizes and the chemocline moves into or out of the photic zone. As a result, mass-occurrences often mark ecological tipping points.
4. Dinoflagellate cysts or dinocysts: They represent the resting cysts of a type of marine plankton. The fossil group appears in the Triassic and starts radiating from the Late Toarcian onward (Fensome et al., 1996). Evolution is fast, so dinocysts are commonly used in biostratigraphy. They are essentially restricted to a wide array of marine environments.
5. Sporomorphs: This is a general term for all occurring pollen and spores. In Jurassic times, the pollen record was only represented by gymnospermous pollen (e.g. from conifers). Angiosperm pollen only appear later, in the Cretaceous.
6. Some other groups also reach abundance in the studied record: Botryococcus represents a type of fresh-water-tolerant algae, that proliferates under brackish conditions. Cymatiosphaera and Pterospermella are both prasinophyte algae, related to *Tasmanites*.

When combined the organic matter data and the palynological provide information regarding the overall rate of primary productivity, degree of surface-water stratification and terrestrial influence. These parameters give rise to five biofacies types according to the following the scheme.

🟦 “Normal” shallow marine
🟥 Tasmanites acme: Chemocline moves in/out photic zone
🟨 Strong stratification and high export productivity: Chemocline around or just below photic zone
🟧 Extreme stratification and export productivity: Chemocline within photic zone
🟩 Strong stratification and high export productivity: Remarkably high terrestrial influence
⬜ Barren: Relation with oil expulsion?

Normal shallow marine conditions (**blue**) are characterized by the abundant presence of organic-walled dinoflagellate cysts and acritarchs. Mass occurrences of the prasinophyte *Tasmanites* likely indicate a transition of the chemocline into- or out of the photic zone (**red**, see section 4.1.2 for more discussion). When organic matter assembalges are dominated by Structureless Organic Matter Type 1, we infer elevated export productivity and strong surface-water stratification (**yellow,** see section 4.1.2 for more discussion), whereas even denser clusters of SOM (Type 2) indicate extreme stratification and export productivity (**orange**). For Loon op Zand we rely on old data, that were not generated using UV-fluorescence microsocopy, it is therefore difficult to disentangle between the orange and yellow biofacies types. Next to that, we noted an interval with high abundance of sporomorphs in assemblages dominated by SOM, this is indicated in **green**.

For the organic-matter typing used for comparison with the Rock-Eval analyses, we also recognized another biofacies type. This type is dominated by *Tasmanites* but is not accompanied by dominant SOM-Type organic matter, likely indicating that the chemocline moved into the photic zone, starting off with normal marine conditions. This type is indicated in **pink** (see section 2.5). In well F11-01 we note an interval that is barren of palynomorphs, this is indicated in **grey**, possibly a consequence of oil-generation and expulsion.

2.4.3 *Results*

2.4.3.1 *Whitby*

The following is a summary and re-interpretation of the results from the palynological study carried out during Phase 1 of the Sweet Spot Project, now scaled against the carbon isotope timelines used in this study (Figure 2-31).

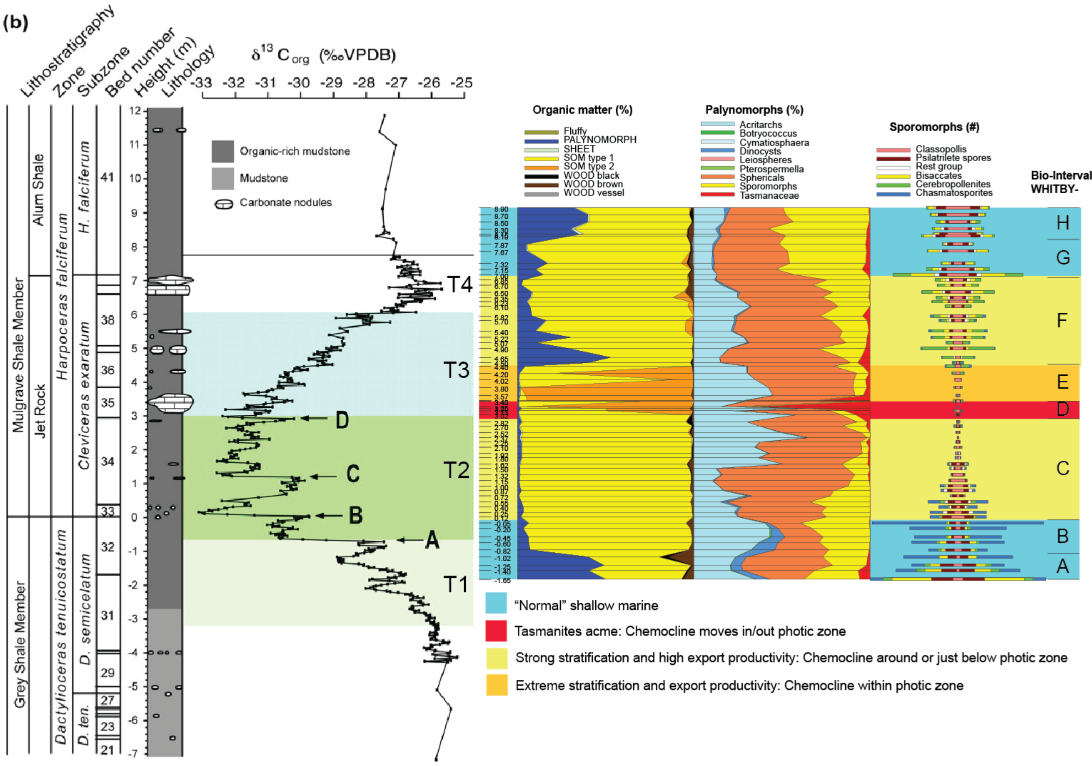

Figure 2-31 Results of palynological study of the Whitby section scaled against the carbon isotope record of Kemp et al. (2005, 2011). The left diagram indicates the composition of the organic material (%), the middle diagram the composition (%) of the palynological associations and at the right the composition of the sporomorph communities. The shading indicates the paleo-environmental zonation discussed in the text.

In general, all samples yield abundant organic matter. From base to top, a trend is observed from organic matter assemblages with abundant palynomorphs, such as dinoflagellate cysts and pollen and spores, towards organic matter assemblages completely dominated by marine SOM, and back again to organic matter assemblages with abundant palynomorphs. The middle part of the section, with the maximum in TOC, is characterized by a major acme of *Tasmanites* followed by dominance of the large and massive SOM-2. Based on the changes in the organic matter and palynomorphs assemblages, 8 biofacies intervals are distinguished WHITBY-A to WHITBY-H (see Figure 2-31). Altogether the record spans the entire CIE (Isotope Zones T1 to T4) and a small part of the post-CIE interval (T5).

WHITBY-A -1.65 – -1.00 m (depth relative to base Jet Rock)

Age: T1

Organic Matter Assemblages:
Abundant palynomorphs (50%). Wood is relatively
common (between 5 and 20%), the highest number reached in the entire section.

Palynomorph Assemblages:
A minor peak of Tasmanites is recorded at the base, which show a gradual decrease towards the top of this zone. Sphericals are recorded in together with acritarchs and dinocysts. The fresh/brackish water algae *Botryococcus* is also present.

WHITBY-B -0.82 – -0.05 m

Age: T1-T2

Organic Matter Assemblages:
Palynomorphs are less abundant than in WHITBY-A, but nevertheless make up between 5 and 15% of the organic matter assemblage. SOM-Type-1 is now the dominant component of the organic matter assemblages.

Palynomorph Assemblages:
Acritarchs, sphericals, dinocysts and sporomorphs are abundant. The relative abundance of sporomorphs increases throughout this interval.

WHITBY-C 0.12 – 2.82 m

Age: T2

Organic Matter Assemblages:
Palynomorphs are now rare, below 5%. SOM-Type 1 dominates the assemblages completely.

Palynomorph Assemblages:
Dinocysts are very rare and often absent. Sporomorphs are still common at the base, but decrease in abundance upwards. Sphericals dominate the palynomorphs assemblages.

WHITBY-D 3.02 – 3.40 m

Age: T2 - T3

Organic Matter Assemblages:
SOM is very dominant. Palynomorphs are very rare,
below 3%. SOM Type 2 is now recorded, starting to reach abundant values.

Palynomorph Assemblages:
Dinocysts and sporomorphs are extremely rare to absent. Sphericals and acritarchs are common, but the most striking element is Tasmanaceae, which reach up to 80% in the palynomorph assemblages.

WHITBY-E 3.42 – 4.40 m

Age: T3

Organic Matter Assemblages:
SOM is very dominant. Palynomorphs are very rare, below 3%. SOM-Type 2 is the most abundant but SOM-Type 1 also occurs.

Palynomorph Assemblages:
Sphericals and acritarchs together dominate the assemblages to 90%, implying a strong relative demise in the influx of terrestrial palynomorphs or increase in marine export productivity.

WHITBY-F 4.50 – 6.85 m

Age: T3 – T4

Organic Matter Assemblages:
SOM-Type 1 and palynomorphs are more equally distributed at the base. Upwards, palynomorphs decrease again from 50% to about 10% at the top. SOM-Type 1 is now again the dominant type. In contrast to the majority of the Jet Rock succession, wood is recorded again.

Palynomorph Assemblages:
Acritarchs and sphericals are dominant at the base, but decrease slightly towards the top. Sporomorphs increase towards the top. Dinocysts remain very rare.

WHITBY-G 7.00 – 8.00 m

Age: T4

Organic Matter Assemblages:
SOM-Type 1 is dominant. Palynomorphs constitute 10-20% of the total abundance. Wood is recorded in low abundance.

Palynomorph Assemblages:
Sporomorphs and sphaericals are dominant. Dinocysts and Tasmanites are rare but consistently present.

WHITBY-H 8.10 – 8.90 m

Age: T5

Organic Matter Assemblages:
SOM-Type 1 is still dominant but palynomorphs have increased up to 30-40%.

Palynomorph Assemblages:
Sporomorphs are abundant, up to 50%. Sphericals and acritarchs make up the other 50%. Dinocysts are rare but consistently present. Remarkably, Tasmanites becomes absent in this interval.

Conclusions

- Predominantly normal marine conditions are inferred for WHITBY-A and WHITBY-B, corresponding to the initial phases of the CIE (**Isotope Zone T1-T2**). This inference is based on the common occurrence of dinocysts and acritarchs. In WHITBY-B, the first indications for enhanced productivity and stratification are reflected by the increased amounts of marine SOM. The higher abundance of Tasmanites at the base of the investigated succession indicates that the chemocline fluctuated just beneath the photic zone.

- Given the strong dominance of SOM, the depositional environment of the main body of the CIE (**Isotope Zone T2**) and the initial recovery phase of the CIE (**Lower Isotope Zone T3**) is interpreted as being subjected to “persistent high export productivity” (WHITBY-C to WHITBY-E). The dominance of marine Structureless Organic Matter (SOM), indicates that exported organic-matter aggregates overwrote/diluted ‘normal-marine’ background sedimentation of palynomorphs.

- WHITBY-D reflects the transitional phase into the most heavily stratified and strongest export productivity regime. During this interval, the chemocline moved into the photic zone as indicated by the massive bloom of *Tasmanites*, co-occurring with the inception of the recovery towards more positive values of the CIE (**T2-T3 Isotope Zone boundary**). WHITBY-E (**Lower Isotope Zone T3**) reflects the most intense export productivity regime, indicated by dominant large and massive aggregates of SOM-Type 2.

- A sharp boundary between WHITBY-E and WHITBY-F is recorded during the recovery of the CIE (**Upper Isotope Zone T3**). The massive SOM-Type-2 aggregates disappear and the relative abundance of palynomorphs increases at the expense of SOM. Alternations between the presence of dinocysts and *Tasmanites* in WHITBY-F indicate that the chemocline fluctuated at or just below the photic zone.

- In WHITBY-G to WHITBY-H (**Isotope Zone T4-T5**) predominantly marine conditions progressively occur again. High abundance of sporomorphs at the expense of sphaericals, suggest that terrestrial influence also increases indicating a very proximal marine environment. The chemocline has deepened below the photic zone.

2.4.3.2 Rijswijk (RWK-01)

42 samples were analysed for palynological organic-matter typing. In order to get some control on trends in the concentration of the palynomorphs a known number of exote *Lycopodium* spores were added to a known sample mass (Figure 2-32).

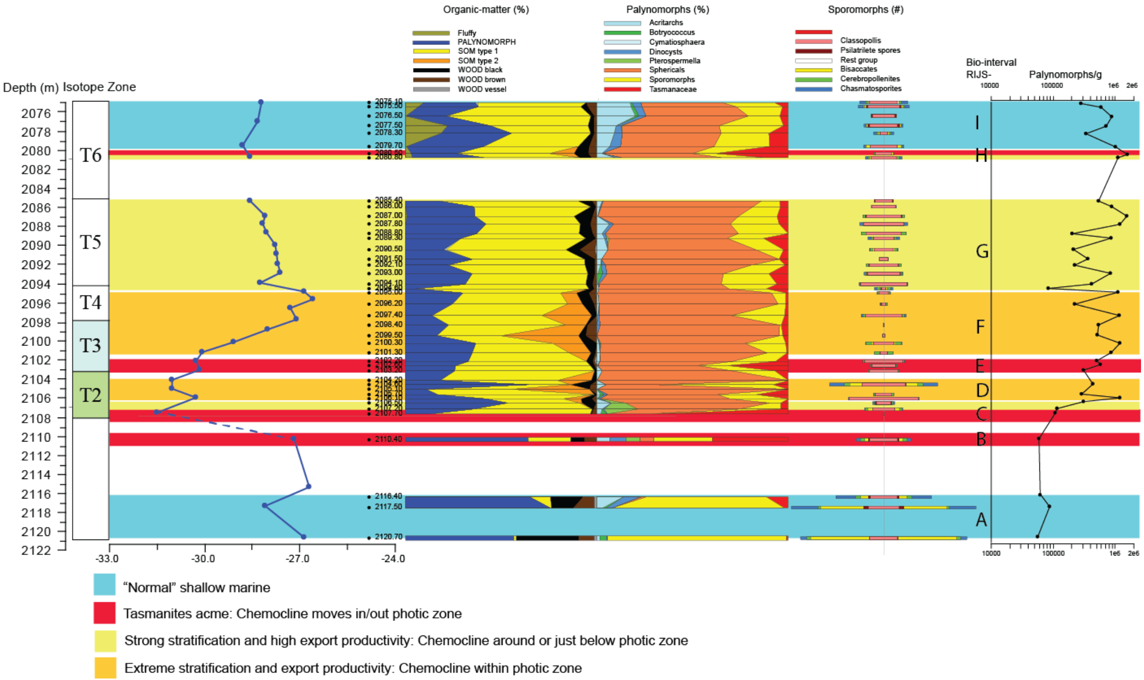

Figure 2-32 Results of palynological study of the Rijwijk (RWK-01) core scaled against the carbon isotope record. From left to right: (I) The composition of the organic material (%) (II) the composition (%) of the palynological associations (III) the composition of the sporomorph associations and (IV) the concentration of palynomorphs/g. The shading indicates the paleo-environmental zonation discussed in the text.

All samples yielded abundant organic matter. Note that the stratigraphic record is truncated between 2110 and 2108 m depth, where the pre-TOAE sediments of the Aalburg Fm. underly sediments corresponding to the "body" of the negative carbon isotope excursion (T2). The remainder of the record corresponds to the CIE-recovery and the post-CIE interval (T3 through T6). From base to top, a trend is observed from organic matter assemblages with abundant palynomorphs, such as dinoflagellate cysts and pollen and spores (RIJS-A, Aalburg Fm.) towards organic matter assemblages that are dominated by SOM (RIJS-C to RIJS-G) corresponding to the CIE (Isotope Zones T2 to T4). In these intervals, we note quite some variability in the organic matter type and palynomorphs associations, with varying abundance of sporomorphs, *Tasmanites* and presence of SOM Type-1 and SOM Type-2. Organic matter assemblages with abundant palynomorphs, indicating more normal marine conditions only occur way above the CIE (Isotope Zone T6). We also note that the absolute abundance of palynomorphs is consistently elevated during the inferred high-productivity zones manifested by dominance of SOM.

RIJS-A: 2120.7 – 2116.4 m

Age: ?Pliensbachian, predates T-OAE

Organic Matter Assemblages:
Palynomorphs and wood-remains are dominant. Very few SOM-Type 1 particles are recorded.

Palynomorph Assemblages:
Sporomorphs are dominant, the presence of dinocysts and acritarchs increases throughout the interval, but do not become abundant. Bisaccate pollen and *Chasmatosporites* spp. are the dominant pollen types.

RIJS-B: 2110.4 m

Age: ?Pliensbachian: predates T-OAE.

Organic Matter Assemblages:
Palynomorphs are dominant. SOM-Type 1 is also recorded but not dominantly. Wood-fragments are present in low quantity.

Palynomorph Assemblages:
The high abundance of the prasinophyte algae *Tasmanites* and to a lesser extent *Pterospermella* characterize this interval. Acritarchs, dinocysts, spaericals and sporomorphs are also present.

RIJS-C: 2107.7 – 2106.5 m

Age: T2

Organic Matter Assemblages:
This interval is dominated by SOM-Type 1. The number of palynomorphs increases up-section, these predominantly reflect sphaericals. Wood-remains are consistently present in low abundance.

Palynomorph Assemblages:
The lowermost sample at 2107.7 m is dominated by *Tasmanites* (90%). In the overlying samples sphericals are dominant (80-90%). Sporomorphs are consistently abundant (~20%), and predominantly constitute *Classopollis* spp. Remarkably, the prasinophyte *Pterospermella* is also recorded abundantly (10%). Acritarchs are consistently present, but dinocysts are not recorded.

RIJS-D: 2106.1 – 2104.2 m

Age: T2

Organic Matter Assemblages:
This interval is characterized by high abundance of both SOM-Type 1 and Type 2 (together about 70%). There is a clear peak in the presence of palynomorphs at 2104.6 m reaching 60%. Wood-remains are consistently present in low abundance.

Palynomorph Assemblages:
Overall sphaericals are dominant, but spormorphs episodically increase at their expense. *Tasmanites* and acritarchs are both consistently present (<10%). Pterospermella is no longer recorded. The increase in palynomorphs at 2104.6 is caused by a major increase in various sporomorphs; *Classopollis* spp., *Chasmatosporites* spp., bisaccates and *Cerebropollenites* spp.

RIJS-E: 2103.2 – 2102.2 m

Age: T3

Organic Matter Assemblages:
SOM-Type-1 is dominant (70%), SOM-Type 2 is no longer recorded. Palynomorphs constitute about 20%.

Palynomorph Assemblages:
Tasmanites is now more abundant (30%), sphaericals remain dominant. Sporomorphs are consistently present (~10%). Very low numbers of acritarchs are recorded.

RIJS-F: 2101.3 – 2095 m

Age: T3-T4

Organic Matter Assemblages:
SOM Type 1 and Type 2 are dominant. Palynomorphs are quite abundant as well. These are predominantly sphaericals occurring in the dense SOM-clusters under UV-illumination.

Palynomorph Assemblages:
Sphaericals are dominant. Sporomorphs (predominantly *Classopollis*) wax and wane episodically in abundance (~20 %). Acritarchs are hardly recorded. *Tasmanites* is consistently present in low abundance.

RIJS-G: 2094.6 – 2085.4 m

Age: T5

Organic Matter Assemblages:
SOM-Type 1 is now dominant, SOM-Type 2 is now absent. Palynomorphs increase, decrease and then increase again throughout the interval, reaching a maximum of about 30%. Wood-fragments are quite abundant too (10%).

Palynomorph Assemblages:
Sphaericals continue to be dominant. Remarkably, acritarchs and dinocysts are now again recorded quite consistently as is *Tasmanites*. Sporomorphs are also more abundant (up to 20%) wax and wane episodically, with minima at 2091.5 m and 2085.4 m.

RIJS-H: 2080.8 – 2080.5 m

Age: T6

Organic Matter Assemblages:
There is a clear appearance of a new organic-matter type; fine translucent clusters of fluorescent organic-material (referred to as "fluffy"). The biological affinity of this type remains unknown. It is possible that these fragments represent degraded parts of larger marine palymomorphs like dinocysts. SOM Type 1 remains dominant. Palynomorphs represent 20% of the organic matter particles.

Palynomorph Assemblages:
The palynomorphs associations reflect high abundance of *Tasmanites* (30%). Sphericals remain dominant, sporomorphs constitue ~10% of the assemblage. Acritarchs and dinocysts are present but not recorded in substantial abundance.

RIJS-I: 2079.7 – 2075.1 m

Age: T6

Organic Matter Assemblages:
SOM-Type-1 remains the dominant OM-type. Palynomorphs and the fluffy material are also abundant. Wood-fragments are consistently present.

Palynomorph Assemblages:
Acritarchs and dinocysts increase substantially in abundance, reflecting the return of more normal marine conditions. Sphaericals and sporomorphs are also dominantly to abundantly recorded.

Conclusions

- A first striking observation is that, given the overall strong dominance of SOM, the depositional environment of the Rijswijk core is subjected to "persistent strong to extreme stratification and productivity". This implies that this regime is sustained a lot longer than for the UK-section. This is supported by the observation of substantially elevated numbers of recovered palynomorphs per gram of sediment (Figure 2-32), showing that the SOM-clusters not simply dilute the signals of the palynomorphs.

- The most severe high productivity is characterized by RIJS-D and RIJS-F, corresponding to the maximum CIE and its recovery (**Isotope Zones T2-T4**). A distinct *Tasmanites* peak is found near the base of the equivalent T2-Isotope Zone, indicating that the chemocline moves into the photic zone. High-order changes between the presence of sphaericals, SOM-Type-1, SOM-Type-2 and the presence of *Tasmanites* are interpreted to reflect subtle migrations of the chemocline in- and out of the photic zone.

- Above the recovery (**Isotope Zone T5**), minor occurrences of acritarchs and dinocysts are recorded. These probably indicate that the chemocline moved below the photic zone and thus reflect an initial return towards more normal marine conditions. A next major step is recorded at about 2081 m, where marine palynomorphs become more prominent.

- High abundance occurrences of *Tasmanites*, indicating strong surface water stratification associated with transitional environments are recorded in the lower part of the maximum isotope excursion (**Isotope Zone T2**), at the base of the CIE-recovery (**Isotope Zone T3**) and near the X-event (**Isotope T6**).

- Below the fault that truncates the basal part of the CIE, conditions are shallow marine with substantial fluvial influence, as reflected by diverse pollen- and spore assemblages. It appears that the top of the section (RIJS-I) is more marine (i.e., in a more distal depositional setting) than the base (RIJS-A).

- In contrast Loon op Zand and Whitby, the CIE and post-CIE interval at Rijswijk are characterized by pollen and spore assemblages that are dominated by *Classopollis*, rather than *Cerebropollenites* and *Chasmatosporites*. *Classopollis* typically indicates relatively arid hinterland conditions. Given the overall low relative abundance of sporomorphs at Rijswijk an alternative explanation may be that fluvial influence is limited.

2.4.3.3 F11-01

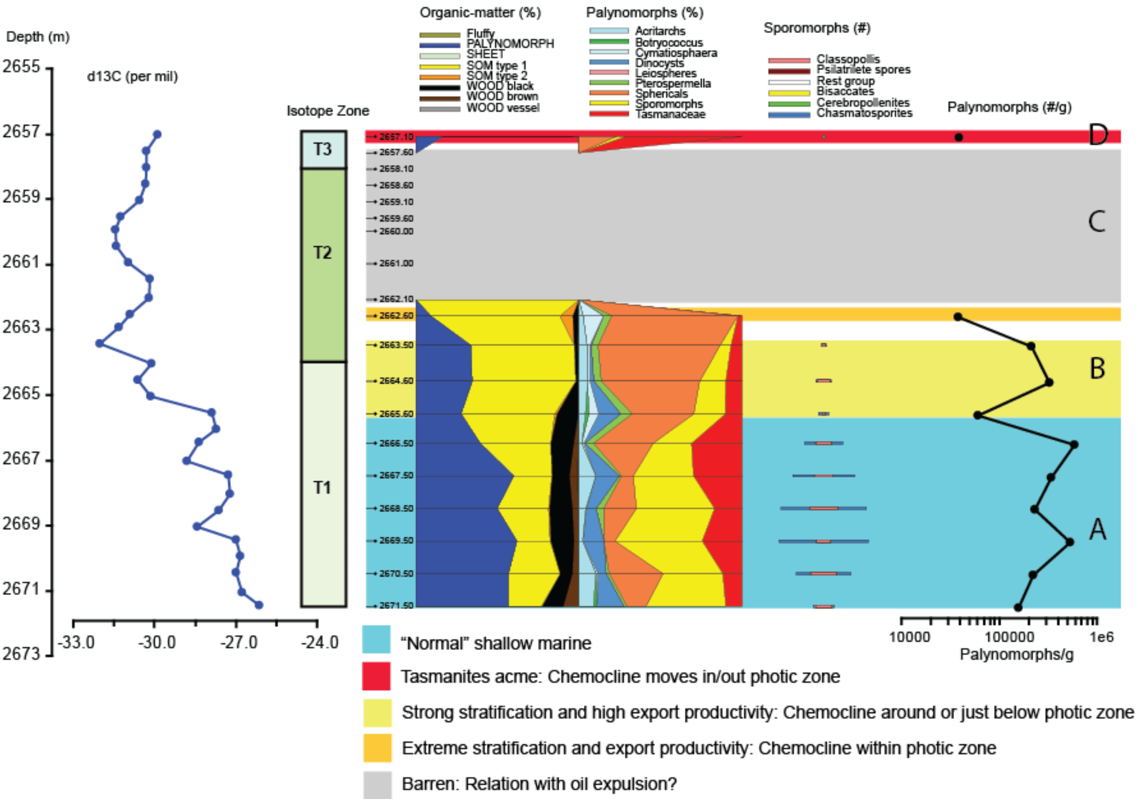

Figure 2-33 Results of palynological study of the F11-01 core scaled against the carbon isotope record. From left to right: (I) The composition of the organic material (%), (II) the composition (%) of the palynological associations, (III) the composition of the sporomorph associations and (IV) the concentration of palynomorphs/g. The shading indicates the paleo-environmental zonation discussed in the text.

We have analysed 19 samples for palynological organic-matter typing. In order get control on trends in the concentration of the palynomorphs a known number of exote *Lycopodium* spores were added to a known sample mass (Figure 2-33).

The cored section from well F11-01 corresponds to the lower half of the CIE; i.e., the initial shift (Isotope Zone T1), maximum CIE (Isotope Zone T2) and the start of the CIE-recovery (Isotope Zone T3). Below 2662.1 m depth, samples yield abundant organic matter but between 2662.1 and 2657.6 no palynomorphs are recorded. Here, only highly degraded SOM is found. From base to top, a trend is observed from organic matter assemblages with abundant palynomorphs, such as dinoflagellate cysts and pollen and spores (F11-A) towards organic matter assemblages that are dominated by SOM (F11-B) and sphaericals as dominant palynomorphs. Above the barren interval (F11-C), albeit poorly preserved the uppermost sample yields dominant of *Tasmanites* (F11-D). In contrast to Rijswijk, the absolute abundance data (palynomorphs/g) remain relatively stable through the basal part of the record. There is a clear imprint of diminished preservation for the upper two productive samples.

F11-A: 2671.5 – 2666.5 m

Age: T1

Organic Matter Assemblages:
Palynomorphs are the dominant organic matter-type. Towards the top of the interval, SOM Type-1 increases in abundance. Wood-fragments are consistently present.

Palynomorph Assemblages:
The palynomorph assemblages are relatively diverse, constituting abundant proportions of acritarchs, dinocysts, sporomorphs and *Tasmanites*. The relatively high proportions of *Tasmanites* indicate that at least seasonally stratification persisted. The sporomorph associations are dominated by *Chasmatosporites* spp..

F11-B: 2671.5 – 2666.5 m

Age: T1-T2

Organic Matter Assemblages:
SOM-Type-1 is now the dominant OM-type and its abundance increases through the interval to >90%. Wood-fragments decrease substantially in abundance and now occur sporadically.

Palynomorph Assemblages:
Sphaericals are the dominant palynomorphs and increase further in abundance throughout the interval, mainly at the expense of sporomorphs. Dinocysts are no longer recorded. The uppermost sample is already affected by signs of dissolution and also yields a substantially lower absolute palynological yield (#/g).

F11-C: 2662.1 – 2657.6 m

Age: T2-T3

Organic Matter Assemblages:
The organic-matter is degraded and reflecting signs of dissolution, perhaps related to oil-generation and/or expulsion.

Palynomorph Assemblages:
No palynomorphs are preserved.

F11-D: 2657.1 m

Age: T3

Organic Matter Assemblages:
The organic matter assemblages are dominated by SOM-Type-1, approximately 20% palynomorphs are found. Few wood particles complete the assemblage.

Palynomorph Assemblages:
Tasmanites dominates the palynological assemblage (80%). The remainder consists of sphaericals. Many palynomorphs remain reveal signs of dissolution. The absolute abundance of palynomorphs is remarkably low.

Conclusions

- The record from F11-01 reflects the gradual transition from relatively normal marine conditions during the initial stages of the CIE (**Isotope Zone T1**) into the strongly stratified high productivity regime. *Tasmanites* spp. is continuously present reflecting that the chemocline fluctuated around the photic zone. Pollen and spore assemblages are dominated by *Chasmatosporites* and *Classopollis*, indicating relatively arid hinterland conditions.

- During maximum excursion values (**Isotope Zone T2**) the typical high-stratification and productivity regime as recorded elsewhere is observed. The barren interval possibly relates to oil expulsion during this interval.

- The topmost sample, corresponding to the initial recovery of the CIE (**Isotope Zone T3**) is characterized by a prominent *Tasmanites* acme, suggesting a time-equivalent change in stratification regime as observed at the other sites.

2.4.3.4 Loon op Zand (LOZ-01)

Palynological results from LOZ-01 are based on an internal TNO Report (Verreussel et al., 2011). By the time, the analyses were not carried out using the new UV-method so a direct comparison with Whitby, Rijswijk-01 and F11-01 is not possible, especially with regards to the distribution of SOM and fluorescent sphaericals and acritarchs. Nevertheless, we were able to apply the same colour coding for the biofacies intervals based on these data (Figure 2-34). An exception is the interval that is massively dominated by sporomorphs corresponding to the recovery of the CIE (shaded in green). The record is spans the entire CIE.

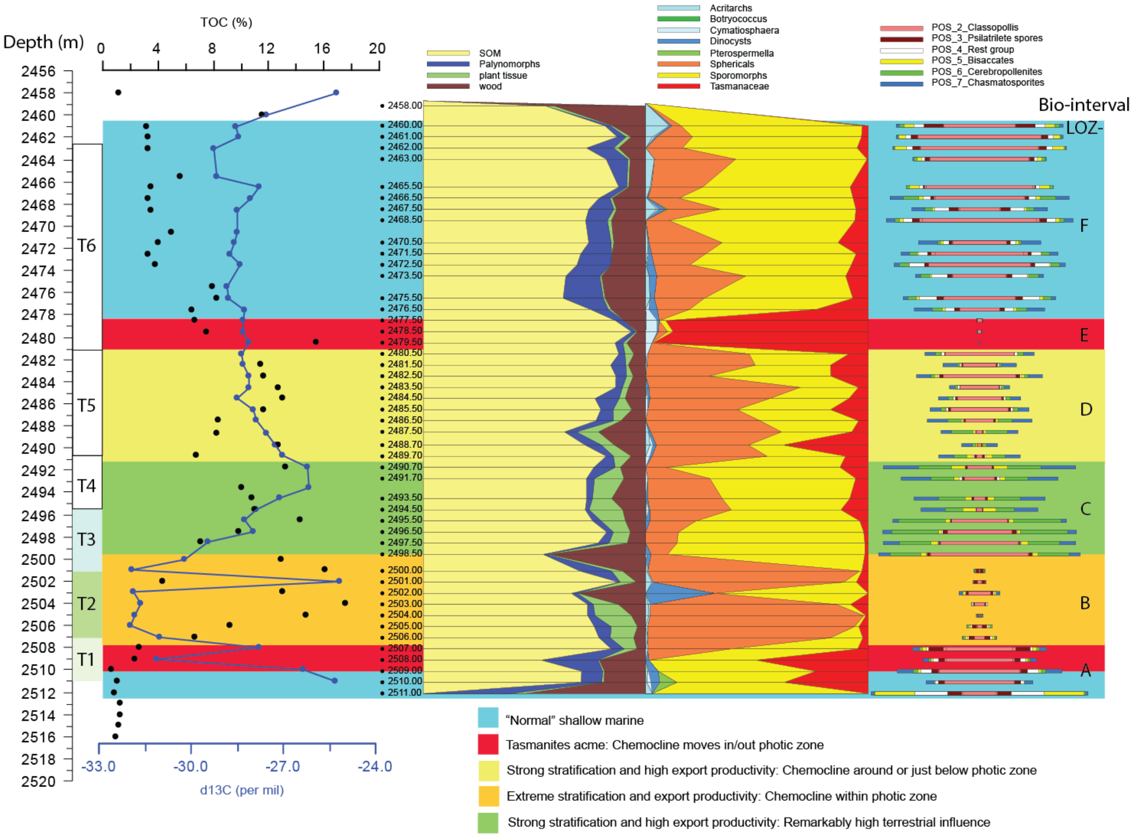

Figure 2-34 Results of palynological study of the Loon op Zand (LOZ-01) scaled against the carbon isotope and TOC records. From left to right: (I) The composition of the organic material (%) (II) the composition (%) of the palynological associations (III) the composition of the sporomorph associations. The shading indicates the paleo-environmental zonation discussed in the text.

LOZ-A: 2511 m

Age: T1

Organic Matter Assemblages:
SOM is dominant but substantial amounts of wood remains are also recorded.

Palynomorph Assemblages:
Tasmanites increases up-section, becoming dominant. Dinocysts are rare but consistently present.

LOZ-B: 2508-2511 m

Age: T2-T3

Organic Matter Assemblages:
SOM remains dominant. Wood-remains and plant-tissue increase throughout this interval

Palynomorph Assemblages:
Two acmes of sphericals are recorded in this interval. The interruption represented by the incursion of dinocysts corresponds to an outlier in the $\delta^{13}C$ values as well, this sample is suspect.

LOZ-C: 2500-2507 m

Age: T3-T4

Organic Matter Assemblages:
SOM remains dominant. Wood-remains and plant-tissue remain abundant throughout this interval.

Palynomorph Assemblages:
Both sphericals and Tasmanites are common, but not superabundant. Sporomorphs are dominant and show a strong increase in Cerebropollenites. Also Chasmatosporites increases, both at the expense of Classopollis.

LOZ-D: 2490-2498 m

Age: T5

Organic Matter Assemblages:
SOM remains dominant. Wood-remains and plant-tissue decline in abundance throughout this interval.

Palynomorph Assemblages:
Sphericals are dominant again Cerebropollenites decreases in relative abundance.

LOZ-E: 2480.5-2489.7 m

Age: T5-T6

Organic Matter Assemblages:
SOM is dominant.

Palynomorph Assemblages:
A massive acme of Tasmanites is recorded in this interval. Acritarchs and sporomorphs are rare.

LOZ-F: 2477.5 – 2479.5 m

Age: T6

Organic Matter Assemblages:
SOM remains dominant but palynomorphs become abundant again.

Palynomorph Assemblages:
Sporomorphs are now dominant. Dinocysts and acritarchs are recorded consistently and sphaericals remain abundant. A gradual increase of Classopollis is observed, from 40 to 75%, likely reflecting the shift to more arid hinterland conditions.

Conclusions

- Although the palynological analyses from Loon op Zand were not carried out using the same gentle processing techniques and using UV-fluorescence microscopy, useful and important trends can be deducted. A careful re-investigation remains however desired but exceeds the scope of this project.

- Before the isotope shift, relatively shallow marine conditions prevail; the pollen- and spore assemblages indicate fluvial influence from a relatively arid hinterland. The water column was not stratified nor characterized by elevated primary productivity.

- During **Isotope Zone T1** the chemocline shoaled into the photic zone and an extremely stratified and productive surface-water regime was installed subsequently. This regime was maintained during the maximum CIE interval (**Isotope Zone T2**) and the initial recovery (**lower Isotope Zone T3**). Given the overall absence of dinocysts and the dominance of sphaericals it appears that the chemocline remained within the photic zone. It is not clear what happens in terms differences in terrestrial influence because the high abundance of sphaericals may have overwritten the relative abundance of sporomorphs.

- A clear increase of sporomorphs at the expense of sphaericals is recorded equivalently to the isotope recovery phase (**upper Isotope Zone T3 and T4**). These sporomorph associations indicate relatively humid conditions (more *Cerebropollenites* and *Chasmatosporites* than *Classopollis*). The relatively high abundance of *Tasmanites* indicates that the chemocline fluctuated just below the photic zone. Hence, it appears that stratification and marine productivity diminished slightly and that terrestrial influence has increased locally.

- Equivalent to **Isotope Zone T5**, increased presence of sphaericals likely indicates somewhat stronger marine stratification and/or a demise in fluvial influence. The chemocline fluctuates around the photic zone.

- At the base of **Isotope Zone T6**, the chemocline moves through the photic zone again given the acme of *Tasmanites*, subsequently stratification diminishes given the return of dinocysts and acritarchs and the absence of *Tasmanites*. Fluvial influence becomes more prominent and the hinterland assemblages are more characterized by arid *Classopollis*.

2.5 Organic Geochemistry

The organic geochemistry was executed in cooperation with the RWTH Aachen University in the context of the PhD thesis of Jinli Song. The results presented here are part of her PhD thesis and publications and are therefore until their publication (expected in December 2015) confidential.

2.5.1 Methodology (as described in Song et al. in prep)

2.5.1.1 Bulk elemental compositions

Total organic carbon (TOC) and total inorganic carbon (TIC) contents were measured on all samples from the SA and FA of SW-Germany, Runswick Bay of UK, LOZ-1 of NL using a temperature ramp method, without previous acidification, in a liquiTOC II analyzer which enables a direct determination of TOC and TIC. Aliquots of approx. 100 mg of rock powder were heated (300°C/min) and held at 550°C for 600 seconds during which the TOC peak was recorded. The temperature was then raised to 1000°C and held for 400 seconds during which the TIC was recorded. The released CO_2 at every heating stage was measured with a non-dispersive infra-red detector (NDIR) (detection limit 10 ppm; TOC error 0.6%; TIC error 1.7%). The $CaCO_3$ content was calculated, assuming that most of the inorganic carbon (TIC) is locked in calcite, using the formula $CaCO_3 = TIC \cdot 8.333$. Total sulfur (TS) content was measured in all samples using a Leco S200 analyzer (detection limit 20 ppm; error < 5%).

2.5.1.2 Rock-Eval pyrolysis

Selected samples covering the entire section for each locality were analyzed by Rock-Eval pyrolysis performed with a DELSI INC Rock-Eval VI instrument according to guidelines published by Espitalié et al. (1985) and Lafargue et al. (1998). About 100 mg of powdered sample were used for TOC contents ranging between 2 and 8%, whereas 50 mg were used for those between 8 and 20%.

2.5.1.3 Organic petrography

Whole-rock core samples were embedded in resin in an orientation perpendicular to bedding for microscopic analyses, prepared according to Littke et al. (2012). Organic petrographic analyses were carried out on a Zeiss Axio Imager microscope for measurement of vitrinite reflectance (VRr) and maceral analyses in reflected white light and incident light fluorescence mode.

2.5.1.4 Gas chromatography-flame ionization detector (GC-FID)

Approx. 10 g of each powdered sample were extracted by ultra-sonication with 40 ml dichloromethane. Polarity chromatography induced fractionation was performed over a fused silica packed baker bond column into three fractions using 5 ml pentane for the aliphatic hydrocarbons, 5 ml pentane/DCM (40:60) for the aromatic hydrocarbons and 5 ml methanol for the resins and asphaltenes. GC-FID analysis was carried out for the saturated fraction on a Fisons Instruments GC 8000 series equipped with split/splitless injector and a flame ionization detector using a Zebron ZB-1 capillary column (30m length, 0.25mm i.d., 0.25µm film thickness). Chromatographic conditions were: 1 µL split-splitless injection with a splitless time of 60s; temperature program: 80 °C for 5 min, then programmed at 5 °C /min to 300 °C and held for 20 min.

2.5.2 *Results*

2.5.2.1 *Bulk elemental composition and Rock-Eval pyrolysis*

TOC, TIC, TS and Rock-Eval results are available for samples from Whitby and LOZ-01, measured by Jinli Song in the context of her PhD thesis, further results for Whitby, L05-04, F11-01 and Luxembourg were collected from literature (French et al., 2014, Trabucho-Alexandre et al., 2012, Song et al., 2014, Salem, 2013, nlog.nl)

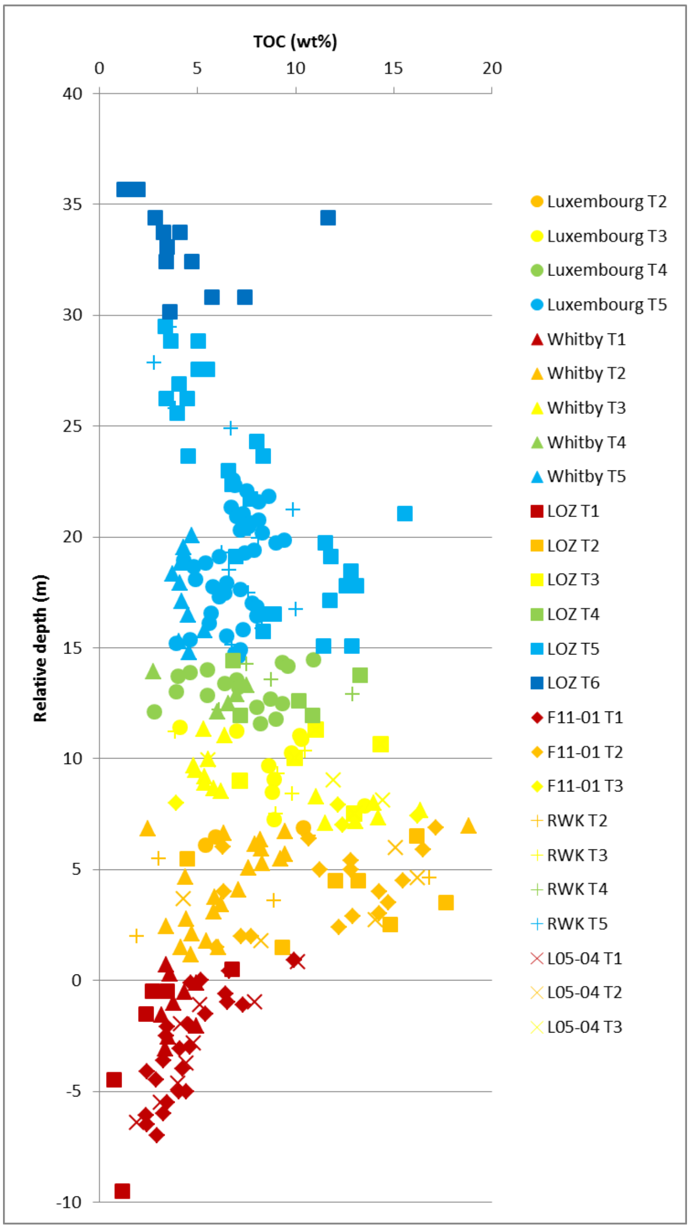

Figure 2-35 Measured TOC for all studied sections against relative depth, subdivided into different Isotope zones T1 to T6

In all studied sections TOC increases drastically from zone T1 to T2. The maximum values are measured in zones T2 and T3 with values of up to ~19 %. In the upper zones T4 and T5 TOC values return to around 5 % in Whitby while they stay higher (around 10 %) in all locations in the Netherlands until it also returns to values below

5 in the upper part of zone T5 and T6. Measured TOC in the well in Luxembourg is lower in general (maximum ~13 and an average of 8).

2.5.2.2 *Maturity and type of organic matter*

Vitrinite reflectance was measured on samples from Whitby, LOZ-01, L05-04 and F11-01. Measuring vitrinite reflectance in marine shales is usually difficult as vitrinite is a land plant particle which can be rare in these type of sediments. More conclusive are the results of the Rock-Eval T_{max} measurements, which however have to be interpreted together with the source rock type (Tissot and Welte, 1984).

Measured vitrinite reflectance for F11-01 is 0.23 %Ro which is extremely low and cannot be considered to be accurate. T_{max} values are on average 439 ºC which is considered to be in the early oil window. On the other hand measured vitrinite reflectance from well L05-04 is 0.95 %Ro which is oil window maturity, T_{max} values however show a much lower maturity of 428 ºC, which is considered to be still immature. For the other two locations LOZ-01 and Whitby both methods show comparable results, Whitby has an average vitrinite reflectance of 0.55 %Ro and a T_{max} of 433 ºC while the results for LOZ-01 are slightly lower with an average vitrinite reflectance of 0.49 %Ro and T_{max} of 427 ºC. Both locations are therefore considered immature for hydrocarbon generation.

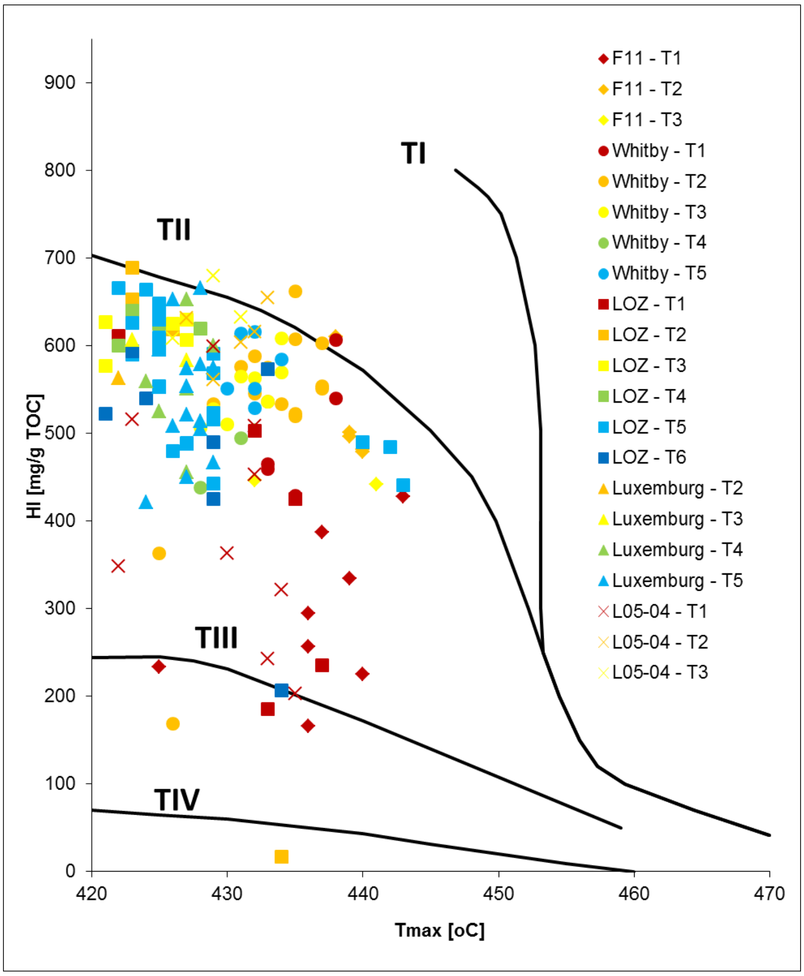

Figure 2-36 HI – T_{max} crossplot showing source rock quality and maturity for the different locations and time zones

The general maturity trend based on the T_{max} measurements LOZ<L05-04<Whitby<F11-01 can also be seen in the T_{max}/HI plot (Figure 2-36) that shows the type of organic matter and the respective maturity. In this plot it is obvious that in zone T1 a different type of organic matter (type II to III) was deposited with much lower HI values while the values from the other zones plot nicely in the range of a typical type II source rock. The only other exception are three values from zone T4 of LOZ-01 that show significant higher T_{max} values and also corresponding higher vitrinite reflectance. This phenomenon could be related to hot fluids migrating through this zone or localized influence from magmatism, such as the magmatic dyke that was drilled about 100 m further down in the Aalburg Formation.

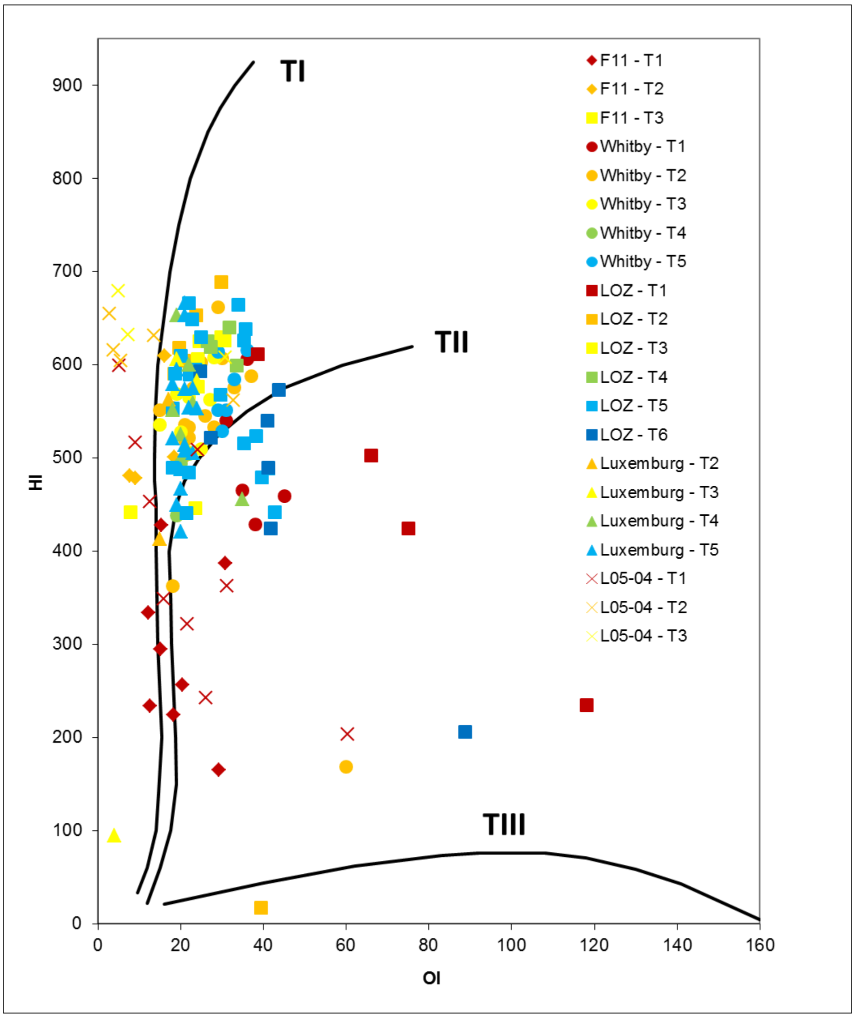

Figure 2-37 Modified van Krevelen diagram showing source rock classification and maturity for the different locations and time zones

Another plot where the type of organic matter can be visualized based on Rock-Eval results is the modified or pseudo van Krevelen diagram where the OI is plotted against the HI (Figure 2-37). For all locations the results of zone T1 plot in an area with lower HI and higher OI which is generally considered to be a type II/III source rock with significant terrestrial input. Most values from zones T2 to T5 plot in part of the diagram that represents type II (marine) source rocks. Some samples, especially those of L05-04 show even lower OI values and might be considered type I source rocks. In the uppermost part of well LOZ-01 the samples show again lower HI and higher OI results which is an indicator for again more influence of terrestrial organic matter and a type II/III source rock.

The HI in well F11-01 is lower than in Whitby or LOZ-01 because of the higher maturity. This source rock in this well has already generated and probably expelled oil, reducing the HI of the source.

2.5.2.3 Biomarkers

Organic geochemical biomarkers were analysed by the RWTH Aachen on samples from Whitby and LOZ-01. During interpretation of the results from LOZ-01 several inconsistencies were recognised in the analysis results, mainly with respect to maturity. Vitrinite reflectance as well as Rock-Eval results show very low maturities while the GC-FID trace of the OM extracts as well as all biomarkers that were analysed show a very mature pattern. After review of the initial drilling documents it was discovered that diesel was added to the mud during drilling of the Jurassic section of LOZ-01. The results of the GC-FID of LOZ-01 are therefore not usable for the purpose of this study as they mainly show the proxies of the diesel-oil that was used during drilling.

We therefore focus on the results of Whitby, where we included results from other published sources as well, to get a better overview of the depositional setting. For this purpose we selected biomarker that record changes in redox conditions.

Homohopane Index

The Homohopane Index (HHI, C_{35}/[C_{31}-$_{35}$] αβ-hopanes; Peters & Moldowan, 1991) is often applied as an indicator of redox conditions in marine sediments. Higher values (> ca. 0.1) are associated with anoxic marine conditions, and are often notable in having the C_{35} hopanes more abundant than the C_{34} homologues (Peters & Moldowan, 1993; Bishop & Farrimond, 1995; Peters et al., 2005).

The Homohopane Index is calculated using the following formula:

$$HHI = C_{35}\alpha\beta(S+R) / (\Sigma C_{31}\text{-}C_{35}\alpha\beta S+R)$$

Equation 2-2 Formula used to calculate the Homohopane Index

There is no absolute value of the HHI for oxic vs. anoxic conditions but generally higher C_{35} compared to C_{34} is an indicator for anoxia. The HHI however does decrease with maturity, making it less reliable for mature source rocks.

The data show a clear transition from the Grey Shales into the Jet Rock (T0 to T1). The samples from the Grey Shales show a clear oxic signal while the results from the Jet Rock are in the transition zone towards clearly anoxic conditions with only a few samples above the 0.1 cutoff.

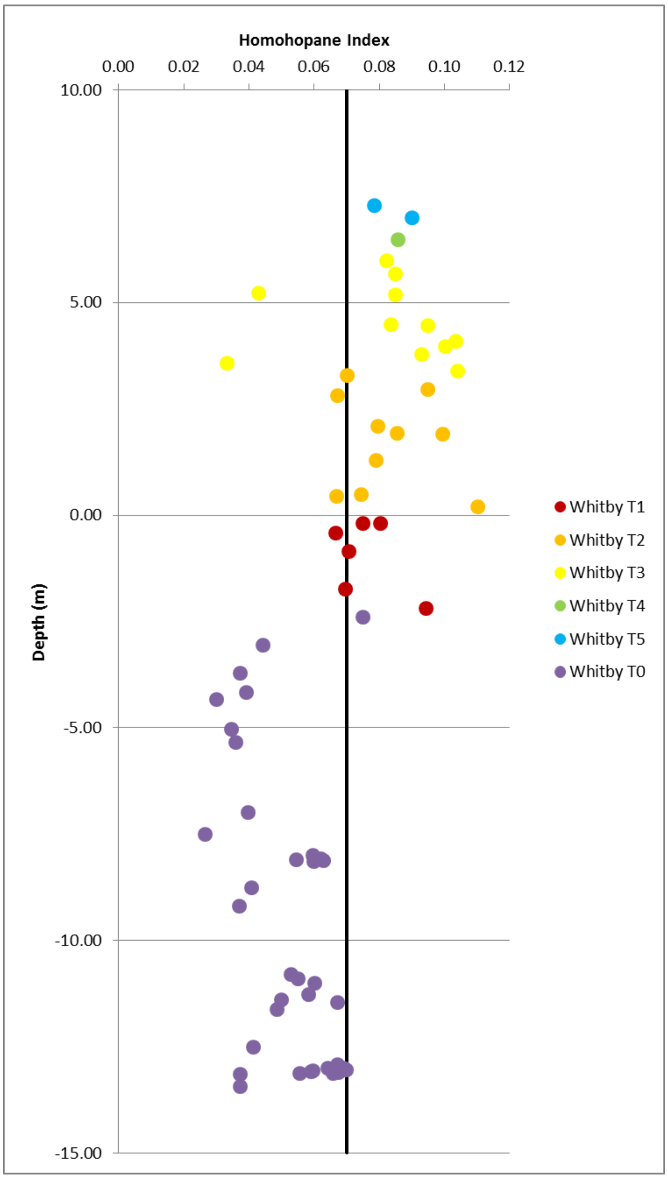

Figure 2-38 Homohopane index against depth for the different timezones of the Whitby section

Pristane/Phytane

Pristane and phytane are two common acylic isoprenoid alkanes. The most abundant source is the phytyl side chain of chlorophyll a in phototrophic organisms and bacteriochlorophylla and b in purple sulphur bacteria. In reducing or anoxic conditions the formation of phytane is favoured while in oxic conditions pristane is formed. The ratio of pristane vs phytane is therefore considered a proxy for depositional redox conditions. However there are a couple of other parameter that influence the pristane/phytane ratio such as variable source input, different rates of early HC generation, variations at higher maturity and analytical uncertainties. In general it can be said that pristane/phytane ratios of < 0.8 indicate saline to hypersaline conditions that are associated with evaporiate and carbonate depositions while ratios of > 3.0 indicate terrigeneous plant input deposited under oxic to suboxic conditions. Everything in between should not be interpreted without additional information (Peters et al. 2005).

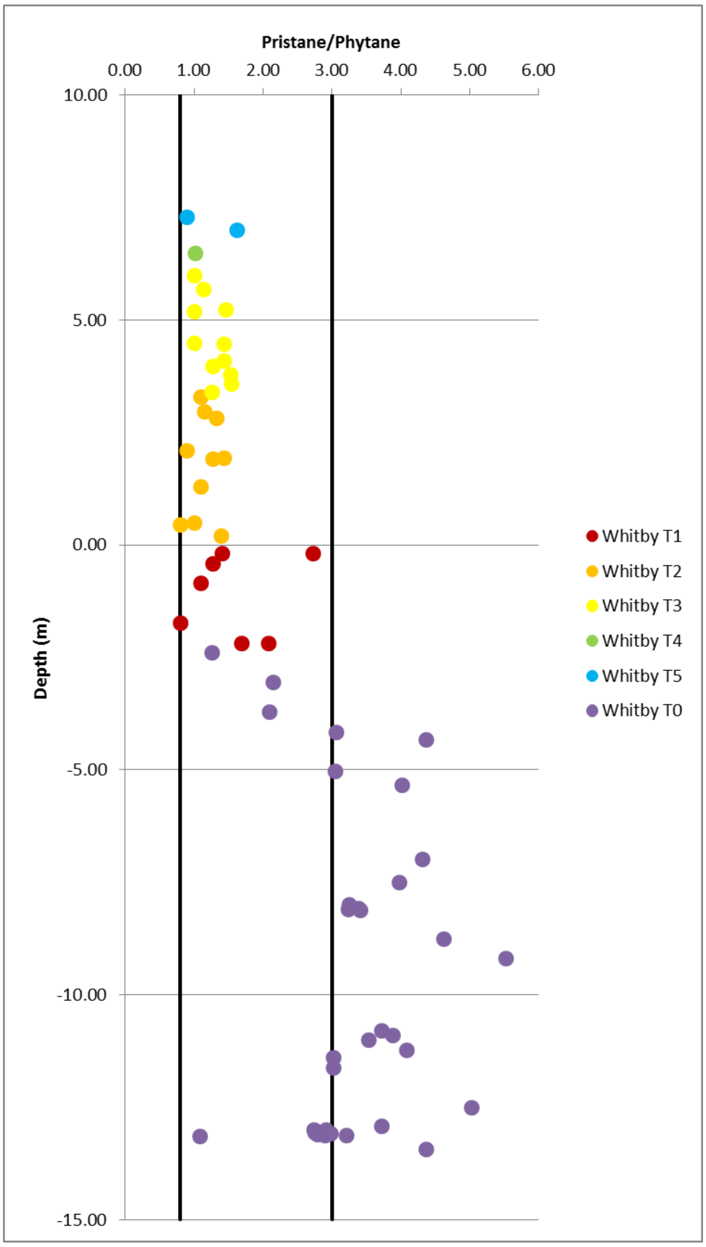

Figure 2-39 Pristane/Phytane against depth for the different timezones of the Whitby section

The pristane/phytane ratios of the samples from Whitby show a clear transition from oxic to suboxic conditions with values well above 3 in the Grey Shales (Zone T0), a transition zone where the pristane/phytane ratio continuously decreases towards the base of the Jet Rock (upper part of T0 and T1) and then stable values around a value of 1. Considering that the general depositional environment of the Jet Rock is neither carbonaceous nor evaporitic, values below 0.8 could not be expected. However a clear trend towards anoxic conditions can be seen.

Isorenieratane

Isorenieratane originates from green sulphur bacteria that indicate, when present in source rock extracts of oils, photic zone anoxia (Peters et al., 2005).

The results from Whitby (data from Salem, 2013) show different amounts of Isorenieratane in the samples, however it is found from the base of zone T1 upwards, throughout the whole of the Jet Rock Formation. In several layers in the Grey Shales Isorenieratane was also found. These layers have been termed Sulphur Bands and are described by Salem (2013) in detail. Isorenieratane was not measured in the samples studied in Aachen, no information about its presence or absence is available for the upper zones.

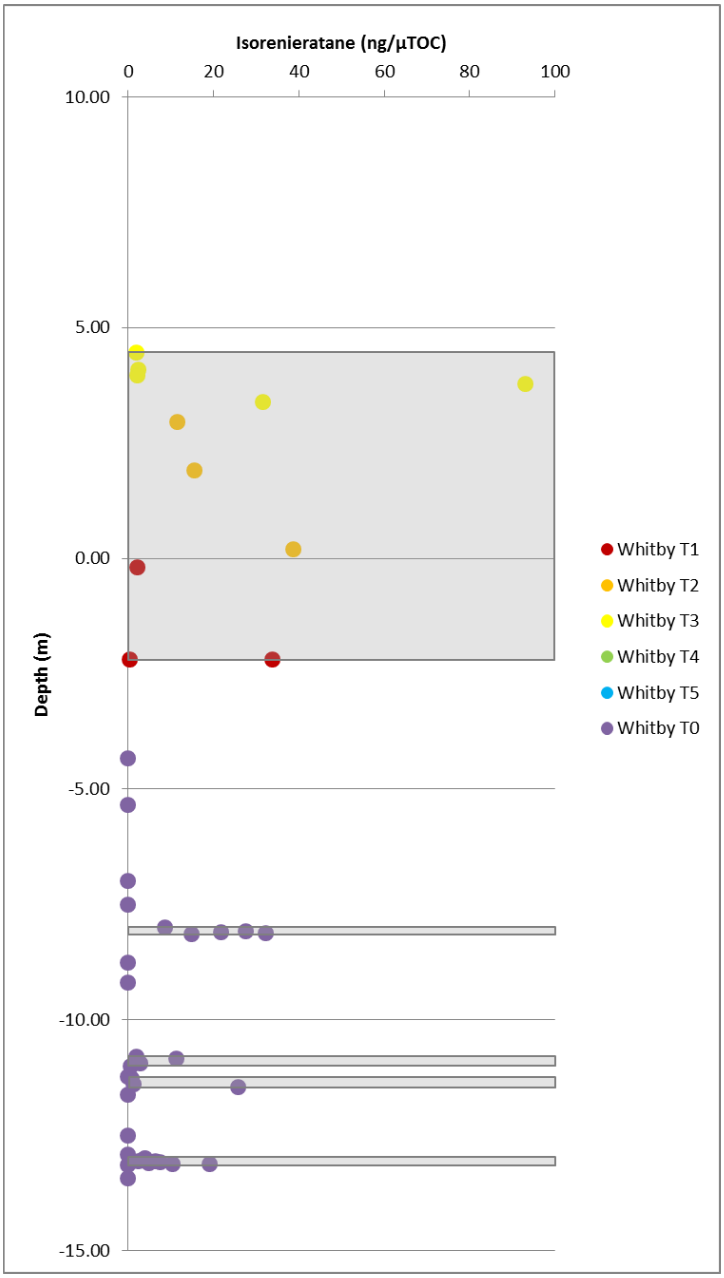

Figure 2-40 Isorenieratane against depth for the different timezones of the Whitby section

Gammacerane Index

Gammacerane is an indicator for a stratified water column either due to hypersalinity at depth or temperature gradient in marine and non-marine depositional environments (Peters et al. 2005). The Gammacerane Index is defined as

GI = 10 x Gammacerane/(Gammacerane + C30 Hopane)

Equation 2-3 Formula used to calculate the Gammacerane Index (GI)

No results for Gammacerane were available for the Grey Shales below the Jet Rock, however, the GI shows an increase from the base of the Jet Rock (zone T0 and T1) towards the top (T2 to 4) suggesting increased stratification of the water column during the CIE.

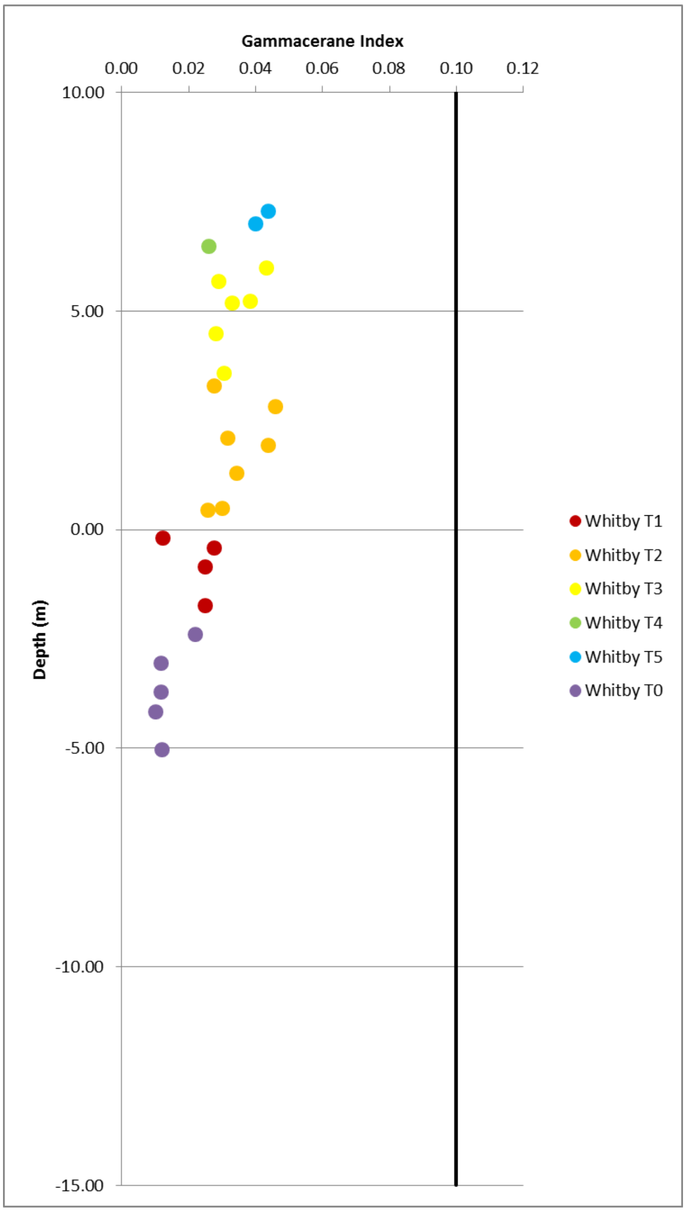

Figure 2-41 Gammacerane index against depth of the different timezones of the Whitby section

2.5.3 *Synthesis*

The results of the organic geochemistry all point to a drastic change in depositional environment at the beginning of the Toarcian from more oxic conditions with influence of terrestrial material to dys- to anoxic conditions with occasional photic zone anoxia. TOC content is highest in isotope zones T2 and T3, which is especially evident in the Whitby section, where TOC levels of up to 19 % were measured at the transition between zones T2 and T3 while it is around 5 % in the rest of the section. Interestingly the biomarker results do not show huge differences in this interval. The Homohopane Index is slightly increased, Isorenieratane levels are highest but this interval does not show a huge shift in depositional environment that could explain the increased TOC levels. The high TOC content however does correlate with changes in the biozones (see chapter 2.4, Figure 2-42) where the TOC peak correlates with biozones orange and red for Whitby and RWK-01 while F11-01 has the highest TOC in zone grey (which appears to be influenced by hydrocarbon generations) and LOZ-01 shows the highest values in zones yellow and green – which can be, however, not be distinguished from zones orange because of the different preparation method..

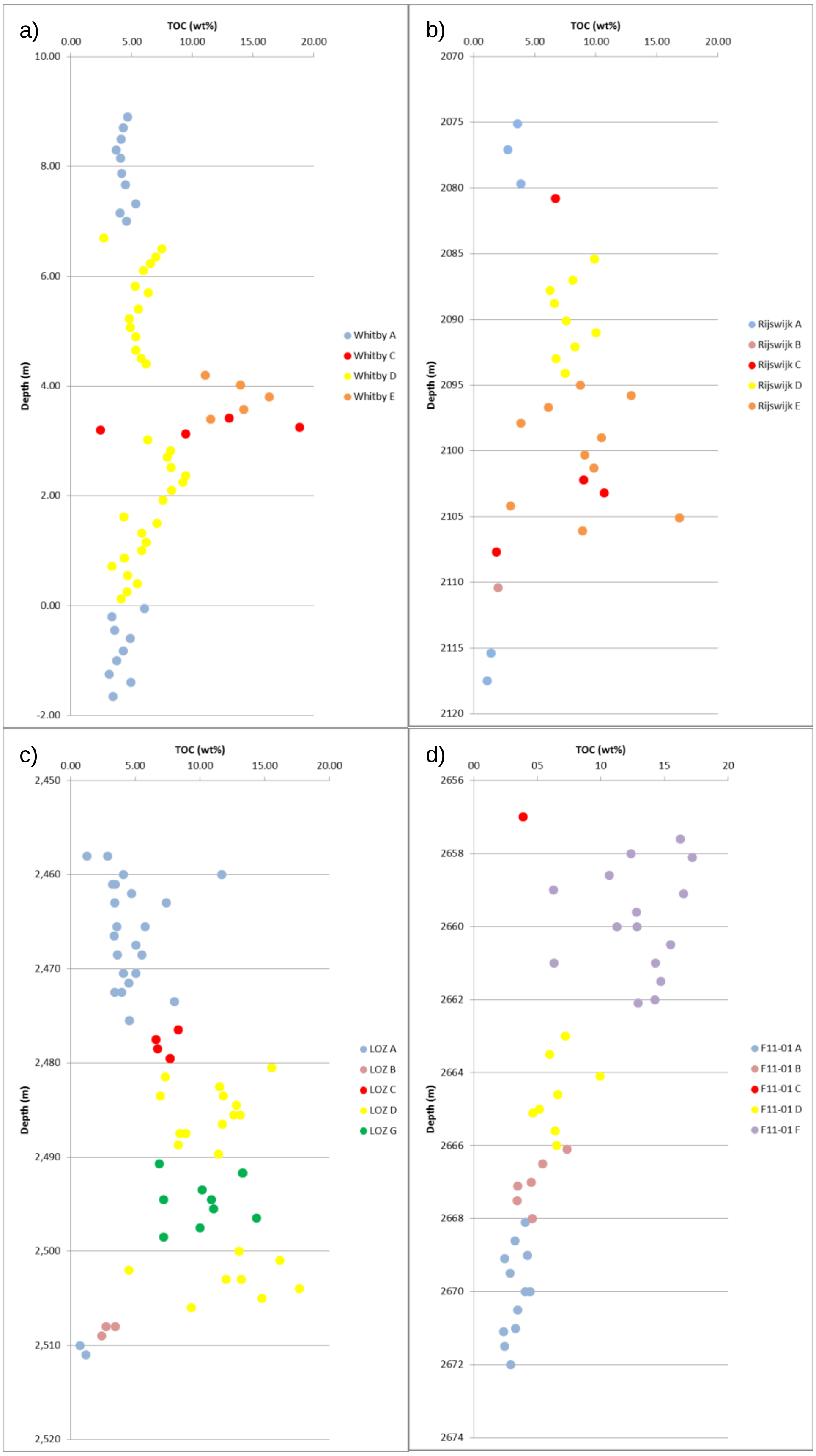

Figure 2-42 TOC content of Whitby (a), RWK-01 (b), LOZ-01 (c) and F11-01 (d) according to the biozones described in chapter 2.4.3.

2.6 Log correlation

The detailed log correlation was performed to get a good overview of the lateral changes of the Posidonia Shale Formation (ATPO) in the Dutch subsurface and to be able to create interpolated thickness and other property maps. For this purpose all exploration wells that drilled through the formation were selected and analysed for log availability and quality.

2.6.1 Methodology

2.6.1.1 Starting points

The starting points for the well log zonation and regional correlation were threefold:

1. Compliance as much as possible with the existing zonation in the Central Graben & West-Netherlands Basin (as defined by Zijp (2010) and ten Veen et al. (2014));
2. Compliance as much as possible with the existing time-zonation based on $\delta^{13}C$ curve in wells RWK-01, LOZ-01, L05-04, F11-01, and the Whitby outcrop;
3. Use as many logs as possible to arrive at a meaningful litho-porosity zonation.

Ad 1) Zijp (2010) defined a subdivision of the Posidonia Shale Formation into four zones, based on the gamma ray, density, and sonic logs: a Basal, Base, Middle, and Upper Zone. This zonation was later refined and extended into a subdivision of six zones. From top to base, these are TP, TZU, TZL, MZU, MZL, BZ.

Ad 2) Five time lines (T1-T5) were defined on the basis of inflection points of the $\delta^{13}C$ curve (See Chapter 2.1). Although in theory the established timelines might well cross lithostratigraphic boundaries, we decided to adopt a 'hemi-pelagic' approach, in which we assign time markers to lithostratigraphic markers, at least in the first stage of the correlation process.

Ad 3) Especially in the West Netherlands Basin where many wells were drilled in the 1950's to 1970's, there are not many wells with a comprehensive log suite. Ideally a log suite would contain a spectral gamma ray log, a bulk density log, a PEF log, a neutron log, a shear sonic log, and a deep and shallow resistivity log. This ideal combination was not encountered in any of the wells that penetrated the Posidonia. Most of the wells had GR, DT, and induction logs. In some wells a neutron-density combination was run, and an occasional well had a spectral gamma ray log. None of the wells had a shear sonic log, which is a pity because of its value for geomechanical characterization.

2.6.1.2 Inventory of wells, logs, and completeness of ATPO

A total of 106 wells were initially selected for Posidonia correlation and mapping of various properties (zone thickness, TOC, brittleness). An initial inventory was made to see whether there were enough logs available for each well to meet the requirements, and also to see whether the reported Posidonia section in each well was large enough to include in the correlation. The basins where Posidonia is found nowadays have been subjected to major tectonic events. Especially the Broad Fourteens Basin has experienced severe structuration. The result is that quite a few wells were discarded because large portions of the Posidonia were faulted out. Other wells were discarded because we found that the official (nlog.nl) stratigraphic interpretation of the Posidonia was probably not correct: in these cases we think there is no Posidonia at all. In total 37 wells were left out of the analysis for the above-mentioned reasons. The remainder of this chapter is based on 69 wells. Figure 2-43 shows a map of the wells eventually used for the correlation.

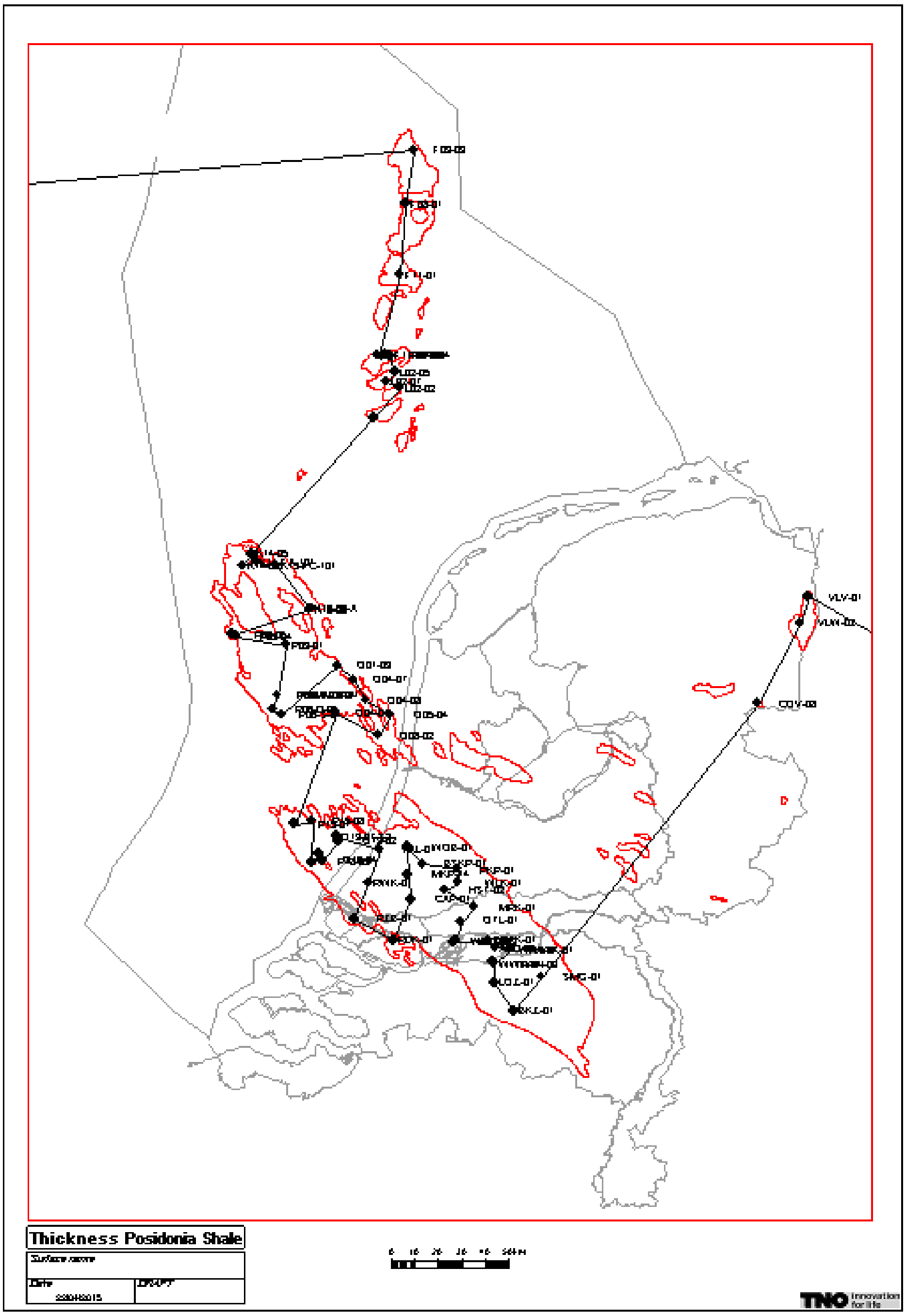

Figure 2-43 Overview of the wells used in the current Posidonia well log correlation

During the inventory of the wells, it became clear that most drilling companies use KCL mud during the drilling of the Lower Jurassic shales. This affects the gamma ray log. In some instances shifts of +70 API units were observed. It will be clear that this will complicate correlation attempts, especially when GR colour coding is used. A provisional workaround was found in a simple subtraction, such that the values of the GR log were more or less the same as those from wells drilled with oil-based mud or just benthonite mud. Later, when all the correlations were established, a more sophisticated method (z-score transform) was used to normalize the gamma ray logs. This will be dealt with later in the report.

Appendix A gives an overview of all the wells that have been included in the correlations; Appendix B contains a list of comments on the presence and quality of the well logs for each well.

2.6.1.3 *Well log interpretation and zonation*

Starting with the existing Zijp-zonation in the West Netherlands Basin, one or more wells were required that had a complete Posidonia section, and enough well logs to make inferences about the lithology, porosity, TOC, etc. In the West Netherlands Basin well MRK-01 amongst others satisfied these constraints. In order to highlight as much as possible the lithological character of the Posidonia, a special well log display was developed, shown in Figure 2-44. This display tries to maximize the information from the various well logs: mineralogy, porosity, and amount of organic matter.

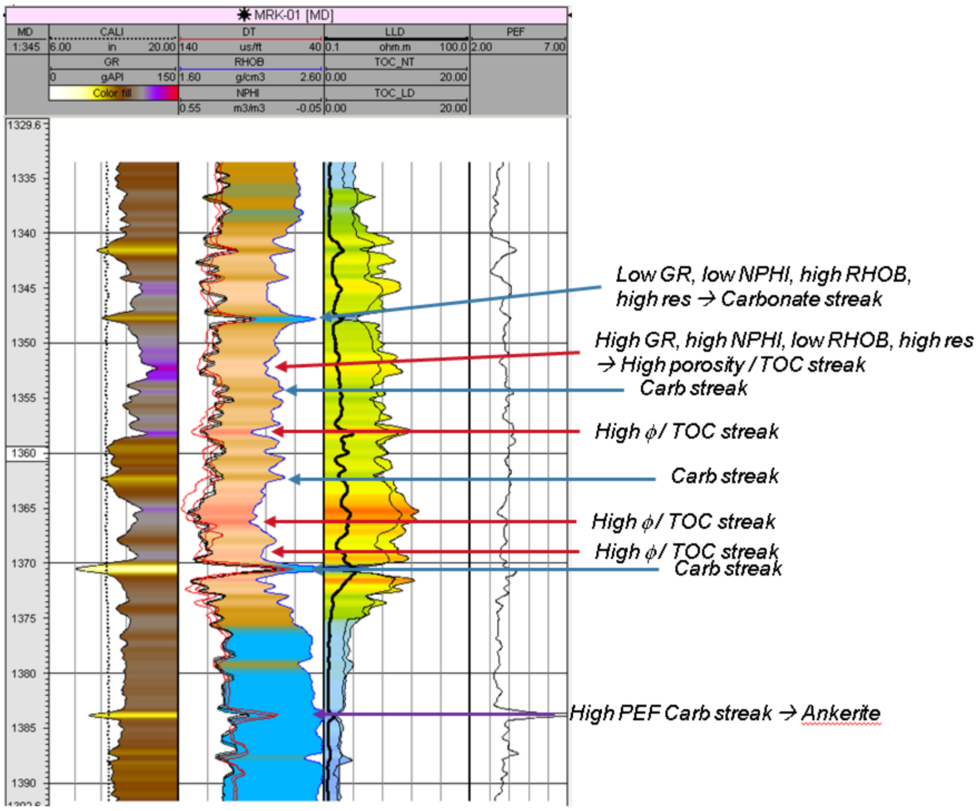

Figure 2-44 Well MRK-01 showing a good suite of well logs through the Posidonia. Track 1: depth in m; track 2: GR with GR colour coding; track 3: DT, RHOB and NPHI with RHOB

colour coding; track 4: TOC calculated by TNO (TNO_LD) and NuTech (TOC_NT), and a deep resistivity log (LLD); track 5: PEF.

Several observations can be made (see Figure 2-44). Firstly, there is a distinct pattern in the gamma ray log (sharp low peaks, sharp high peaks) that corresponds to a pattern of peaks in the porosity logs. Low GR peaks have low neutron porosities and high bulk densities and are interpreted to consist of carbonate streaks, or possibly concretions. Given the relatively low PEF values (around 4.3 Barns/cc) the carbonate is most likely calcite, which has a listed PEF value of 5.1 (Schlumberger, 2009). It cannot be dolomite, as this has a low PEF value of around 3.1.

A remarkable carbonate layer or concretion is found at the base of the Posidonia (in MRK-01 at 1384 m), which has a high PEF value of 7.9, close to the ankerite value of 9.0. The carbonate bed is therefore interpreted to consist of ankerite. At the other end of the spectrum, high GR peaks always coincide with high neutron and low bulk density values plus high resistivity values, and are interpreted to represent high porosity, high TOC streaks. Both types of streaks are rarely more than a meter thick.

Another feature which is readily apparent from Figure 2-45, is that the average porosity increases rapidly from 1380 to 1365 m, decreases somewhat until 1360 m, then remains more or less constant up to the top of the Posidonia (around 1337 m). It is also apparent that this porosity pattern is more or less independent from the GR log.

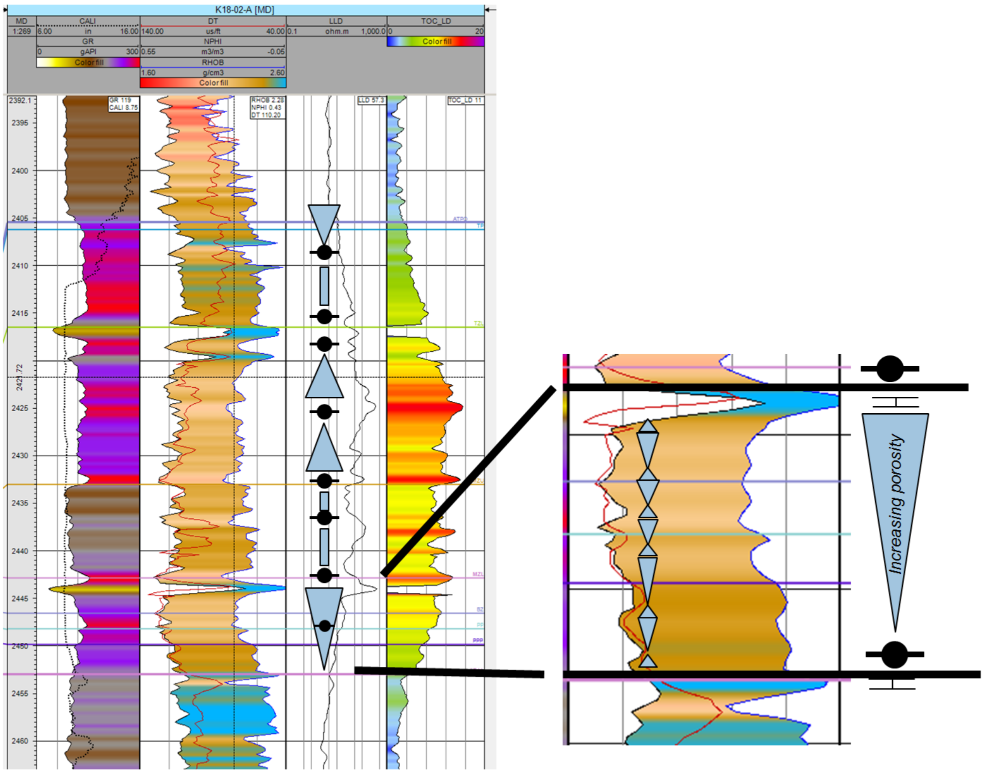

Figure 2-45 Well K18-02-A showing well-developed well log patterns in the Posidonia, which form the basis for the log zonation and correlation. Blue triangles denote porosity patterns. See text for explanation.

The porosity patterns through the Posidonia are illustrated in more detail in well K18-02-A (Figure 2-45). Building upon the carbonate streaks, the high por / high TOC streaks, and the porosity development the following observations were made.
The Posidonia Shale is made up of packages of a few meters thick (in K18-02-A on average five meters), which start and end in a high porosity, high TOC streak of around a meter thickness. Carbonate streaks usually occur just below the high por-high TOC streaks. It should be noted that most of the carbonate streaks occur either in the lower packages of the Posidonia, or in the upper packages. Carbonates are only rarely developed in the middle packages.

In total, nine of these packages were recognized, and these form the basis for the log zonation as well as for the regional well-to-well correlation.

The porosity development in each of these packages can vary. The lowest package displays a clear upward increase in porosity, but others show an upward decrease, or remain stable.

Another interesting observation is the smaller-scale cyclicity of the porosity in these packages. Each package has four to six of these cycles; the neutron porosity varies from peak to trough by about two porosity units. These small-scale cycles have been previously described in this interval by Kemp et al. (2005) and Boulila et al. (2014). They attributed the phenomenon to Milankovitch cyclicity, most notably the precession and obliquity periods. This will be elaborated in more detail below.

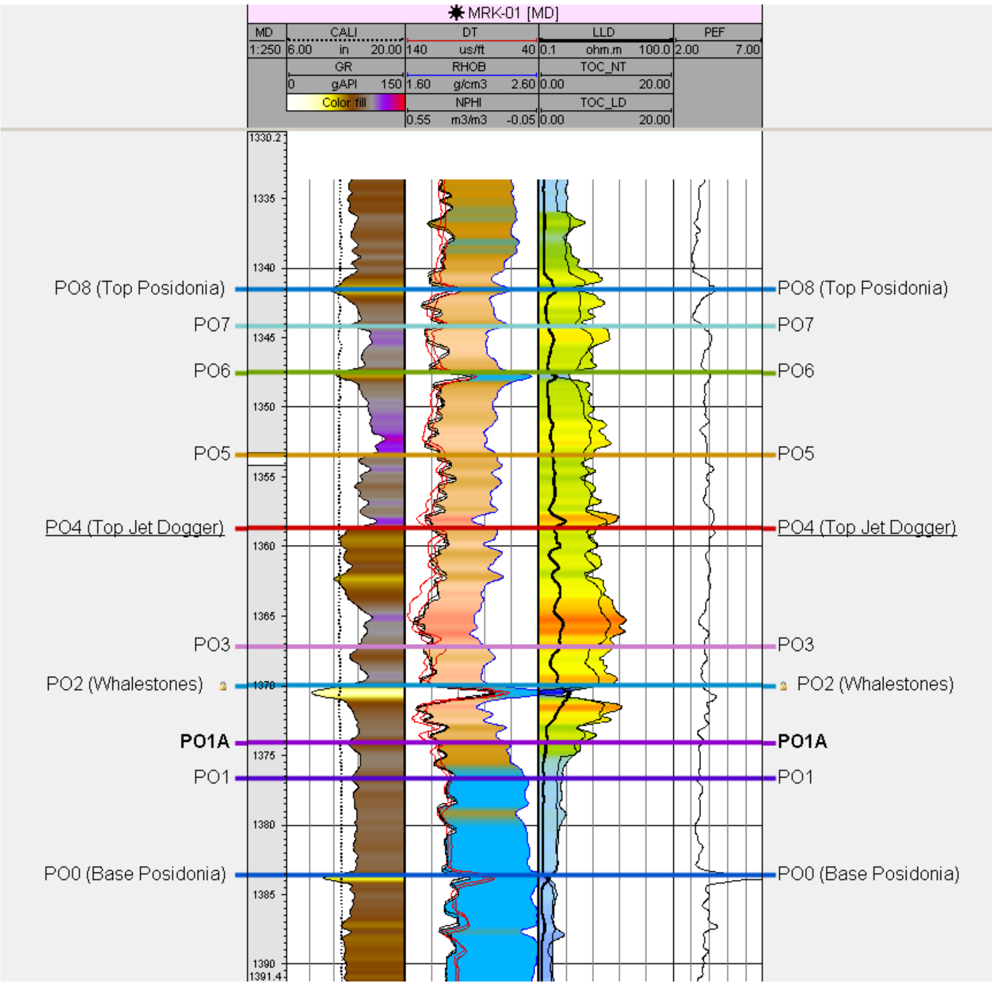

Figure 2-46 Proposed lithostratigraphic subdivision of the Posidonia Shale.

So, the packages thus observed formed the basis for the new zonation. Figure 2-46 shows the proposed lithostratigraphic subdivision of the Posidonia Shale Formation. Well tops were named “PO0” to “PO8”. The corresponding zones bear the name of its upper boundary. The inflection points of the logs (GR, DT, RHOB, NPHI) at the transition from normal shale to high por / high TOC streak were designated as the boundary of each package, and thus constitute the well tops.

Figure 2-47 shows a comparison in well F11-01 of the new proposed Posidonia subdivision with the $\delta^{13}C$ timelines and zonation from Zijp (2010). The timelines established by picking inflection points on the $\delta^{13}C$ curve compare favourably to the new proposed lithostratigraphic subdivision. When the four wells that have $\delta^{13}C$ curves are plotted (Figure 2-48), we see that the lithology closely follows the timelines from $\delta^{13}C$; only occasionally a crossing occurs. This is not surprising, as one would expect core shifts (F11-01 for example, has a core shift of +1.5 m at the top of the core, and +0.5 m at the base).

With regard to the previous lithostratigraphic zonation scheme: in general, it can be observed that the two zonation schemes are more or less the same. Changes were applied in some of the wells. We believe that the new one is better, because we have a complete overview of all the wells, and are thus better able to pick the well tops.

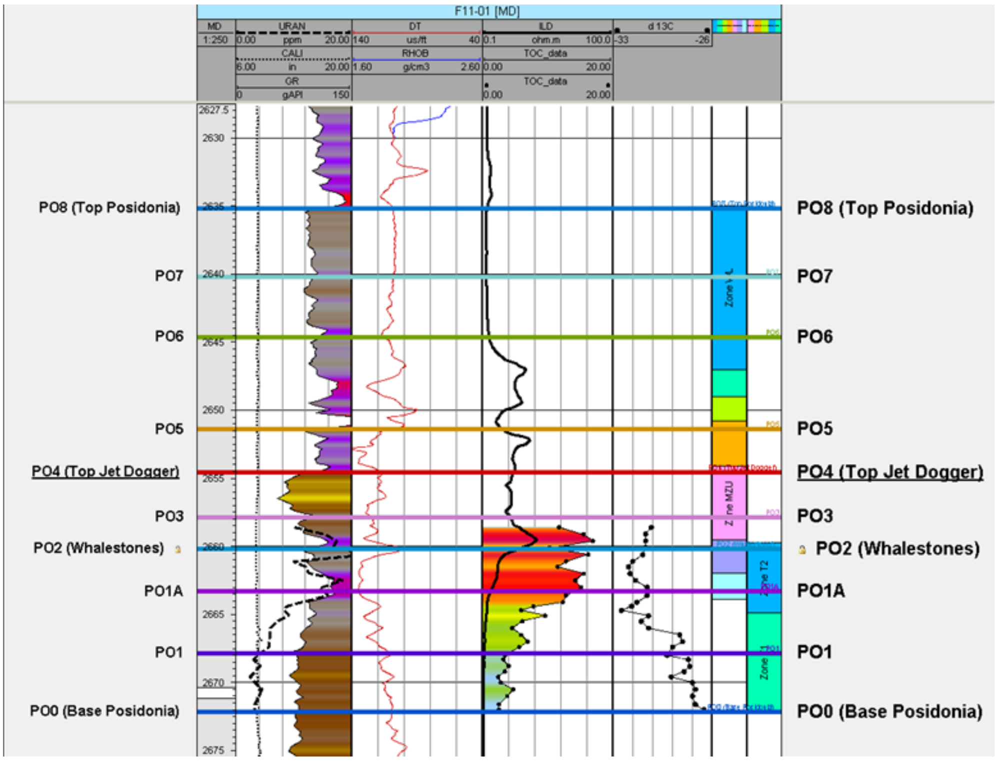

Figure 2-47 Comparison in well F11-01 of the new proposed Posidonia subdivision with the δ^{13}C timelines (rightmost tracks) and zonation from Zijp (2010) (second track from the right).

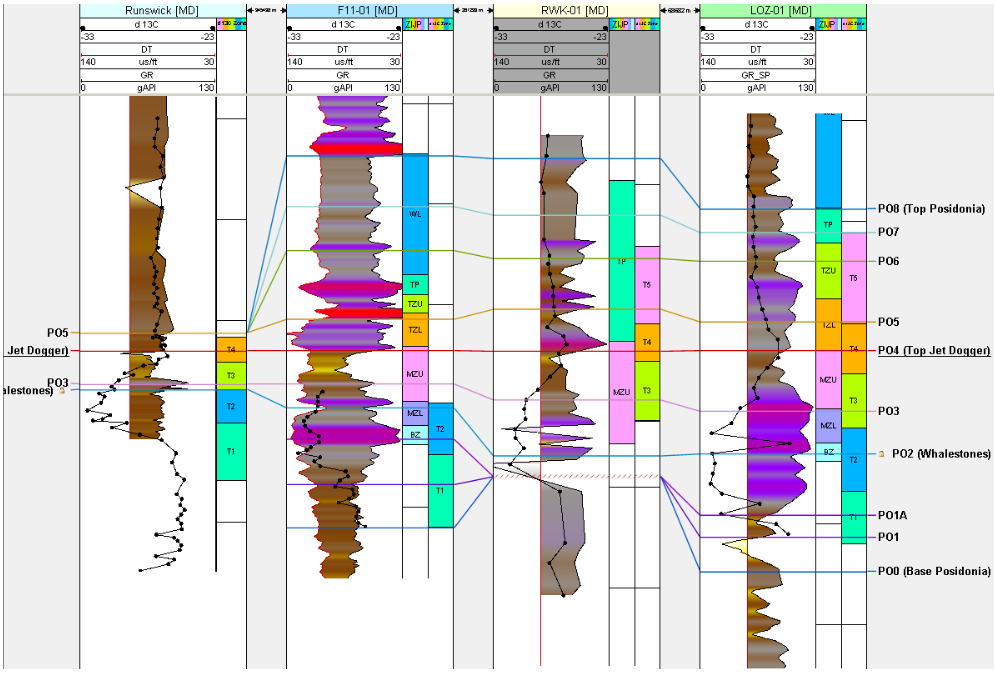

Figure 2-48 Comparison in wells Runswick, F11-01, RWK-01, and LOZ-01 of the new proposed Posidonia subdivision with the δ^{13}C timelines (rightmost tracks) and zonation from Zijp (2010) (second track from the right).

2.6.1.4 *Well to well correlation*

Since most of the wells only had GR-DT-ILD instead of a full log suite, a special log display was developed to help recognize the cycles that were so prominent in the combined GR-NPHI-RHOB-ILD display. Since the recognition of most of the cycles is based on porosity, the display should have a strong focus on porosity, in this case the sonic log. Figure 2-49 shows this setup.

During the process of correlating the wells throughout the four basins, the surprising result emerged that the lithostratigraphic zonation turned out to be valid in nearly all the investigated wells. Individual zones showed thickness variations as well as property variations (see next section), but all zones seem to be present in the entire Dutch subsurface. Once realized that this was actually the case, this feature was used to delineate faults (which occur quite frequently in the WNB and BFB) with a fault gap. In one case (P15-01) even a reverse fault was detected near the top of the Posidonia.

Figure 2-50 to Figure 2-55 show the correlations done in each of the four basins. The three East Netherlands wells were included in the WNB panel. Two versions are displayed: the classic view with only gamma ray, and the 'shale-enhanced' view, where the sonic log is the dominant log. Note that in each display panel, only a selection of wells is displayed. The complete set of correlations can be found in Appendices D1 to D3. Appendix C shows a correlation panel of all wells in this project, with GR only and the new log zonation used in the present study.

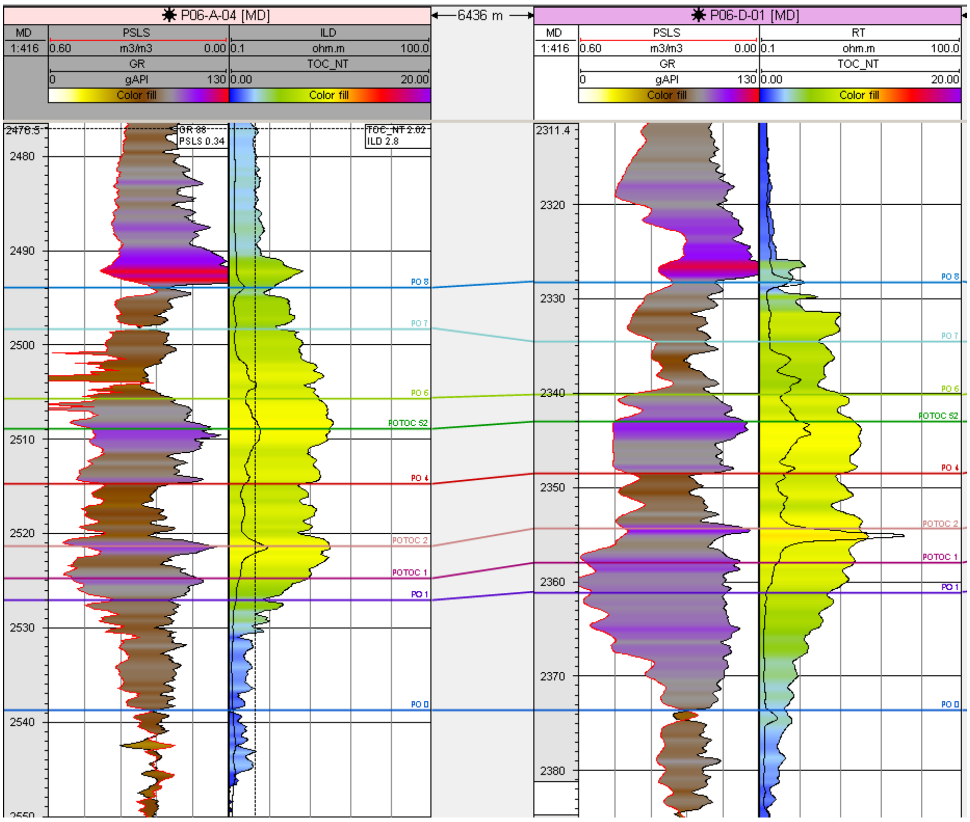

Figure 2-49 Optimised display for Posidonia. Track 1: measured depth; Track 2: GR [0-130], DT or PSLS [0.6-0], GR colour fill; Track 3: Deep Res [0.1-100 Ohm.m], TOC (NuTech, data, or TNO).

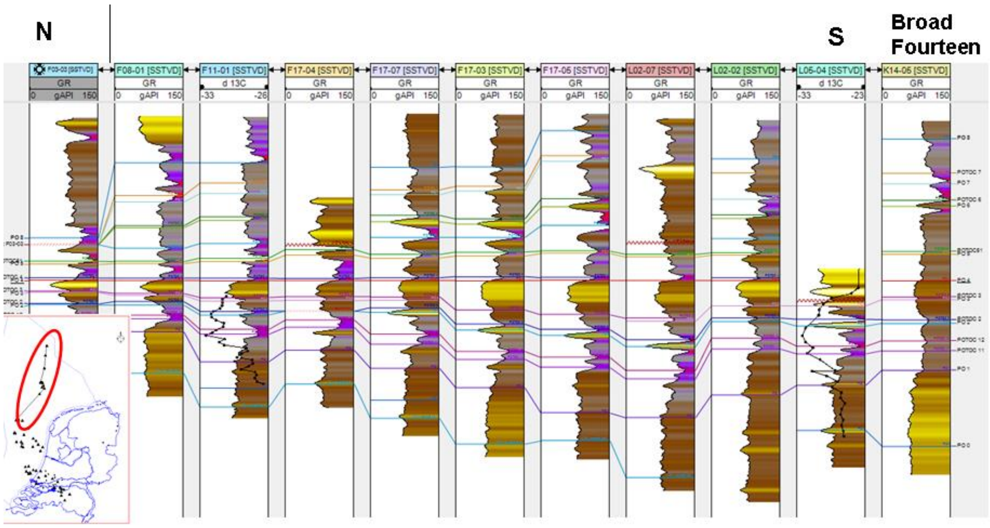

Figure 2-50 Overview of Posidonia correlation in the Dutch Central Graben (classic view: GR only).

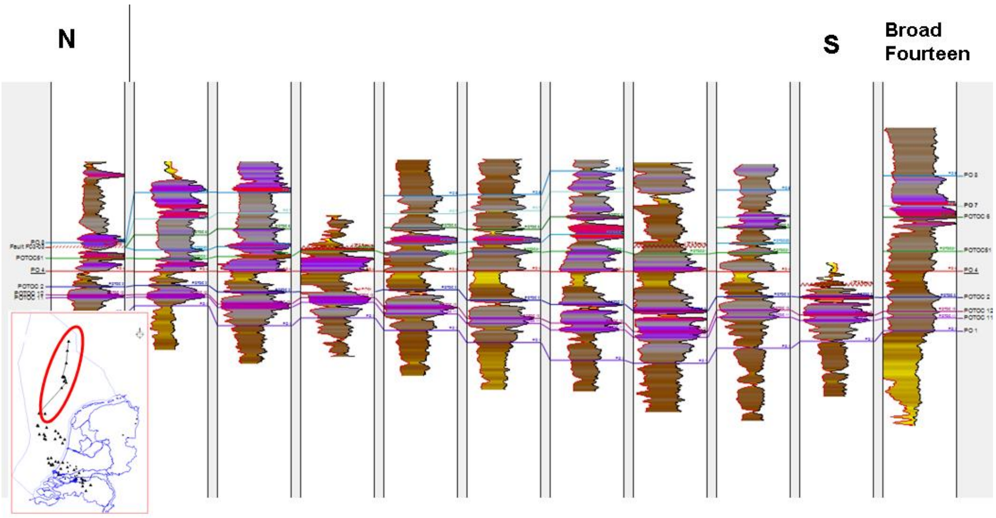

Figure 2-51 Overview Posidonia correlation the Dutch Central Graben (shale-enhanced view: GR & DT)

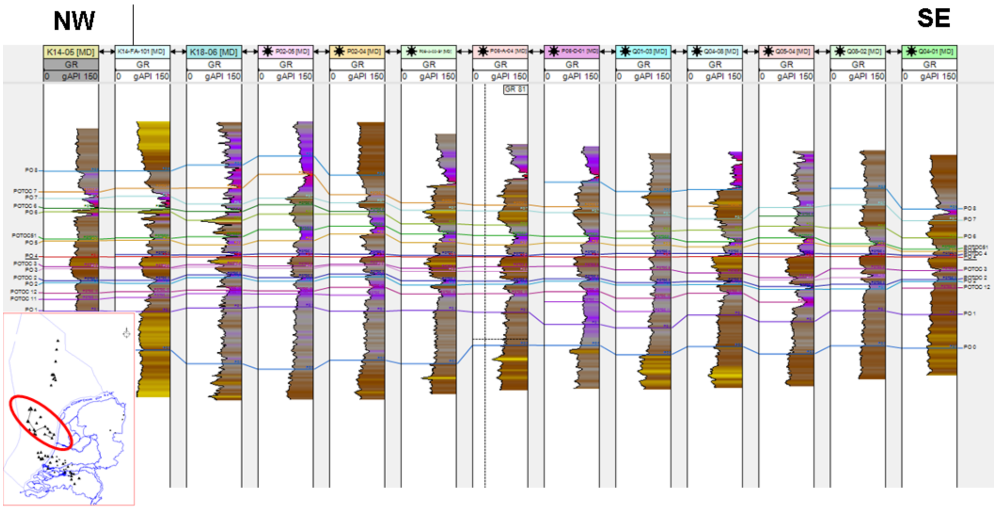

Figure 2-52 Overview of Posidonia correlation in the Broad Fourteens Basin (classic view: GR only).

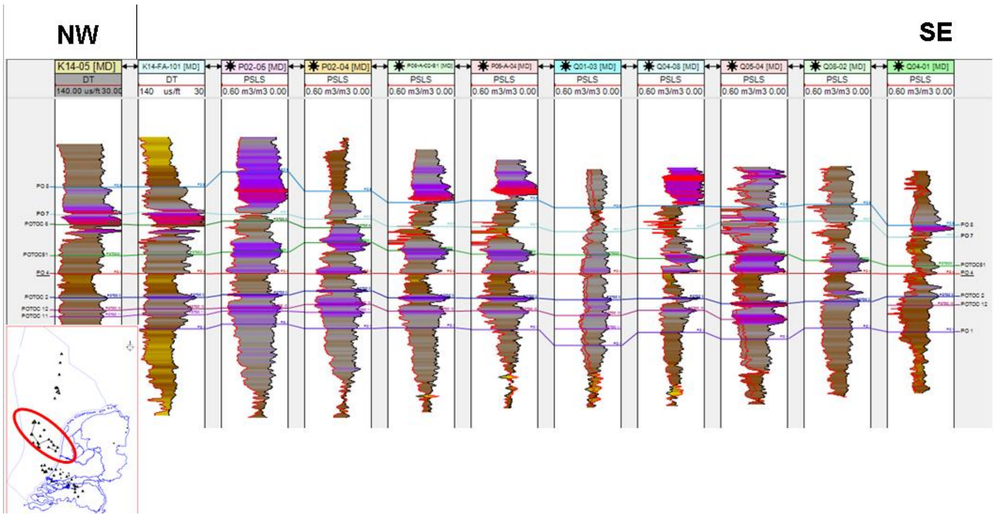

Figure 2-53 Overview Posidonia correlation Broad Fourteens Basin (shale-enhanced view: GR & DT)

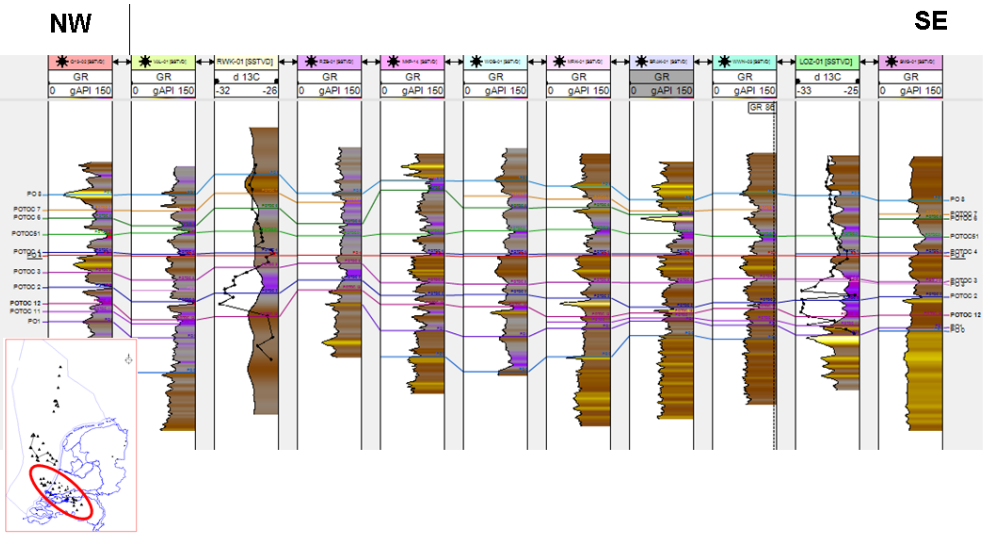

Figure 2-54 Overview of Posidonia correlation in the West Netherlands Basin (classic view: GR only).

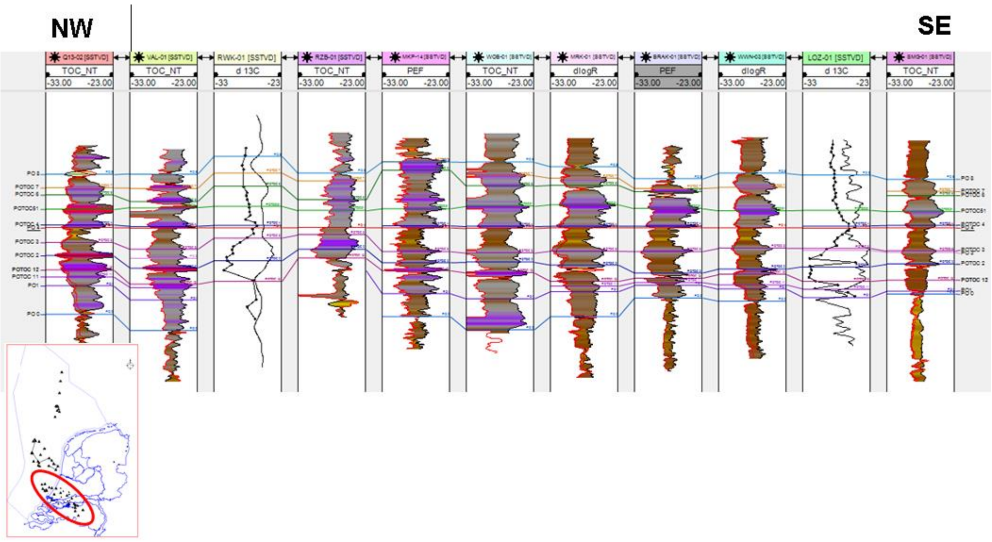

Figure 2-55 Overview Posidonia correlation West Netherlands Basin (shale-enhanced view: GR & DT)

2.6.2 *Results*

The correlations as described above formed the basis for a series of maps. All maps have the zero-edge outline of the Posidonia Shale as an overlay. This outline of the Posidonia was established by GDN dd Nov 2014 (courtesy Johan ten Veen).

2.6.2.1 *Thickness*

Firstly, the thicknesses were mapped. Appendices E1 to E11 show the isochore maps for zones PO1 to PO8, as well as for the combined zones PO1 – PO4 (the lower half of the Posidonia) and PO5 to PO8 (upper half of the Posidonia). Isochore maps were gridded using the “isochore” algorithm of Petrel, which is a modified version of the convergent gridding algorithm (one that does not interpolate and extrapolate values below zero).

2.6.2.2 *Average TOC*

The average TOC values for each zone were derived from the TOC logs, which were either calculated by NuTech or by TNO in previous studies (Zijp, 2010). The logs were averaged through the Well Tops attributes, converted to points, and gridded using the “isochore” algorithm. Maps are shown in Appendix F1 to F9.

2.6.2.3 *Brittleness*

Brittleness values were created from the sonic and bulk density logs according to Rickman et al (2008)’s recipe, the details of which are described in chapter 3.4 Maps are shown in Appendix G1 to G9.

2.6.3 *Synthesis*

- There is a strong cyclic signal present in the well log response of the Posidonia Shale. From base to top of the Posidonia, a total of nine cycles have been recognized. In the current definition of a cycle, it shows a high porosity / high TOC streak at the base, and “normal” clay-sized sediment for the remainder of the cycle. The top of a cycle may consist of (diagenetic) carbonate, but in general this only occurs in either the lowermost or the uppermost cycles.

- Based on these cycles a subdivision was made in the Posidonia Shale, where each cycle constitutes one zone. 69 wells were correlated using this subdivision. In the entire Dutch subsurface all nine zones were recognized and correlated.

- Thicknesses of individual zones show some lateral variation, but a clear pattern is difficult to recognize. When zones are lumped into an upper and a lower half, it becomes clear that the Broad Fourteen Basin has the thickest Posidonia. Another striking feature is the increasing thickness in the Central Graben from North to South.

- TOC percentages do not differ much throughout the area, at least not in a systematic way. There is one important exception: the area around well F17-04, which has a very high TOC. The reason for it is as yet unclear.

- TOC percentages do vary in a vertical sense. Zones PO3 and PO4 have on average the highest TOC.

- For those wells that had sonic and/or bulk density logs, a brittleness index was calculated based on an average Poisson’s Ratio and Young’s Modulus brittleness index. In general, three brittle zones are recognized in the Posidonia: the top part, the bottom part, and a thinner middle part. Two ductile, high TOC layers separate these three brittle layers.

- One area seems to have a higher brittleness than the rest of The Netherlands. It is located in the west of the WNB, near Q13. The rest of The Netherlands shows quite some fluctuations in brittleness, the cause of which remains speculative.

3 Section 3 – Interpretation

3.1 Calibration of the mineralogical model

In Sweetspot I phase mineral concentrations were calculated by Chemostrat from the major element composition for the Runswick Bay section. In Sweetspot II XRD was performed on samples from Runswick Bay (10 samples), RWK-01 (5 samples) and F11-01 (4 samples). XRD data from Runswick Bay was compared to the mineralogical calculation, referred to as “mineral model”, from Chemostrat.

The results showed that quartz was highly underestimated by the mineral model compared to XRD quartz content. Ankerite and siderite values were quite close to each other (Table 3-1). Several minerals (kaolinite, quartz, K-feldspar and siderite) had a poor correlation between XRD and modelled data (Table 3-1)

Table 3-1 Difference between the modelled and XRD mineralogy. The comparison between XRD and the old model is Runswick Bay data only.

mineral	old model		new model	
	similarity	correlation (R)	similarity	correlation (R)
Illite	0.14	0.71	0.20	0.82
kaolinite	0.13	-0.24	0.05	0.82
chlorite	0.34	0.61	0.02	0.43
quartz	0.46	0.40	0.12	0.81
K-feldspar	0.02	0.16	0.02	0.42
plagioclase	0.05	0.77	0.03	0.71
calcite	0.13	0.96	0.11	0.96
ankerite	0.05	0.94	0.11	0.83
siderite	0.02	-0.34	0.02	-0.28

Correlation factors (Pearson’s R values) and similarity were calculated with Past 3.04 software. Similarity is calculated as the Gower similarity or distance (d), which the distance between 2 points that averages the difference over all variables with each term normalized for the range of that variable (Equation 3-1). The higher the number, the higher is the difference between two parameters.

$$d_{jk} = \frac{1}{n} \sum_i \frac{\left| x_{ji} - x_{ki} \right|}{\max\limits_s x_{si} - \min\limits_s x_{si}} .$$

Equation 3-1 j and k indices refer to the 2 parameters of comparison.

Chemostrat used the XRD data to calibrate their model. The results shown in Table 3-1 for the new model have an overall better correlation for most minerals. Similarity between the XRD and modelled quartz and chlorite data was significantly improved. However, illite and ankerite are further apart, despite good correlation. Illite-XRD content is larger in than modelled XRD. It is quite possible that the actual illite content is lower than the XRD-illite content because the illite peak overlaps with the mica peak. Mica is thus calculated together with illite, which leads to illite overestimation in mica bearing rocks. We thus assume that the modelled illite content to be more reliable. Ankerite on the other hand is very difficult to model because ankerite is a solid solution. Ankerite (Fe,Mg,Mn[CaCO3]) has variable contents of Fe, Mg and Mn. The XRD data is therefore more reliable.

The mineralogical composition (taken from the mineral model) of the RWK dataset is plotted in Figure 3-1 along with the studied samples using SEM indicated by the black symbol outline in the carbonate/calcite data series. The relative mineral abundance corresponds well with the SEM observations of high and low calite and dolomite versus matrix. The calculated mineralogy also shows the correlation between clay and quartz. Note that in the SEM section we always refer to dolomite while for the mineral model all ‘dolomite’ is called ankerite for the (small) iron content.

- RWK-01-10 (2080.5): Low Mg, Medium Ca, Medium Al & Si
  → Average mineralogy
- RWK-01-25 (2091.5): Medium Mg, High Ca, Low Al & Si
  → High carbonate/calcite
- RWK-01-37 (2097.2): Low Mg, High Ca, Low Al & Si
  → High carbonate/calcite
- RWK-01-44 (2100.8): Low Mg, Low Ca, High Al & Si
  → Low carbonate/calcite
- RWK-01-54 (2105.7): High Mg, High Ca, Low Al & Si
  → High carbonate/ankerite

Unfortunately none of the very high ankerite/dolomite samples were selected for thinsection preparation and hence this carbonate enrichment could not be studied.

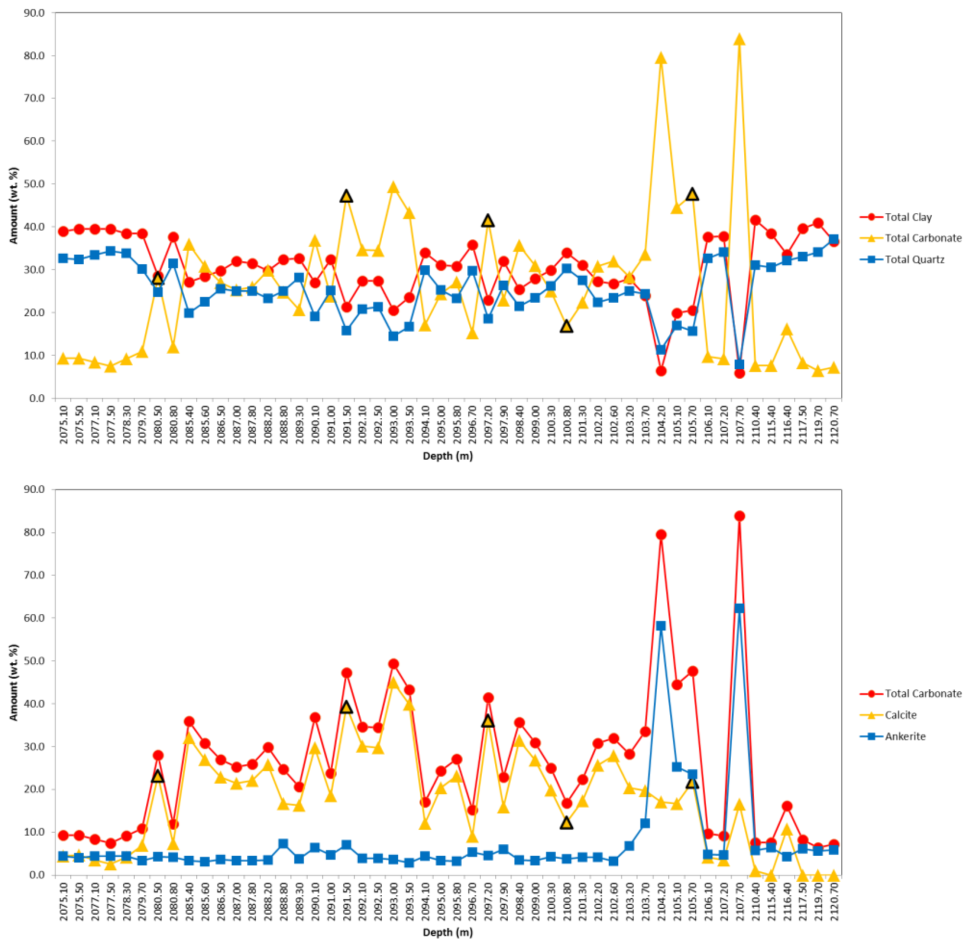

Figure 3-1 Plots of the calculated mineralogy

3.2 Stable C isotopes correlation and stratigraphic context

The very characteristic stable carbon isotope record of the Toarcian gives good stratigraphic control based on isotope correlations. In this study the Posidonia Shale Formation was subdivided into 6 zones based on the stable carbon isotope curves (Figure 3-2). These zones however are not linked to cyclostratigraphy such as published by Ruebsam et al. (2014) or Boulila et al. (2014). Several publications have proven that the characteristic negative and positive CIE in the Toarcian is a global phenomenon and can be used for detailed correlation (e.g. Gröcke et al (2011). It gives a more detailed subdivision than the commonly used ammonite zonations. The transition from T1 to T2 is equivalent with the boundary of the teuicostatum and the falciferum ammonite zones. The maximum peak of the positive isotope excursion in zone 4 is commonly correlated to the boundary between the exeratum/egantulum and falciferum ammonite subzones. The stable carbon isotopes measured in the context of this study can be correlated to literature isotope curves e.g., from the southern Paris Basin, France (Hernonso and Pellenard, 2014), Cardigan Basin, UK (Jenkyns and Clayton, 1997) Katsuyama, Japan (Gröcke et al. 2011) and Peniche, Portugal (Hesselbo et al. 2007). In the literature stable carbon isotopes from organic matter are commonly compared to those from carbonate, in this study only measurements on organic matter are used.

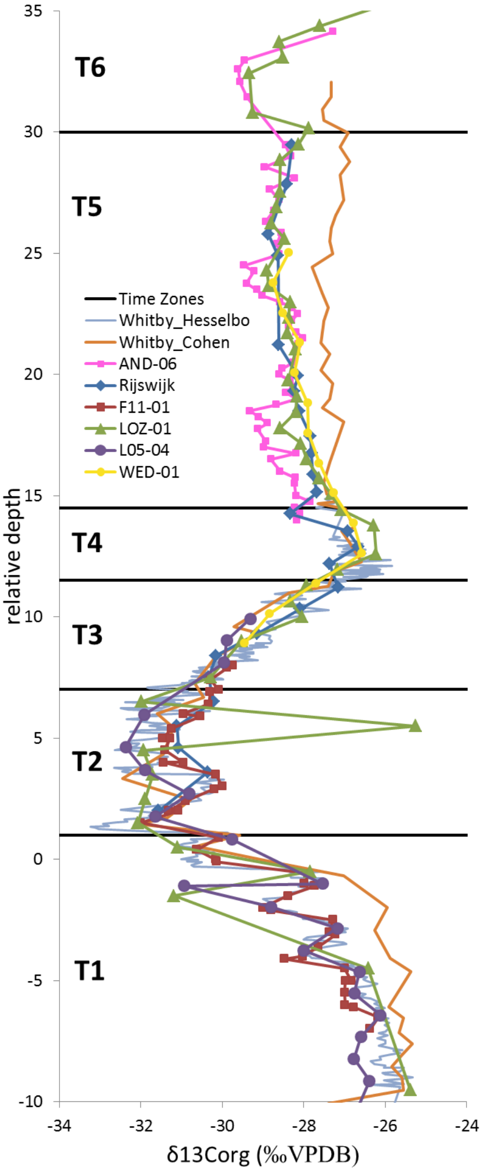

Figure 3-2 Correlation of the different stable carbon isotope curves from the Netherlands on and offshore and from two different publication from the area of Whitby in the Cleaveland Basin.

Through the possibility to correlate time equivalents by calculating relative depths per interval it is possible to calculate differences in sedimentation rate. For this purpose we use the cyclostratigraphic interpretation of Ruebsam et al (2014) who concluded that the total duration of the exeratum/egantulum subzone is 790 kyr. However the duration of the Toarcian isotope excursion is still under discussion (e.g., Ruebsam et al. 2014, 2015, Boulila et al. 2014, Boulila and Hinnov, 2015), other interpretations are possible.

Thickness of the interval T2 to T4 was calculated for wells F11-01, L05-04, RWK-01 and LOZ-01 and the locations Whitby, Dotternhausen and Luxembourg (Table 3-2). Maximum thickness for this interval can be seen in the two onshore wells (RWK-01 and LOZ-01) in the Netherlands while the interval is thinnest in Dotternhausen. Sedimentation rates are in accordance with this, however the sedimentation rates for the well in Luxembourg show very low sedimentation rates for intervals T2 and

T3 and are highest for interval T4 indicating a strong increase in sedimentation towards the top of the section.

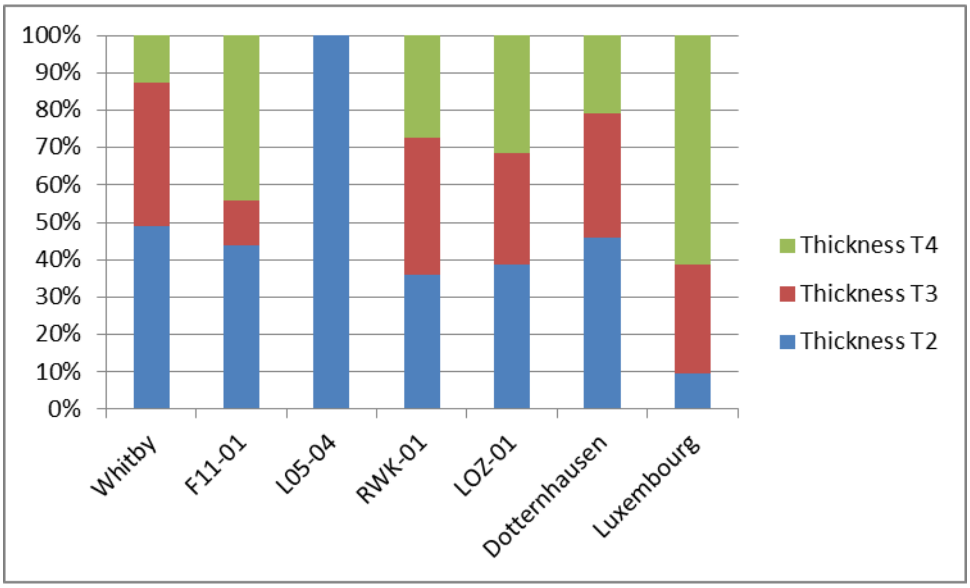

Figure 3-3 Thickness in percent of zones 2 to 5 of the different locations. The top of well L05-04 is eroded, the base of well RWK-01 is missing due to a fault and the well in Luxembourg stops in zone 2 and has not been drilled deeper.

Table 3-2 Detailed calculation of the sedimentation rate and the individual thicknesses of zones 2 to 4. Sedimentation rates were calculated based on Ruebsam et al. (2014) using 790 kyr for T2-4, 290 kyr for T4 and 500 kyr for T2 and T3.

	Whitby	F11-01	L05-04	RWK-01	LOZ-01	Dottern-hausen	Luxem-bourg
Top T4	7,00	2651?	eroded	2093,5	2489.7	5.4	23,9
Top T3	6,10	2656,5?	eroded	2097,4	2495	6,2	29,6
Top T2	3,40	2658	2827,35	2102,6	2500	7,5	32,3
Base T2	-0,05	2663,5	2833,71	2107,7 (unconf)	2506.5	9,3	33,2 (max d)
Thickness T2-T4	7,05	12,5		14,2	16,8	3,9	9,3
Thickness T2	3,45	5,5	6,36	5,1	6,5	1,8	0,9
Thickness T3	2,70	1,5		5,2	5	1,3	2,7
Thickness T4	0,90	5,5		3,9	5,3	0,8	5,7
Total SR (cm/kyr)	0,89	1,58		1,8	2,13	0,49	1,18
SR T2-3 (cm/kyr)	1,23	1,4	1,27	2,06	2,3	0,61	0,72
SR T4 (cm/kyr)	0,31	1,9		1,34	1,83	0,28	1,97

3.3 Carbonates

Carbonates in the studied sections consist of three main phases, with calcite being the most abundant (0 to 63%, average 9% of whole rock), followed by ankerite (2-61%, average 6%, of whole rock) and a small amount of siderite (0-5%, average 1% of whole rock).

Carbonate origin was studied in detail in the RWK-1 and LOZ sections. Calcite consists primarily of carbonaceous nanoplankton (such as Coccolithophores and Schizoaphaerellen) and subdominantly of macrofauna (mostly bilvalve shells). Secondary (diagenetic) calcite was not observed in the RWK-1 or LOZ sections. Ankerite was formed during early diagenesis, prior to compaction but post pyrite formation. The genesis of ankerite is related to a redox zonation within the sediment. During bacterial sulphate reduction (1) and anaerobic methane oxidation (2) organic carbon is converted to inorganic carbon. Fe- and Mn-reduction also leads to the decay of organic matter and carbonate release (e.g. Raiswell and Fisher 2004; Lash and Blood, 2004).

$$SO_4^{2-} + CH_4 \rightarrow H_2S + 2HCO_3^- \qquad (1)$$

$$SO_4^{2-} + 2CH_2O \rightarrow HS^- + 2HCO_3^- + H_2O \qquad (2)$$

Alkalinity can become oversaturated within pore-water and promotes carbonate precipitation. Carbonate however will not readily precipitate in the presence of significant H_2S amounts, due to the low pH. As H_2S is converted to Fe-sulfides (e.g. pyrite) or escapes to the upper water column pH increases and carbonate can precipitate, mostly in form of concretions, prior to compaction. Early diagenetic carbonate can be in the form of calcite but as Ca is consumed Mg and Fe is taken into the crystal structure to form dolomite and/or ankerite. Bacterial sulphate reduction and production H2S creates a weak acidic environment that can lead to primary calcite dissolution, thus contributing further HCO^{3-} and Ca^{2+} to the pore-waters.

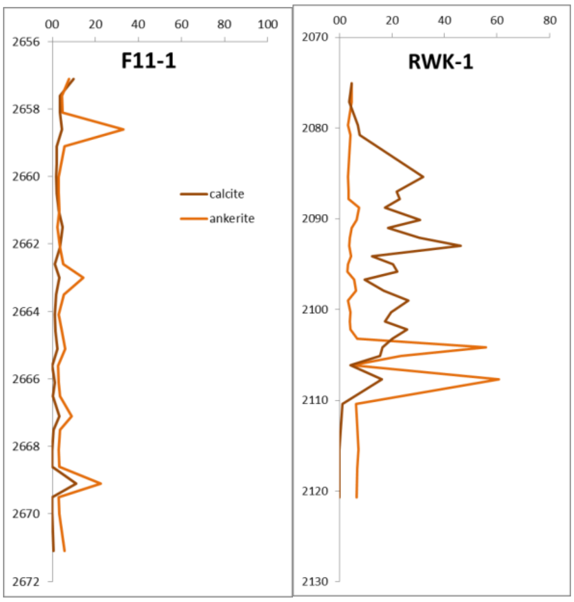

Figure 3-4 Calcite vs. ankerite content in F11-1 and RWK-1.

In F11-1 calcite content is rather low and the carbonate is dominanted by ankerite (Figure 3-4). Primary calcareous nanoplankton is either absent or low in the studied interval of F11-1. Carbonate concretions of early diagenetic origin have been observed in F11-01. However the F11-1 core is dominated by fibrous carbonate veins and lenses that are have been referred to as BEEF (Figure 3-5). The BEEF structures are bedding parallel with a suture in the middle that depicts the beginning of crystal growth. The fibrous crystals have grown vertically from the suture, either in episodes or continuously. BEEFs are interpreted as late digenetic infilling of cracks, caused by tensile fracturing and vertical dilation during burial (Cobbold et al., 2013). Some authors argued for an early origin of BEEF, before significant dewatering of the shale (e.g. Gilman & Metzger, 1967). Although the timing of BEEF formation is unclear it is likely that formation occurred during burial and later than the carbonate concretions.

Interestingly, the formation of carbonate BEEF has been linked to fluid overpressure during petroleum generation (Cobbold et al., 2013). In this case oil expulsion would have caused hydrofracturing of the shale and subsequent growth of carbonate in the fractures.

Figure 3-5 (A) F11-01, ca. 2661m core depth, (B) Albert Heijn beef.

In Runswick carbonate concretions were not sampled. For this reason the cannonball, whalestone and curlingstone levels are not evident from the modelled mineralogy (Figure 3-6). The Jet Dogger bank is evident by the calcite increase at ~ 6 to 7m above Base Jet Rock. The concretions are purely diagenetic and can be described by the previously explained processes. The diagenetic carbonate concretions consist of mostly siderite, calcite and secondary dolomite (ten Veen et al. 2014). However, the increase in calcite content is most probably related to the calcareous nanoplancton. The continuous limestone layer at the Top Jet Dogger was described in the SS1 report as a layer consisting of (partly recrystallized) coccolithophores. Although calcite layers can be formed diagenetically (e.g. Tribovillard et al., 2012) it is fair to speculate that the increase of calcite is related to an increase in the calcareous nanoplankton.

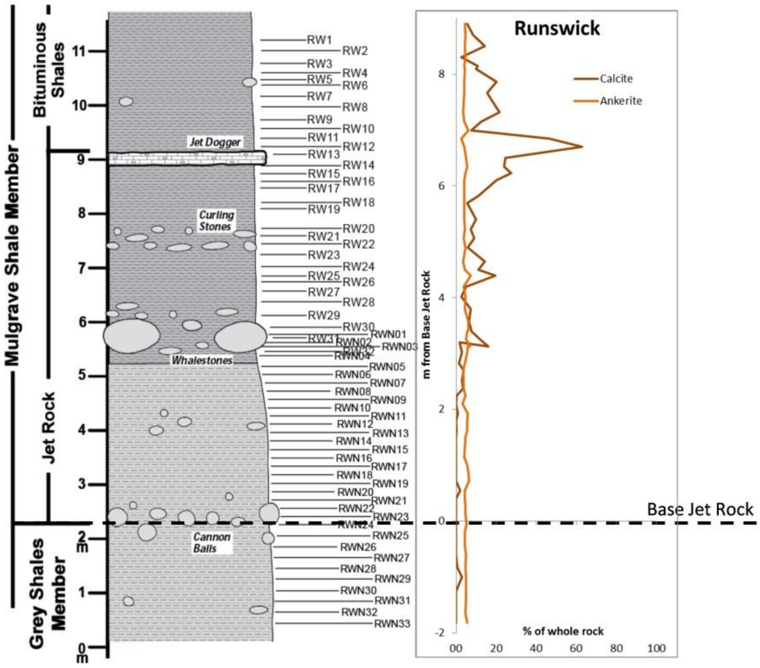

Figure 3-6 Runswick Bay lithology and carbonate content.

3.4 Brittleness from mineralogy and well logs

Successful exploitation of shale gas is dependant not only on the amount of gas but also on the susceptibility of a reservoir to hydraulic fracturing. Fraccability is connected to the brittleness of a rock. Brittleness is controlled by many factors including rock mineralogy, porosity, saturation, TOC, temperature, strain rate, in situ stress, etc. (King, 2010; Yang et al, 2013). This has resulted in a variety of brittleness descriptions and characterizations, which makes it difficult to choose a proper one for the delineation of sweet spots in the Posidonia Shale Formation. The various brittleness indices can be subdivided into three categories: A) those that are based on geomechanical measurements on cores; B) those based on geomechanical properties derived from well logs; and C) a group that is based on mineralogical constituents derived from core or well logs.

A full geomechanical testing procure on a variety of Posidonia samples was beyond the scope of the current project, therefore brittleness indices from category (A) were excluded from this study. Brittleness indices from the other two groups were calculated. The mineralogy-based ones were calculated only for those wells for which mineralogical analyses were available (RWK-01, LOZ-01, F11-01, Whitby); the well-log based geomechanical brittleness index was calculated for all wells.

3.4.1 Brittleness from mineralogy

As mineralogy is a major factor controlling brittleness the mineralogical brittleness index (BI_{min}) has also been consulted to understand the brittleness of a rock. The classical brittleness index suggested by Jarvie et al. (2007), based on their work on the Barnett Shale, considered the amount of quartz to be the main brittleness driver, while clay and carbonate are the ductile components.

$$BI_{min} = \frac{quartz}{quartz+clay+carbonate}$$

Equation 3-2 BI_{min} after Jarvie et al. 2007

$$BI_{min} = \frac{quartz+dolomite+0.5limestone}{quartz+dolomite+limestone+clay+TOC} \; f(Ro)$$

Equation 3-3 BI_{min} after Wang & Gale, 2009

$$BI_{min} = \frac{quartz+1.35carbonate+feldspar}{quartz+carbonate+feldspar+clay+TOC}$$

Equation 3-4 BI_{min} as calculated in the Sweetspot I report, ten Veen et al., 2014

This was considered to be too simplistic and was elaborated by Wang & Gale (2009). They assumed that the presence of carbonate tends to increase brittleness of shales. Because dolomite is more brittle than limestone, the limestone content was thus halved. Additionally, organic matter was considered to increase ductility (Wells, 2004) and was thus added to the denominator. Perez and Marfurt (2013) also applied the Wang & Gale model, however, they found that TOC did not increase the ductility of the rock in the case of the Barnett Shale.

Wang and Gale (2009) further added vitrinite reflectance (Ro) that they proposed to mirror maximum paleotemperatures related to diagenesis and the amount of compaction. The maturity was considered to increase brittleness.

Finally, during Sweetspot 1 project the Wang and Gale (2009) calculation was partially adapted. However, total carbonate was given weighing factor of 1.35 because carbonate layers were considered to positively influence brittleness compared to fine crystalline quartz. Feldspar was added to the nominator, as an enhancer of brittleness.

In this work we use the modelled minerals to calculate BI_{min}. Wang and Gale model was calculated without Ro. Vitrinite reflectance is a measure of maturity which is mainly temperature related. The amount of compaction and thus pore space reduction is not directly related to the vitrinite reflectance.

Experimental results also showed that increased porosity decreased the strength of a rock (Reinicke at al., 2010). Since the porosity was not measured in most cores, this parameter has not been taken in account in this study.

3.4.2 *Brittleness from geomechanical well logs*

It has been proposed in literature that brittleness should reflect both Poisson's Ratio and Young's Modulus (Grieser et al., 2006; Rickman et al, 2008). The idea is that the Poisson's Ratio (PR) represents a rock's ability to fail, and Young's Modulus (YM) the ability to maintain the fracture. So a brittleness index was defined which combines both Young's modulus and Poisson Ratio (Figure 3-7). Each of the two properties is scaled between a minimum and maximum value, and the two resulting brittleness indices are averaged (Rickman et al, 2008). An additional advantage of this method is that both PR and YM can be derived from well logs (sonic and density logs) which are readily available for most wells.

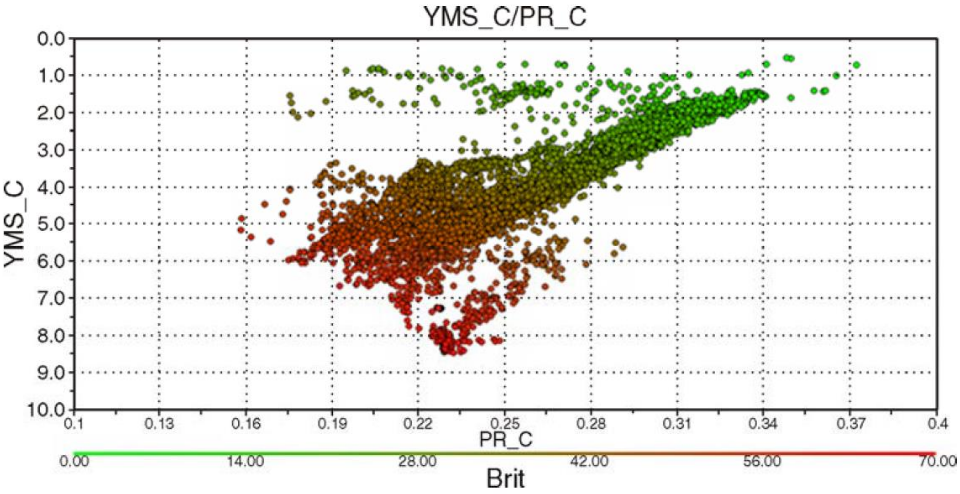

Figure 3-7 A cross plot of Young's Modulus and Poisson's Ratio showing the brittleness percentage increasing to the southwest corner of the plot (Rickman et al., 2008).

The following equations were used to calculate the brittleness index:
YM_BRIT = ((YMS_C – YMSmin)/(YMSmax – YMSmin)) * 100
PR_BRIT = ((PR_C – PRmax)/(PRmin-PRmax)) *100
BRIT = (YM_BRIT + PR_BRIT) / 2

Where:
YM_BRIT is the brittleness index from Young's Modulus;
YMS_C is the measured static Young's Modulus (subscripts min and max refer to minimum and maximum measured Young's Modulus);
PR_BRIT is the brittleness index from Poisson's Ratio;
PR_C is the measured Poisson's Ratio (subscripts min and max refer to minimum and maximum measured Poisson's Ratio).

In the absence of cores, PR and YM are derived from sonic and density logs:

YMdyn=RHOB*Vs*Vs*(3*Vp*Vp-4*Vs*Vs)/(Vp*Vp-Vs*Vs)
PR = 0.5*((Vp*Vp)-(2*(Vs*Vs)))/((Vp*Vp)-(Vs*Vs))

Where Vp and Vs are the seismic compressional and shear velocities, respectively, and RHOB is the bulk density.

The static Young's Modulus is much more useful than the dynamic. Unlike ordinary, non-prospective shales, for gas-bearing shales a good correlation exists between the static and dynamic YM. According to King (2010), this relation is similar to tight sandstone clastics (Figure 3-8). The relation can be written as follows:

YMstat= 10^0.02*(RHOB*YMdyn)^0.77

When no shear sonic is available Vs is derived from Vp, using the mudstone relation from Castagna et al (1985):

Vs = (Vp-1.36)/1.16

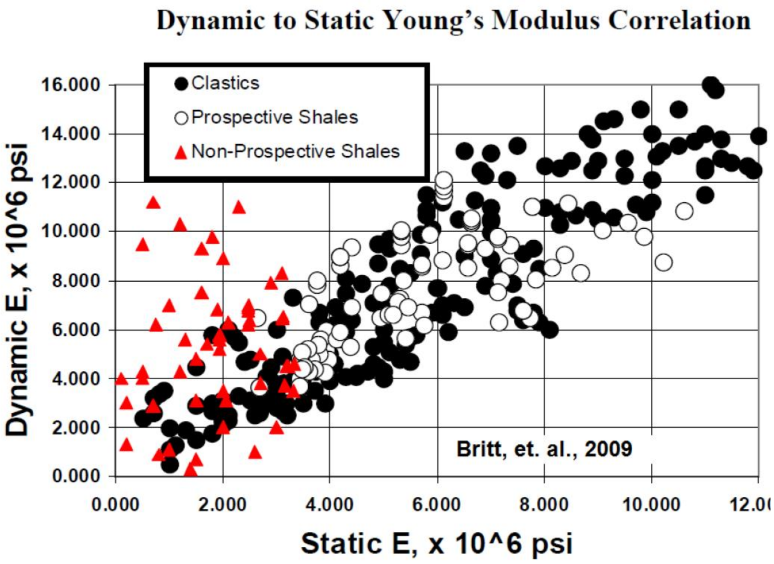

Figure 3-8 Correlation between static (cores) and Dynamic (logs) Young's Modulus. From King, 2010.

3.4.3 *Rate of penetration as a proxy for brittleness*

The rate of penetration (ROP) during drilling, expressed as meters/time, may also reflect the brittleness of a rock. Altindag (2002) postulated for ROP to decrease with brittleness. The question is whether his results (an analysis of percussion drilling in boreholes for mining exploration, exclusively hard rock) can be directly applied to the rather ductile Posidonia Shale. Figure 3-9 shows a formation evaluation log that includes the ROP of well VAL-01. The drilling rate of the Posidonia is only half the rate of the overlying Lower Werkendam shale, so if Altindag's (2002) conclusion is right, the brittleness of the Posidonia would be higher than the overlying shale. This is counterintuitive as the Wekendam Formation is much more sandy.

For five wells (F11-01, F17-04, VAL-01, OTL-01, and RDK-01) the ROP was compared to various well logs, and if available, with mineralogical constituents and brittleness indices.

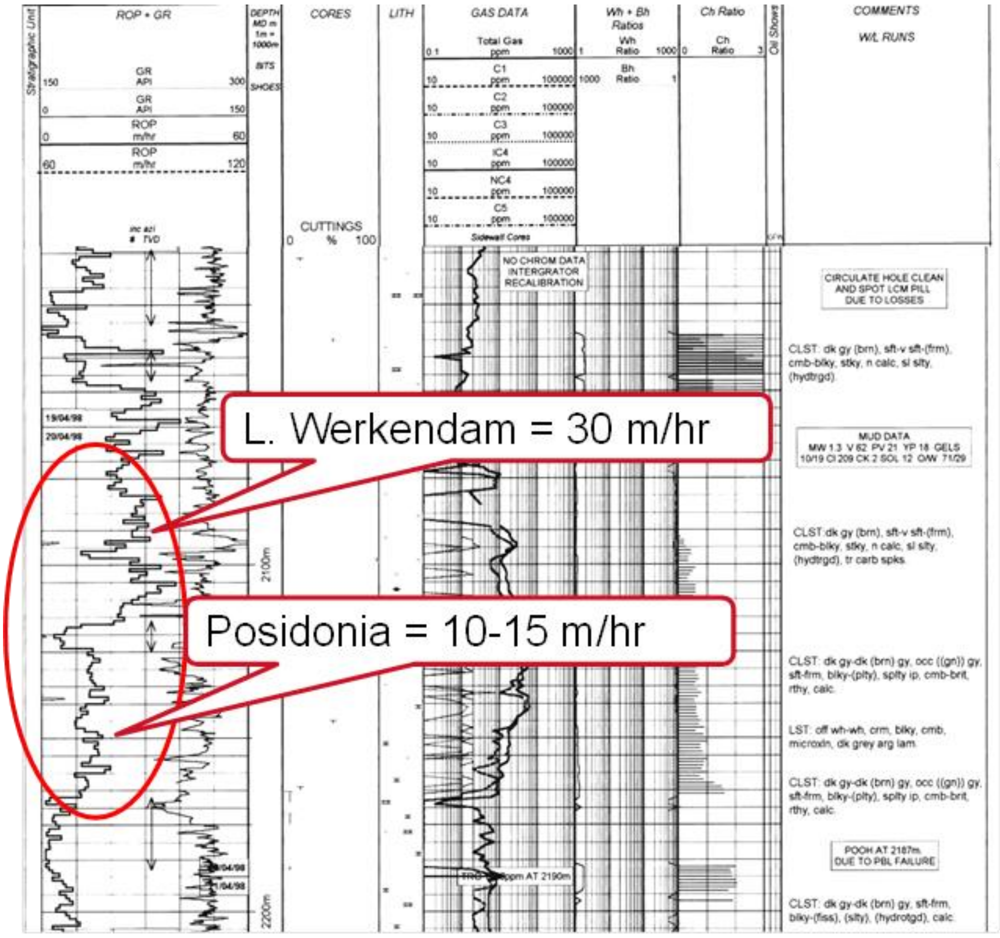

Figure 3-9 Formation evaluation log of the drilling of well VAL-01. Note that the drilling speed in the Posidonia drops to half of the Lower Werkendam's.

3.4.4 *Results*

To start with the usefulness of the rate of penetration (ROP) as a proxy for brittleness, we see contradictory results from the five investigated wells. For the entire Posidonia, Altindag's (2002) conclusion that the more brittle the formation is, the slower the drilling rate will be, does not seems to be justified. In detail, the wells yield contradictory results. Wells F11-01 and VAL-01 have higher drilling rates in low TOC, low porosity zones, but wells F17-04 and RDK-01 show a completely opposite relation. Drilling speed in well OTL-01 does not seem to be influenced at all by mineralogy, TOC, or porosity. It is questionable whether the ROP log, which is evaluated at best every meter, has the proper resolution to allow comparisons with other logs. Furthermore, the depth of the ROP log is recorded as driller's depth, which can be off by several meters to logger's depth. It will be clear that the use of cross plots with such variables needs to be treated with great caution.

The main conclusion therefore is that it is unclear which constituents in the Posidonia control the Rate of Penetration. It is unwise to use ROP as a proxy for brittleness.

The three mineralogical BI_{min} are plotted for Runswick, F11-01 and RWK-01 (Figure 3-10).

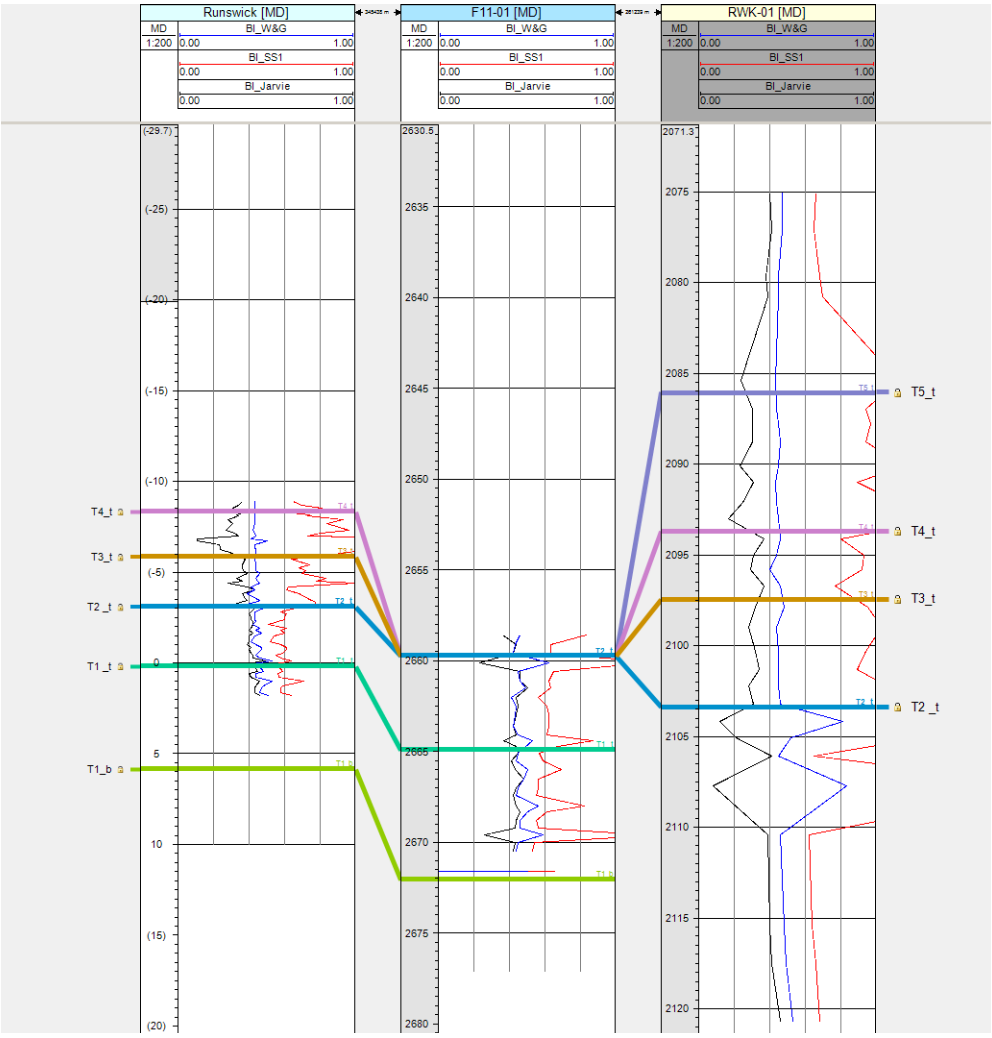

Figure 3-10 Comparison of the three mineralogical brittleness indices for three wells

The brittleness calculated by Jarvie differs significantly with the SSI1 $\mathrm{BI}_{\mathrm{min}}$ and also W&G $\mathrm{BI}_{\mathrm{min}}$, the reason being the carbonate content. The Jarvie $\mathrm{BI}_{\mathrm{min}}$ has a negative correlation with the SSI1 $\mathrm{BI}_{\mathrm{min}}$. Wang&Gale $\mathrm{BI}_{\mathrm{min}}$ does not vary much, except in RWK-01 in the ankerite-rich level. Average $\mathrm{BI}_{\mathrm{min}}$ values do not differ much between the sections when comparing each index (Table 3-3). As clay and quartz contents do not change significantly throughout the sections, the brittleness indices varies mainly with the carbonate content with depth.

Table 3-3 Averages of the mineralogical brittleness index.

	Jarvie	SS1	W&G
F11-1	0.4	0.7	0.5
RWK-1	0.3	1.0	0.5
Runswick	0.4	0.7	0.4

Only section F11-01 qualified for the comparison of the different brittleness indices because it contains both sufficient log data and geochemical analyses.

Comparison between YM-PR brittleness and BI_{min} (Figure 3-11) for the F11-01 section. The YM-PR brittleness shows a general decrease up section (studied interval only), with peaks throughout the section that correlate with the peaks in BI_{min} (W&G) and BI_{min} SSI1. The largest peak at the top of T2 is related to the higher carbonate content. The BI_{min} (Jarvie) does not correlate with the YM-PR brittleness.

3.4.5 Conclusions

The rate of penetration is not a good indicator of brittleness, at least not within the Posidonia Shale. BI_{min}-W&G and BI_{min}-SSI1 are possibly reasonable indicators of brittleness, whereas the Jarvie BI_{min} index seems more unreliable. The downside of the BI_{min} indices is that they do not include the effect of porosity on brittleness. Another disadvantage is that they do not include the influence of confining stress on the brittleness. Because the YM-PR brittleness index is primarily based on the sonic log response it accounts for porosity and in parts for mineralogy, but also partly for the confining stress (as much as it is related to depth of burial).

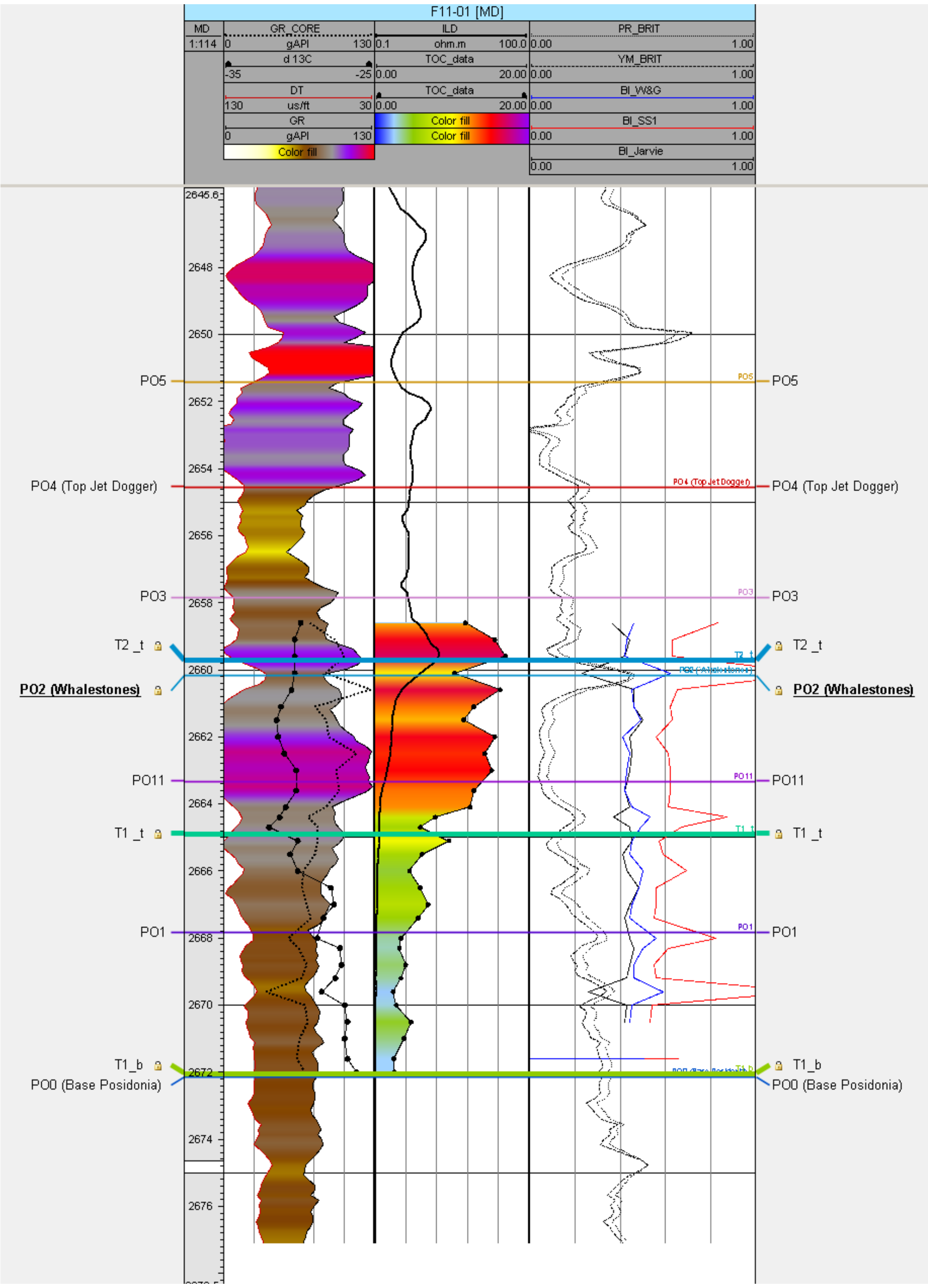

Figure 3-11 The brittleness indices (YM-PR and BI_{min}) plotted along GR and DT, TOC and ILD logs. The TOC log is from measured (coloured area) data.

3.5 Lateral changes

Maps created using the log correlation and other available maps were used to identify regional trends and when linked to the detailed results from the core analyses (organic geochemistry, mineralogy, palynology) to determine lateral processes that drive these changes.

3.5.1 Thickness

During the log correlation it became evident, that the Posidonia Shale Formation is incomplete in several wells, either due to erosion or to faulting. In 19 out of 72 wells an incomplete section was encountered. For the analysis of the total thickness these wells were not considered.

The Posidonia Shale Formation is thickest in the Broad Fourteens Basin with average thicknesses of 36 m, while average thickness in the West Netherlands Basin is about 33 m. Thickness in the Dutch Central Graben increases southwards from about 28 m to 38 m with a local maximum of 46 m in well F17-05. Such a local maximum can also be observed in the Broad Fourteens Basin in well K18-2-A with a thickness of 42 m. These local thickness maxima are probably related to salt movement during deposition and the creation of rim synclines. An interpreted seismic section through the F17 and L02 blocks shows that the whole lower Jurassic is thickening to the north of the salt diapir (Figure 3-12), suggesting a local subsidence centre. It is possible that a similar thickening occurred in the south, however erosion removed at least parts of the formation in this area. Well K18-2-A was also drilled in the vicinity of a salt diaper, suggesting a similar process at work there. Detailed seismic interpretation of that area might support that theory (Figure 3-13).

Along with general thickness, detailed thickness maps for each log interval were created. These maps do not show any variation, that cannot already be seen on the general thickness map of the Posidonia Shale Formation (Appendix E). However interval PO3 to PO4 shows a very interesting trend (Figure 3-14). This interval shows a clear thickening towards the onshore with a thickness increase from 2 m in the offshore to around 8 m in the south and east of the Netherlands. This interval is related to the recovery stage of the isotope excursion (upper part of T3, lower part of T4) and is characterized on the logs by low GR and high DT, which can be interpreted as either high carbonate or quartz content.

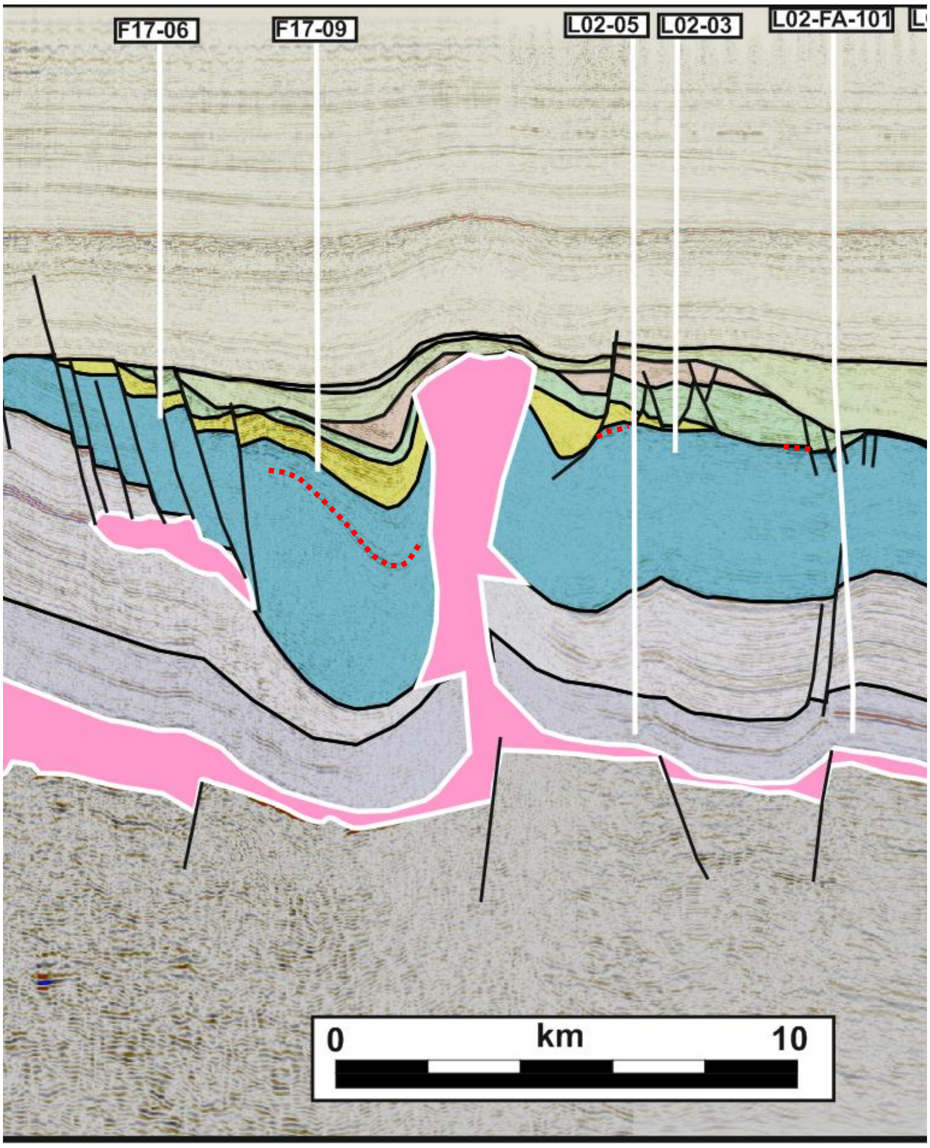

Figure 3-12 Interpreted seismic section through the southern part of the Dutch Central Graben. The dashed red line shows the position of the Posidonia Shale Formation. From Bouroullec et al. (2015)

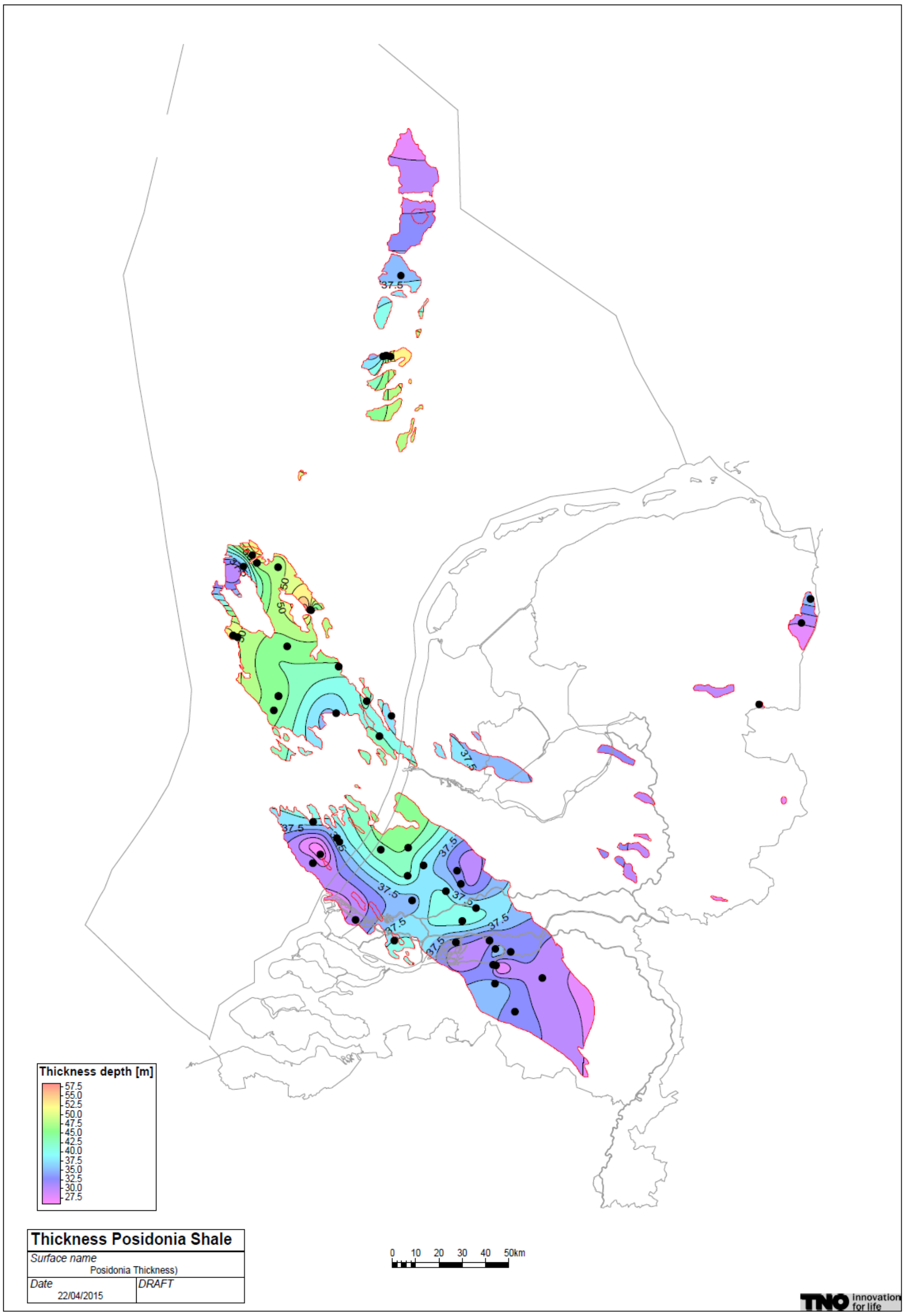

Figure 3-13 Total thickness map of the Posidonia Shale Formation according to detailed log correlation.

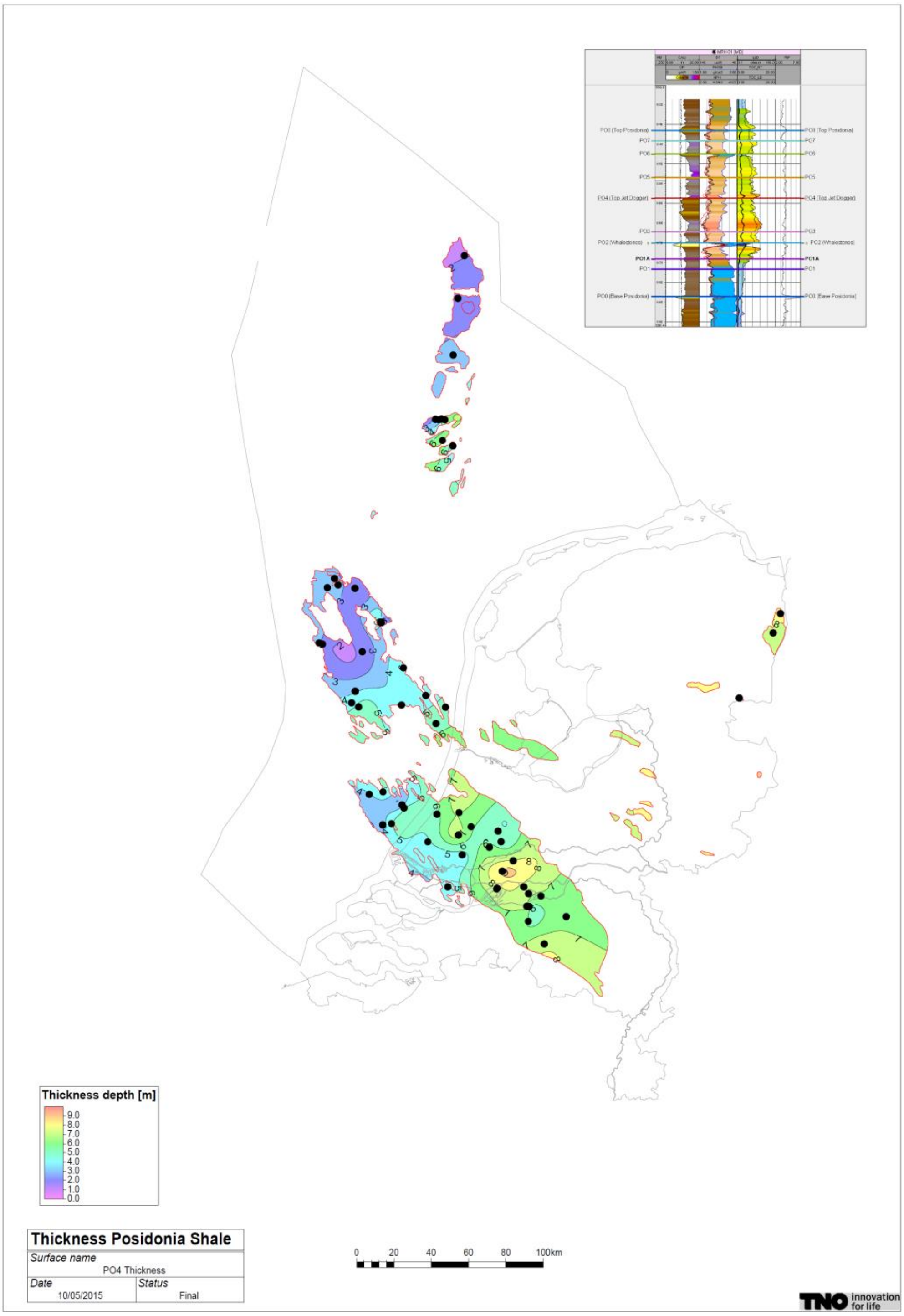

Figure 3-14 Thickness map of the log interval PO3 to PO4

3.5.2 *Maturity*

In the context of the Knowledge Investment Projects (KIP) and the tasks as geological survey of the Netherlands (GIP) multiple 3D basin models of the Dutch subsurface were constructed in the years from 2008 to 2013. These models were used to create a map of the thermal maturity of the Posidonia Shale Formation in the Netherlands, calibrated to vitrinite reflectance measurements. Additional information on the different basin models and the used input data can be found in the public reports and publications for the different studies (Verweij et al., 2009 and 2010, Nelskamp and Verweij, 2012, Abdul Fattah et al., 2012a, 2012b and 2012c).

The calculated and calibrated maturity of the top of the Posidonia Shale Formation shows low levels of maturity <1 %Ro for most of the onshore area. Higher maturity (1.0 to 1.3 %Ro) is restricted to the area around the towns of The Hague and Gouda. Offshore, in the Broad Fourteens Basin and in the Dutch Central Graben, the maturity can be higher and locally even reach levels of > 2 %Ro, which can be considered overmature for oil and gas generation. Vitrinite reflectance measurements from wells were used as calibration data, however, these wells were usually drilled for oil and gas exploration and are therefore situated on structural highs, showing lower maturities. The presented map is the result of basin modelling, and is subject to the usual uncertainties related to basin modelling. Furthermore it has a resolution of 1km x 1km, smaller features such as specific shallow or deep structures might be below the resolution of the map.

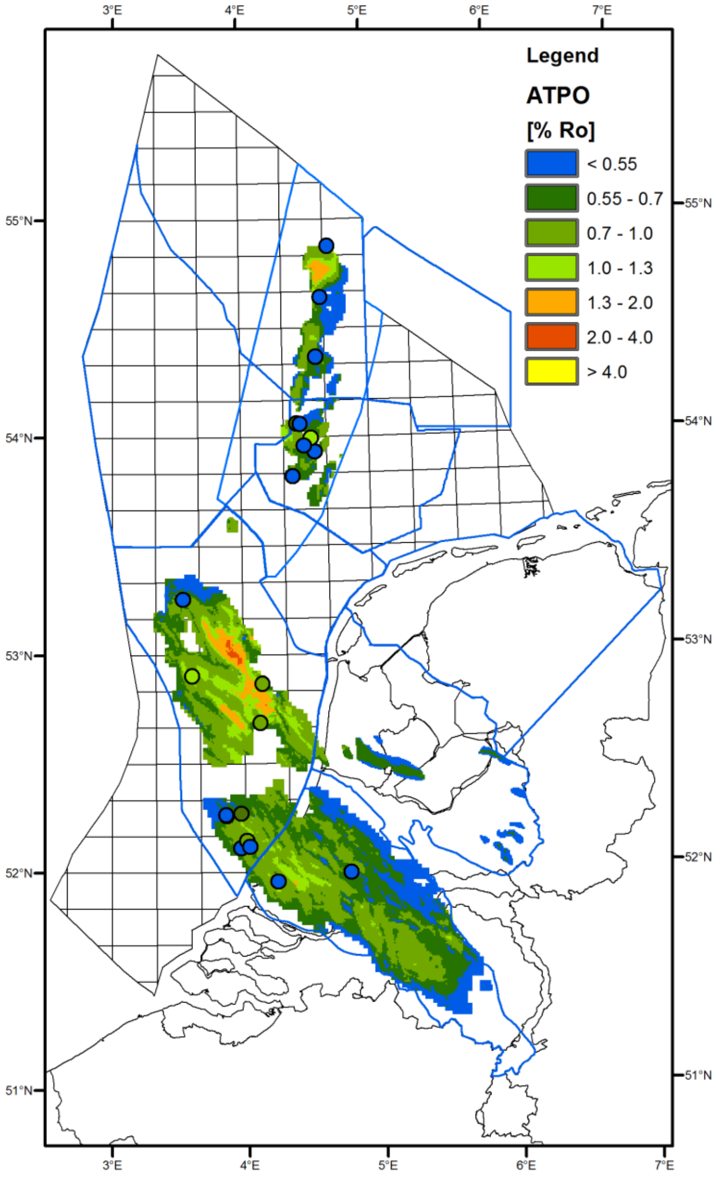

Figure 3-15 Calculated maturity of the Posidonia Shale Formation

3.5.3 *Total organic carbon (TOC)*

Measured TOC from Whitby, LOZ-01, RWK-01 and F11-01 indicate that the highest TOC in each section is concentrated in the lower part during the CIE (zones T2 and T3). Maximum values of ~19 % were measured in Whitby, in the Dutch wells values vary between 10 and 17 %. TOC measurements from Luxembourg are the lowest with values of around 10 %. However the highest TOC values in Whitby are concentrated in a thin layer while the rest of the section shows lower values of around 5 % while the TOC in the Dutch wells stays high well into isotope zone T5. On the logs several intervals were interpreted that show very high GR and low DT and RHOB. These intervals are generally interpreted as organic carbon rich intervals. These intervals were very well correlatable on the logs in the Dutch subsurface and could also be seen in the detailed TOC measurements (e.g. LOZ-01). According to recent sequence stratigraphic analyses (Slatt and Rodriguez, 2012) these intervals could represent maximum flooding surfaces or condensed sections.

The log based TOC levels do not change significantly throughout the studied region (Appendix F), the strongest variations are still in the horizontal section, with the increase in TOC from isotope zone T1 to T2, the maximum in zones T2 and T3 and the decrease in zone T5.

The only exception is the very high log based TOC in well F17-04,with values of up to 30 % TOC. The gas log of this well shows very high gas reading for the Posidonia Shale Formation with a maximum of 50% gas in the drilling fluid. The log based calculation of the TOC includes already generated in place hydrocarbons, including natural gas which is generally not included in sample measurements. A high contribution of natural gas could explain the extremely high log based TOC in this area. Rock-Eval measurements on cuttings and cores of wells F17-04, F17-05 and F17-07 from internal TNO sources and published values (Doornenbal and Stevenson, 2010) suggest that the Posidonia Shale Formation in this area is immature (T_{max} values of 420-430) while vitrinite reflectance measurements on the same samples show ambiguous results (0.5 to 1.1 %Ro). TOC measurements from these samples vary between 7 and 18%. Basin modelling results suggest higher mature areas (calculated values of 1-1.3 %Ro) to the south west of the investigated wells (Figure 3-15) so that migrated hydrocarbons from these deeper areas could contribute to the high log based TOC results.

3.5.4 *Brittleness*

In general, the calculated brittleness of the Posidonia Shale Formation is lower compared to the underlying Aalburg Formation and the overlying Werkendam Formation. In the Posidonia itself the brittleness is higher along the south-west border of the West Netherlands Basin and decreases towards the east. Another clearly visible trend is the increase in brittleness in the Dutch Central Graben from the south to the north (Figure 3-16).

There are several different processes that have an influence on the brittleness, the most obvious are the mineralogy, quartz, carbonate, clay and organic matter content and the depth of the formation. Based on the mineralogical analyses, the mineralogical composition does not change drastically between the three investigated wells. However, according to the depth map of the Posidonia (Figure 3-17), the formation is deepest in the south west of the Netherlands Basin and in the north of the Dutch Central Graben, these large scale trends can therefore probably be attributed to compaction related to depth of burial.

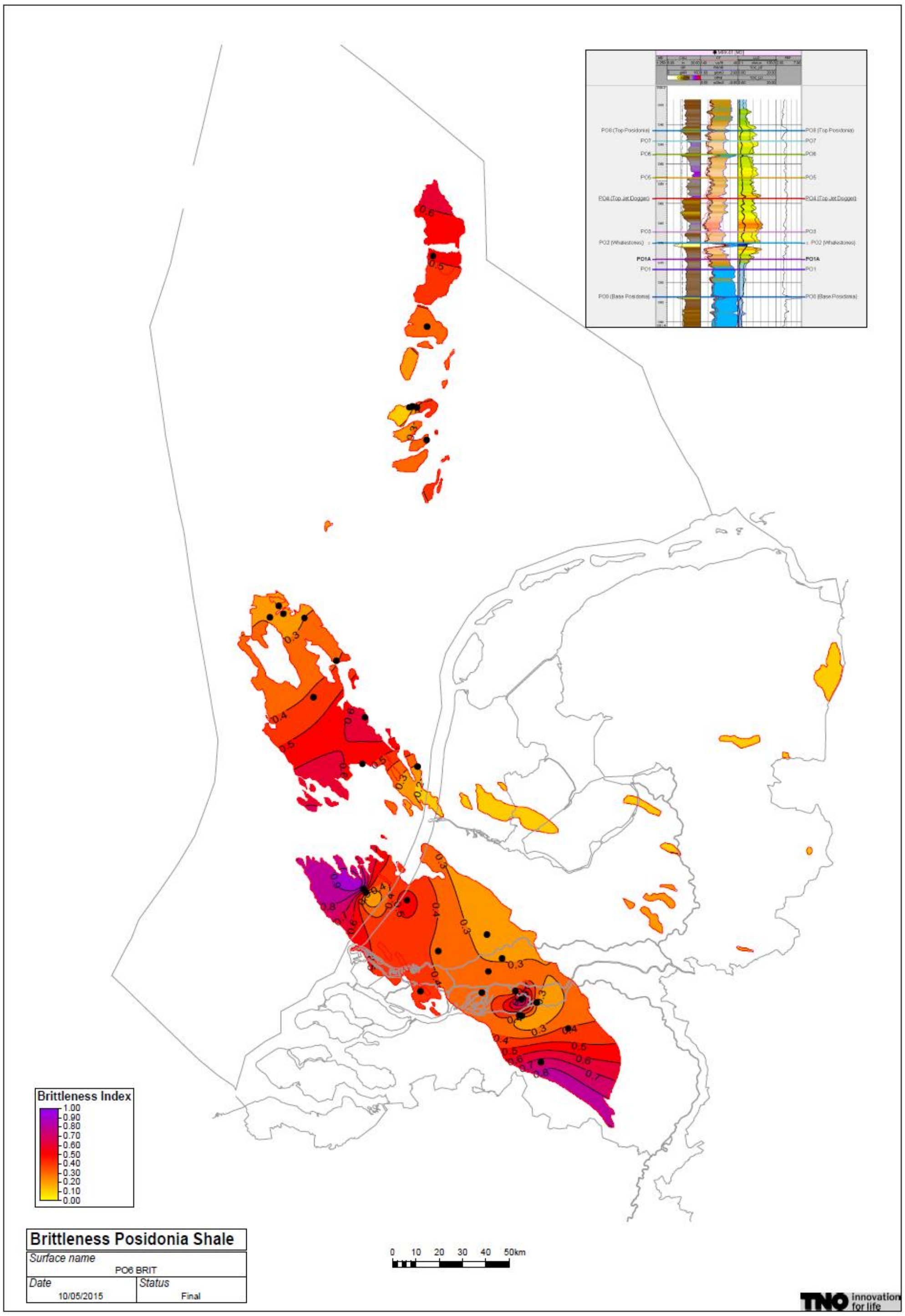

Figure 3-16 Calculated brittleness of interval PO6

There are however some exceptions. Well Q13-07-S2 shows relatively high brittleness compared to the surrounding wells, while the wells in block F17 show very low brittleness compared to the burial depth of the Posidonia in that area. The high brittleness in well Q13-07-S2 might be related to local cementation or faulting.

On the other hand, the low brittleness in the wells of F17 could be related to the high organic matter/gas content found in these wells, either because of undercompaction due to overpressure related to gas generation or because high amounts of organic matter reduce the brittleness of the rock.

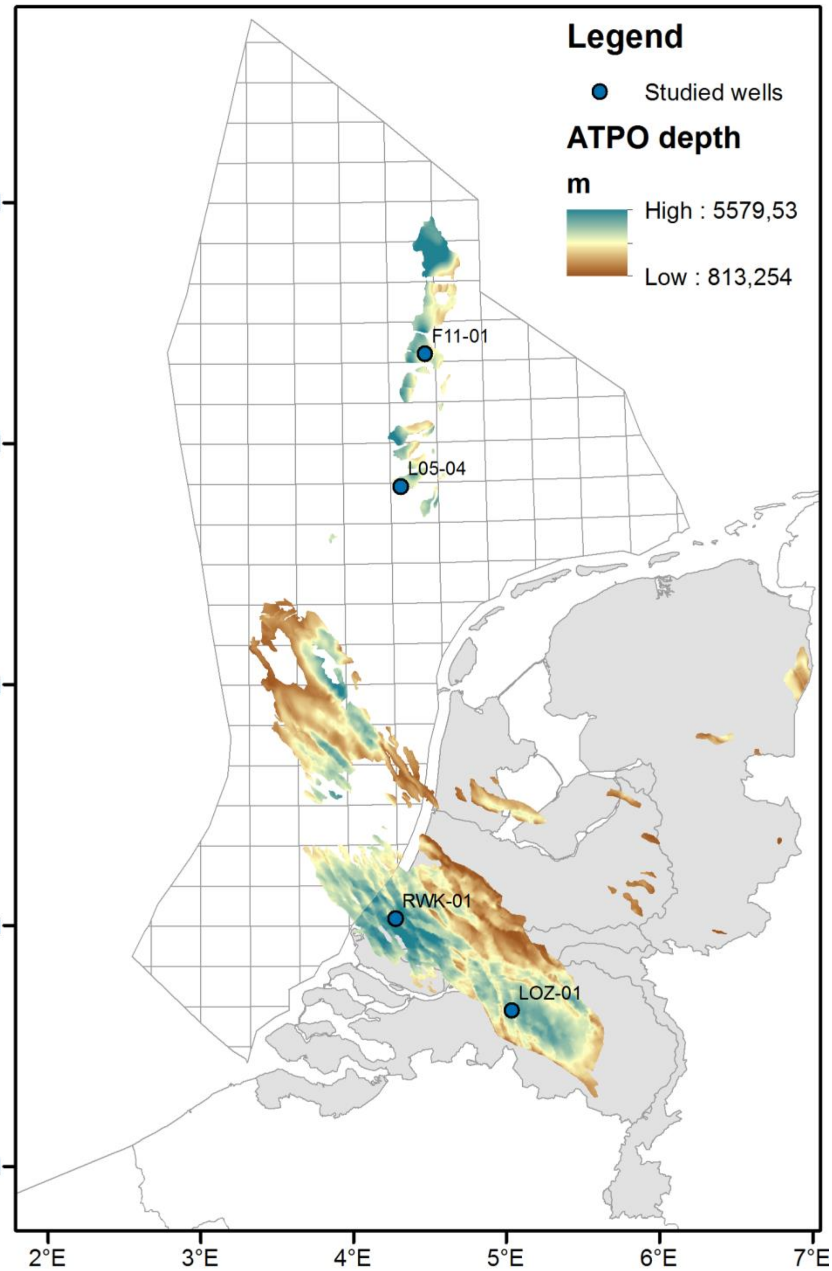

Figure 3-17 Depth map of the Posidonia Shale Formation in the Netherlands (www.nlog.nl, retrieved 2014)

4 Section 4 – Integration

4.1 Controlling parameters

Based on the palynological and geochemical analyses, the most important driving factors of depositional heterogeneity and implications for TOC- and carbonate patterns are discussed in the following section.

4.1.1 Climatic and oceanographic setting

During Early Jurassic times, the large landmasses of the supercontinent Pangaea still existed. Overall, the Early Jurassic is considered as a large 1st order transgressive sequence, culminating in the late Early Toarcian. It is this major flooding that contributed to the widespread marine shale deposition in Central and Western Europe (see also Röhl et al., 2001).

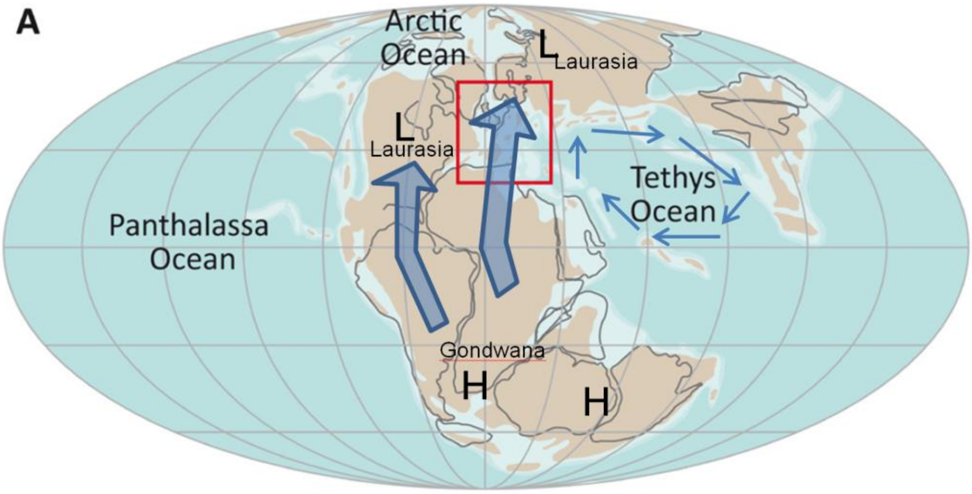

Figure 4-1 Paleogeographic configuration of the Early Jurassic and the position of the epicontinental sea that covered Western and Central Europe during the Toarcian (red square). Modified after Rubsam et al., 2014. The thick arrows indicate the direction of large-scale monsoonal wind-patterns moving across the warm and moist Western Tethys Ocean thereby gaining a lot of humidity, supplying run-off to the epicontinental NW-European basins during the Northern Hemisphere summer.

Apart from the large-scale drowning of this epicontinental platform, the paleoclimatic and oceanographic situation in line with a major climatic perturbation prompted the characteristic depositional environment giving rise to the important source-rock accumulations of the Lower Toarcian.

Given the paleogeographic configuration during the Early Jurassic (Figure 4-1), a strong monsoonal climate prevailed in Northwest Europe. The large land-masses situated between 30˚ and 60˚ latitude gave rise to a strong meridional overturning regime with vigorous monsoon- and trade winds (Dera and Donnadieu, 2012; Röhl et al., 2001). During the northern hemisphere summer, low pressure cells formed over the land masses of Laurasia. This configuration favoured a north-ward directed wind-system crossing the Western Tethys Ocean, thereby taking up substantial moisture (Dera et al., 2009, Dera and Donnadieu, 2012, Röhl et al., 2001). As part of this summer monsoonal system, enhanced rainfall led to major river discharge leading to intensified nutrient influx and reduction of surface-water salinity in the NW-European epicontinental sea. In contrast, during the Northern Hemisphere winter, high-pressure atmospheric cells existed over the Laurasian land-masses and Central Gondwana, causing a reversal of the wind system; with trade winds blowing essentially away from NW-Europe in a south-westward direction, thereby giving rise to relatively arid conditions with diminished runoff, nutrient influx and enhanced evaporation. Given the relative distance to the Tethyan teleconnection in the southeast, and the minor degree to which saline Tethyan waters were able to return to the basin, these strong seasonal contrasts likely enhanced the establishment of a strongly stratified marine basin throughout the majority of the year (Figure 4-2). This is also reflected by fossil assemblages of benthic macrofauna such as *Bositra buchii*, constituting incomplete life-stadia so characteristic for the Posidonia Shale Formation and its regional equivalents (Röhl et al., 2001). Hence, although there may have been substantial seasonal variability, enhanced fresh-water, nutrient input and photosynthetic productivity during summer/spring gave rise to strongly stratified and at least partly anoxic conditions year-round.

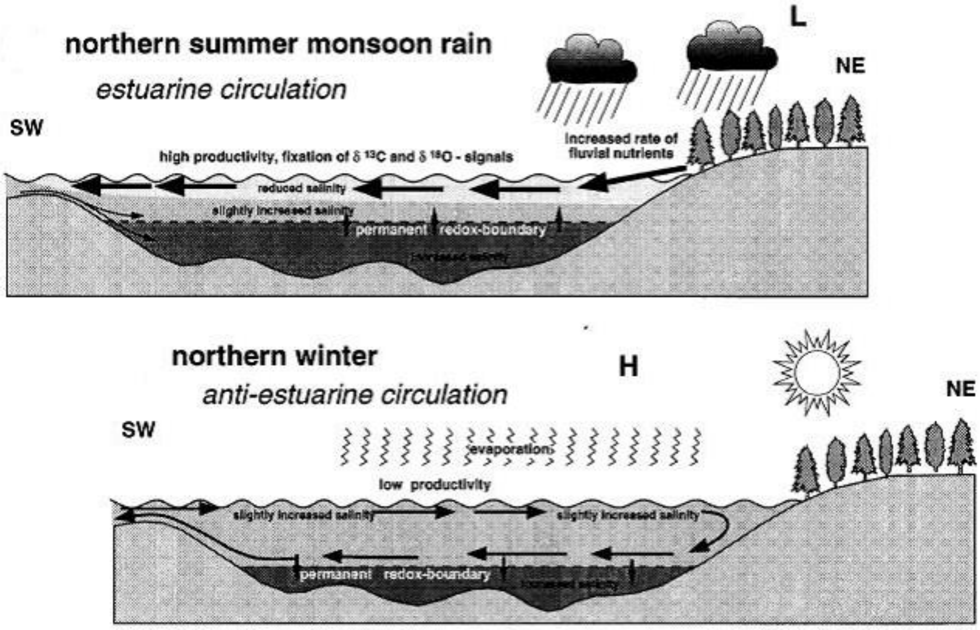

Figure 4-2 Schematic diagram illustrating the depositional model for organic-rich mudstones in NW-Europe. Modified after Röhl et al. (2001).

Many intervals of organic carbon accumulations are characterized by significant positive carbon isotope excursions (related to the burial of isotopically light carbon in organic-matter). In contrast, the Early Toarcian OAE stands out as a prominent negative excursion. The occurrence of this global negative shift in many substrates (marine carbonates and terrestrial wood fragments, Hesselbo et al., 2000) indicates that all reservoirs were affected and that this occurs despite of the enhanced burial of organic-carbon. This argues for a voluminous and rapid release of isotopically light carbon, either from methane gas hydrates or the combustion of organic-matter in large igneous provinces. The CIE invokes a rapid increase in atmospheric CO_2 concentrations and a subsequent drawdown that must have dramatically affected global and regional climate trends and climate-feedbacks. Important climate feedbacks include intensification of monsoonal circulation due to polar amplification of warming (see e.g., Huber and Caballero, 2003). Secondly, thermal expansion of sea-water in warmer climates leads to subsequent sea-level rise. Next to that, both a rapid pulse of CO_2 injection into the ocean-atmosphere system and organic-matter accumulations themselves exert a strong control on marine carbonate-ion chemistry, affecting calcification processes. These environmental forcings and effects form the basis for conceptualizing the link between the dynamic depositional environment and resultant sweet spots that will be discussed in this section.

4.1.2 Redox conditions and stratification in relation to organic-carbon accumulation

Due to the inhibition of biological oxidation/consumption, organic material is preferentially preserved under anoxic conditions. One hypothesis maintains that the development of anoxic conditions in the NW-European epicontinental sea in the Toarcian is related with intense freshwater runoff during the early Toarcian warm climatic conditions, leading to the development of a sharp pycnocline (e.g. Bailey, 2003). This pycnocline (chemocline) reflects salinity stratification of the water column with less saline water at the top and more saline water at the bottom. The pycnocline restricts mixing between the top and bottom water layers. The lack of water-column mixing may lead to oxygen depletion deeper in the water column due to the oxidative decay of ascending organic matter. High primary productivity and strong density-driven stratification both contribute to cause anoxic conditions. The data generated during this study contribute to decipher the relative impact of stratification, anoxia and productivity.

The Rijswijk core provides the only record of the interval predating the Early Toarcian CIE. Here, Fe-speciation and TOC/P in the Aalburg Formation samples indicate dysoxic to fully oxic bottom water conditions. Redox sensitive trace elements remain low. The palynological data indicate relatively normal shallow marine conditions without indications for a shallow or persistent chemocline. A similar palynological pattern is also recorded in the Loon op Zand core. Oxygenated bottom waters are also encountered in the lower part of the Grey Shales in Whitby, predating the Early Toarcian CIE, with the exception of reoccurring anoxic spikes, which were termed “sulfidic bands” (Salem, 2013). These may be considered as transient precursors to the Early Toarcian OAE.

Together with the start of negative carbon isotope excursion, the combined geochemical data (Fe-speciation and TOC/P-ratios as well as biomarker) point to persistent anoxic bottom water conditions at all sites. The indicator of sulphidic (euxinic) conditions (FeP/FeHR) displays some lateral differences. In Whitby, values are mostly at or above the threshold to euxinic conditions, indicating that hydrogen sulphide was present in bottom waters, albeit not permanently. At Well F11-01 and at Rijswijk, euxinic conditions occur slightly later, when the CIE reaches stable excursion values (Isotope Zone T2 to T3). The fact that TOC peaks in this interval indicates that oceanic primary productivity would have continued to thrive in the upper part of the water column but a high death and decay rate may have caused severe anoxic conditions leading to good preservation of organic matter. This increase in TOC is also seen in a change in biofacies, areas with highest TOC correlate with Biozones D, E and F (Figure 2-42). Both at Rijswijk and Whitby, intermittent euxinic conditions prevail beyond the recovery of the CIE (Isotope Zone

T5). Fe-speciation data only show the bottom-water redox conditions below the redoxcline.

Note however that the upper water column may in fact, still be fully oxic when bottom waters are anoxic. Both the palynological as well as biomolecular data provide insight into the redox conditions across the vertical water-column. Nitrogen is often considered a limiting nutrient in the marine realm. When waters become suboxic to anoxic, a distinct vertical chemical redox zonation of the water column develops, resulting in differences in the chemospecies of nitrogen and sulphur that are available within the photic zone (Figure 4-3). Marine green algae (Prasinophytes) have the ability to use reduced or recycled nitrogen compounds, such as nitrite or ammonium much more effectively than other algal groups. In marine environments, these reduced or regenerated nitrogen chemospecies are generally found in higher concentrations in oxygen minimum zones, thus below the pycnocline (Jenkyns et al., 2001 and Prauss, 2007). Therefore, the productivity of Prasinophytes will be generally stimulated during intervals when the nitrous and nitric zones move into the photic zone. This adaptation represents a selective advantage over algal groups that, even under nitrate limitation, preserve a high physiologic potential for fast nitrate assimilation. The palynomorphs known as *Tasmanites* are characteristically linked to modern-day Prasinophytes.

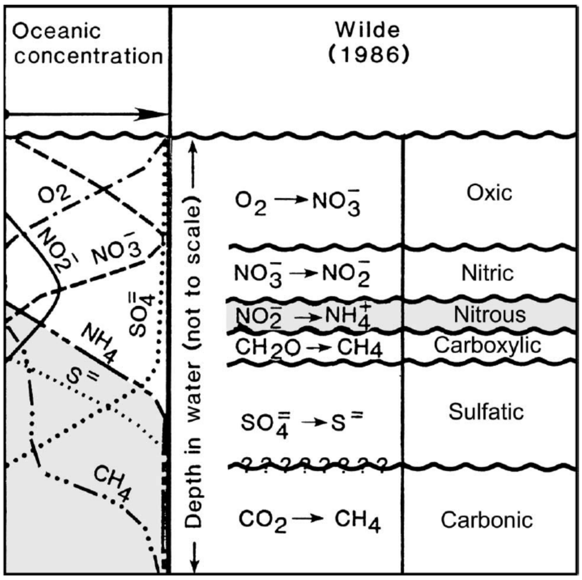

Figure 4-3 Profile of oceanic redox zones (modified after Wilde and Berry, 1986). The distribution of ammonium within a redox profile is shaded in gray. Prasinophyte algae fossilizing as *Tasmanites* are a good indicator of nitric to nitrous conditions whereas biomarkers like isorenieratane indicate toxic euxinic conditions. Modified after Prauss, 2007.

Importantly, the vertical extent of toxic euxinic conditions can also be reconstructed by detecting derivatives of anoxygenic phototropic green sulphur bacteria, such as isorenieratienes (e.g., Peters et al. 2005). If present, they indicate that the water column was anoxic and contained toxic sulphide up to the photic zone. Isorenieratane, 2.3.6-aryl isoprenoids and chlorobactene were found in variable amounts in throughout the succession of Whitby, even in the Grey Shales (Chapter 2.5.2.3, French et al., 2014 and Salem, 2013). Several other biomarkers, such gammacerane, homohopane, pristine and phytane are also indicative of redox stratification. These indicators show a change from oxic to anoxic conditions in the

Grey Shales (ca. 3 m below Jet Rock). This is also consistent with Fe-speciation that records anoxic conditions in the top part of the Grey Shales and throughout the Jet Rock. Better oxygenated bottom waters are encountered in the lower part of the grey shales, with the exception of reoccurring anoxic spikes, which were termed “sulfidic bands” (Salem, 2014). This confirms the presence of intermittent or seasonal euxinic conditions intervals into the lower photic zone in the Jet Rock. It seems likely that presence of such conditions even inhibited the full-stage growth of prasinophytes like *Tasmanites*, giving rise to the characteristic sphaericals. Therefore the distinct abundance optima of these palynomorphs can be used to detect intervals when euxinic conditions moved in- or out of the photic zone.

Consistently, mass occurrences of *Tasmanites* predate and postdate intervals that are characterized by overwhelming abundance of structureless organic matter (SOM, marine snow) that under UV-radiation appear populated by these sphaericals. Importantly, these SOM-dominated intervals coincide with levels of high TOC. If a *Tasmanites* acme is overlain by dense SOM and palynomorphs assemblages dominated by sphaericals, the chemocline must have shoaled into the photic zone. The successive disappearance of *Tasmanites* may in turn relate to the installation of toxic sulfidic conditions in the photic zone as indicated by the biomarker data. The other way round, when dinoflagellates and acritarchs return above a *Tasmanites* acme, the chemocline migrated to a level substantially below the photic zone, removing the competitional adavantage of prasinophytes over red-pigmented algae.

Based on the combined palynological and geochemical data we conclude that there is a clear relationship between the depth/intensity of (upper) water column anoxia and the preservation of organic-carbon (TOC, Figure 4-4). In contrast, there does not appear to be a prominent relation between bottom-water anoxia and TOC-accumulations. This implies that substantial organic carbon is respired within the water column during the deposition of relatively low TOC-intervals. This may be considered remarkable given the relatively shallow depositional setting of the Early Jurassic basin of NW-Europe. It is hypothesized that this relates to the relatively high paleotemperatures that spurred microbial activity.

The transitional intervals marked by the *Tasmanites* acmes appear consistently at important steps of the carbon isotope excursion, particularly at the onset of this event. This implies that there is a prominent link between the intensity of photic zone anoxia, euxinia and CO_2-induced climate change. The maximum TOC-values are consistently characterized by the biofacies type reflecting a very shallow chemocline, definitely within the photic zone and occur near the maximum excursion values and the beginning of the recovery phase (Isotope Zone 2-3). A first important and coeval chemocline shoaling occurs in correspondence with the initial isotope shift (Isotope Zone 1). It seems plausible that the hydrological cycle increasingly intensified during the global warming phase associated with the CIE, a pattern widely recorded during such episodes of transient greenhouse warmth (Huber and Caballero, 2003; Dera and Donnadieu, 2012). Note that this in fact would have been counteracted by the transgression resulting from thermal expansion of the sea-water, which would have enhanced winter mixing. Whereas the bottom water anoxia clearly lasted beyond the CIE (into Isotope Zone T6 at Rijswijk and Loon op Zand, see Figure 4-4). The photic zone anoxia started to decrease earlier in Yorkshire, immediately after the recovery phase, negatively affecting TOC-levels.

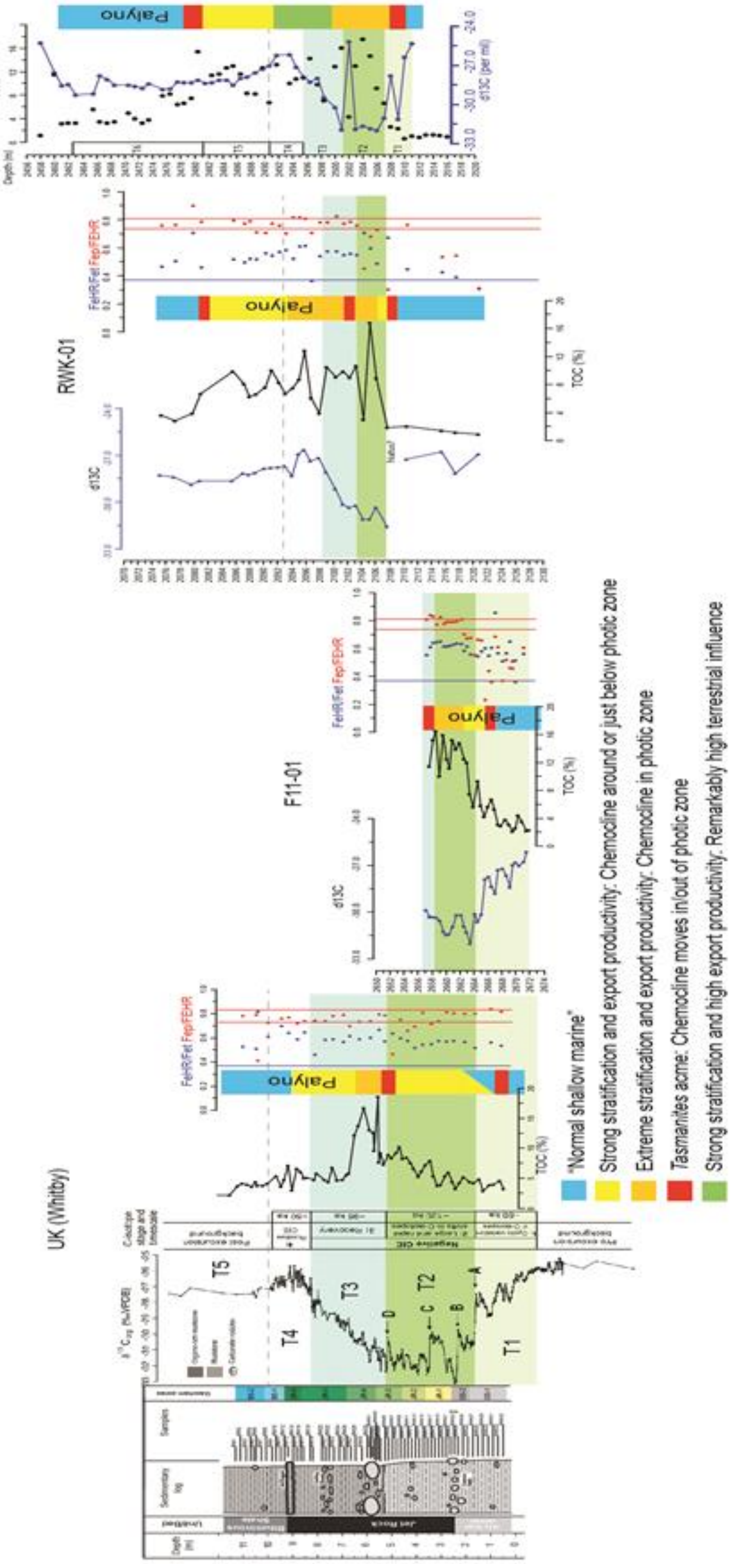

Figure 4-4 Integration of TOC analyses, palynological patterns and Fe-speciation information for anoxia and euxinia. Note that Tasmanites acmes consistently straddle the intervals characterized by photic zone anoxia and euxinia.

4.1.3 *Productivity vs. Stratification and Ventilation*

The combined palynological and geochemical data indicate that the most organic-rich deposition is associated with photic-zone anoxia and euxinia. Under such conditions, phototrophic Green Sulphur Bacteria (GSB) were likely important primary producers (see also Van de Schootbrugge et al., 2013). The consistently recorded palynological expression of high TOC-zones with dense SOM-clusers, the overall absence of ‘normal marine palynomorphs’ and the dominance (also in absolute abundance) of sphaericals which represent incomplete growth stages of prasinophyte algae corroborates the hypothesis that primary productivity did not collapse at all. In contrast all this evidence points towards a regime in which predominantly photobacterial primary productivity is substantially elevated. It thus becomes increasingly clear that relatively rapid CO_2-induced climatic change and an enhanced hydrological cycle exerted a strong control on nutrient availability and fresh water influx leading to widely dispersed stratified water conditions throughout the study basin already below the CIE. This implies that the climatic perturbation across the Early Toarcian itself was the most important driver for the development of prosperous source-rock properties. By driving an enhanced hydrological cycle, the basin strongly stratified and was progressively saturated with nutrients. This nutrient-rich and stratified regime was able to sustain a unique surface-water ecosystem boasting vast primary productivity. Successive export to the sea-floor was of course extremely efficient because of the absence of oxic remineralization. So far, there are no indications that the onset of such stratified water-conditions was strongly heterogeneous throughout the basin. This implies that local point sources of river discharge are not important in shaping TOC-sweet spots. However, we do note a heterogeneous termination, occurring earlier in Yorkshire. Possibly, this relates to a shallower depositional environment that was more susceptible to wind-driven mixing or the expected geostrophically-driven western boundary current in the western edge of the basin.

Isotope Zone T1

Locality	Chemocline	Stratification and Productivity	Terrestrial influence	Bottom water
Whitby	Below photic zone	Increases to ++	+++ shift to humid climate	Anoxic: Intermittent Euxinia
F11-01	Below photic zone	Increases to ++	++ shift to humid climate	Anoxic: Non-euxinic
Loon op Zand	Moves into photic zone	Increases to +++	++ shift to humid climate	

Isotope Zone T2

Locality	Chemocline	Stratification and Productivity	Terrestrial influence	Bottom water
Whitby	Below photic zone	++	+ Overwritten by marine productivity	Anoxic: Intermittent Euxinia
F11-01	Below photic zone	++	+ Overwritten by marine productivity	Anoxic: Euxinic
Rijswijk	Fluctuates around photic zone	+++	+/++	Anoxic: Non-euxinic
Loon op Zand	In photic zone	+++	+ Overwritten by marine productivity	

Isotope Zone T3

Locality	Chemocline	Stratification and Productivity	Terrestrial influence	Bottom water
Whitby	Lower: in photic zone Upper: fluctuates around photic zone	Lower: +++ Upper: ++	Lower: + Upper: ++ humid	Anoxic: Intermittent Euxinia
F11-01	Shoals into photic zone	+++	+	Anoxic: Euxinic
Rijswijk	Shoals into photic zone	+++	+	Anoxic: (mostly) Euxinic
Loon op Zand	Fluctuates around photic zone	+++	+++ humid	

Isotope Zone T4

Locality	Chemocline	Stratification and Productivity	Terrestrial influence	Bottom water
Whitby	Below photic zone	++	++/+++ shift to arid	Anoxic: Intermittent Euxinia
Rijswijk	Fluctuates below photic zone	++	+	Anoxic: fluctuating euxinia
Loon op Zand	Fluctuates below photic zone	++	+++ humid	

Isotope Zone T5

Locality	Chemocline	Stratification and Productivity	Terrestrial influence	Bottom water
Whitby	Below photic zone	+	++ arid	Anoxic: Intermittent Euxinia
F11-01	-	-	-	
Rijswijk	Fluctuates below photic zone	++	++ arid	Anoxic: Intermittent Euxinia
Loon op Zand	Fluctuates below photic zone	++	++ arid	

Isotope Zone T6

Locality	Chemocline	Stratification and Productivity	Terrestrial influence	Bottom water
Rijswijk	Deepens below photic zone	+	++ arid	Anoxic: mostly euxinic
Loon op Zand	Deepens below photic zone	+	+++ arid	

4.2 Important factors for shale gas exploration in the Posidonia Shale Formation in the Netherlands

4.2.1 *Thickness*

The Posidonia Shale Formation is thickest in the Dutch offshore region of the Broad Fourteens Basin with an average thickness of 36 m and local maxima of up to 46 m. According to the AAPG EMD mid-year report (2010) a thickness of > 20m is necessary, while for successful shale gas production an average thickness of 65m is generally considered (Slatt and Rodriguez, 2012).

4.2.2 *TOC and type of organic matter*

Sample measurements from different wells and calibrated log based TOC calculations suggest TOC values between 7 and 20% with local maxima of up to 30%. Even in less rich intervals (T1 and T5-6) the TOC still has average values of around 5%. This is well above the required threshold of 2-3% (Evans et al. 2001, Slatt and Rodriguez, 2012). The type of organic matter in the Posidonia Shale Formation (T2-T5) was identified to be of type II while it is of type II/III just below and above (T1 and T6). Type II organic matter is required for a successful shale gas play as stated by Kabula et al. (2003) and Slatt and Rodriguez (2012).

4.2.3 *Maturity*

The maturity of the Posidonia Shale Formation in the Netherlands is generally low with values between 0.55 and 1.0 %Ro. Onshore calculated vitrinite reflectance reaches values of 1.3 %Ro locally (Figure 3-15), offshore maturities of >2 %Ro can be reached. According to literature maturities of > 1.1 %Ro or even > 1.4 %Ro are favourable for shale gas plays (Slatt and Rodriguez, 2012 and Jarvie et al., 2007 respectively).

4.2.4 *Mineralogy/Brittleness*

The Young's Modulus (YM) and Poisson's Ratio (PR) represent a good measure of the brittleness, being primarily based on the sonic log response, which accounts for porosity, in parts for mineralogy, and also partly for the confining pressure. Comparison of the YM-PR brittleness index to mineralogy has shown that carbonates are not insignificant for the fraccability of a rock and tent to enhance brittleness, rather than suppress it. The distribution of brittleness of the Posidonia depends not only on the mineralogy but also on the porosity that is essentially related to the degree of compaction. Lastly, confining pressure plays a significant role in increasing ductility.

4.3 Cross-reference to other shale gas plays

Slatt and Rodriguez (2012) published a combined sequence stratigraphic/organic geochemical approach for several successful gas shale plays from the US, that is in parts comparable with our approach. In their conclusions they list several features that they recognized in all shale plays. In this section we compare our results to these features.

1. All shales rest on an unconformity surface which is interpreted as a combined sequence boundary formed during drop in relative sea level

   The Posidonia Shale Formation rests conformably on the Aalburg Formation and was deposited during a phase of overall rise of sea level. Deposition of organic rich shales was probably initiated by changes in atmospheric conditions.
2. High GR intervals are interpreted as organic rich shales that correspond to transgressive system tracts (TST) or condensed sections (CS) and rest either on a transgressive surface of erosion (TSE) or cap a fining upwards trend, the top of the high GR is a maximum flooding surface (MFS).

   Several high GR intervals were interpreted in the logs of the Posidonia Shale Formation. A detailed sequence stratigraphic study is needed to see whether these intervals represent TST's or CS's. However during the log correlation it became evident, that the Posidonia Shale Formation consists of several distinct cycles, that might be similar to the cycles identified in the US shales.
3. Above the MFS is an area of reduced GR highstand system tract (HST)

   In the logs the GR usually decreases after the high GR/high TOC intervals, however in the Posidonia the section just below these bands shows the lowest GR values. This might be related to cementation with early diagenetic carbonate rather than a difference in sea level.
4. The observed cycles are related to 2nd, 3rd and 4th level cyclicity.

   Ruebsam et al. (2014), Kemp et al, (2005) and Boulila et al. (2014) all relate the observed cyclicity in the Posidonia Shale Formation to 2nd, 3rd and 4th level cyclicity.
5. None are uniform black shales, all show varying degrees of stratification that can be related to climate/eustatic processes

   The same can definitively be said for the Posidonia Shale Formation, even though the differences within the Posidonia are less pronounced than the transition at the base and at the top of the Formation. One of the main differences of the Posidonia Shale

Formation when compared to the US shale gas plays is the shorter period of deposition (~1.2-1.5 Ma compared to Barnett – 22 Ma, Woodford – 33 Ma, New Albany – 20 Ma, Haynesville – 15 Ma, Eagle Ford – 7 Ma). It is therefore apparent, that the depositional conditions that lead to the deposition of organic-rich shales that are favourable for shale gas production, continued for much longer periods in time in the US shales compared to the Posidonia Shale Formation. If one, however, includes the Aalburg Formation below the Posidonia and the Werkendam Formation above into the whole assessment, the shales might be comparable.

6. TST's or CS have the highest potential for gas content, which are generally interbedded with more brittle rocks which can be better stimulated.

    Log based TOC and sample measurements support the idea, that the high GR events have the highest gas potential, however the intermittent rocks in the Posidonia Shale Formation are still very clay rich and below most of these horizons layers with extremely low porosity can be found, which might limit gas migration into the more brittle rocks. Furthermore the intermittent more brittle sections in the Posidonia Shale Formation are relatively thin compared to the US shales.

In addition to the general characteristics of the US shale gas plays that were identified using sequence stratigraphy, Slatt and Rodriguez (2012) also defined typical organic geochemical characteristics.

1. The US shales are very organic rich with TOC values of >3% and HI higher than 350 mgHC/gTOC. They are of type II oil prone organic material and consist of amorphous organic matter of >93% and H/C ratios of >1.4 for e.g., the Barnett Shale and of 80% of amorphous organic matter and H/C ratios of 1.14-1.21 for the Woodford Shale.

    Similar values were found in the organic geochemical analyses from all studied locations, the Aalburg Formation on average has less TOC (1-5%), and is of type II/III organic material.

2. Phosphatic nodules were found in the Barnett Shale, the Woodford Shale and the Monteney Shale, pyrite was found in the Barnett, Haynesville, Marcellus, Woodford and Horn River Shale
    a. Pyrite levels are high in the Posidonia Shale Formation, phosphatic nodules were not found in the study area.
3. US shale gas plays show changes in redox conditions during deposition,, variations of the amount of terrigeneous material, more oxic conditions in organic poor areas and phases of photic zone anoxia.

    According to the biomarker analysis of Whitby as well as the results of the palynology and iron-speciation all these features are also seen in the Posidonia Shale Formation.

4. The organic rich section should be thicker than 65m as thicker source rocks retain more hydrocarbons that are then available for gas generation in later stages.

    The thickness of the Posidonia Shale Formation in the Netherlands is between 27 and 48 m.

5. The maturity of the shale should be above 1.1 % Ro, e.g., the Barnett Shale has a maturity of 1.3 %Ro in the main producing area.

> There are areas in the Netherlands where the maturity of the Posidonia Shale Formation exceeds 1.1 % Ro, there are however mainly located in the offshore.

According to these features, regions of the Posidonia Shale Formation in the Dutch offshore region can be considered to be interesting targets for shale gas exploration. The onshore area might be interesting for shale oil exploration. More interesting areas might be identified when the Aalburg Formation is included in the assessment.

5 Conclusions

The results of this study can be grouped into three main parameters that are important for shale gas exploration:

- Thickness and distribution of the shale
- Organic matter composition and content
- Brittleness

In the following section the most important findings are summarised.

Thickness and distribution:

- A regional and even global correlation can be achieved using the very distinct Toarcian stable carbon isotope excursion (CIE) assuming different sedimentation rates and hiatuses. This allows a comprehensive comparison in terms of thickness variation and identification of sedimentation rate variations.
- A strong cyclic signal is present in the well log response of the Posidonia Shale, which formed the basis for a new subdivision.
- All zones are present in the entire Dutch subsurface if nothing was eroded or faulted out. No onlapping features on the surrounding massifs were observed.
- Depositional thickness variations of the Posidonia in the Netherlands are minimal (~28-36m). Local thickness maxima are observed in the vicinity of salt domes in the Dutch Central Graben area, probably related to creation of accommodation space in salt rim synclines.
- Based on the isotope correlation thickness and sedimentation rate of different locations in central Europe could be compared. The sedimentation rate during the negative shift of the CIE is low in Luxembourg and Dotternhausen (0.7 and 0.6 cm/kyr respectively) and high in RWK-01 and LOZ-01 (2.1 and 2.3 cm/kyr respectively). During the positive shift of the CIE sedimentation rate is low in Whitby and Dotternhausen (both 0.3 cm/kyr) and high in F11-01 and Luxembourg (1.9 and 2.0 cm/kyr respectively).

Organic matter composition and distribution

- According to both measurements and log calculations, the TOC of the Posidonia Shale Formation and its equivalents is overall high (4-18 %). Vertically the variations are stronger than laterally. Lowest average TOCs were measured in Luxembourg. The highest TOCs, although based on log calculation only, were recorded in the area with the highest subsidence rate/accommodation space (F-blocks of the Dutch Central Graben).
- In all studied sections the highest TOCs are invariably found in the middle zones of the formation, coinciding with the main body of the CIE. The palynological organic matter typing, persistently indicates that TOC-maxima co-occur with dominant SOM and indications for overall elevated productivity.
- According to the Fe-speciation results, bottom water conditions were persistently anoxic in the Lower Toarcian. Sulfidic bottom-water conditions are intermittently recorded.
- No direct link between TOC% and bottom water redox conditions could be observed.
- Molybdenum and Uranium concentrations suggest restricted water masses with little connection to the Tethyan or Arctic oceans during the time of the CIE

(T2-3). Intensification of surface-water mixing implying termination of basinal restriction is recorded above the CIE (T4-6), based on increases in Mo/Al ratio.

- Biomarker-, geochemical and palynological data all depict a strong change at the base of the Toarcian CIE (T1 and before): from more oxic well-ventilated near-shore surface-water conditions to strongly stratified conditions, with high marine productivity during the main body of the CIE (T2-T3). This regime is sustained throughout the Posidonia Shale Fm., also after the CIE (T4-T5).
- There is a clear link between TOC% and surface water biofacies type. The highest TOC contents occur in biozones “orange” and “red”, which are both dominated by structureless organic matter (SOM).
- In all studied sections SOM and spherical dominance is preceded and post-dated by mass-occurrences of Tasmanites, a prasinophyte green algae. Based on the characteristic ecology of this group, we infer these occurrences to mark the transition of the chemocline into- or out of the photic zone. This likely implies that euxinic conditions migrate substantially throughout the water-column, even into the photic zone and back.
- This leads to the interpretation that TOC maxima are caused by/related to shoaling of the chemocline into the photic zone, rather than local nutrient supply boosting productivity. Low-salinity induced stratification in conjunction with ample nutrient availability thus sets the stage for a highly productive, largely microbial ecosystem. The anoxic underlying water-column causes extremely efficient organic-matter export.
- The increasing overall net productivity is caused by the addition of an anoxygenic photosynthetic ecological niche.

Brittleness

- The Brittleness of the Posidonia Shale Formation is mainly related to carbonate content and depth. Due to the high clay and organic matter content of the formation it is generally lower than surrounding formations.
- Calcite content relates to initial in situ sedimentation of fossil (-fragments) while dolomite/ankerite content is related to early pre-compaction diagenetic processes. Late diagenetic carbonate (Beef or fibrous calcite), possibly related to fluid/hydrocarbon expulsion, has only been detected in F11-01.
- Log based brittleness shows zones of higher brittleness alternating with zones of lower brittleness.

Based on these results the Posidonia Shale Formation can be compared to productive shale gas formations from the US, as summarised by Slatt and Rodriguez (2012). It is however, generally thinner and less mature than the respective US shales.

6 Implications and recommendations

The results of this study suggest that it might be useful to include the whole of the Lower Jurassic into the shale gas assessment. The Posidonia Shale Formation itself is an excellent oil source rock with a very homogeneous lateral distribution in the Netherlands but due to lower thickness and maturity (onshore) it seems better suited for a shale oil than a shale gas target. Other studies suggest environmental precursors that may provide additional source rock intervals in the Lower Jurassic of the Cleveland Basin (Salem, 2013, Littler et al., 2009). Including these deeper and more mature source-rock layers, together with more brittle rocks of the organic-poor intervals in between could give a much better shale gas target.

In order to understand the driving forces of black shale deposition in more detail (e.g., what are the effects of the small massifs compared to sediment supply from large Laurasian landmasses), it would be useful to include other formations from other events into the study or to look at Toarcian black shales from different paleogeographical areas such as Portugal, Argentina or Japan. Nevertheless, we have shown that high TOCs are likely to occur in the deepest and subsiding areas (F-blocks of the DCG). This may suggest that there is a link between initial topography in such relatively isolated epicontental settings that are affected by low-salinity induced stratification.

Finally, to achieve a better correlation between samples and log-based calculations a cored section recovered from a well with a good/modern log suite is much needed. Hesselbo et al. (2013) put forward a proposal to drill a shallow research well in the area of West Wales in the context of the ICDP which has the Lower Jurassic as a target. The planned drilling time is October 2015 to March 2016. Provided that access to sample material and log suites is available, this would be a good opportunity to improve the correlation.

7 References

AAPG EMD mid-year report November 2010, 42p.

Abdul Fattah, R., Verweij, J.M., Witmans, N., ten Veen, J., 2012a. 4D Basin modelling of the Broad Fourteens Basin and offshore West Netherlands Basin; Erosion and heat flow reconstruction and its influence on temperature, maturity and hydrocarbon generation. TNO report, TNO2012R10670, 167p.

Abdul Fattah, R., Verweij, J.M., Witmans, N., 2012b. Reconstruction or burial history, temperature, source rock maturity and hydrocarbon generation for the NCP-2D area, Dutch Offshore. TNO report, TNO-034-UT-2010-0223, 72p.

Abdul Fattah, R., Verweij, J.M., Witmans, N., ten Veen, J.H., 2012c. Reconstruction of burial history, temperature, source rock maturity and hydrocarbon generation in the northwestern Dutch offshore. Netherlands Journal of Geosciences, 91(4), 535-554.

Algeo, T.J., 2004. Can marine anoxic events draw down the trace element inventory of seawater. Geology, 32(12), 1057-1060.

Algeo, T.J., Ignall, E., 2007. Sedimentary C_{org}: P ratios, paleocean ventilation, and Phanerozoic atmospheric pO_2. Paleogeography, Paleoclimatology, Paleoecology, 256(3), 130-155.

Algeo T. J. and Lyons T. W. (2006) Mo-total organic carbon covariation in modern anoxic marine environments: Implication for analysis of paleoredox and paleohydrographic conditions. Paleoceanography 21, 1016-1029

Algeo, T.J. Tribovillard, N., 2009. Environmental analysis of paleoceanographic systems based onmolybdenum–uranium covariation. Chemical Geology, 268, pp. 211–225

Algeo, T.J., Hannigan, R., Rowe, H., Brookfield, M.E., Baud, A., Krystyn, L., 2007. Sequencing Events across the Permian-Triassic Bounday, Duryul Ravine. Paleogeography, Paleoclimatology, Paleoecology, 252(1-2), 328-346.

Altindag, R., 2002. The evaluation of rock brittleness concept on rotary blast hole drills. Journal of The South African Institute of Mining and Metallurgy, 102(1), 61-66.

Anderson T. F. and Raiswell R. (2004) Sources and mechanisms for the enrichment of highly reactive iron in euxinic Black Sea sediments. American Journal of Science 304, 203–233

Anderson R.F., LeHuray A.P., Fleisher M.Q., Murray J.W., 1989. Uranium deposition in Saanich Inlet sediments, Vancouver Island. Geochim. Cosmochim. Acta, 53, 2205–2213.

Andruleit, H., Bahr, A., Bönnemann, C., Erbacher, J., Franke, D., Gerling, J.P., Gestermann, N., Himmelsbach, T., Kosinowski, M., Krug, S., Pierau, R., Pletsch, T., Rogalla, U., Schlömer, S., NiKo-Projekt-Team, 2012. Abschätzung des Erdgaspotentials aus dichten Tongesteinen (Schiefergas) in Deutschland. Bundesanstalt für Geowissenschaften (BGR), Hannover, 57p.

Bailey, T.R., Rosenthal, Y., McArthur, J.M., van de Schootbrugge, B., Thirwall, M.F., 2003. Paleoceanographic changes of the Late Pliensbachian–Early Toarcian interval: a possible link to the genesis of an Oceanic Anoxic Event. Earth Planet. Sci. Lett. 212, 307–320.

Barnes C. E. and Cochran J. K. (1993) Uranium geochemistry in estuarine sediments: Controls on removal and release processes. Geochim. Cosmochim. Acta 57: 555-569

Bishop, A.N. & Farrimond, P. (1995). A new method of comparing extended hopane distributions. In: Organic Geochemistry vol. 23, 987-990.

Boulila, S., Galbrun, B., Huret, E., Hinnov, L.A., Rouget, I., Gardin, S., Bartolini, A., 2014. Astronomical calibration of the Toarcian Stage: implications for sequence stratigraphy and duration of the early Toarcian OAE. Earth Planet. Sci. Lett.386, 98–111.

Boulila, S., Hinnov, L.A., 2015. Comment on “Chronology of the Early Toarcian environmental crisis in the Lorraine Sub-Basin (NE Paris Basin)” by W. Ruebsam, P. Münzberger, and L. Schwark [Earth and Planetary Science Letters 404 (2014) 273-282]. Earth and Planetary Science Letters, 416, 143-146.

Bouroullec, R., Focus project team, 2015. Report of the Focus TKI project.

Breit, G.N., Wanty, R.B., 1991. Vanadium accumulation in carbonaceous rocks: a review of geochemical controls during deposition and diagenesis. Chemical Geology, 91(2), 83-97.

Brumsack, H.J., Gieskers, J.M., 1983. Intersitial water trace-metal chemistry of laminated sediments from the Gulf of California, Mexico. Marine Chemistry, 14(1), 89-106.

Canfield D. E. (1989) Reactive iron in marine sediments. Geochimica et Cosmochimica Acta 53, 619-632

Canfield D. E., Raiswell R. and Bottrell S. (1992) The reactivity of sedimentary iron mineral toward sulphide. American Journal of Science 292, 659-683

Castagna, J.P., Batzle, M.L., Eastwood, R.L., 1985. Relationships between compressional-wave and shear-wave velocities in clastic silicate rocks. Geophysics, 50(4), 571-581.

Cobbold, P.R., Zanella, A., Rodrigues, N., Løseth, H., 2013. Bedding-parallel fibrous veins (beef and cone-in-cone): worldwide occurrence and possible significance in terms of fluid overpressure, hydrocarbon generation and mineralization. Marine and Petroleum Geology 43, 1–20.

de Jager, J., Doyle, M.A., Grantham, P.J., Mabillard, J.E., 1996. Hydrocarbon habitat in the West Netherlands Basin. In : Rondeel, H.E., Batjes, D.A.J, Nieuwenhuis, W.H. (eds.) Geology of Oil and Gas under the Netherlands. Royal Geological and Mining Society, the Netherlands. Kluwer Academic Publishers, Dordrecht, 191-209.

Dera, G., Pucéat, E., Pellenard, P., Neige, P., Delsate, D., Joachimski, M.M., Reisberg, L., Martinez, M., 2009. Water mass exchange and variations in seawater temperature in the NW Tethys during the Early Jurassic: Evidence from neodymium and oxygen isotopes of fish teeth and belemnites. Earth and Planetary Science Letters, 286, 198-207.

Dera, G., Donnadieu, Y. (2012) Modelling evidences for global warming, Arctic seawater freshening and sluggish oceanic circulation during the Early Toarcian anoxic event. Paleoceanography 27.

Doornenbal, H., Stevenson, A., 2010. Petroleum Geological Atlas of the Southern Permian Basin Area. EAGE Publications b.v., Houten, 354p.

Dunk R. M., Jenkins W. J., and Mills R. A. (2002) A re-evaluation of the oceanic uranium budget. Chemical Geology. 190 45-67.

Emerson S. R. and Huested S. S. (1991) Ocean anoxia and the concentrations of molybdenum and vanadium in seawater. Marine Chem. 34: 177-196.

Espitalié, J., Deroo, G., Marquis, F., 1985. La pyrolyse Rock–Eval et ses applications. Revue de l'Institut Français du Pétrole 40, 563–579.

Evans, D., C. Graham, A. Armour and P. Bathurst 2003. The Millenium Atlas: Petroleum Geology of the central and Northern North Sea. London, Geological Society of London.

Fensome, R.A., MacRae, Ra., Moldowan, J.M., Taylor, F.J.R., Williams, G.L. (1996) The early Mesozoic radiation of dinoflagellates. Paleobiology 22, 329-338.

French, K.L., Sepúlveda, J., Trabucho-Alexandre, J., Gröcke, D.R., Summons, R.E., 2014. Organic geochemistry of the early Toarcian oceanic anoxic event in Hawser Bottoms, Yorkshire, England. ?????

Frimmel, A., Oschmann, W., Schwark, L., 2004. Chemostratigraphy of the Posidonia Black Shale, SW Germany: I. Influence of sea-level variation on organic facies evolution. Chemical Geology, 206, 199-230.

Gasparik, M., Ghanizadeh, A., Bertier, P., Gensterblum, Y., Bouw, S., Krooss, B.M., 2012. High-Pressure Methane Sorption Isotherms of Black Shales from The Netherlands. Energy Fuels, 26, 4995-5004.

Ghadeer, S.G., Macquaker, J.H.S., 2011. Sediment transport processes in an ancient mud-dominated succession: a comparison of processes operating in marine offshore settings and anoxic basinal environments. Journal of the Geological Society of London, 168, 835-846.

Gilman, R.A., Metzger, W.J., 1967. Cone-in-cone concretions from western New York: Jour. Sedimentary Petrology, 37, 87-95.

Grieser, B., B. Shelley, B.J. Johnson, E.O. Fielder, J.R. Heinze, and J.R. Werline (2006) Data analysis of Barnett shale completions. Paper SPE 100674 presented at the Annual Technical Conference and Exhibition, San Antonio, TX, 24–27 September.

Gröcke D. R., Hori R. S., Trabucho-Alexandre J., Kemp D. B. and Schwark L. (2011) An open ocean record of the Toarcian oceanic anoxic event. Solid Earth 2, 245-257

Hermoso, M., Pellenard, P., 2014. Continental weathering and climatic changes inferred from clay mineralogy and paired carbon isotopes across the early to middle Toarcian in the Paris Basin. Palaeogeogr. Palaeoclimatol. Palaeoecol.399, 385–393.

Helz, G.R., Vorlicek, T.P., Kahn, M.D., 2004. Molybdenum scavenging by iron monosulfide. Environ. Sci. Technol. 38, 4263–4268.

Hesselbo, S.P., Gröcke, D.R., Jenkyns, H.C., Bjerrum, C.J., Farrimond, P., MorgansBell, H.S., Green, O.R., 2000. Massive dissociation of gas hydrate during a Jurassic oceanic anoxic event. Nature, 406, 392-395.

Hesselbo, S.P., Jenkyns, H.C., Duarte, L.V., Oliveira, L.C.V., 2007. Carbon-isotope record of the Early Jurassic (Toarcian) oceanic anoxic event from fossil wood and marine carbonate (Lusitanian Basin, Portugal). Earth Planet. Sci. Lett. 253, 455–470.

Hesselbo, S. P., Bjerrum, C. J., Hinnov, L. A., MacNiocaill, C., Miller, K. G., Riding, J. B., & van de Schootbrugge, B., 2013. Mochras borehole revisited: a new global standard for Early Jurassic earth history. Scientific Drilling, 16, 81-91.

Huber, M. and Caballero, R. (2003) Eocene El Nino: Evidence for Robust Tropical Dynamics in the “Hothouse”. Science, 299, 877-881.

Jarvie, D. M., R. J. Hill, T. E. Ruble, and R. M. Pollastro (2007) Unconventional shale-gas systems: The Mississippian Barnett Shale of north-central Texas as one model for thermogenic shale-gas assessment: AAPG bulletin, v. 91, p. 475-499.

Jenkyns, H.C., Clayton, C.J., 1997. Lower Jurassic epicontinental carbonates and mud-stones from England and Wales: chemostratigraphic signals and the Early Toarcian anoxic event. Sedimentology44, 687–706.

Jenkyns, H. C., Gröcke, D. R., Hesselbo, S. P, 2001. Nitrogen isotope evidence for water mass denitrification during the early Toarcian (Jurassic) oceanic anoxic event. Palaeoceanography 16, 593–-603.

Kabula, M., M. Bastow, S. Thompson, I. Scotchman and K. Oygard 2003. Geothermal regime, petroleum generation and migration. In: D. Evans, C. Graham,

A. Armour and P. Bathurst, The Millenium Atlas: Petroleum Geology of the central and northern North sea. London, Geological Society of London, 289-315.

Kemp, D.B., Coe, A.L., Cohen, A.S., Schwark, L., 2005. Astronomical pacing of methane release in the Early Jurassic period. Nature 437, 396–399.

Kemp, D.B., Coe, A.L., Cohen, A.S., Weedon, G.P., 2011. Astronomical forc-ing and chronology of the early Toarcian (Early Jurassic) Oceanic Anoxic Event in Yorkshire, UK. Paleoceanography 26, PA4210. http://dx.doi.org/10.1029/2011PA002122.

King, G.E. (2010) Thirty Years of Gas Shale Fracturing: What Have We Learned? Society of Petroleum Engineers Annual Technical Conference, 19-22 September, Florence, Italy. SPE Paper 133456, 50 p.

Klinkhammer, G.P., Palmer, M.R., 1991. Uranium in the Oceans – Where it Goes and Why. Geochimical et Cosmochimica Acta, 55(7), 1799-1806.

Lafargue, E., Marquis, F. Pillot, D., 1998. Rock-Eval 6 Applications in Hydrocarbon Exploration, Production, and Soil Contamination Studies. Oil & Gas Science and Technology - Rev. IFP 53 (4), 421-437.

Lash, G.G., Blood, D., 2004. Geochemical and textural evidence for early (shallow) diagenetic growth of stratigraphically confined carbonate concretions, Upper Devonian Rhinestreet black shale, western New York. Chemical Geology, 206, 407-424.

Leythaeuser, D., Littke, R., Radke, M., Schaefer, R.G., 1988. Geochemical effects of petroleum migration and expulsion from Toarcian source rocks in the Hils syncline area, NW-Germany. Org. Geochem. 13, 489–502.

Littke, R., Baker, D.R., Leythaeuser, D., 1988. Microscopic and sedimentologic evidence for the generation and migration of hydrocarbons in Toarcian source rocks of different maturities. Org. Geochem. 13, 549–559.

Littke, R., Baker, D.R., Leythaeuser, D., Rullkötter, J., 1991a. Keys to the depositional history of the Posidonia Shale (Toarcian) in the Hils Syncline, northern Germany. Geol. Soc. Lond., Spec. Publ. 58 (1), 311–334.

Littke, R., Urai, J. L., Uffmann, A. K., Risvanis, F., 2012. Reflectance of dispersed vitrinite in Palaeozoic rocks with and without cleavage: Implications for burial and thermal history modeling in the Devonian of Rursee area, northern Rhenish Massif, Germany. International Journal of Coal Geology 89, 41-50.

Littler K., Hesselbo S. P. and Jenkyns H. C. 2009. A carbon-isotope perturbation at the Pliensbachian–Toarcian boundary: evidence from the Lias Group, NE England. Geological Magazine 147, 181-192.

März C., Poulton S. W., Beckmann B., Kuster K., Wagner T. and Kasten S. (2008) Redox sensitivity of P cycling during marine black shale formation: dynamics of sulfidic and anoxic, non-sulsulfidic bottom waters. Geochimica et Cosmochimica Acta 72, 3703-3717

Mann, U., Müller, P.J., 1987. Source rock evaluation by well log analysis (Lower Toarcian, Hils syncline). Advances in Organic Geochemistry, 13(1-3), 109-119.

Mann, U., Leythaeuser, D., Müller, P.J., 1985. Relation between source rock properties and wireline log parameters: An example from Lower Jurassic Posidonia Shale, NW Germany. Advances in Organic Geochemistry, 10, 1105-1112.

McArthur, J.M., Algeo, T.J., Van de Schootbrugge, B., Li, Q., Howarth, R.J., 2008. Basinal restriction, black shales, Re-Os dating, and the early Toarcian (Jurassic) oceanic anoxic event. Paleoceanography, 23, PA4217, doi:10.1029/2008PA001607.

Morford J. L. and Emerson S. (1999) The geochemistry of redox sensitive trace metals in sediments. Geochimica et Cosmochimica Acta 63, 1735-1750

Nelskamp, S., Verweij, J.M., 2012. Using basin modelling for geothermal energy exploration in the Netherlands – an example from the West Netherlands Basin and Roer Vally Graben. TNO report, TNO-060-UT-2012-00245, 113p.

Partin, J. W., Quinn, T. M., Shen, C. C., Emile-Geay, J., Taylor, F.W., Maupin, C. R., Lin, K., Jackson, C. S., Banner, J. L., Sinclair, D. J., 2013. Multidecadal rainfall variability in South Pacific Convergence Zone as revealed by stalagmite geochemistry, Geol, 41(11), 1143–1146..

Passey, Q.R., Bohacs, K.M., Esch, W.L., Klimentidis, R., Sinha, S., ExxonMobil Upstream Research Co., 2010. From Oil-Prone Source Rock to Gas-Producing Shale Reservoir – Geological and Petrophysical Characterization of Unconventional Shale-Gas Reservoirs. SPE 131350,

Pearce C. R., Cohen A. S., Coe A. L. and Burton K. W. (2008) Molybdenum isotope evidence for global ocean anoxia coupled with perturbations to the carbon cycle during the Early Jurassic. Geology 36, 231-234

Perez, R., and Marfurt, K. (2013) Calibration of brittleness to elastic rock properties via mineralogy logs in unconventional reservoirs, AAPG International Conference and Exhibition. American Association of Petroleum Geologists, Cartagena, Colombia.

Peters K. E. and Moldowan M. J. (1991) Effects of source, thermal maturity, and biodegradation on the distribution and isomerization of homohopanes in petroleum. Organic Geochemistry 17, 47–61

Peters K. E. and Moldowan J. M. (1993) The biomarker guide: Interpreting molecular fossils in petroleum and ancient sediments. pp.363. Prentice-Hall, Englewood Cliffs (United States)

Peters K. E., Walters C. C. and Moldowan J. M. (2005) The Biomarker Guide: Volume 1, Biomarkers and Isotopes in the Environment and Human History. Cambridge, UK: Cambridge University Press

Pletsch, T., J. Appel, D. Botor, C. J. Clayton, E. J. T. Duin, E. Faber, W. Górecki, H. Kombrink, P. Kosakowski, G. Kuper, J. Kus, R. Lutz, A. Mathiesen, C. Ostertag-Henning, B. Papiernek and F. Van Bergen 2010. Petroleum generation and migration. Petroleum Geological Atlas of the Southern Permian Basin Area. J.C. Doornenbal and A.G. Stevenson. Houten, EAGE Publications b.v.: 225-253.

Poulton S. W. and Canfield D. E. (2005) Development of a sequential extraction procedure for iron: implications for iron partitioning in continentally derived particulates. Chemical Geology 214, 209– 221

Poulton S. W. and Canfield D. E. (2011) Ferruginous conditions: a dominant feature of the ocean through earth’s history. Elements 7, 107-112

Poulton S. W. and Raiswell R. (2002) The low temperature geochemical cycle of iron from continental fluxes to marine sediment deposition. American Journal of Science 302, 744-805

Poulton S. W., Fralick P. W. and Canfield D. E. (2004) The transition to a sulphidic ocean- 1.84 billion years ago. Nature 431, 173-177

Prauss, M.L. (2007) Availability of reduced nitrogen chemospecies in the photic zone waters as the ultimate cause for fossil prasinophyte prosperity. Palaios 22, 489-499.

Raiswell R. and Canfield D. E. (1998) Sources of iron for pyrite formation in marine sediments. American Journal of Science 298, 219-245

Raiswell, R., Fisher, Q.J., 2004. Rates of carbonate cementation associated with sulphate reduction in DSDP/ODP sediments: implications for the fon-nation of concretions, Chemical Geology, 211, 71-85.

Reinicke, A., Rybacki, E., Stanchits, S., Huenges, E., and Dresen, G., 2010, Hydraulic fracturing stimulation techniques and formation damage mechanisms — Implications from laboratory testing of tight sandstone – proppant systems: Chemie der Erde 70 S3, p. 107–117.

Rickman, R., M. Mullen, J. Petre, W. Grieser, and D. Kundert (2008) A practical use of shale petrophysics for stimulation design optimization: all shale plays are not clones of the Barnett Shale: SPE Annual Technical Conference and Exhibition.

Röhl, H.-J., Schmid-Röhl, A., Oschmann, W., Frimmel, A., Schwark, L., 2001. The Posidonia Shale (Lower Toarcian) of SW-Germany: an oxygen-depleted ecosystem controlled by sea level and palaeoclimate. Palaeogeography, Palaeoclimatology, Palaeoecology, 165, 27-52.

Ruebsam, W., Münzberger, P., Schwark, L., 2014. Chronology of the Early Toarcian environmental crisis in the Lorraine Sub-Basin (NE Paris Basin). Earth and Planetary Science Letters, 404, 273-282.

Ruebsam, W., Münzberger, P., Schwark, L., 2015. Reply to the comment by Boulila and Hinnov towards “Chronology of the Early Toarcian environmental crisis in the Lorraine Sub-Basin (NE Paris Basin)” by W. Ruebsam, P. Münzberger, and L. Schwark [Earth and Planetary Science Letters 404 (2014) 273-282]. Earth and Planetary Science Letters, 416, 147-150.

Rullkötter, J., Leythaeuser, D., Horsfield, B., Littke, R., Mann, U., Muller, P., Radke, M., Schaefer, R., Schenk, H.J., Schwochau, K., Witte, E., Welte, D., 1988. Organic matter maturation under the influence of a deep intrusive heat source: a natural experiment for quantitation of hydrocarbon generation and expulsion from a petroleum source rock (Toarcian shale, northern Germany). Org. Geochem. 13, 847–856.

Salem, N.-E., 2013, Geochemical characterisation of the Pliensbachian-Toarcian boundary during the onset of the Toarcian Oceanic Anoxic Event. North Yorkshire, UK. Thesis, School of Civil Engineering and Geosciences, Newcastle University, UK, 276p.

Schlumberger (2009) Log Interpretation Charts, 2009 Edition. 310 p.

Schwark, L., Frimmel, A., 2004. Chemostratigraphy of the Posidonia Black Shale, SW-Germany: II. Assessment of extent and persistence of photic-zone anoxia using aryl isoprenoid distributions. Chemical Geology, 206, 231-248.

Slatt, R.M., Rodriguez, N.D., 2012. Comparative sequence stratigraphy and organic geochemistry of gas shales: Commonality or coincidence? Journal of Natural Gas Science and Engineering, 8, 68-84.

Song, J., Littke, R., Maquil, R., Weniger, P., 2014. Organic facies variability in the Posidonia Black Shale from Luxembourg: Implications for thermal maturation and depositional environment. Palaeogeography, Palaeoclimatology, Palaeoecology 410, 316-336.

Song, J., Littke, R., Weniger, P., Ostertag-Henning, C., Nelskamp, S., in prep. Shale oil potential and thermal maturity of the Lower Toarcian Posidonia Shale in NW Europe.

Tissot, B.P., Welte, D.H., 1984. Petroleum Formation and Occurrence,
2nd edition, Springer-Verlag, New York, p. 699.

TNO-NITG 2004. Geological Atlas of the Subsurface of the Netherlands - onshore.

Trabucho-Alexandre, J., Dirkx, R., Veld, H., Klaver, G., De Boer, P.L., 2012. Toarcian black shales in the Dutch Central Graben: record of energetic variable depositional conditions during an oceanic anoxic event. Journal of Sedimentary Research, 82, 104-120.

Tribovillard N. P., Algeo T. J., Lyons T. W. and Riboulleau A. (2006) Trace metals as paleoredox and paleoproductivity proxies: An update. Chemical Geology 232, 12-32

Tribovillard, N., Sansjofre, P., Ader, M., Trentesux, A., Averbuch, O., Barbecot, F., 2012. Early diagenetic carbonate bed formation at the sediment-water interface triggered by synsedimentary faults. Chemical Geology, 300-301, 1-13.

Van Adrichem Boogaert, H.A. & Kouwe, W.F.P., 1993-1997. Stratigraphic nomenclature of the Netherlands, revision and update by RGD and NOGEPA, Section A, General. Mededelingen Rijks Geologische Dienst, 50, 1-40.

Van de Schootbrugge, B., Bachan, A., Suan, G., Richoz, R., Payne, J.L. (2013) Microbes, mud and methane: cause and consequence of recurrent Early Jurassic anoxia following the end-Triassic mass extinction. Paleontology 56, 685-709.

Veen, J.H. ten, R.M.C.H. Verreussel, D. Ventra, M.H.A.A. Zijp, T.A.P. Boxem (2014) Improved Sweet Spot Identification and smart development using integrated reservoir characterization. TNO Report 2014 R10265, 110 p. + Enclosures.

Verreussel, R., Horikx, M., Donders, T., Bunnik, F., 2011. Vertical and horizontal characterization of the Posidonia Shale Formation in the Dutch subsurface: a palynological study. TNO report, TNO-060-UT-2011-01497.

Verweij, J.M., Souto Carneiro Echternach, M., Witmans, N., 2009. Terschelling Basin and southern Dutch Central Graben Burial history, temperature, source rock maturity and hydrocarbon generation – Area 2A. TNO report, TNO-034-UT-2009-02065, 46p.

Verweij, J.M., Souto Carneiro Echternach, M., Witmans, N., 2010. Central Offshore Platform – Area NCP2E Burial history, temperature, source rock maturity and hydrocarbon generation. TNO report, TNO-034-UT-2010-01298/A, 70p.

Wang, F. P., and J. F. W. Gale, 2009, Screening criteria for shale-gas systems: Gulf Coast Association of Geological Societies Transactions, v. 59, p. 779-793.

Wanty, R.B., Goldhaber, M.B., 1992. Thermodynamics and kinetics of reactions involving vanadium in natural systems: Accumulation of vanadium in sedimentary rocks. Geochimica et Cosmochimica Acta, 56(4), 1471-1483.

Wells, F., 2004. A new method to help identify unconventional targets for exploration and development through integrative analysis of clastic rock properties: Houston Geological Society Bulletin, 52, 34 – 49.

Wignall, P.B., Newton, R., 1998. Pyrite framboid diameter as a measure of oxygen deficiency in ancient mudrocks. American Journal of Science, 298, 537-552.

Wilde, P., Berry, W.B.N., 1986. Role of oceanographic factors in the generation of global bio-events. In: Global Bio-Events, O. Walliser (ed.); Springer-Verlag, Berlin, 75-91.

Wong, Th.E. (2007) Jurassic. In: Geology of the Netherlands (Eds Th.E. Wong, D.A.J. Batjes and J. de Jager), pp. 107–125. Royal Netherlands Academy of Arts and Sciences, Amsterdam.

Yang, Y, H. Sone, A. Hows, and M.D. Zoback (2013) Comparison of Brittleness Indices in Organic-rich Shale Formations. 47th US Rock Mechanics/Geomechanics Symposium, 7p.

Zheng, Y., Anderson, R. F., van Geen, A., Kuwabara, J., 2000. Authigenic molybdenum formation in marine sediments: A link to pore water sulfide in the Santa Barbara Basin. Geochim. Cosmochim. Acta, 64, 4165–4178.

Zijp, M.H.A.A. (2010) Shale gas possibilities for the Posidonia Formation in the onshore West Netherlands Basin. MSc Thesis, Vrije Universiteit Amsterdam, 35 p. + Enclosures.

APPENDIX A

Wells used for correlation and mapping

Nr	Well Name	Basin	NuTech processed	Posidonia partly faulted out	Surface X (ED50-UTM31)	Surface Y (ED50-UTM31)	Offset [m]	TD TVDSS [m]	TD MD [m]
1	Runswick	Yorkshire			258924,19	6049053,85	0	10	10
2	F03-03	Dutch Central Graben		x	609685	6079120	33,1	3874,4	3917
3	F11-01	Dutch Central Graben			603574	6025743	0	3000	3000
4	F08-01	Dutch Central Graben			606091	6056138	30,6	2560,4	2591
5	F17-05	Dutch Central Graben			599207	5991079	27,1	2307,6	2335
6	F17-03	Dutch Central Graben			597324	5991546	34,5	2165,1	2200
7	F17-04	Dutch Central Graben			594058	5991405	29	2592,9	2624
8	F17-07	Dutch Central Graben			595931	5991152	28,2	2271,5	2300
9	L02-02	Dutch Central Graben			603392	5977115	29,1	4085,7	4130
10	L02-05	Dutch Central Graben		x	601490	5984002	36,2	4217,9	4257
11	L02-07	Dutch Central Graben			597892	5980020	35,3	4144,9	4185
12	L05-04	Dutch Central Graben			592413	5964373	0	3000	3000
13	K14-05	Broad Fourteens Basin			539925	5905992	37,8	3299,2	3337
14	K14-02	Broad Fourteens Basin		x	536137	5901085	27	3186,1	3216
15	K15-FC-101	Broad Fourteens Basin			550976	5900779	29,9	4024,9	4060
16	K18-06	Broad Fourteens Basin			564693	5881980	36	3726,3	4087
17	K14-FA-101	Broad Fourteens Basin			541868	5902560	0	3191,4	3193
18	K18-02-A	Broad Fourteens Basin			564640	5882459	30	2796,9	2835
19	P03-01	Broad Fourteens Basin	x		554817	5866785	0	3777,8	3790
20	Q01-03	Broad Fourteens Basin	x		576918	5858173	31,4	3217,1	3250
21	Q04-01	Broad Fourteens Basin	x		575860	5838210	32,6	3098,2	3138
22	Q05-04	Broad Fourteens Basin	x		599783	5836765	33,7	1420	1558
23	P02-04	Broad Fourteens Basin	x		533546	5870812	35,1	2695,9	2731
24	P02-05	Broad Fourteens Basin	x		531701	5871516	35,9	3679,1	3715
25	P06-A-01-S4	Broad Fourteens Basin	x	x	551124	5845527	36,2	3406,8	3443
26	P06-A-02-S1	Broad Fourteens Basin	x		551125	5845526	36,2	4334,8	4371
27	P06-A-04	Broad Fourteens Basin	x		551124	5845526	36,2	3355,8	3392
28	P06-D-01	Broad Fourteens Basin	x		549107	5839415	0	3815	3815
29	P06-S-01	Broad Fourteens Basin	x	x	552915	5837151	42,7	4050,3	4093
30	Q04-07	Broad Fourteens Basin	x	x	583836	5852158	37,2	3460,8	3498
31	Q04-08	Broad Fourteens Basin	x		588917	5843350	42	2708	2750
32	Q08-02	Broad Fourteens Basin	x		594336	5828277	30,1	2534,9	2565
33	P15-01	West Netherlands Basin	x		558638	5790450	34,3	3202,9	3258
34	P15-08	West Netherlands Basin	x		565956	5791658	36	2264	2300
35	P18-02	West Netherlands Basin	x		565845	5773940	33,5	3732,5	3766
36	Q13-02	West Netherlands Basin	x		577239	5783023	36	-26	10
37	Q13-07-S2	West Netherlands Basin			576044	5784429	37,1	3408,9	3655
38	Q16-03	West Netherlands Basin	x	x	569027	5777713	40,6	2619,4	2660
39	Q16-04	West Netherlands Basin	x	x	570498	5774656	31	3808	3839
40	AND-02	West Netherlands Basin		x	643241	5736935	6	1713	1719
41	LOZ-01	West Netherlands Basin			643876	5722305	17	3045	3062
42	RWK-01	West Netherlands Basin			589966	5764859	5	2570	2575
43	AND-06	West Netherlands Basin	x		643236	5736935	11	2662,4	3136
44	BKZ-01	West Netherlands Basin	x		652386	5710248	17	2672,3	2702
45	BRAK-01	West Netherlands Basin	x		641549	5740991	11	2552,3	2689
46	CAP-01	West Netherlands Basin	x		608386	5757883	4	3696	3700
47	KWK-01	West Netherlands Basin	x		650569	5735364	12	3098,1	3281
48	WOB-01	West Netherlands Basin			606671	5780524	0	1947,4	1983
49	MRK-01	West Netherlands Basin	x		636041	5754827	9,2	2712	2813
50	OTL-01	West Netherlands Basin	x		629977	5749743	9	2753,8	3096
51	PKP-01	West Netherlands Basin	x		627235	5770403	7,9	2397,9	2751
52	RDK-01	West Netherlands Basin	x		600559	5741116	9,3	2962	3053
53	SMG-01	West Netherlands Basin	x		664160	5724721	11	3327	3338
54	WED-02	West Netherlands Basin	x		626868	5739578	7	3505,4	3516
55	WED-03	West Netherlands Basin	x		626870	5739609	11	3031,8	3125
56	WLK-01	West Netherlands Basin	x		629557	5764861	8	2409,9	2666
57	WWK-01	West Netherlands Basin	x		645456	5730439	10	3077,5	3802
58	WWN-03	West Netherlands Basin	x		642786	5729529	11	2950,7	3639
59	BSKP-01	West Netherlands Basin			613189	5772944	0	2256,3	2261
60	HST-02	West Netherlands Basin			622886	5761894	0	2245,6	2275
61	MKP-14	West Netherlands Basin			606232	5768639	0	2690,1	2820
62	RZB-01	West Netherlands Basin		x	584904	5749722	0	3084,6	3244
63	VAL-01	West Netherlands Basin			595813	5780283	0	2850	3222
64	COV-08	Lower Saxony			757006	5841949	0	2525	2526
65	VLV-01	Lower Saxony			779136	5887189	0	4026,9	4191
66	VLW-02	Lower Saxony			775225	5876869	0	4357,8	4457
67	Dielmissen	Hils syncline			954343,38	5778465,25	0	80	80
68	Haddesen	Hils syncline			932904,24	5799183,36	0	80	80
69	Wenzen	Hils syncline		x	969500,13	5769760,48	0	80	80

Earth, Life & Social Sciences
Princetonlaan 6
3584 CB Utrecht
P.O. Box 80015
3508 TA Utrecht
The Netherlands

www.tno.nl

T +31 88 866 42 56
F +31 88 866 44 75

To
EBN B.V. & Wintershall Noordzee B.V.

From
TNO Project Team; Sweet Spot Identification Phase 2

Subject
Appendix B - Review of the usability and completeness of NuTech

Date
1 June 2015

Our reference
060.05919

E-mail
thijs.boxem@tno.nl

Direct dialling
+31 88 866 36 81

Broad Fourteens Basin

- ☹ P02-03 No Nutech logs
- **P02-04** ok. No density or neutron logs in ATPO. No Nutech DT
- **P02-05** ok. No density or neutron logs in ATPO. No Nutech DT
- **P03-01** ok. No density, neutron & R logs in ATPO
- **P05-03 OK** Doubtful nlog strat interpr.
- **P06-06** ok. No density or neutron logs in ATPO. No Nutech DT. GR needs large KCL fix.
- ☹ P06-10 No Nutech logs in ATPO
- **P06-A01-S4** ok. No density or neutron logs in ATPO. No Nutech DT. Check strat!
- **P06-A02-S1** ok. No density or neutron logs in ATPO. No Nutech DT.
- **P06-A04** ok. No density or neutron logs in ATPO. No Nutech DT.
- **P06-D-01** ok. No density or neutron logs in ATPO. No Nutech DT.
- **P06-S-01** ok. No density or neutron logs in ATPO. No Nutech DT. GR very low values. ?thru casing?
- **P09-01** ok. No Nutech neutron log in ATPO.
- ☹ P09-07 no ATPO (Unc)
- **P15-01 OK**
- **P15-08** ok. No density or neutron logs in ATPO. No Nutech DT.
- **P18-01** ok. No density or neutron logs in ATPO. No Nutech DT.
- **P18-02** ok. No density or neutron logs in ATPO. No Nutech DT.
- **P18-A-02** ok. No density or neutron logs in ATPO. No Nutech DT. GR needs KCL fix.
- **Q01-03 OK.** GR needs KCL fix.
- **Q04-01** ok. No density or neutron logs in ATPO.
- ☹ Q04-03 No density or neutron logs in ATPO. No Nutech DT. Doubtful NuTech TOC. Doubtful stratigraphy.
- ☹ Q04-05 No Nutech logs in ATPO
- **Q04-07** ok. No density or neutron logs in ATPO. No Nutech GR & DT. Truncated top.
- **Q04-08** ok. No density or neutron logs in ATPO. No Nutech DT.
- **Q05-04 OK.** Clay squeeze at PO7 marker.
- **Q08-02** ok. No density or neutron logs in ATPO. No Nutech DT. GR needs serious KCL fix. Nlog strat seems 20 m deep
- **Q13-02 OK.** GR needs serious KCL fix.

- **Q04-03** ok. No density or neutron logs in ATPO. Low R.
- ☹ Q13-07-S2 No Nutech logs in ATPO
- ☹ Q16-02 Doubtful nlog strat
- **Q16-03** ok. No density or neutron logs in ATPO. No Nutech DT.
- **Q16-04** ok. No density or neutron logs in ATPO. No Nutech DT.
- ☹ Q16-05 No Nutech logs in ATPO
- ☹ Q16-FA-101 No Nutech logs in ATPO

West Netherlands Basin

- ☹ AND-06 no resistivity log in ATPO. GR needs KCL fix
- **☹** IJS-64 / IJS-64-S1 / IJS-64-S2 no logs in ATPO (NuTech)
- **KWK-01** ok; but no NPHI
- ☹ MKP-10 no logs in ATPO
- **MKP-14** ok . GR needs KCL fix
- **☹** MOL-02 / MOL-02-S2 no logs in ATPO (nutech)
- **MRK-01** ok
- ☹ OBL-01 no logs in ATPO
- **OTL-01** ok. GR needs KCL fix
- **PKP-01** ok. GR needs KCL fix. Top ATPO faulted out (CWL)?
- ☹ PRW-04 no logs in ATPO; Trias production well
- **RDK-01** ok. no RDeep, so no TOC_ld
- **☹** RKK-32-S3 no logs in ATPO. Logs ATPO in main hole
- **RZB-01** ok. No density or neutron logs in ATPO
- **SMG-01** ok. No density log in ATPO
- **SPC-01** ok. No density or neutron logs in ATPO; Rdeep doubtful
- **☹** SPG-01 does not reach ATPO. Logs in Sidetrack 2
- **☹** SPKW-01 no logs in ATPO (NuTech only).
- **VAL-01** ok. No density or neutron logs in ATPO
- **WAA-01** ok. No neutron log in ATPO
- **WED-02** ok. No neutron log in ATPO
- **WED-03 OK!**
- **WLK-01** ok**.** GR needs KCL fix
- **WOB** ok. No density or neutron logs in ATPO
- **WWK-01** ok. No density, neutron & R logs in ATPO
- **☹** WWN-02-S4 no logs in ATPO: Logs ATPO in main hole
- **WWN-03** ok. No density or neutron logs in ATPO
- **☹** WWS-01-S1 no logs in ATPO: Logs ATPO in main hole
- ☹ WWS-02 no logs in ATPO

East-Netherlands (Lower Saxony Basin)

- ☹ OLZ-06 only GR through casing
- **☹** COV-09 no NuTech logs in ATPO
- **COV-08** ok. No density or neutron logs in ATPO. No Nutech DT
- **☹** VLW-03-S5 No logs in ATPO. Logs ATPO in main hole
- **VLW-02** ok. No density or neutron logs in ATPO. No Nutech DT
- **VLV-01** ok. No density or neutron logs in ATPO. No Nutech DT


PO5
O4 (Top Jet Dogger)
PO3
PO2 (Whalestones)
PO1A
PO1
PO0 (Base Posidonia)
GR
gAPI
0
150
Color fill
d 13C
PO8
PO7
PO6
PO5
PO4
Fault Wenz
PO2 (Whale
PO1A
PO1
PO0 (Base


Runswick [SSTVD]
d 13C
-33
-23
DT001
140
US/F
30
GR
0
gAPI
130
Color fill
351957 m
F03-03 [SSTVD]
DT003
23200 m
F08-01 [SSTVD]
30500 m
F11-01 [SSTVD]
DT002
35661 m
F17-04 [SSTVD]
1830 m
F17-07 [SSTVD]
1433 m
F17-03 [SSTVD]
1949 m
F17-05 [SSTVD]
7464 m
L02-05 [SSTVD]
5434 m
L02-07 [SSTVD]
6297 m
L02-02 [SSTVD]
16916 m
L05-04 [SSTVD]
78507 m
K14-05 [SSTVD]
ATPO Erosive
PO8 (Top Posidonia)
PO7
PO6
PO5
PO4 (Top Jet Dogger)
PO3
PO2 (Whalestones)
PO1A
PO1
PO0 (Base Posidonia)


PO8 (Top Posidonia)
PO7
PO6
PO5
PO4 (Top Jet Dogger)
PO3
PO2 (Whalestones)
PO1A
PO1
PO0 (Base Posidonia)
K14-05 [SSTVD]
K14-02 [SSTVD]
K14-FA-101 [SSTVD]
K15-FC-101 [SSTVD]
K18-02-A [SSTVD]
K18-06 [SSTVD]
P02-05 [SSTVD]
P02-04 [SSTVD]
P03-01 [SSTVD]
P06-A-01-S4 [SSTVD]
P06-A-02-S1 [SSTVD]
P06-A-04 [SSTVD]
P06-D-01 [SSTVD]
P06-S-01 [SSTVD]
Q01-03 [SSTVD]
Q04-07 [SSTVD]
Q04-08 [SSTVD]
Q05-04 [SSTVD]
Q08-02 [SSTVD]
Q04-01 [SSTVD]
PSLS
m3/m3
DT003
US/F
GR
gAPI
Color fill
2 m
1 m


P06-A-02-S1 [SSTVD]
1 m
P06-A-04 [SSTVD]
6436 m
P06-D-01 [SSTVD]
49933 m
P15-01 [SSTVD]
7672 m
P15-08 [SSTVD]
17719 m
P18-02 [SSTVD]
4936 m
Q16-03 [SSTVD]
3393 m
Q16-04 [SSTVD]
10745 m
Q13-02 [SSTVD]
7054 m
Q13-04 [SSTVD]
10914 m
VAL-01 [SSTVD]
15428 m
RWK-01 [SSTVD]
16363 m
RZB-01 [SSTVD]
19014 m
RDK-01 [SSTVD]
18978 m
CAP-01 [SSTVD]
10616 m
MKP-14 [SSTVD]
12128 m
WOB-01 [SSTVD]
9931 m
BSKP-01 [SSTVD]
15171 m
PKP-01 [SSTVD]
5755 m
WLK-01 [SSTVD]
6485 m
HST-02 [SSTVD]
14551 m
MRK-01 [SSTVD]
8478 m
OTL-01 [SSTVD]
9241 m
WED-02 [SSTVD]
607 m
WED-03 [SSTVD]
14177 m
BRAK-01 [SSTVD]
4447 m
AND-06 [SSTVD]
6062 m
KWK-01 [SSTVD]
9262 m
WWK-01 [SSTVD]
821 m
WWN-03 [SSTVD]
8793 m
LOZ-01 [SSTVD]
14850 m
BKZ-01 [SSTVD]
18762 m
SMG-01 [SSTVD]
149585 m
COV-08 [SSTVD]
38934 m
VLW-02 [SSTVD]
11784 m
VLV-01 [SSTVD]
177893 m
Haddensen [SSTVD]
29815 m
Dielmissen [SSTVD]
DT
140 us/ft 30
PSLS
0.60 m3/m3 0.00
PSLS_SYNTH
DT_SYNTH
GR
GR_SP
0 gAPI 130
d 13C
-33 -23
Color fill
Fault Reverse P15-01
PO 8
POTOC 7
PO 7
POTOC 6
PO 6
POTOC51
PO 5
POTOC 4
PO 4
POTOC 3
PO 3
POTOC 2
PO 2
POTOC 12
POTOC 11
PO1
PO 0

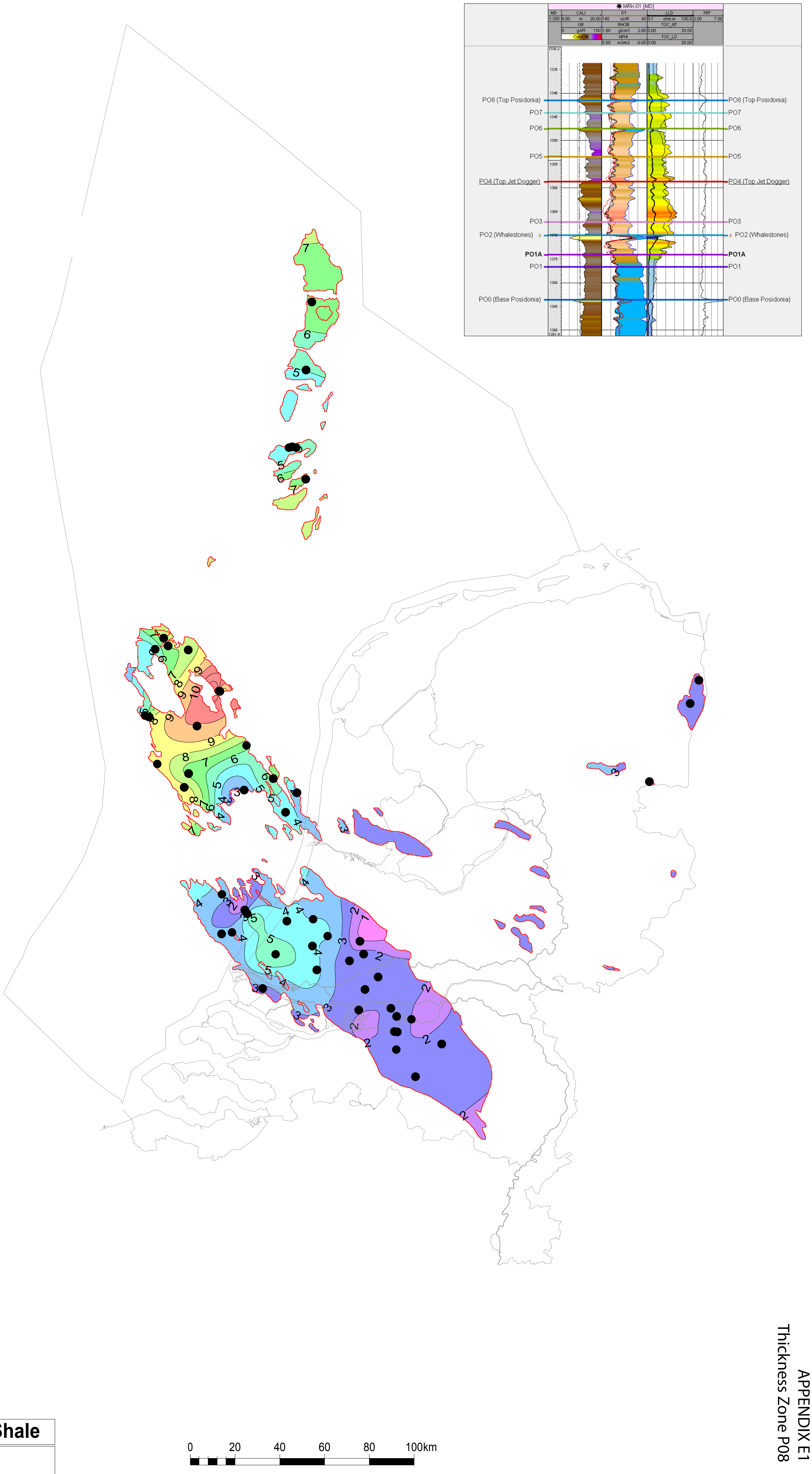

Thickness Posidonia Shale

Surface name	
PO8 Thickness	
Date	*Status*
10/05/2015	Final

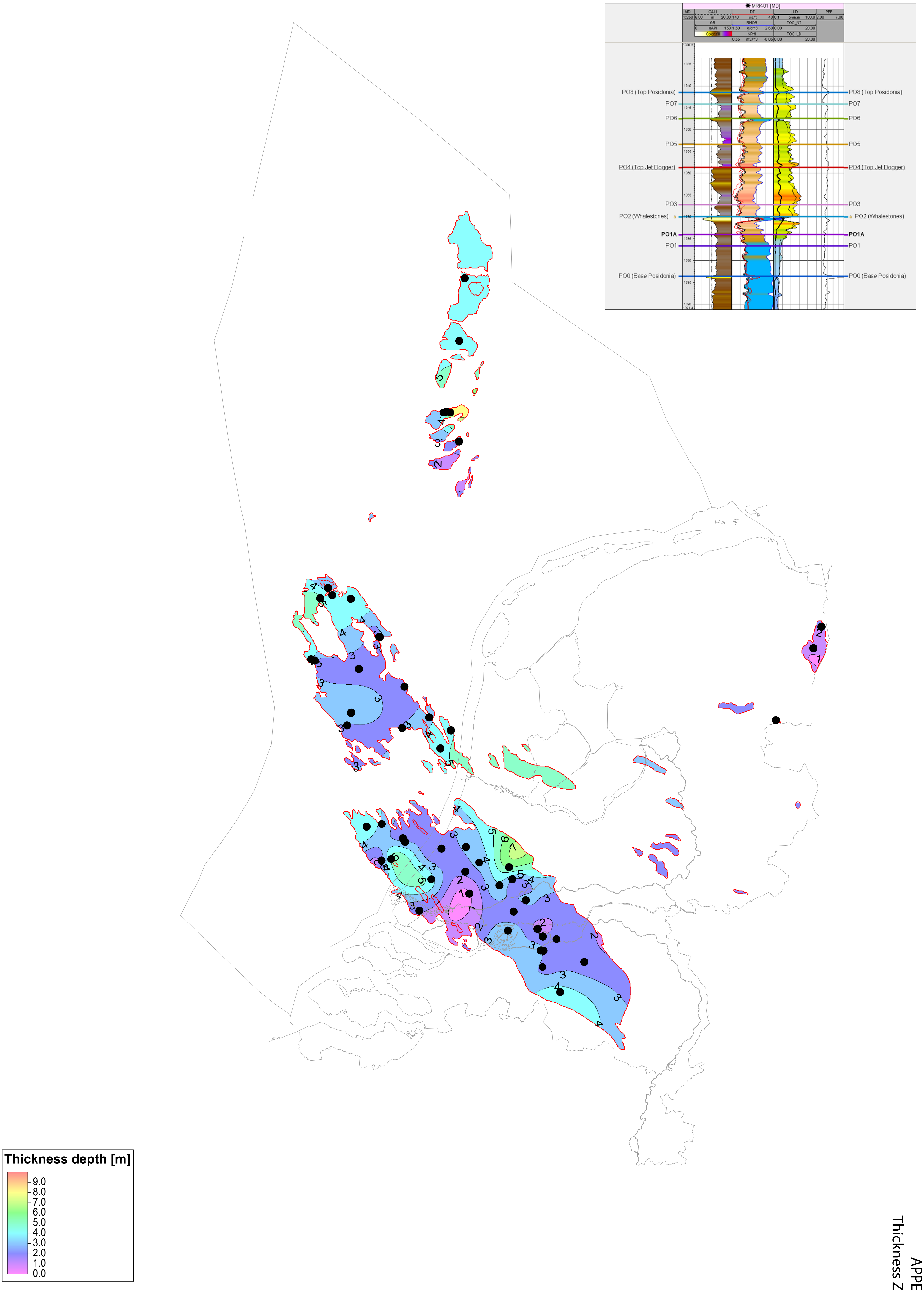

0 20 40 60 80 100km

TNO report TNO 2015 R10740
APPENDIX E2
Thickness Zone P07

Thickness Posidonia Shale

Surface name	
PO7 Thickness	
Date	*Status*
10/05/2015	Final

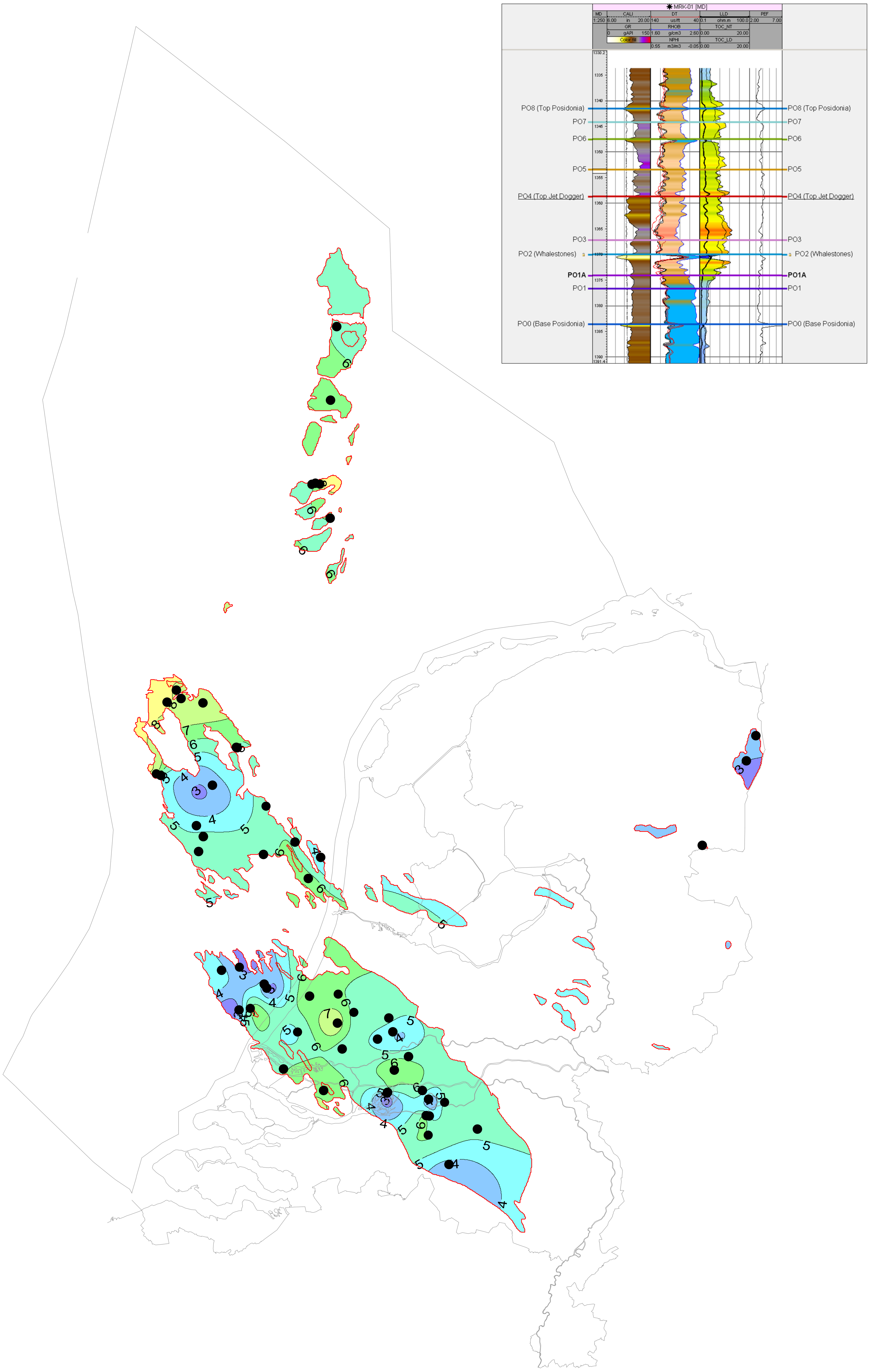

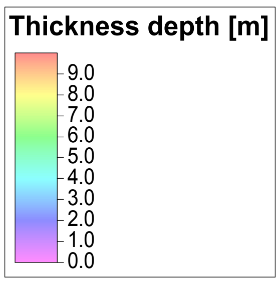

Thickness Posidonia Shale

Surface name PO6 Thickness	
Date 10/05/2015	*Status* Final

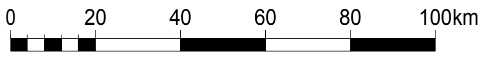

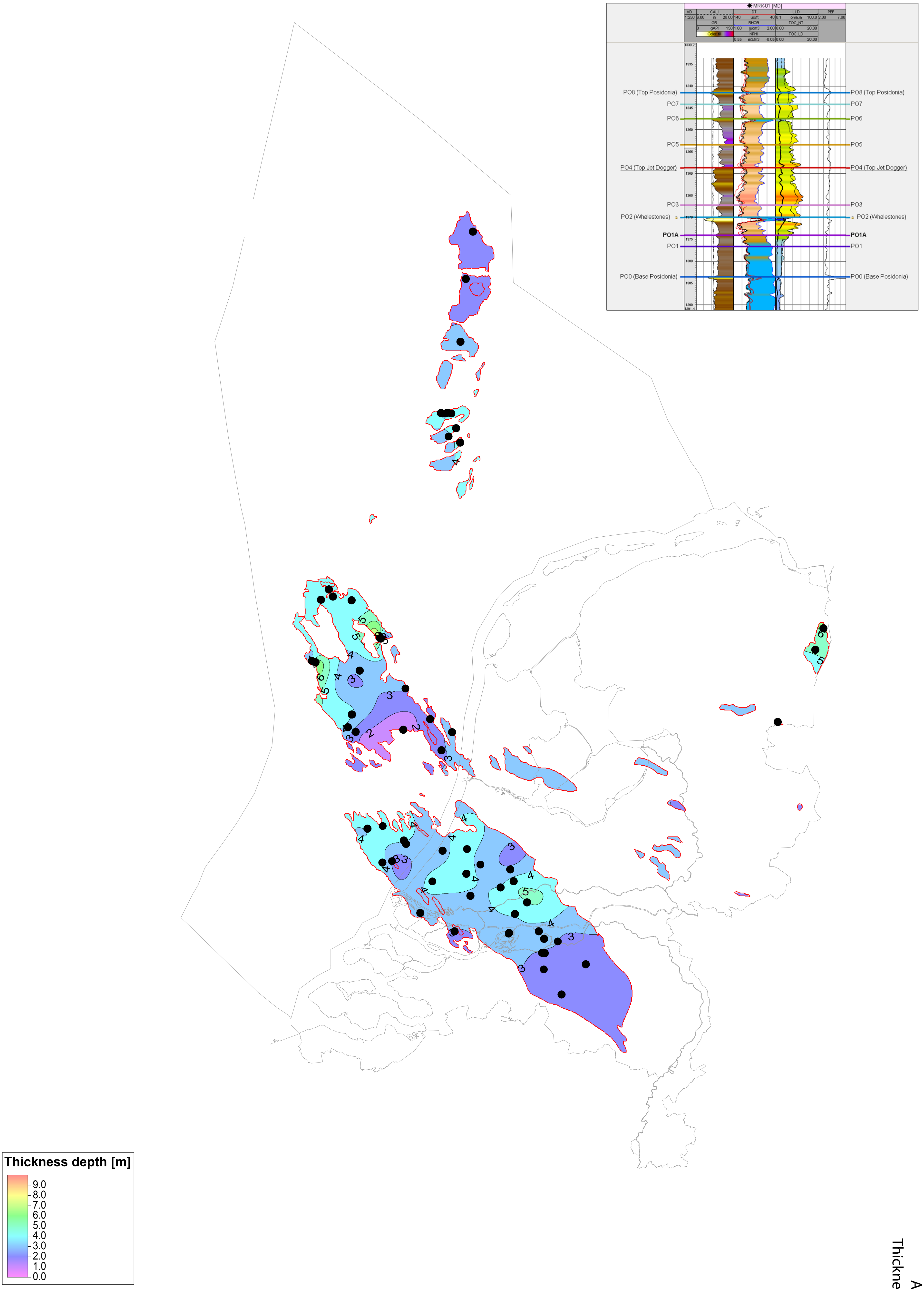

0 20 40 60 80 100km

Thickness Posidonia Shale

Surface name	
PO5 Thickness	
Date	*Status*
10/05/2015	Final

TNO report TNO 2015 R10740
APPENDIX E4
Thickness Zone P05

TNO innovation for life

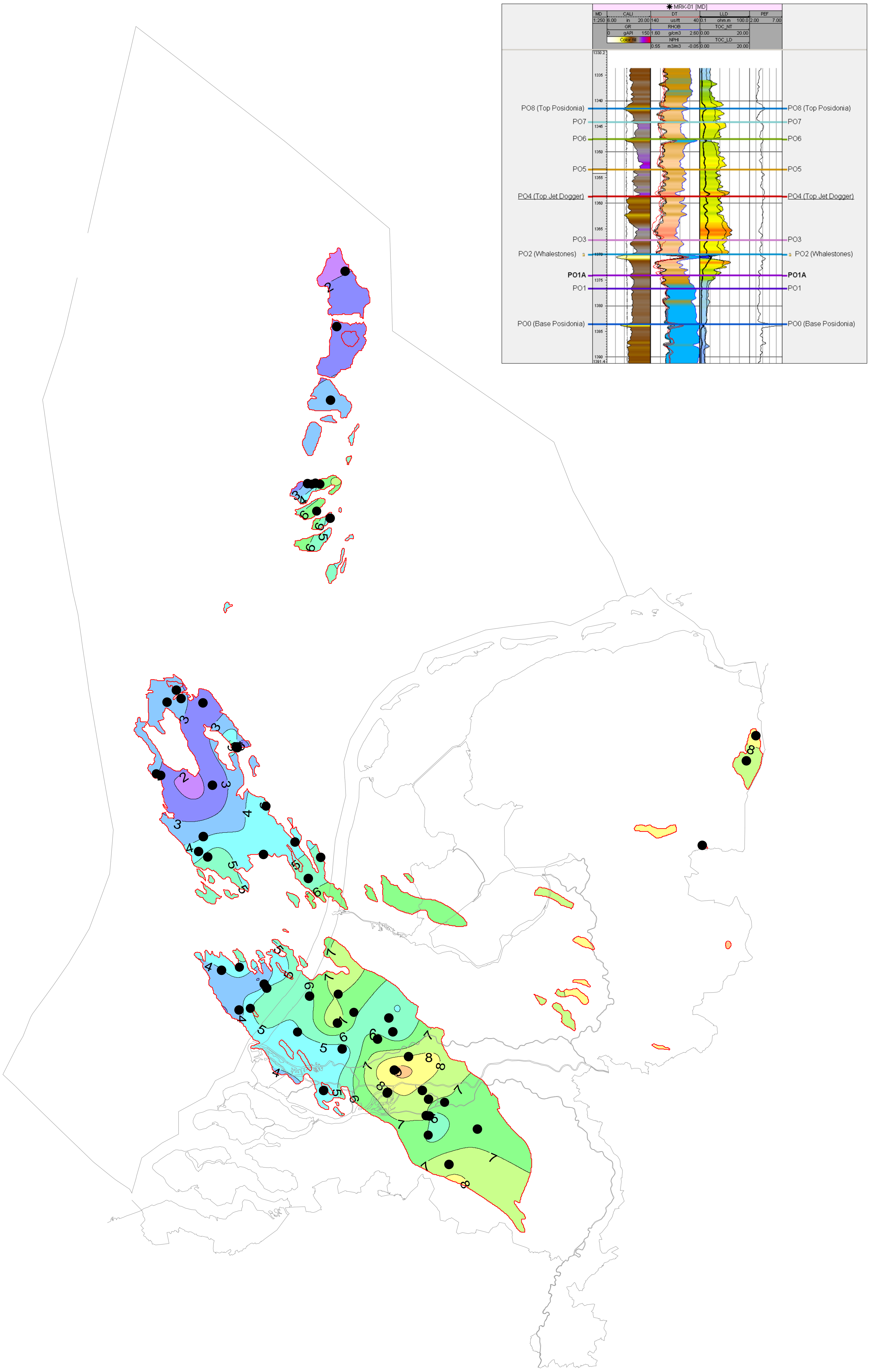

TNO report TNO 2015 R10740
APPENDIX E5
Thickness Zone P04

Thickness Posidonia Shale

Surface name
PO4 Thickness

Date	*Status*
10/05/2015	Final

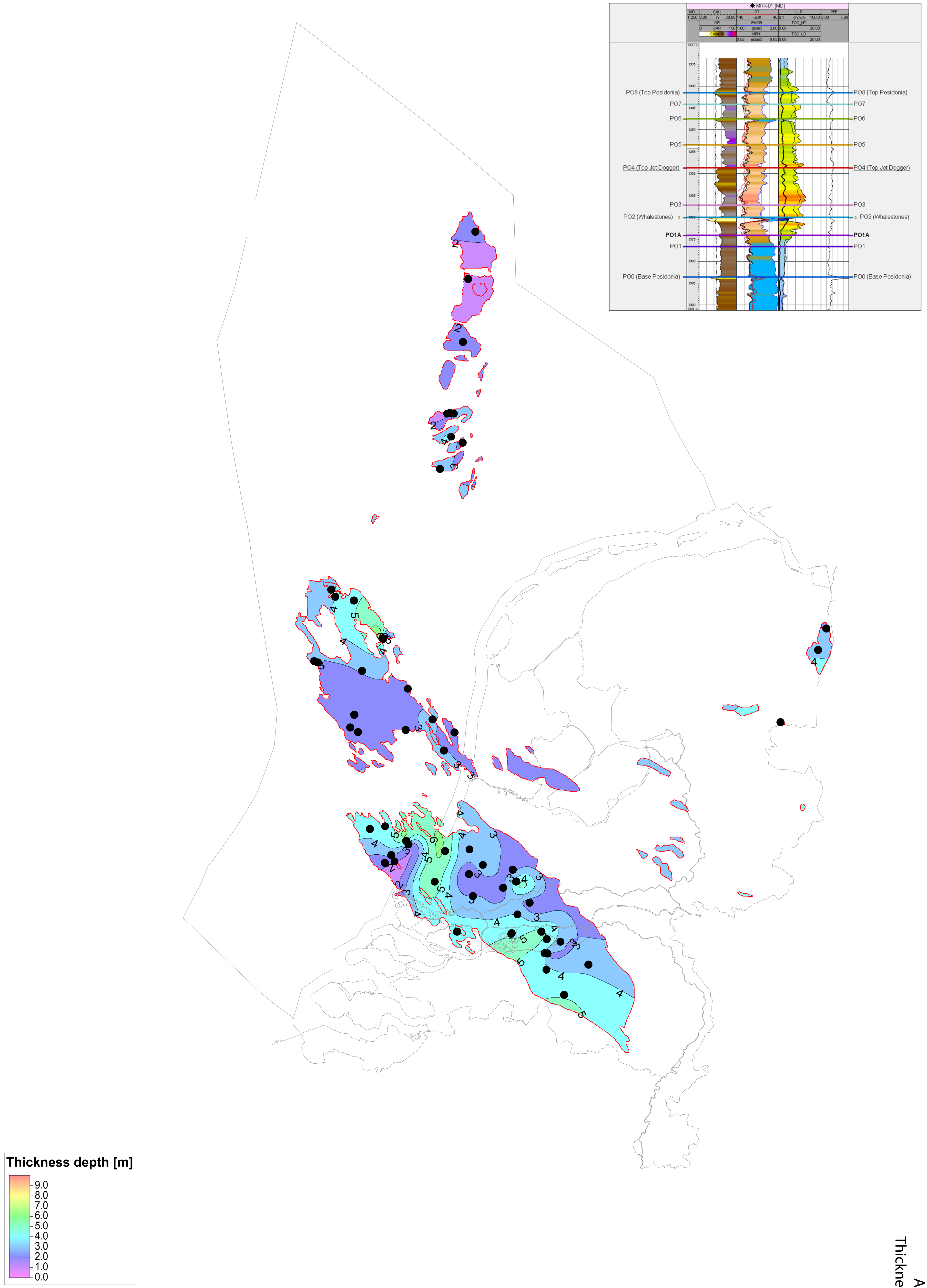

Thickness Posidonia Shale

Surface name	
PO3 Thickness	
Date	*Status*
10/05/2015	Final

TNO report TNO 2015 R10740
APPENDIX E6
Thickness Zone P03

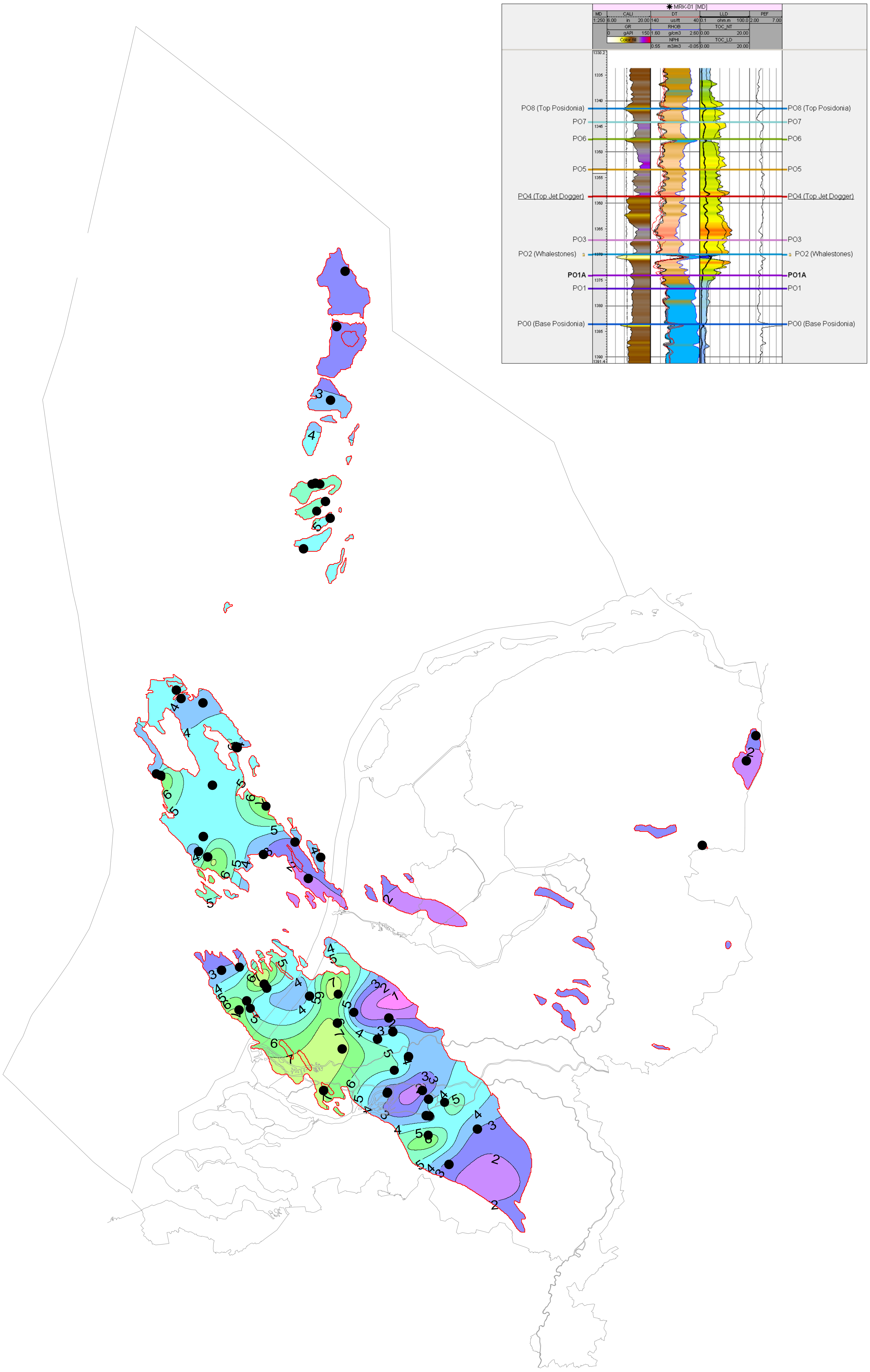

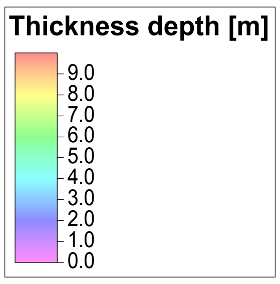

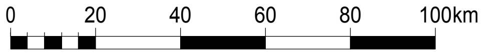

Thickness Posidonia Shale

Surface name PO2 Thickness	
Date 10/05/2015	*Status* Final

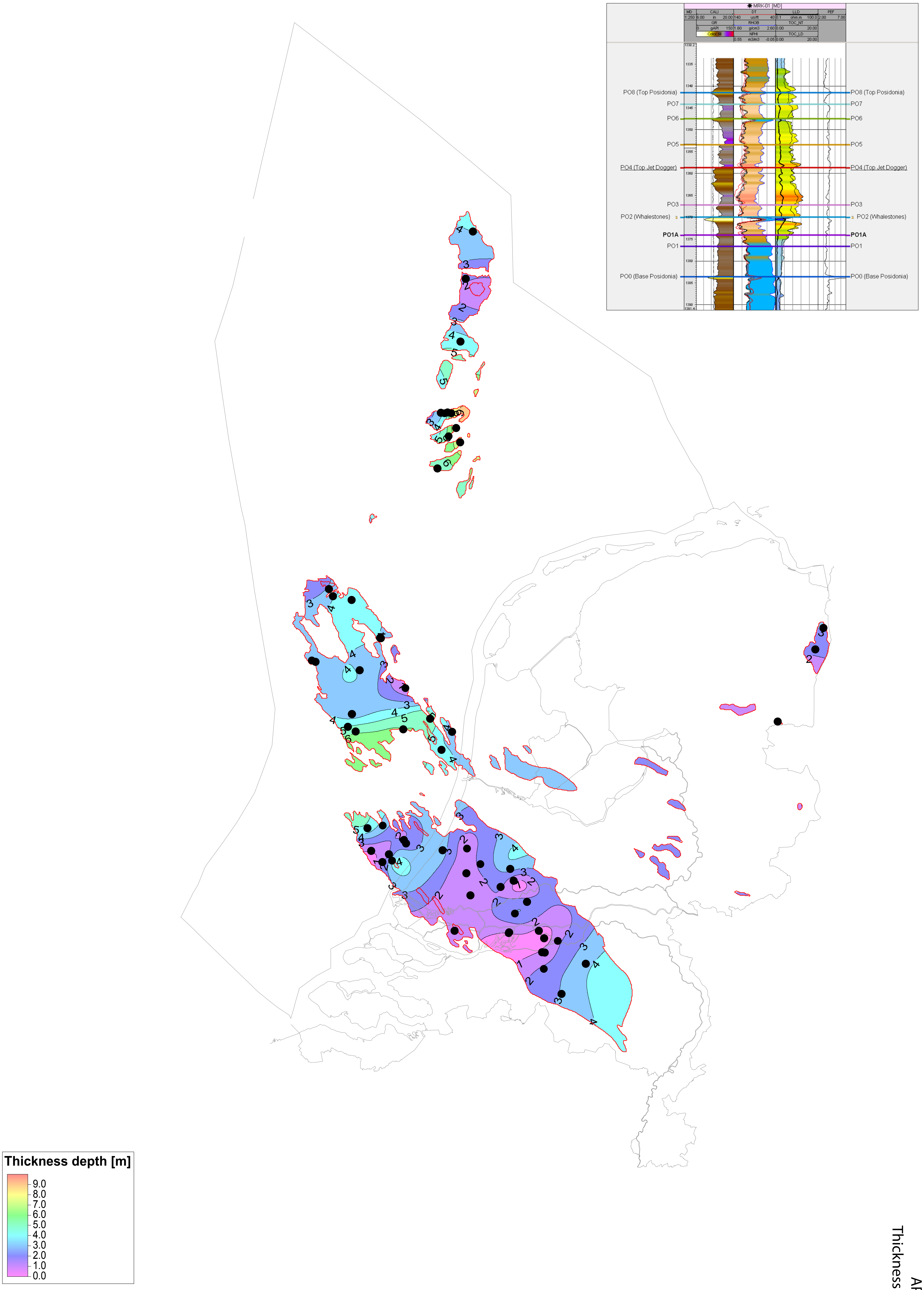

Thickness Posidonia Shale

Surface name	
PO1A Thickness	
Date	*Status*
10/05/2015	Final

TNO report TNO 2015 R10740
APPENDIX E8
Thickness Zone P01A

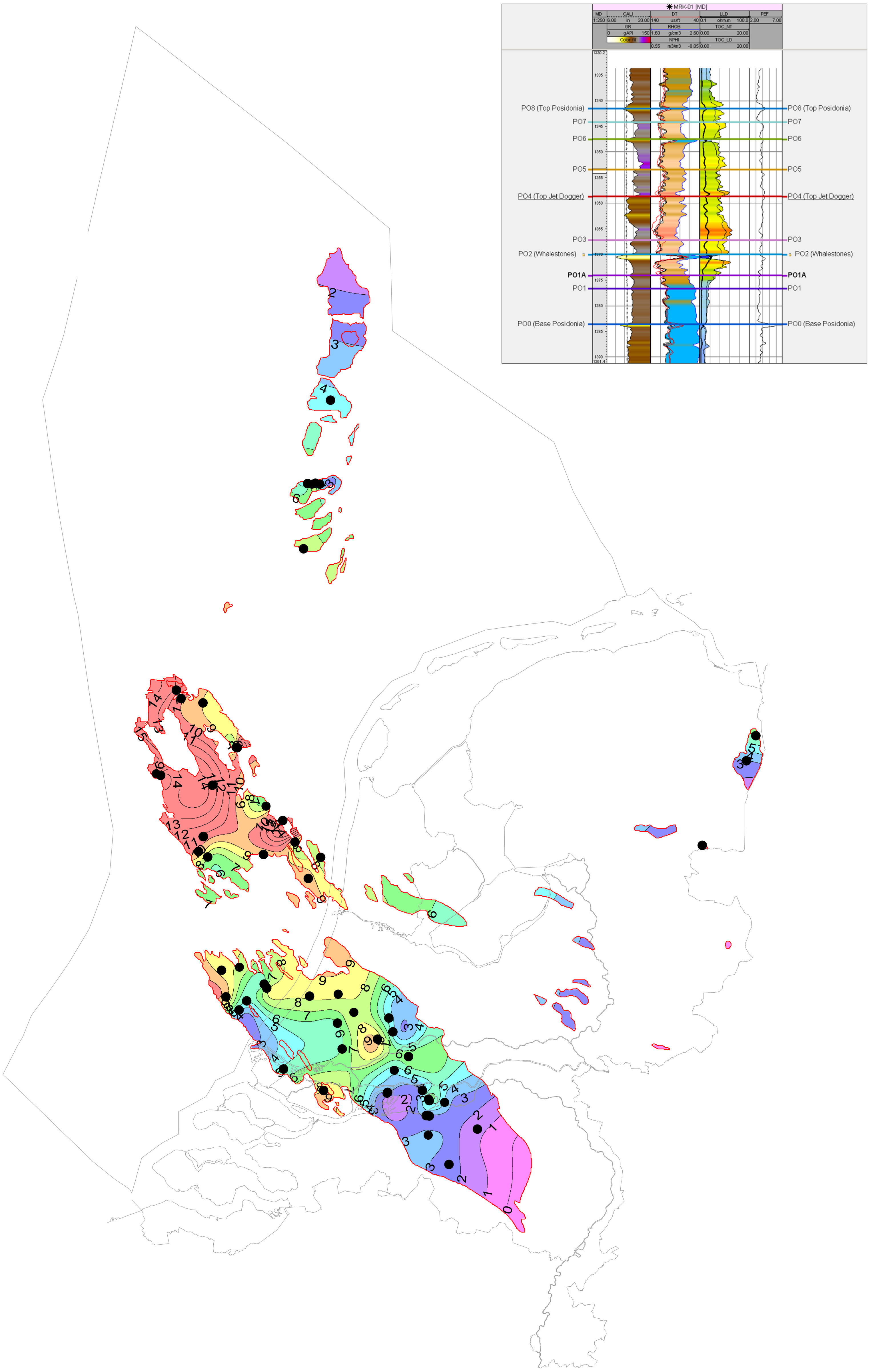

Thickness depth [m]

9.0
8.0
7.0
6.0
5.0
4.0
3.0
2.0
1.0
0.0

0 20 40 60 80 100km

Thickness Posidonia Shale

Surface name
PO1 Thickness

Date	*Status*
10/05/2015	Final

TNO report TNO 2015 R10740
APPENDIX E9
Thickness Zone P01

TNO innovation for life

TNO report TNO 2015 R10740
APPENDIX E10
Thickness Zones P05-P08

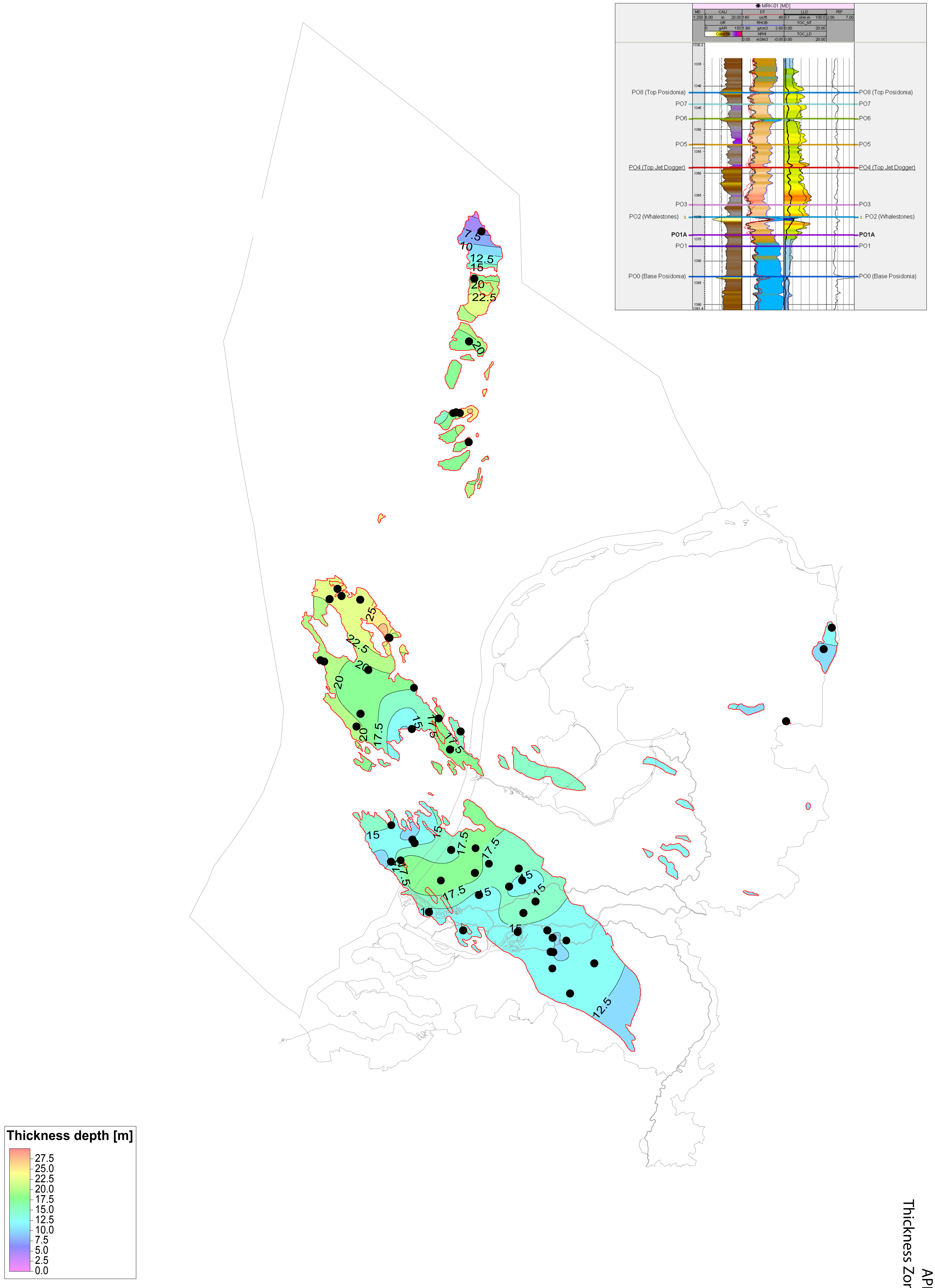

Thickness Posidonia Shale

Surface name
PO4- PO8 Thickness

Date
10/05/2015

Status
Final

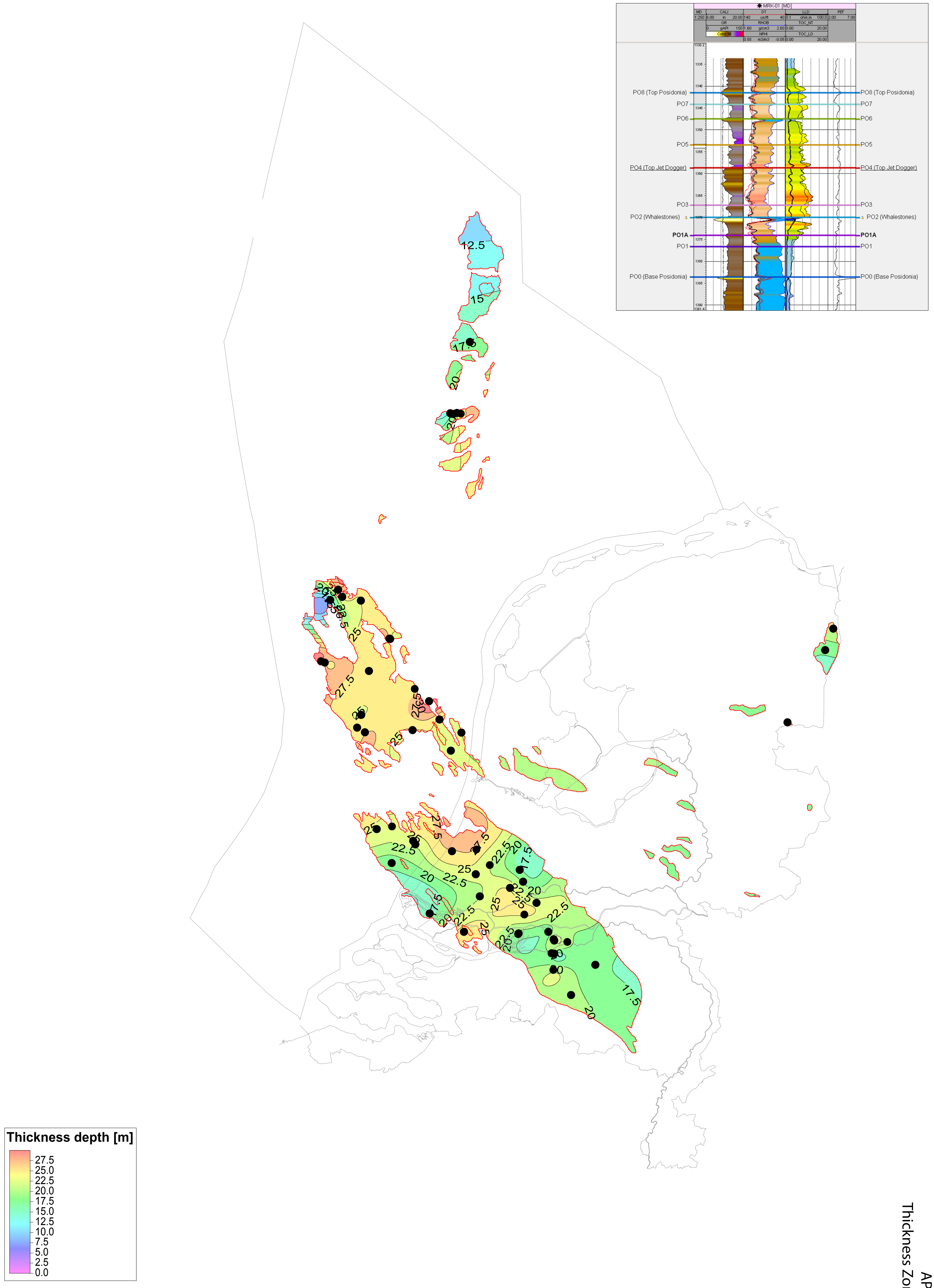

0 20 40 60 80 100km

Thickness Posidonia Shale

Surface name	
PO0 - PO4 Thickness	
Date	*Status*
10/05/2015	Final

TNO innovation for life

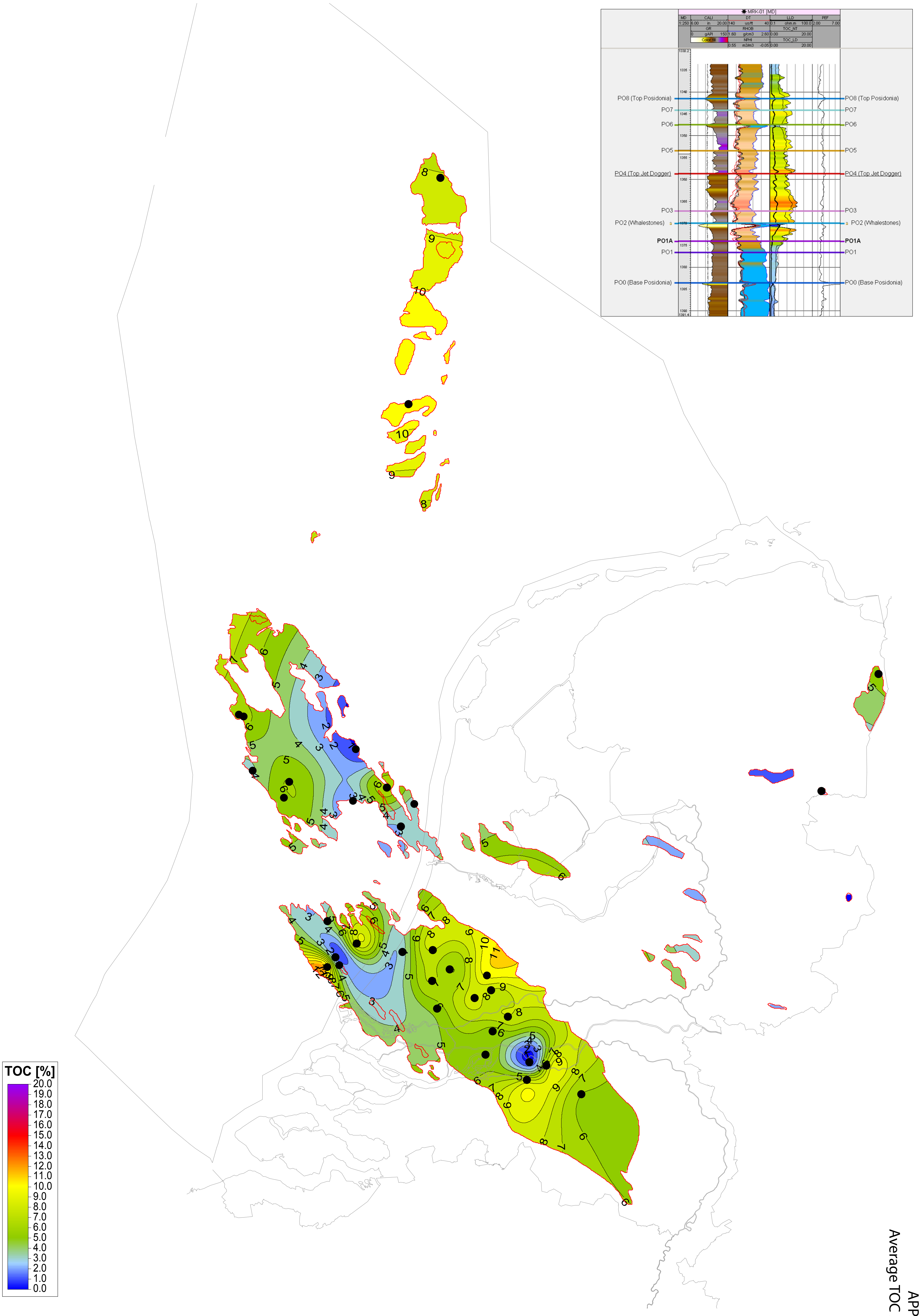

TOC Posidonia Shale

Surface name PO8 avg TOC_NT	
Date 10/05/2015	*Status* Final

Average TOC Zone P08

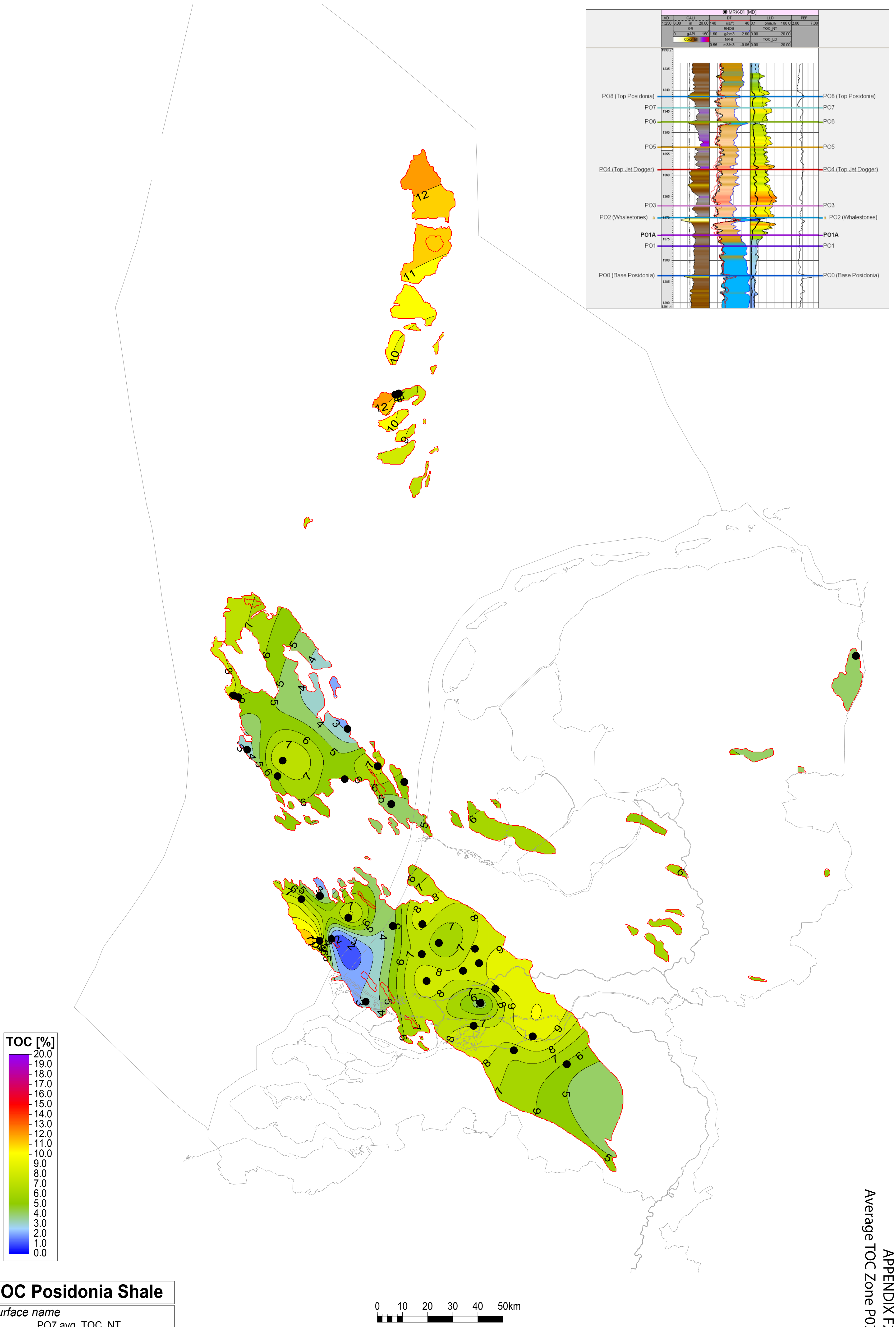

TOC Posidonia Shale

Surface name PO7 avg TOC_NT	
Date 10/05/2015	*Status* Final

TNO report TNO 2015 R10740
APPENDIX F2
Average TOC Zone P07

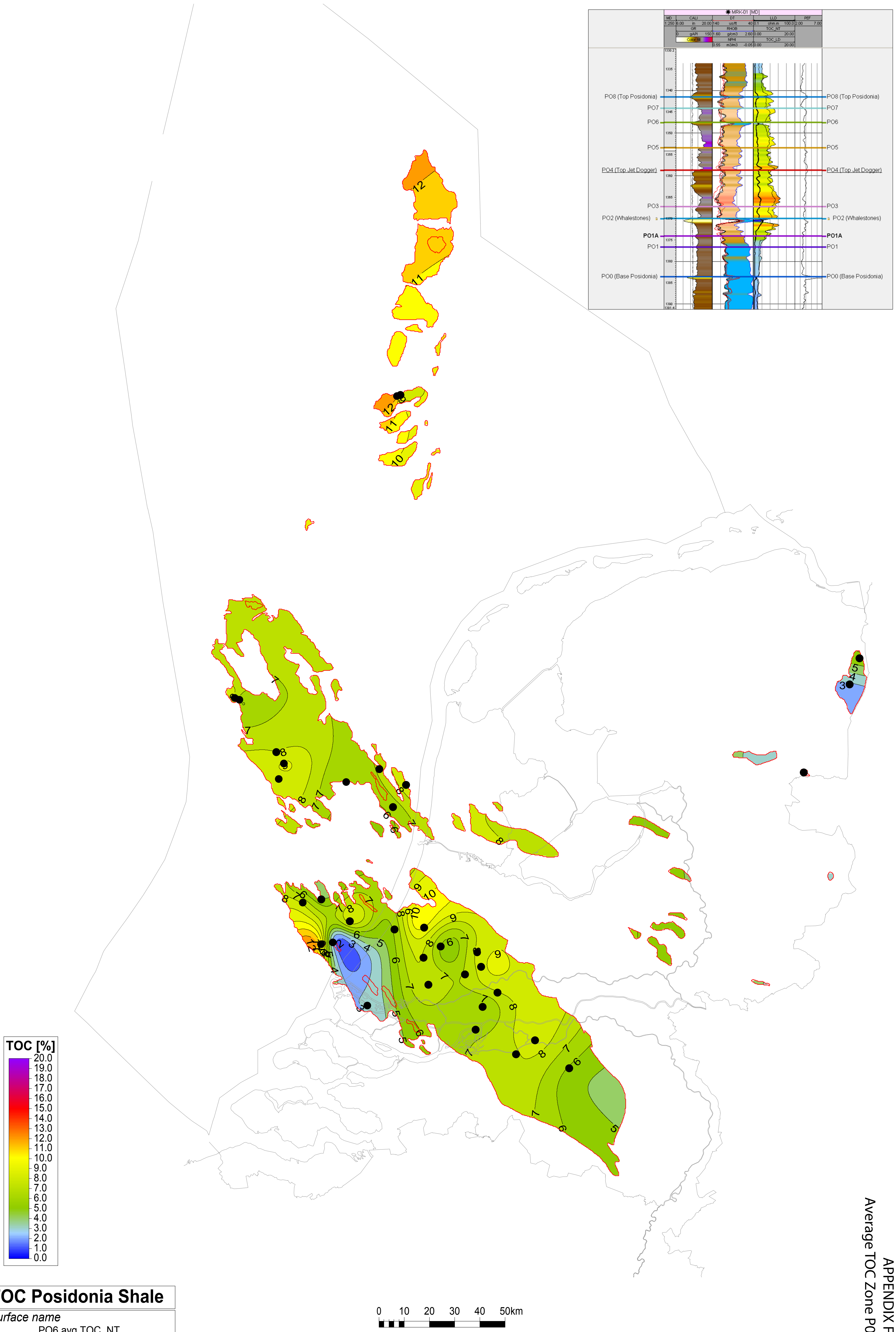

TOC Posidonia Shale

Surface name	
PO6 avg TOC_NT	
Date	*Status*
10/05/2015	Final

TNO report TNO 2015 R10740
APPENDIX F3
Average TOC Zone P06

TNO innovation for life

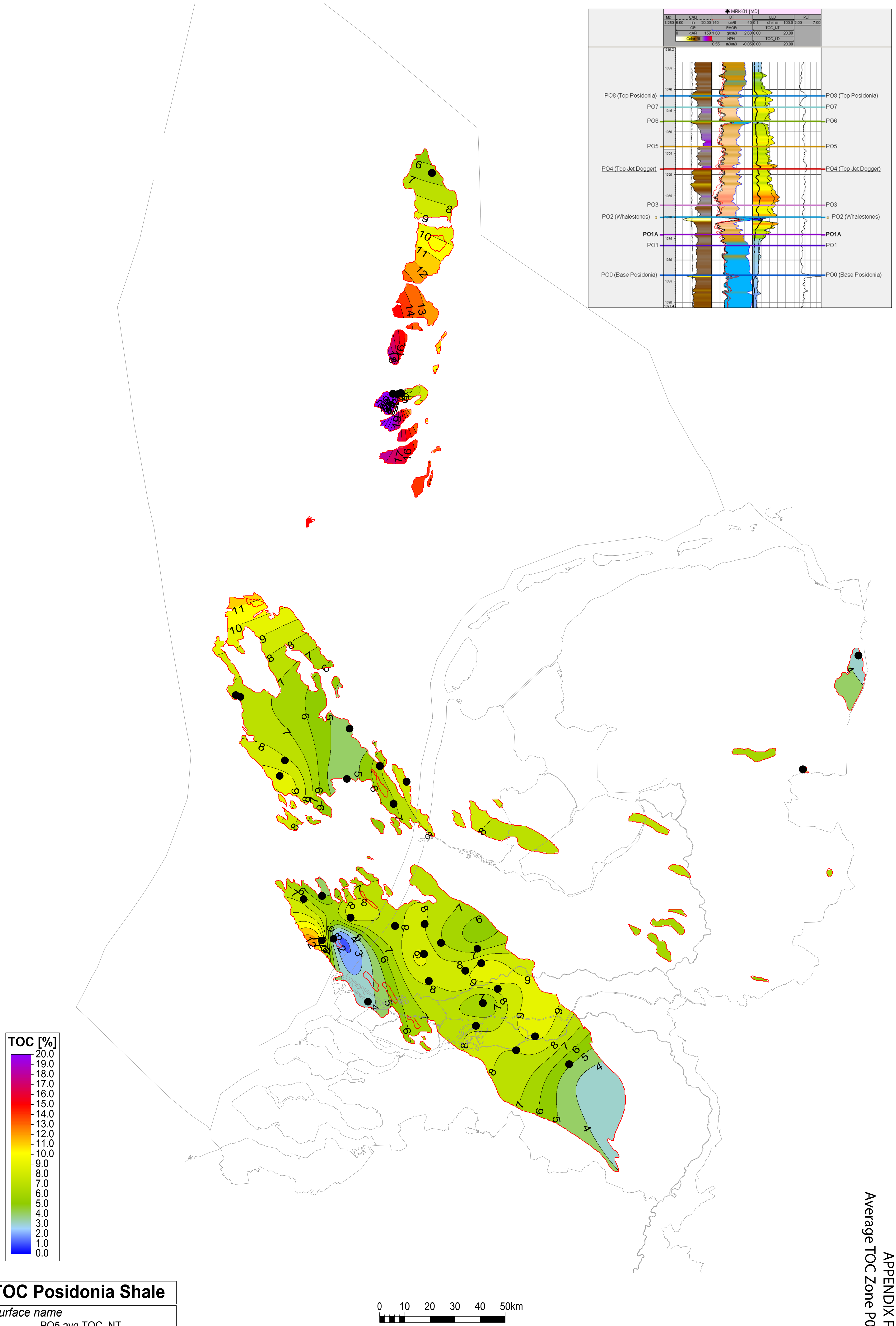

TOC Posidonia Shale

Surface name
PO5 avg TOC_NT

Date	*Status*
10/05/2015	Final

TNO report TNO 2015 R10740
APPENDIX F4
Average TOC Zone P05

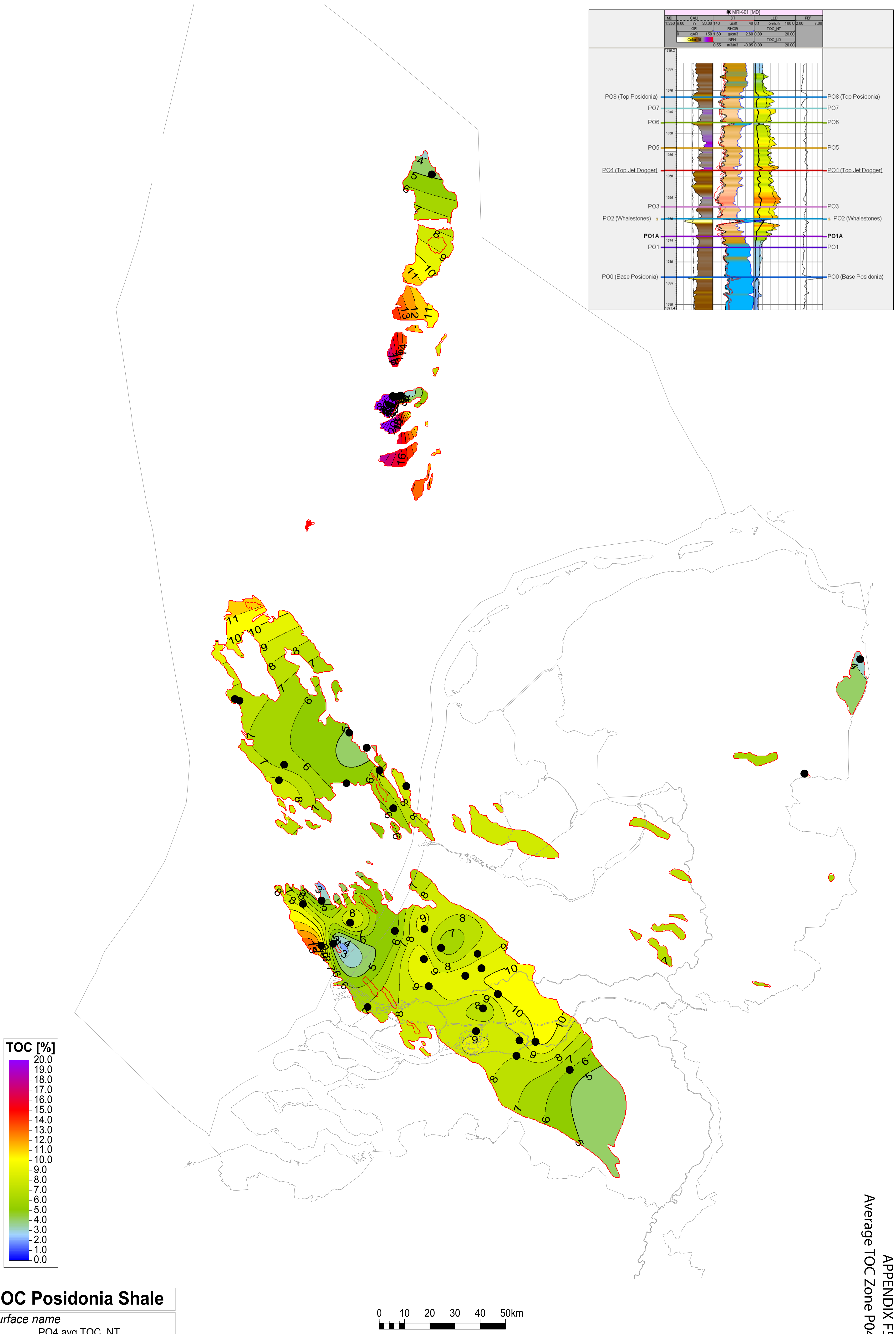

TOC Posidonia Shale

Surface name	
PO4 avg TOC_NT	
Date	*Status*
10/05/2015	Final

TNO report TNO 2015 R10740
APPENDIX F5
Average TOC Zone P04

Average TOC Zone P03

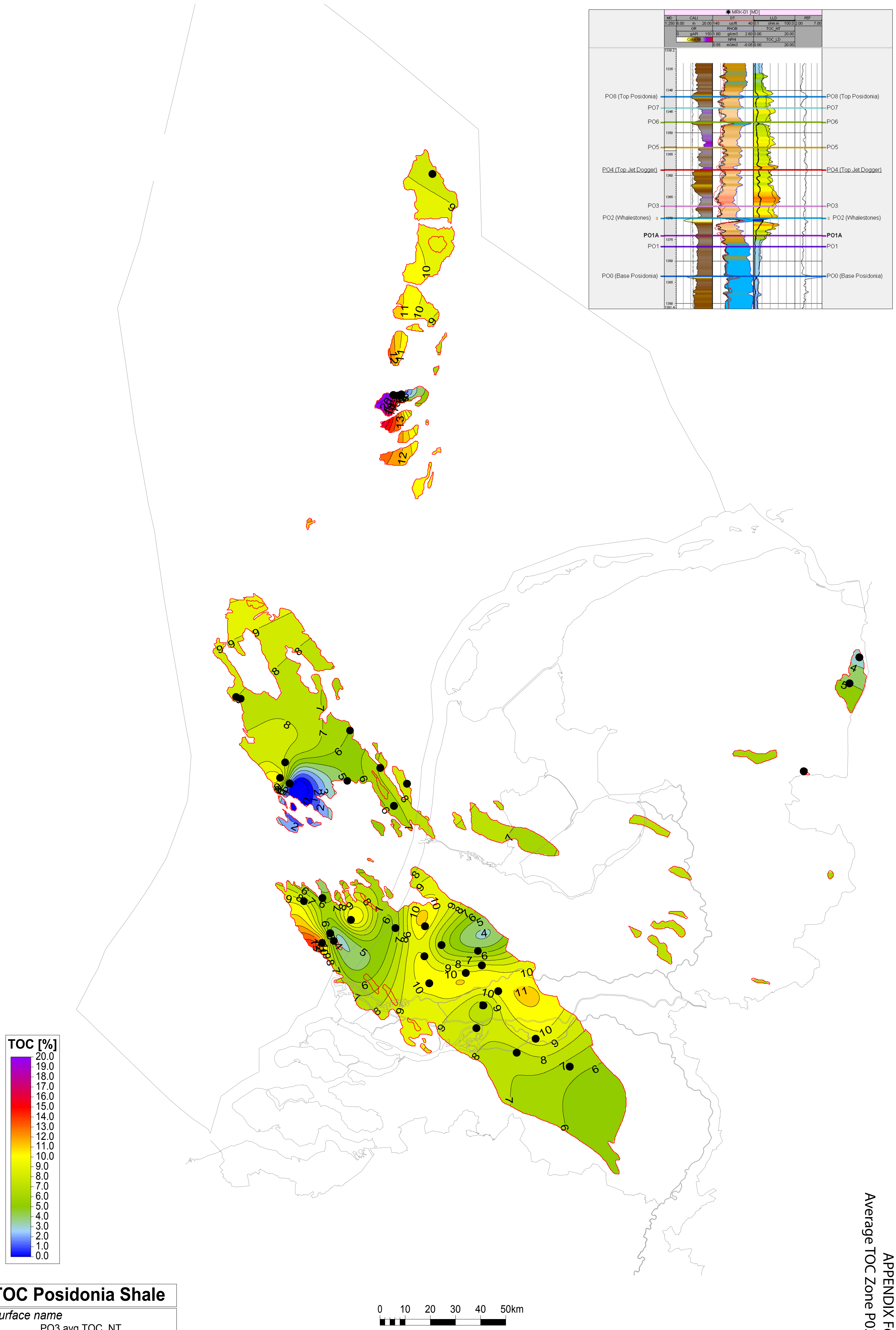

TOC Posidonia Shale

Surface name	
PO3 avg TOC_NT	
Date	*Status*
10/05/2015	Final

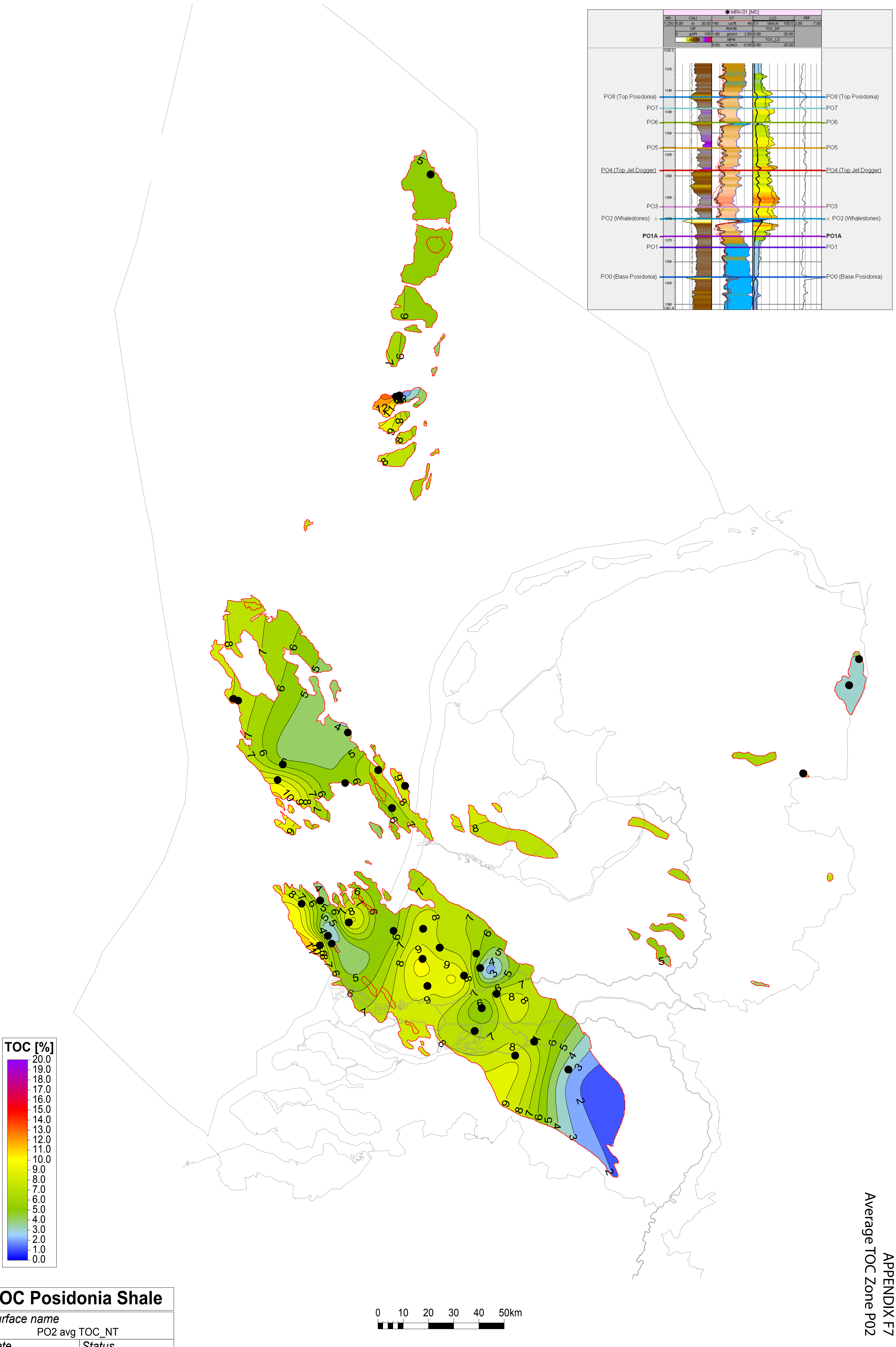

TOC Posidonia Shale

Surface name
PO2 avg TOC_NT

Date 10/05/2015
Status Final

TNO report TNO 2015 R10740
APPENDIX F7
Average TOC Zone P02

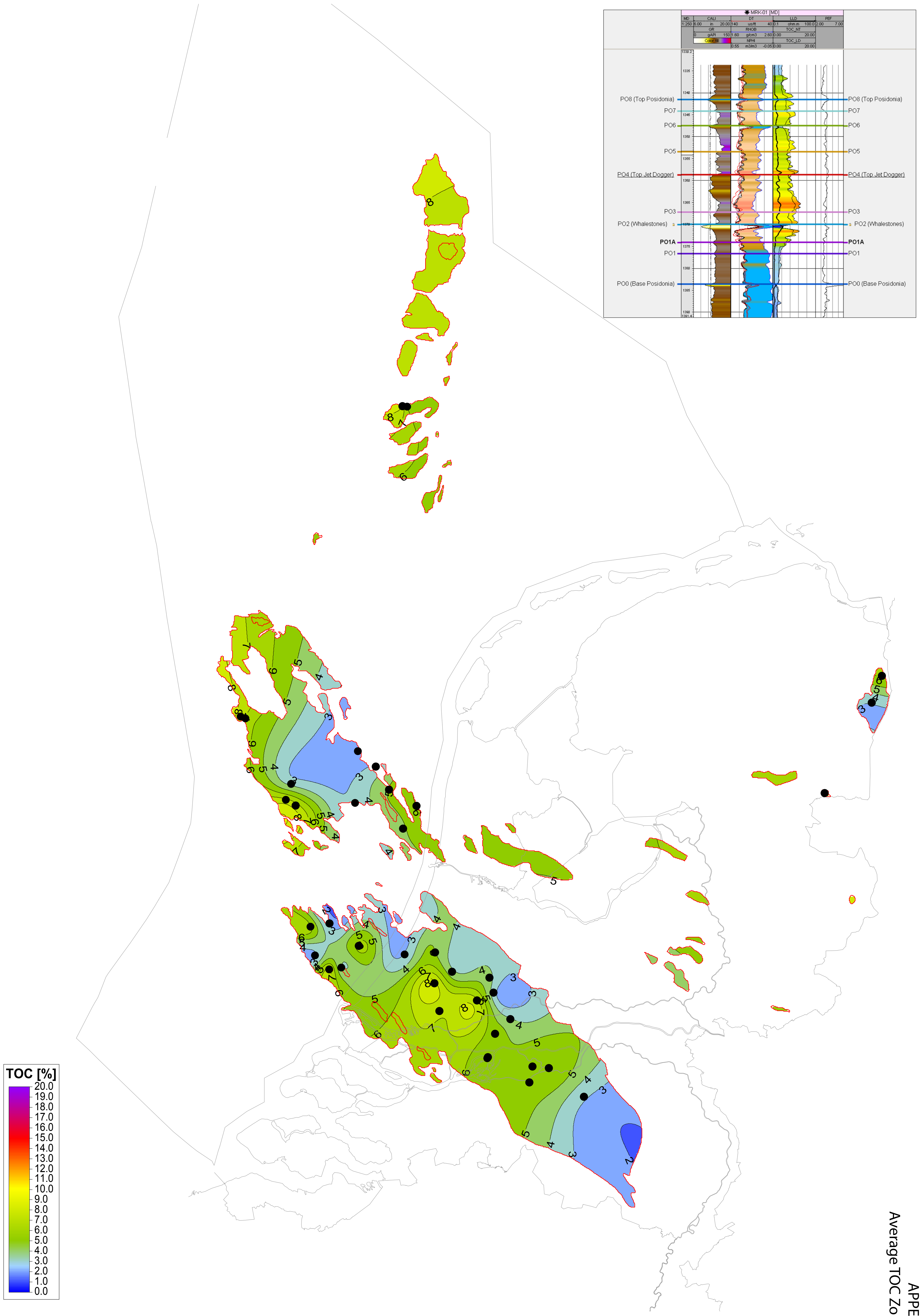

TOC Posidonia Shale

Surface name	
PO1A avg TOC_NT	
Date	*Status*
10/05/2015	Final

0 10 20 30 40 50km

TNO report TNO 2015 R10740
APPENDIX F8
Average TOC Zone P01A

TNO innovation for life

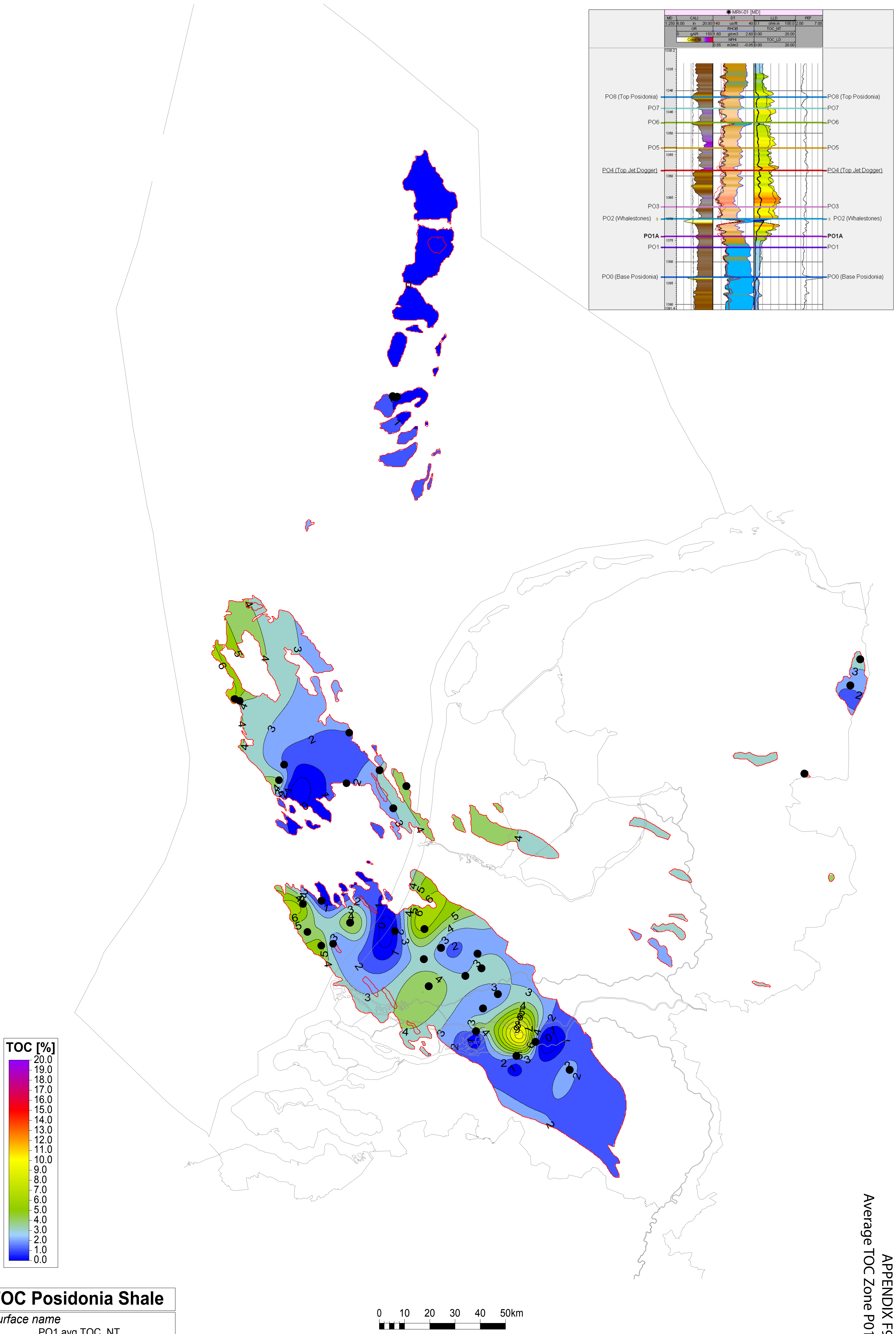

TOC Posidonia Shale

Surface name	
PO1 avg TOC_NT	
Date	*Status*
10/05/2015	Final

TNO report TNO 2015 R10740
APPENDIX F9
Average TOC Zone P01

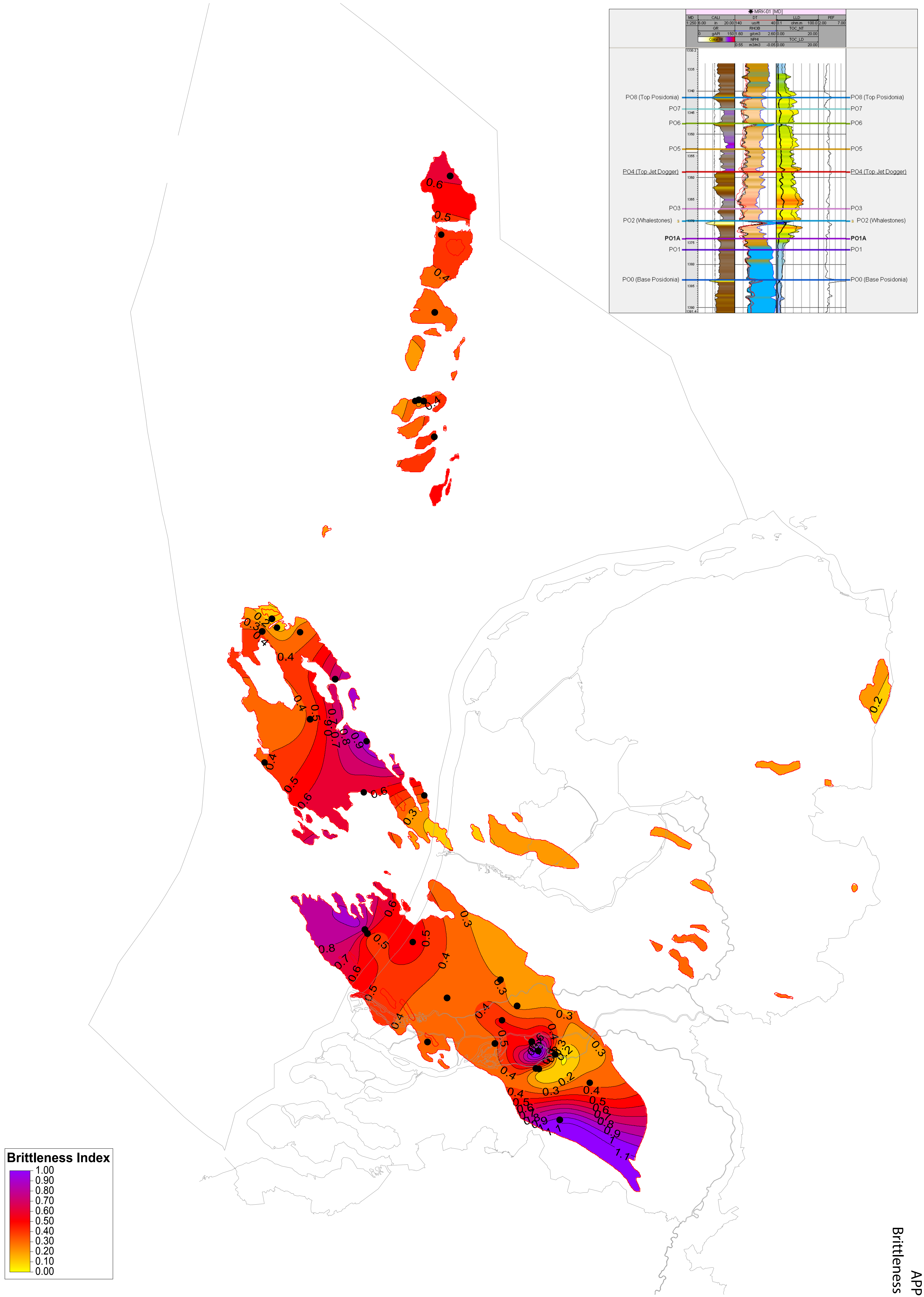

Brittleness Posidonia Shale

Surface name	
PO8 BRIT	
Date	*Status*
10/05/2015	Final

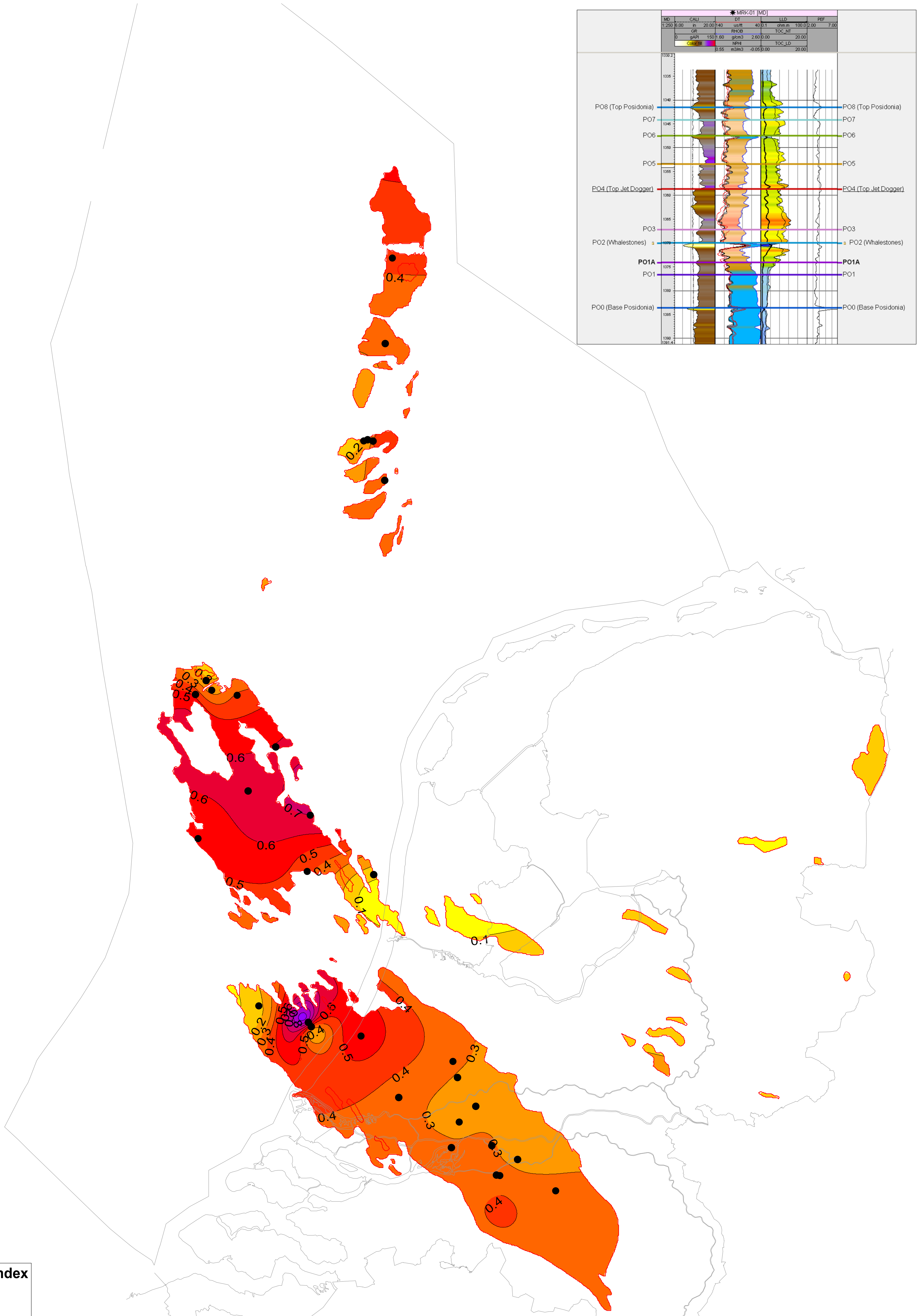

Brittleness Index

	1.00
	0.90
	0.80
	0.70
	0.60
	0.50
	0.40
	0.30
	0.20
	0.10
	0.00

0 10 20 30 40 50km

Brittleness Posidonia Shale

Surface name	
PO7 BRIT	
Date	*Status*
10/05/2015	Final

innovation for life

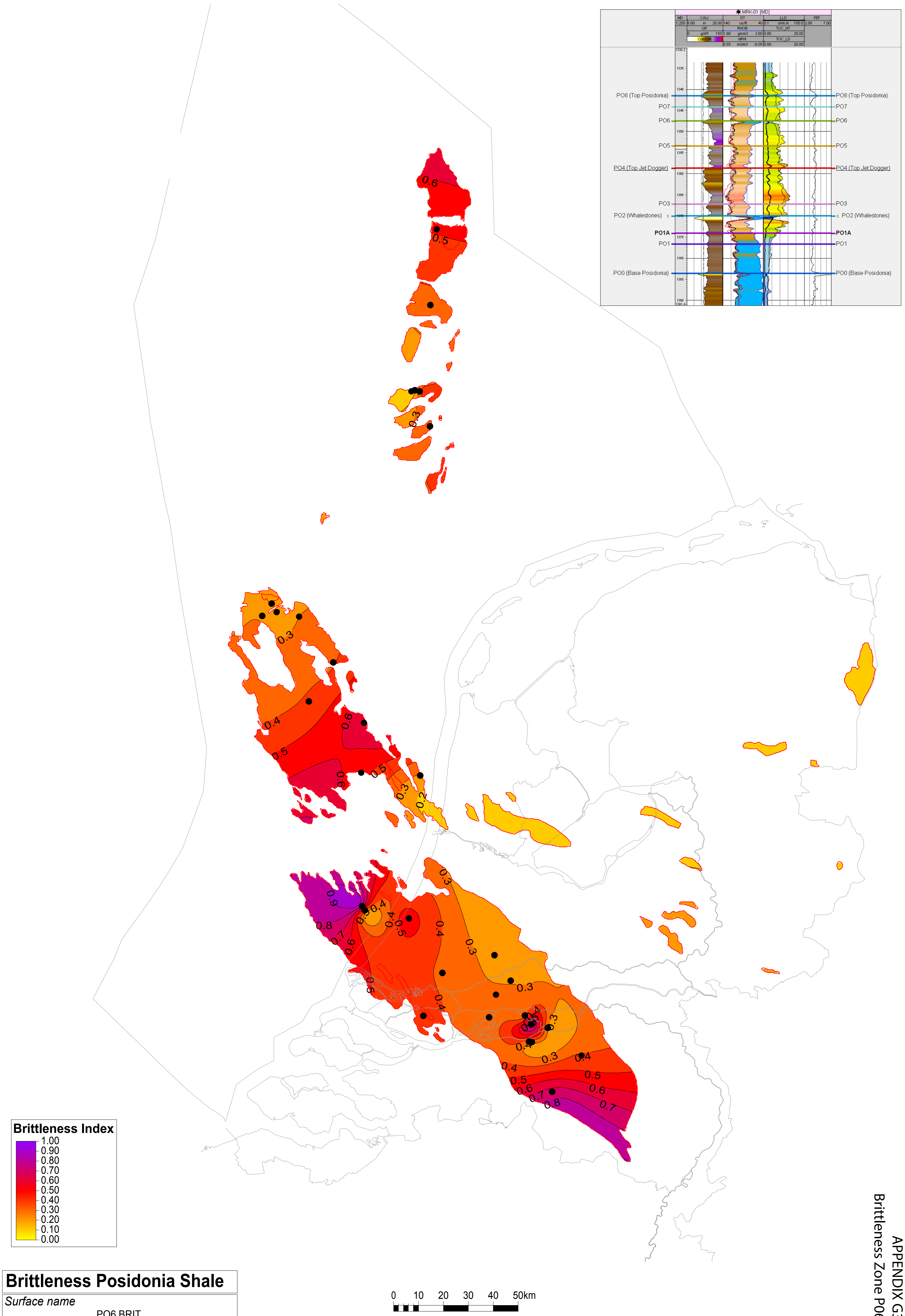

Brittleness Posidonia Shale

Surface name PO6 BRIT	
Date 10/05/2015	*Status* Final

TNO innovation for life

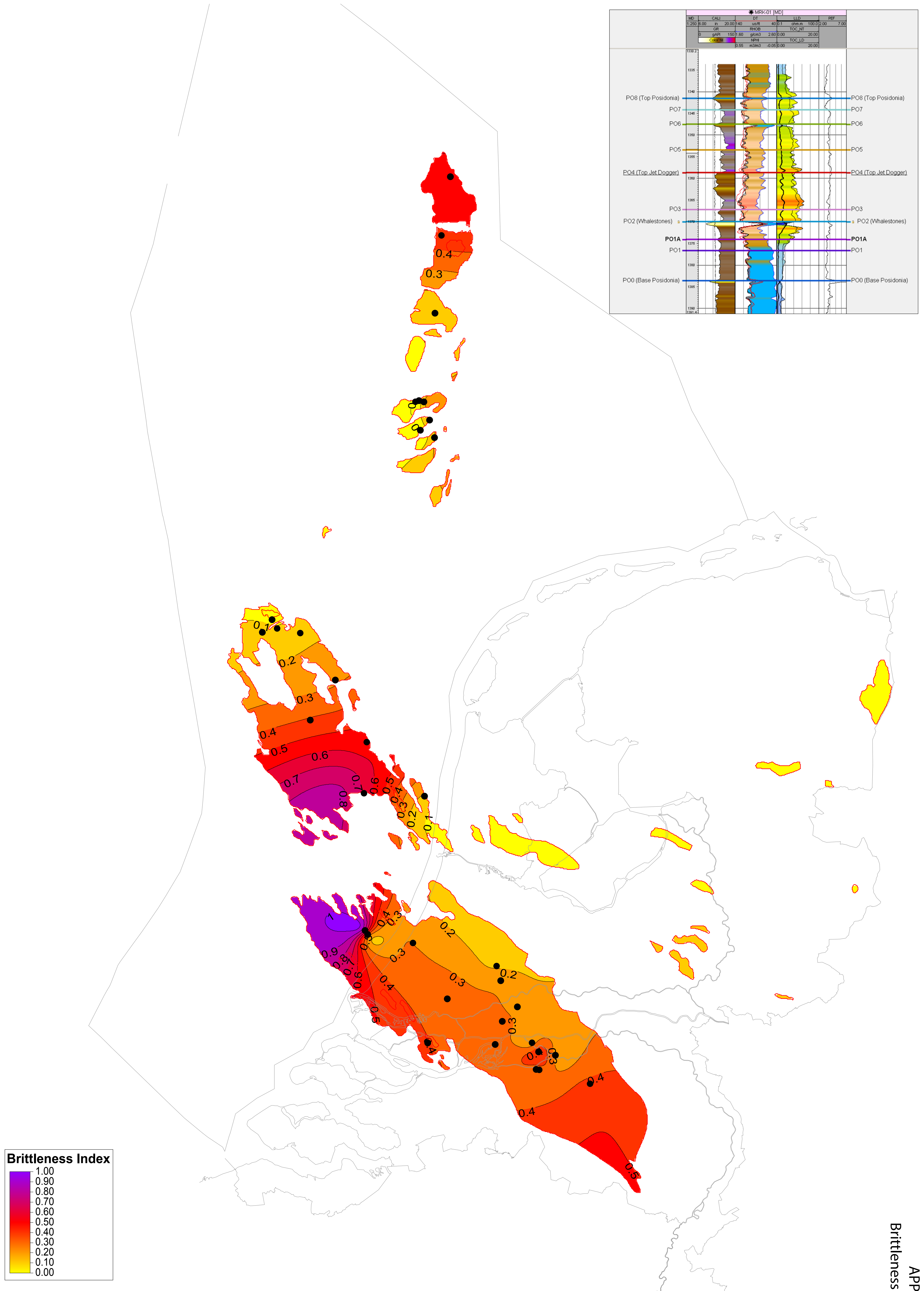

Brittleness Posidonia Shale

Surface name	
PO5 BRIT	
Date	*Status*
10/05/2015	Final

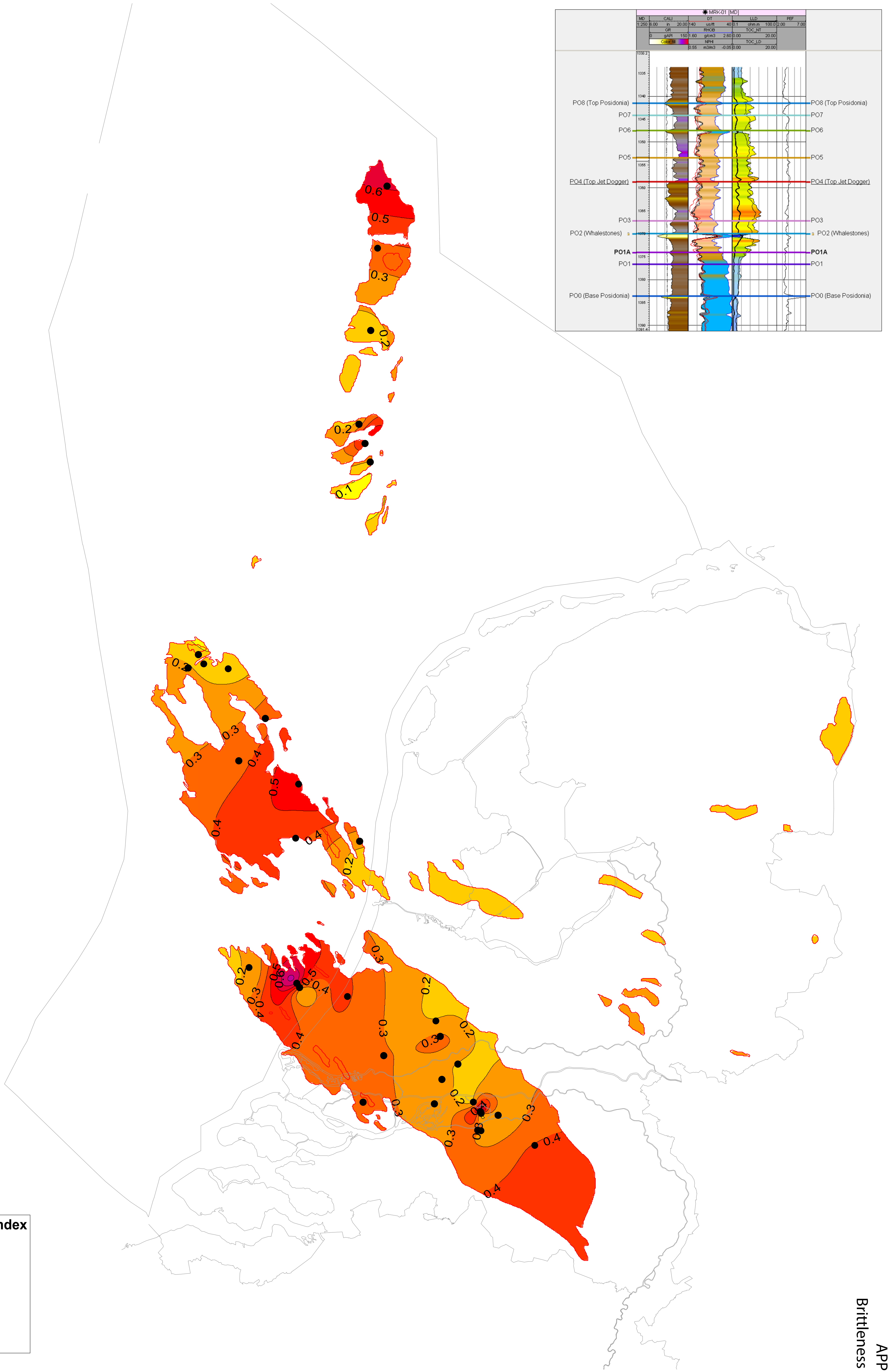

Brittleness Index

🟪	1.00
	0.90
	0.80
	0.70
🟥	0.60
	0.50
	0.40
🟧	0.30
	0.20
	0.10
🟨	0.00

0 10 20 30 40 50km

Brittleness Posidonia Shale

Surface name	
PO4 BRIT	
Date	*Status*
10/05/2015	Final

TNO report TNO 2015 R10740
APPENDIX G5
Brittleness Zone P04

TNO innovation for life

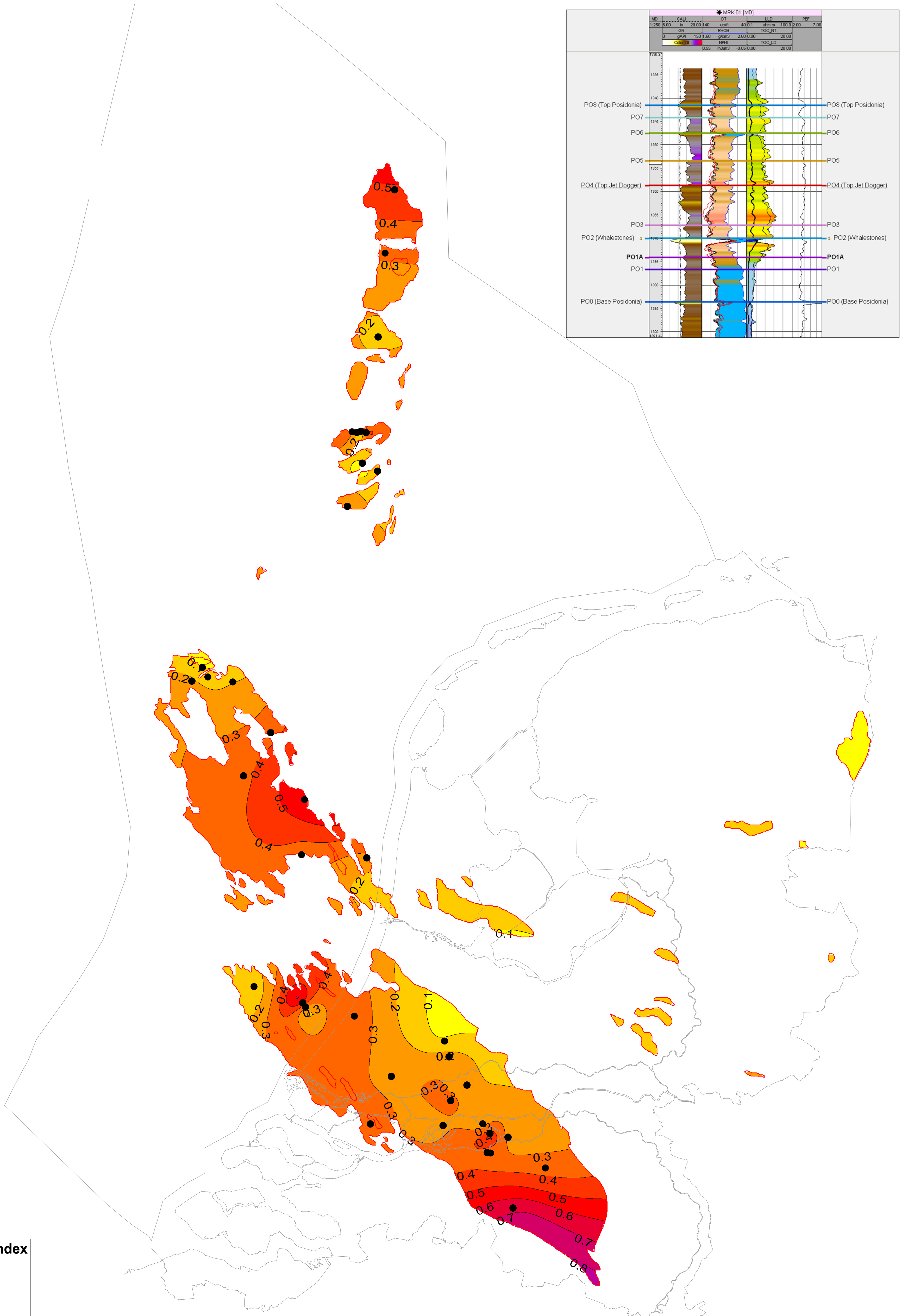

Brittleness Index

- 1.00
- 0.90
- 0.80
- 0.70
- 0.60
- 0.50
- 0.40
- 0.30
- 0.20
- 0.10
- 0.00

0 10 20 30 40 50km

Brittleness Posidonia Shale

Surface name
PO3 BRIT

Date	*Status*
10/05/2015	Final

TNO innovation for life

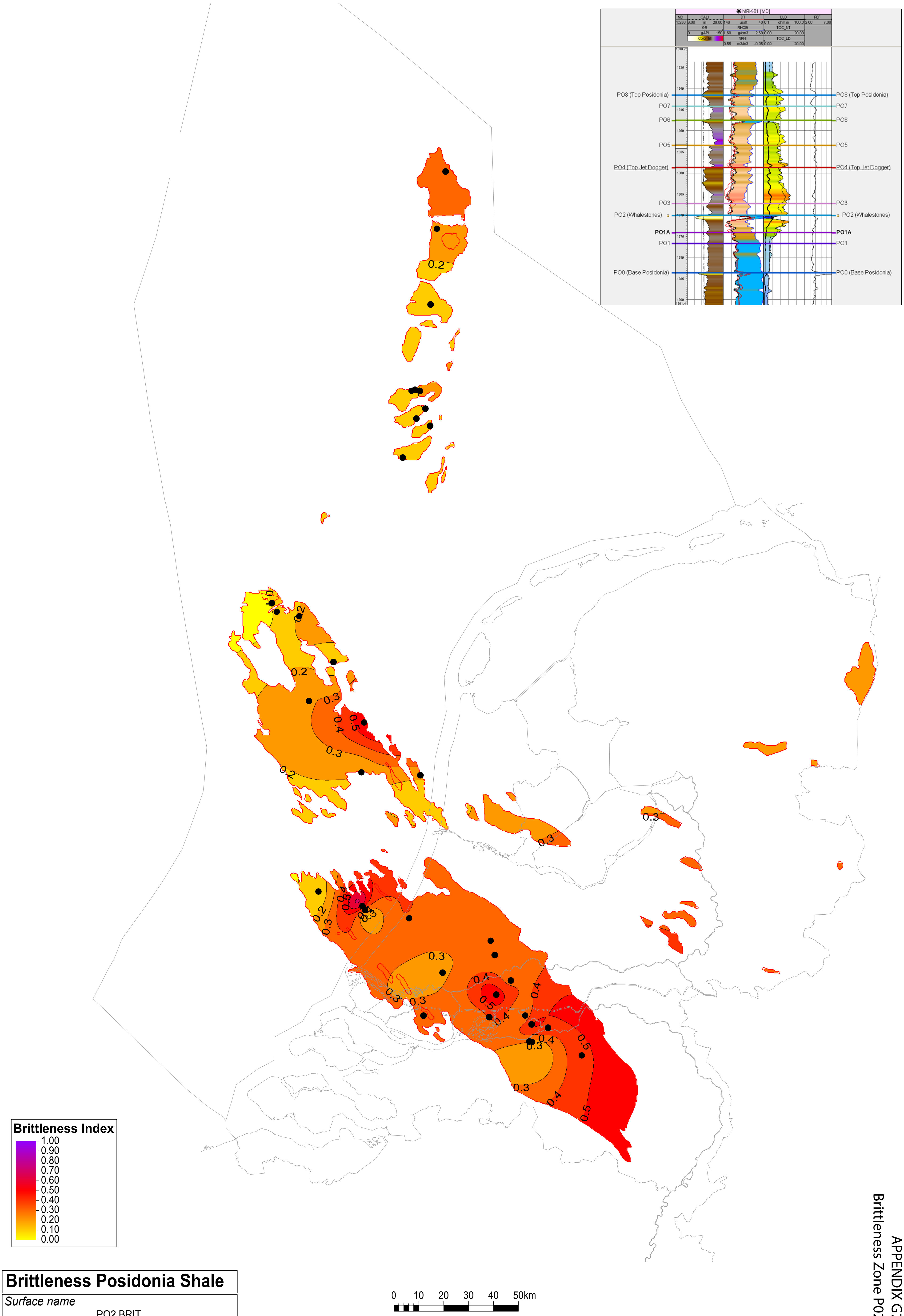

Brittleness Posidonia Shale

Surface name
PO2 BRIT

Date	*Status*
10/05/2015	Final

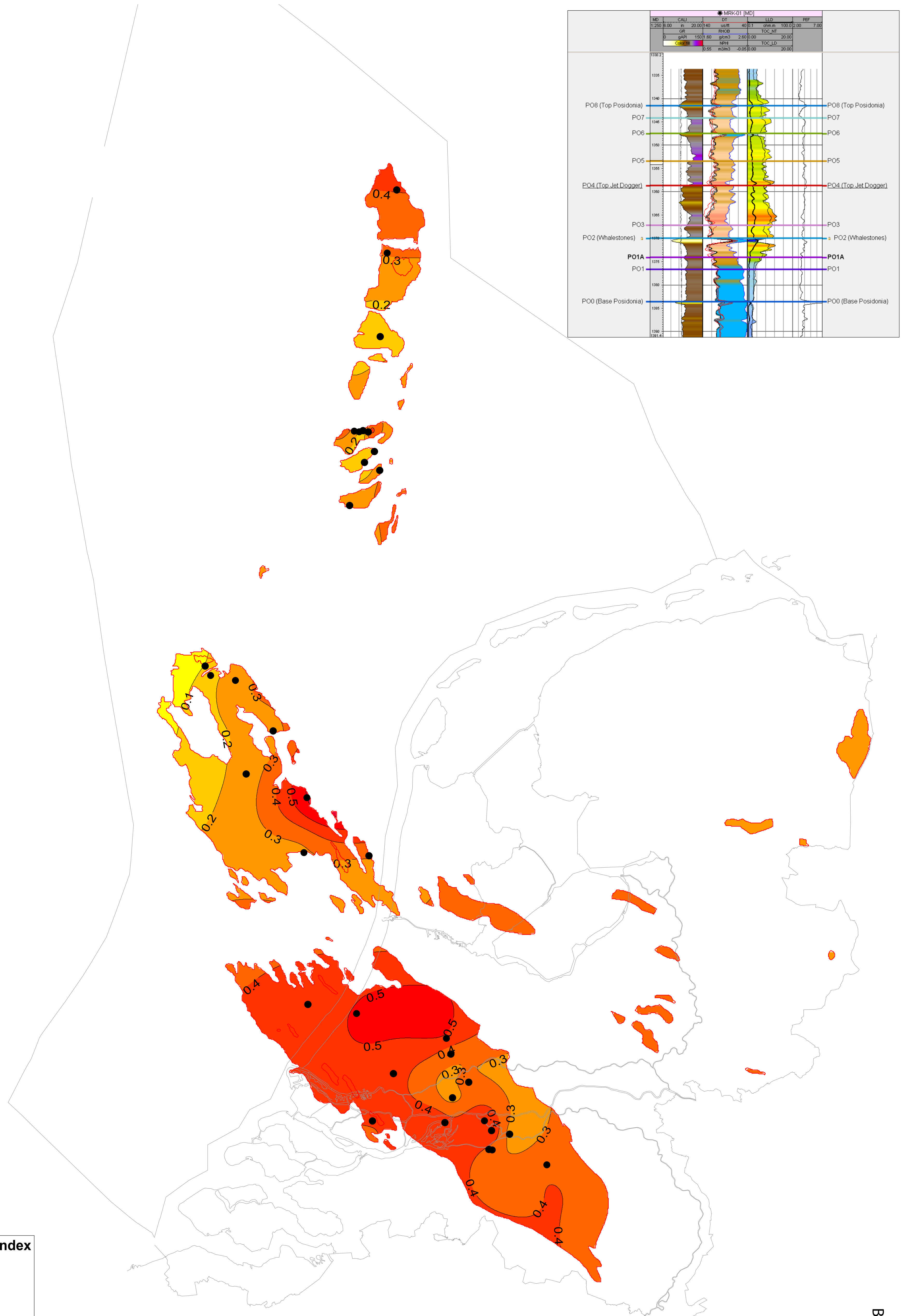

Brittleness Index

- 1.00
- 0.90
- 0.80
- 0.70
- 0.60
- 0.50
- 0.40
- 0.30
- 0.20
- 0.10
- 0.00

Brittleness Posidonia Shale

Surface name PO1A BRIT	
Date 10/05/2015	*Status* Final

TNO report TNO 2015 R10740
APPENDIX G8
Brittleness Zone P01A

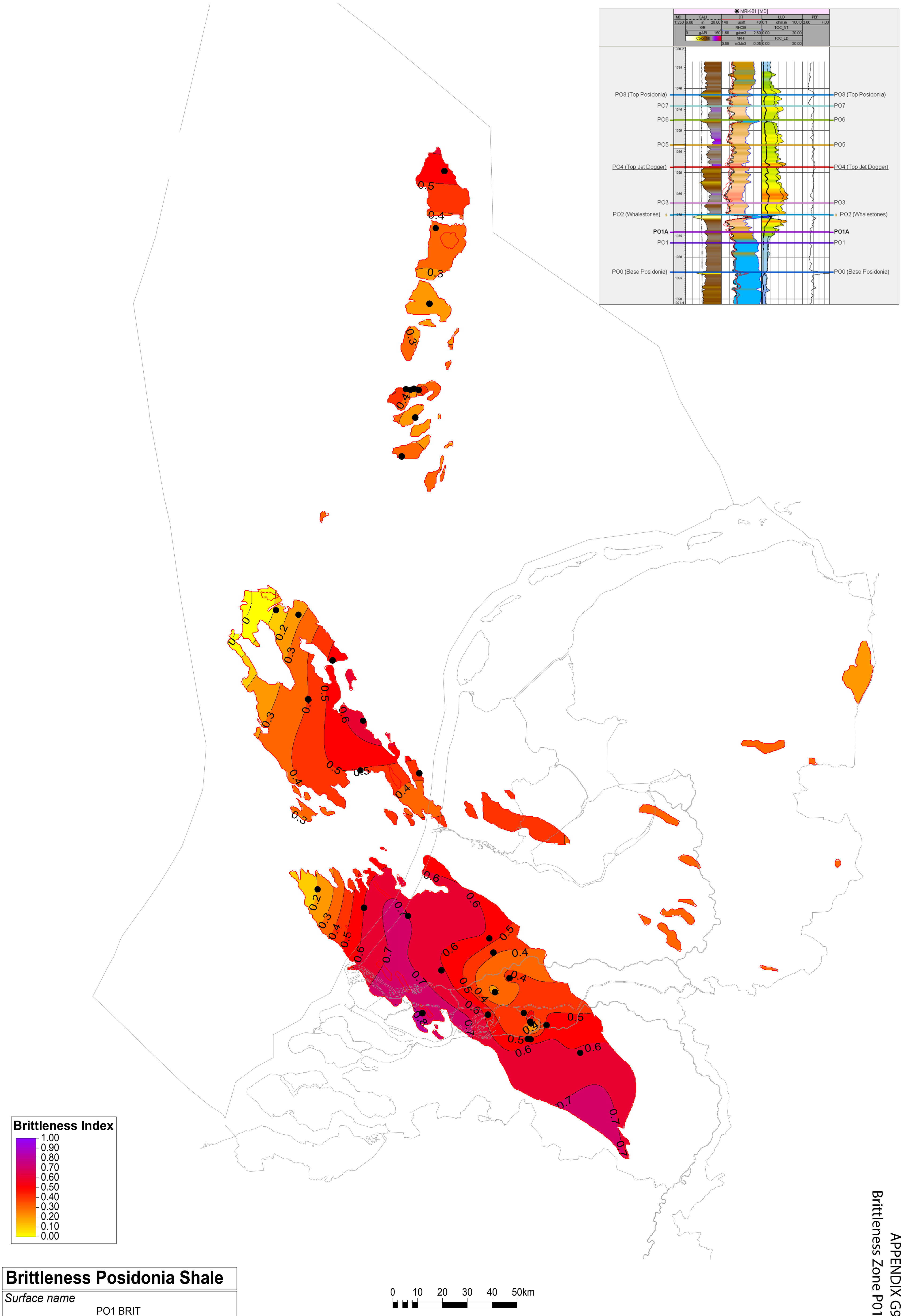

Brittleness Posidonia Shale

Surface name	
PO1 BRIT	
Date	*Status*
10/05/2015	Final

TNO report TNO 2015 R10740
APPENDIX G9
Brittleness Zone P01

innovation for life

Stable isotope correlation